A study of mixing and combustion in a divided chamber turbocharged natural gas engine

Jager, Dennis John

Award date:
1992

Awarding institution:
University of Bath

A STUDY OF MIXING AND COMBUSTION IN A DIVIDED CHAMBER TURBOCHARGED NATURAL GAS ENGINE

Submitted by Dennis John Jager
for the degree of Ph.D. of the
University of Bath 1992

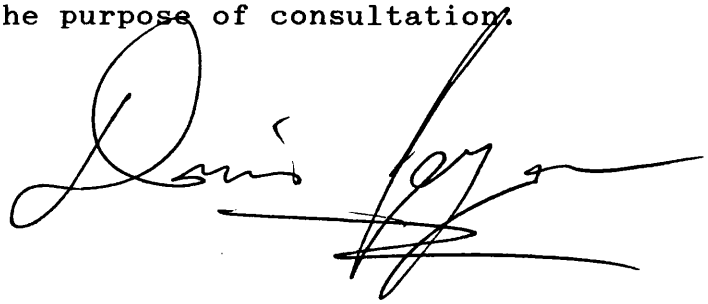

ProQuest LLC
789 East Eisenhower Parkway
P.O. Box 1346
Ann Arbor, MI 48106-1346

To Lizzie

Summary

This thesis describes an investigation into mixing and combustion in a divided chamber turbocharged natural gas engine. This type of engine is able to operate at very lean air-fuel ratios for the purpose of reducing exhaust emissions of NOx. The engine uses a prechamber ignition system to ignite a lean main charge.

Results from engine tests have proven this type of combustion system to be a successful method of reducing NOx emissions from a natural gas engine. Experimental results demonstrate that extremely low (<2g/kWh) emissions of NOx are possible with this system by adopting air-fuel ratios of 27 to 29:1

A fast response FID has been validated and used to measure the mixture strength within the prechamber during compression and combustion. This work has been complemented by a study of mixture variation in the prechamber using CFD modelling.

From the engine tests and prechamber study, it appears that the best control strategy is to operate the prechamber with a pilot supply air-fuel ratio of approximately 3:1 and with a filling ratio just sufficient to fill the prechamber with fresh charge. Results indicate that a mixture concentration close to stoichiometric will then be produced at the spark plug location at the time of ignition.

Acknowledgements

The author wishes to express his thanks to the many people at the University of Bath and Dorman Diesels who have been involved with the project.

In particular the author wishes to thank:

Dr S.J. Charlton for his continuous support and guidance throughout the project.

The technicians Les Duddridge and Don Blake for their excellent work in the installation, maintenance and running of the engine rig.

The employees in the research and development department at Dorman.

The financial support of the Science and Engineering Research Council and Dorman Diesels Ltd. is also acknowledged.

List of Contents

Nomenclature

Abbreviations

afr	air-fuel ratio
bdc	bottom dead centre
bmep	brake mean effective pressure
bsfc	brake specific fuel consumption
CFD	computational fluid dynamic
CR	compression ratio
FID	flame ionisation detector
HFR	high frequency response
TDC	top dead centre

General Notation

k	turbulence kinetic energy
C	courant number
Cd	coefficient of discharge
D	diameter
I	turbulence intensity
l	turbulence mixing length
p	pressure
t	time
T	temperature
u	velocity
V	volume
λ	prechamber filling ratio
ρ	density
γ	ratio of specific heats
β	diametric ratio
ε	turbulence dissipation
τ_v	turbulent diffussion

Chapter 1

1. Introduction

1.1 Subject of Thesis

This thesis reports on an investigation into mixing and combustion in a lean burn natural gas engine which utilises stratified charge combustion by having two combustion chambers, a main chamber and a smaller prechamber (see Appendix A for engine specification). The engine is designed to be operated by igniting a stoichiometric air-fuel mixture in the prechamber with a conventional discharge spark. A high energy flame is produced which propagates into the main combustion chamber through a connecting orifice. This then ignites the leaner main charge. Correct design and operation of the prechamber is thought to be essential for correct running of the engine and it is this subject that this thesis particularly concentrates on.

The study involved three distinct objectives. The first objective was to evaluate the performance and emissions of this engine configuration under typical operating conditions. The second objective was to attempt to optimise operating parameters with respect to thermal efficiency and exhaust emissions. The third objective was to increase our understanding of the combustion processes occurring within the engine by both experimental and computational techniques which would lead to recommended improvements in the design.

1.2 Background to Project

The use of gas in internal combustion engines is not new. Gas engines were widely in use at the turn of the century, but changes in the relative prices of fuels gradually made their continued use uneconomic. However, with the arrival of a new piped fuel,

natural gas, and immense changes in engine technology, the use of gas engines as on-site prime movers has increased in popularity. Natural gas is a low-cost, high-quality substitute for high grade liquid fuels, and is an ideal fuel for internal combustion engines. Reciprocating gas engines consist of two types, dual fuel and spark ignition engines. Dual fuel engines use the compression ignition cycle, where combustion is initiated by a small quantity of liquid fuel. This type of engine has the advantage that it can operate on either a gas/liquid fuel mixture, or on straight liquid fuel. Working approximately on the Otto cycle, spark ignited gas engines are similar in design to the petrol engine, typically having compression ratios between 6:1 and 12:1.

Stringent regulations are being introduced regarding pollution to the environment from the exhaust emissions of internal combustion engines, including those running on natural gas. Manufacturers are having to look at new ways of meeting these new regulations, but as far as possible, without compromising engine performance.

The greatest cause of concern as far as gas engines are concerned, is the emission of oxides of nitrogen (NOx). Emissions of carbon monoxide are only a problem if the engine is operating on the rich side of stoichiometric. In a lean burn engine, the excess air will mean that the fuel carbon will be oxidised to CO_2 in preference to CO.

Production of these harmful oxides of nitrogen is as a result of the high temperatures present in the region behind the flame front during combustion. By operating the engine with lean

mixtures, flame temperatures can be substantially lowered, and hence NOx emission is reduced. However it is not possible to operate a conventional open chamber engine with a mixture lean enough to meet stringent government regulations on NOx emission, such as amendments to the Clean Air Act of 1976 and 1977, because of low flame speeds and high hydrocarbon emissions.

Operating gas engines on extremely lean fuel-air mixtures is one method of reducing NOx emissions. Alternative methods of NOx reduction include the use of catalytic converters and exhaust gas recirculation. Catalytic converters can remove NOx from the exhaust gases before they are released to the environment. However this is an expensive solution as the converters employ precious metals, and in order to be effective, require the engine to be operated at near stoichiometric conditions. This means that efficiency is compromised, and CO emissions are no longer negligible, and so a two way catalyst would be required to remove this as well. Exhaust gas recirculation (EGR) also has the effect of reducing NOx emissions by reducing peak combustion temperatures. This is due to the higher values of specific heat capacity of the residuals in the exhaust gas reducing the rise in temperature as well as reducing oxygen avaliability for NOx formation. A combination of catalytic reduction and EGR can be used to allow NOx emissions to be lowered sufficiently to meet the necessary regulations, but the extra costs of installation and reduced performance make them an undesirable option.

One method of igniting lean fuel-air mixtures is to provide an energy source for ignition that is much greater than the spark alone. In the past, this has been tried successfully using a pilot supply of diesel oil to provide the energy necessary for

reliable ignition of the main charge, and many engines are still in operation using this system. However, benefits in improved combustion efficiency are lost by the extra costs of the pilot fuel and additional equipment. A much more desirable approach is to employ a stratified charge system using a small isolated volume containing a charge of richer mixture ignited by the spark. The energy thus released from this "energy cell" is many times that of the original spark and sufficient to ignite very lean main chamber mixtures. This method of ignition is often referred to as "Torch" or "Jet ignition", and is achieved by using a separate auxiliary pre-combustion chamber with a separate fuel supply system. The processes of mixture preparation, ignition and flame propagation within this small prechamber are complex, but critical to the overall operation of the engine. This system is employed on the Dorman SE1 gas engine, the subject of this thesis.

Dorman Diesels have been developing low emission lean burn natural gas engines for some time. Dorman Diesels produce a wide range of large high speed Diesel and natural gas engines for industrial and power generation applications. Plate 1 shows a Dorman SE6 6 cylinder diesel engine. Traditionally the company has produced natural gas engines by converting the basic Diesel engine design. This involves a reduction of compression ratio, a modified cylinder head design to accept a spark plug and reduce swirl, the incorporation of a gas-air mixer in the intake system and rematched turbocharger. This type of engine operates with an air-fuel ratio close to stoichiometric thereby ensuring stable combustion with acceptable efficiency. However the disadvantage of this type of engine is that exhaust emissions will not meet new international legislation.

Prechamber variants of this engine have been produced and tested by the company with limited success. This was largely due to the restrictions imposed when attempting to perform research and development on a multi cylinder engine. Hence an experimental, single cylinder research engine was designed and manufactured in a collaboration between Bath University and Dorman Diesels. Design and construction of the engine is described by Moore (23). Figure 1.1 shows the SE1 research engine in Diesel form, while plate 2. and figure 1.2 show a section through the prechamber assembly itself.

1.3 Objectives of Project

An aim of the project was to commission the SE1 engine and instrumentation, involving the development of main chamber and prechamber fuel and air supply systems. This was followed by a period of experimental testing. The object of this was to study prechamber mixture requirements for both quality and quantity and the effect on engine performance and emissions. The effect of varying ignition timing and ambient temperature were also to be studied with the object of reducing NOx emissions, improving thermal efficiency and eliminating combustion knock.

These engine experiments were then followed by a detailed investigation of mixture preparation within the prechamber of the engine. Two approaches were used, one experimental, the other computational. Results from the two were then compared and evaluated.

In the experimental study, a novel fast response flame ionisation detector (FID) developed by Collings (9) was used to sample mixture concentration within the prechamber of the running SE1 engine. The high frequency response of the instrument (100-500 Hz) allowed real time measurements over the high pressure part of the engine cycle. A hypodermic probe, providing point measurement of mixture strength, can be moved to different positions to produce limited spatial resolution.

The computational study involved using a computational fluid dynamics (CFD) program employing finite-volume methods to model the mixture preparation within the prechamber. The program features a body-fitted mesh coordinate system, turbulence modelling and a time-marching transient flow facility.

Comparison of the results from these two methods will help to validate the application of CFD and increase our understanding of the complex processes occurring within the prechamber. This has lead to recommendations in both the setting of the engine operating parameters, improvements in engine design, and areas of further research.

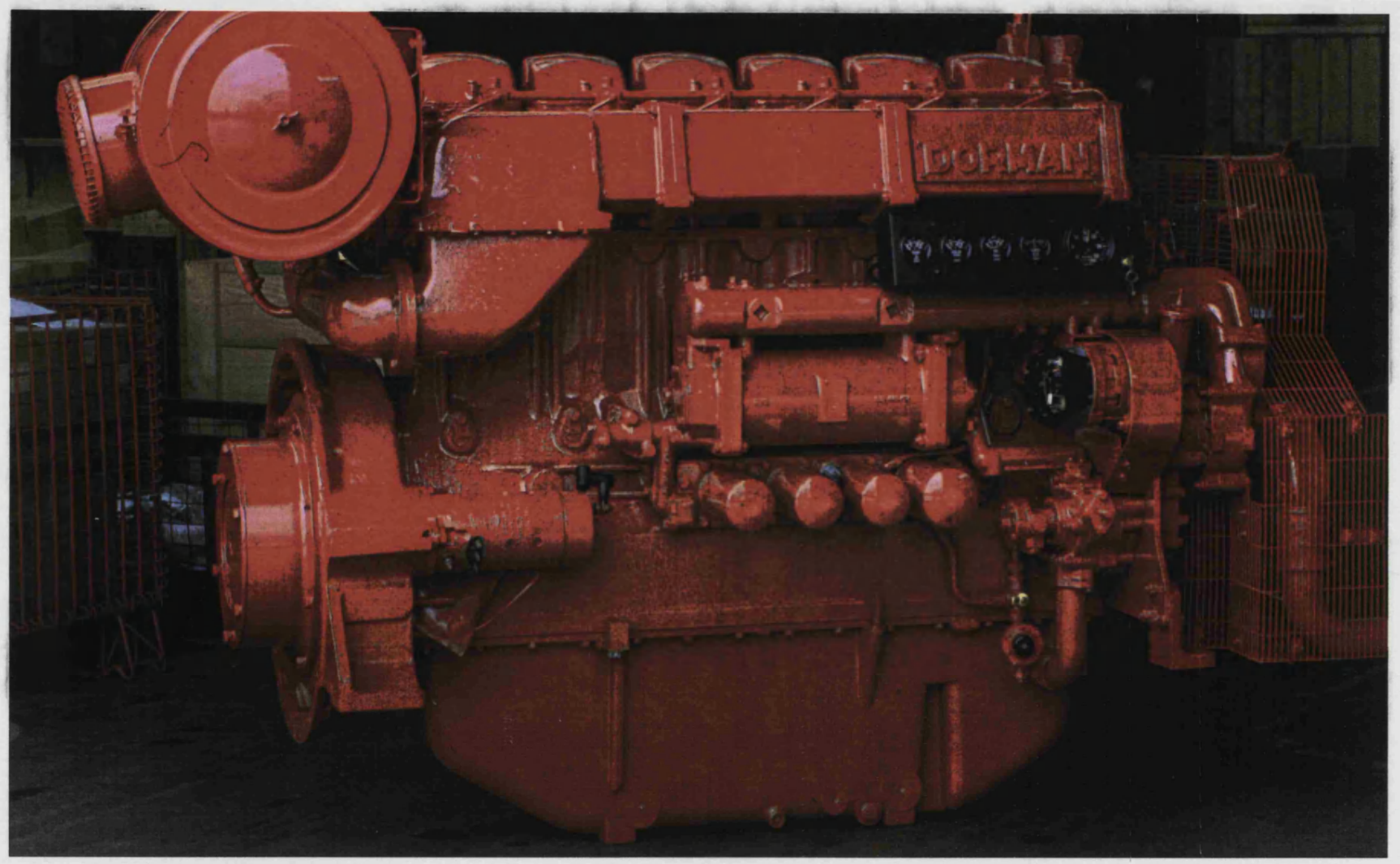

Plate 1. 6 Cylinder Dorman SE6 Diesel Engine

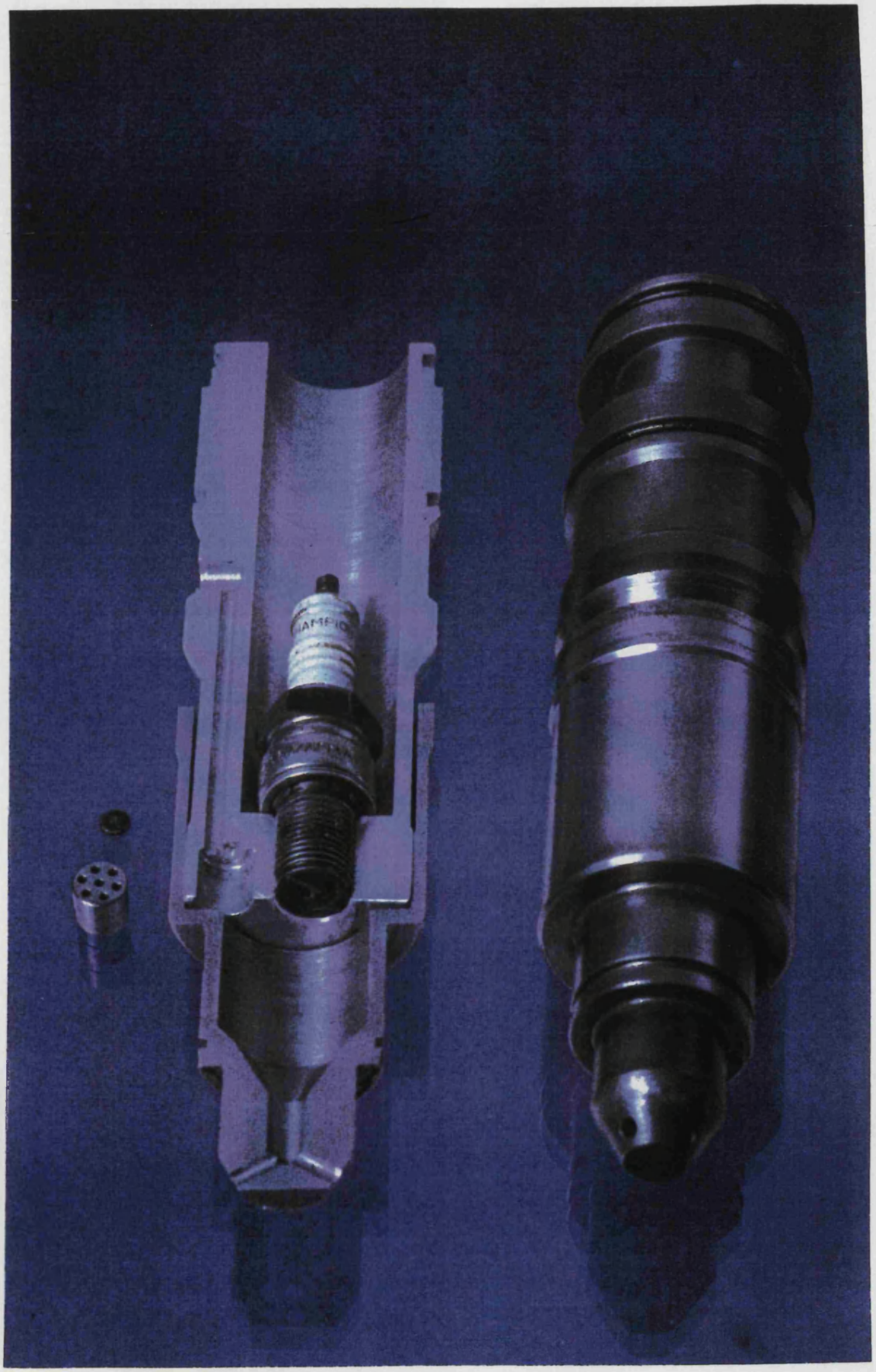

Plate 2. Cross-Section Through and External View of Prechamber Assembly

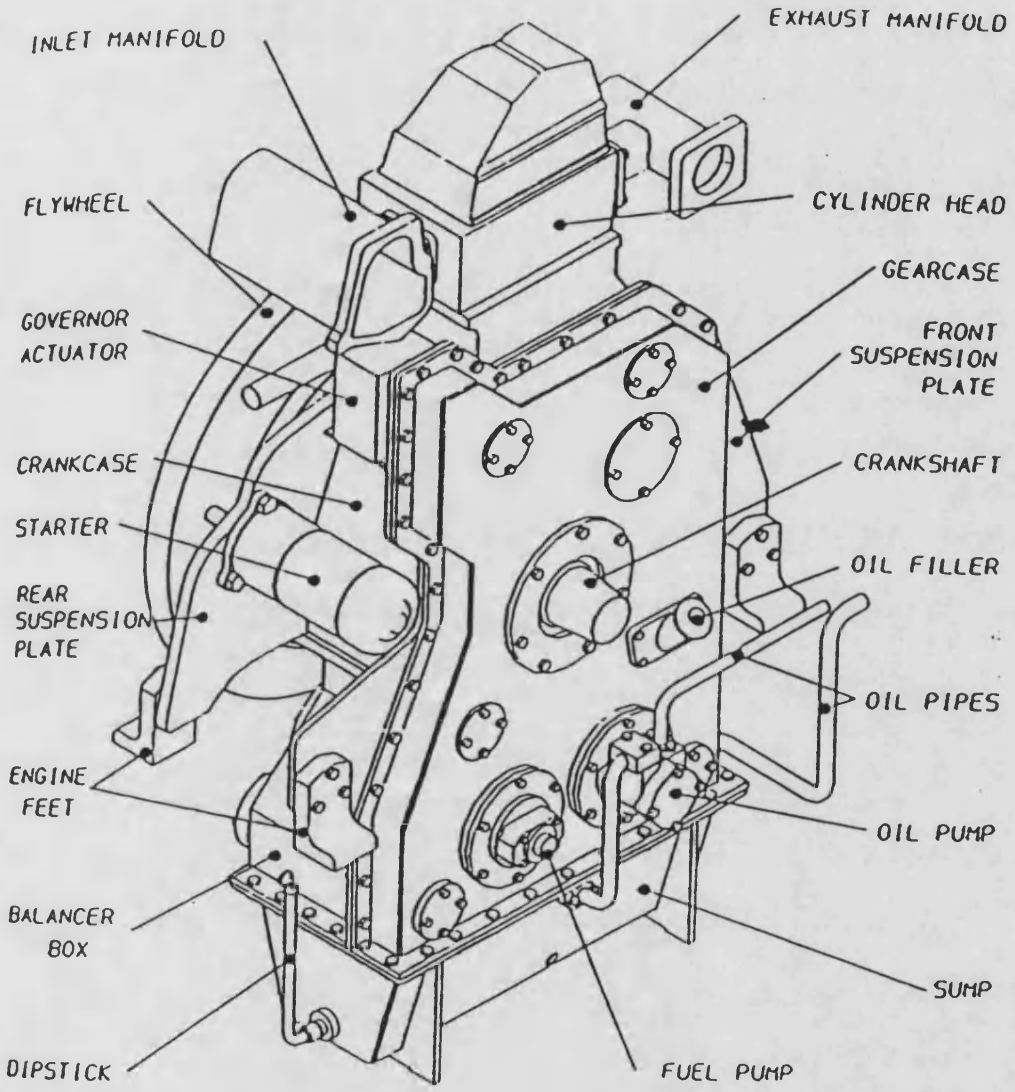

Figure 1.1 The SE1 Research Engine in Diesel Form

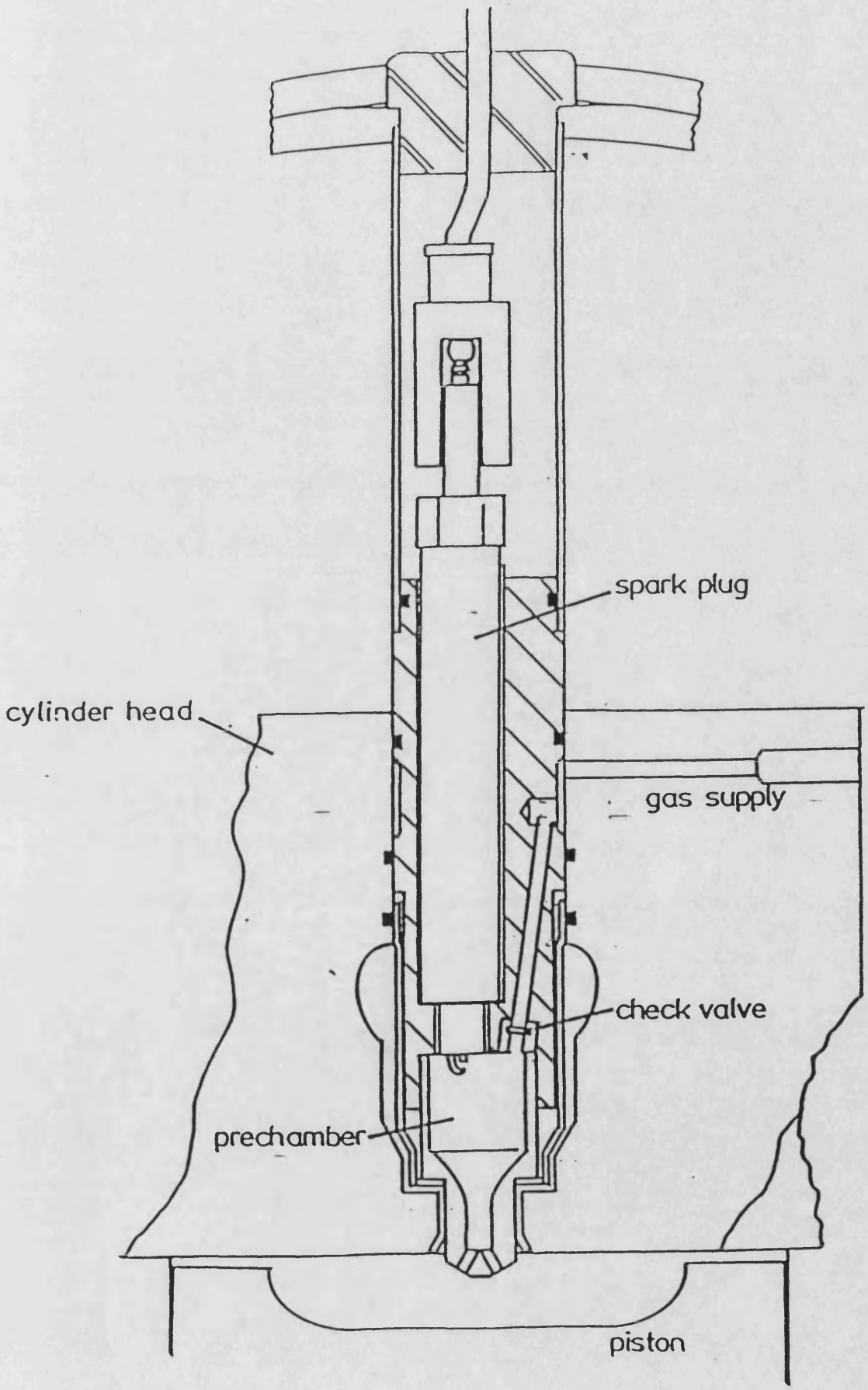

Figure 1.2 Section Through Prechamber Assembly

Chapter 2

2. Literature Review

2.1 Introduction

This chapter reviews the material published by other workers which relates either directly or indirectly to the subject of this thesis. As the quantity of literature is large, only the most relevent material is discussed.

2.2 Exhaust Emissions from Natural Gas Engines

Spark ignition engines, like Diesel engines, constitute a substantial source of urban air pollution. The exhaust from spark ignition engines contains varying quantities of carbon monoxide (CO), organic compounds which are unburned or partially burned hydrocarbons (HC) and oxides of nitrogen (nitric oxide, NO and small quantities of nitrogen dioxide, NO_2, collectively referred to as NOx). The relative amounts of these emissions depends greatly on engine design and operating conditions. Figure 2.1 shows how each of these emissions vary with the most important operating parameter, air-fuel ratio. As an illustrative guide, Heywood (15) suggests emissions from a conventional petrol engine might be of the order: NOx, 500 to 1000 ppm; CO, 1 to 2 percent; and HC 3000 ppm (as C_1). For a natural gas engine, however, HC emissions are of less concern as methane is not considered a pollutant, it is unreactive and does not contribute to photochemical smog. Methane does however contributes to the 'greenhouse effect' resulting in global warming, and therefore emissions of methane should be minimised. CO emissions are only significant if operating close to, or on the rich side of the stoichiometric ratio. The most important emission from natural gas engines is that of NOx, which peaks to the slightly lean side

of stoichiometric.

As a comparison, Heywood (15) states that Diesel engine exhaust contains similar levels of NOx to those from spark ignition engines while hydrocarbon emissions, though still significant, are typically lower by about a factor of 5. However the hydrocarbon emissions from Diesel engines are more apparent as they may condense to form white smoke during start up from cold and certain hydrocarbon compounds in the exhaust are the source of Diesel odour. Diesel engines are also an important source of particulate emissions, primarily consisting of soot and heavier liquid hydrocarbons. Emissions of carbon monoxide are not significant as dissociation of CO2 to CO is reduced due to lower overall combustion temperatures.

Interest in measuring and controlling exhaust emissions from natural gas engines began in the early 1970s, largely as a result of the introduction of government regulation, such as the Clean Air Act of 1970 in the USA. It is the emission of NOx which is the most difficult to minimise as this is greatest at air-fuel ratios close to stoichiometric, where conventional gas engines are designed to operate for best thermal efficiency.

The formation of oxides of nitrogen during combustion is a result of the reactions involving nitrogen and oxygen molecules present within the combustion chamber. It is produced in the burned gases behind the flame front where the temperatures are greatest, rather than in the regions near the combustion chamber surfaces or in the unburned mixture.

The most likely chain reaction, known as the extended

Zeldovich mechanism (28), initiates the primary NO formation as follows:

$$N_2 + O \Rightarrow NO + N$$

$$N + O_2 \Rightarrow NO + O$$

$$N + OH \Rightarrow NO + H$$

NO formed in the flame zone can be rapidly converted to NO_2 and subsequently converted back to NO via reactions such as:

$$NO + HO_2 \Rightarrow NO_2 + OH$$

$$NO_2 + O \Rightarrow NO + O_2$$

These reactions are necessarily rate limited. That is, there are several factors affecting the rate at which the reaction can proceed. The reaction rates in either forward or reverse direction are temperature sensitive and are only significant at high temperatures (> 1500 C). As a result, NO formation occurs only between ignition and the point of rapid cooling caused by rapid expansion of the combustion gases. Peak concentrations are dependent, therefore, on maximum cycle temperature and the time duration available for the reactions. Rate constants for the NO formation mechanism are given in figure 2.2. These are values suggested by Heywood after a critical review of numerous published experimental studies.

The primary engine parameter affecting NOx formation is air-fuel ratio. Figure 2.1 illustrates how exhaust emissions vary with air-fuel ratio. The curve peaks at approximately 10 % leaner than stoichiometric. This is due to the combined effect of high peak temperatures and excess oxygen required for NOx formation. Leaner mixtures have a cooling effect and richer mixtures inhibit NOx formation due to the reduced concentration of the oxygen

reactant.

2.3 Reduction of NOx Emissions From Gas Engines

As governmental regulation of exhaust emissions from stationary gas engines become increasingly more stringent, methods of reducing exhaust emissions have become a necessary element in engine design. A number of options are available to the engine manufacturer that will allow exhaust emissions to meet the relevant legislation, each having associated advantages and disadvantages. Servé (28) and Heywood (15) both report on established methods of NOx reduction.

To some extent, exhaust emission levels can be reduced through adjustment of some of the external operating parameters. The effects of these adjustments on emissions and other critical performance data have long been established by engine manufacturers. For a natural gas engine, these consist of air-fuel ratio, ignition timing, charge air cooling and power deration.

Air-Fuel Ratio

Air-fuel ratio is the dominant parameter that affects emission levels of NOx. Figure 2.3 illustrates the effect of air-fuel ratio on the emission of NO and NO2, NO making up the bulk of NOx emissions. As the engine is run leaner, substantial reductions in NOx are achieved. The fuel consumption penalty is however significant for large NOx reductions and tends to increase exponentially. There are two effects occurring as the equivalence ratio is decreased. Firstly, the additional air provides a cooling effect on the charge resulting in lower cylinder

temperatures throughout the cycle. Secondly, it reduces combustion pressures and temperatures by reducing flame propagation speeds and therefore combustion rates. The net effect is to lower peak cycle temperature with a correspondingly lower NOx formation rate. However, there is obviously a limit to the extent to which the engine can be operated in the lean direction. This limit occurs when combustion becomes too unstable to allow continuous engine operation as cyclic stability, a measure of combustion variation cycle to cycle, has deteriorated to the point where it is unacceptable, with some cycles misfiring or partially burning. As a consequence, hydrocarbon emissions increase.

Charge Cooling

Gains in NOx reduction can be made by the use of charge air cooling. On average, a 25% reduction is realised for a 22 degree Centigrade reduction in air manifold temperature. The advantage of this method of reduction is the negligible effect on specific fuel consumption. A practical limit exists here, however, as most field installations cannot bring the manifold temperature closer than about 5 degrees C of ambient. A chiller could be added to the intercooler circuit, but there would obviously be a fuel penalty involved.

Ignition Timing

Ignition timing has a great effect on NOx emissions. Figure 2.4 shows the effect of retarding the ignition on different air-fuel ratios. In each case, the emissions of NOx are greatly reduced as the timing is retarded. The NOx reductions are, of course, due to the lower peak firing pressures (and therefore cycle temperatures). However, the penalty effects on specific fuel consumption are severe, and this also has the effect of

derating the engine significantly. NOx reduction is also possible by other methods of engine deration since by reducing bmep, combustion temperatures are also reduced, hence leading to reduced NOx production. Capital equipment costs are inversely proportional to the unloading so this is not considered an acceptable method of reduction by either engine manufacturers or users.

The present situation regarding methods of controlling NOx emissions is concisely summed up in a paper by Urban (36). Figure 2.5 refers to known methods of NOx reduction and their potential application to gas engines. Of the methods listed, only three are commercially available with major control potential: NSCR (nonselective catalytic reduction), lean burn combustion, and prestratified charge combustion. Another system with the potential for large scale application is SCR (selective catalytic reduction) which has had some limited field success, but is not at present commercially available.

Nonselective Catalytic Reduction

Nonselective catalytic reduction has been used for over 20 years to convert engine exhaust into a non-reactive gas for use in pressurising oil wells. Application of NSCR for the control of NOx emissions from stationary gas engines began in the late 1970's, but systems that functioned effectively in field use have not become available until recent years. NSCR requires that the engine must be operated on the rich side of stoichiometric so that a fuel rich exhaust may be passed over the precious metal catalyst. An exhaust oxygen sensor is used in an equivalence ratio (λ) controller to maintain λ in a narrow band slightly rich of stoichiometric. The catalyst generally has a platinum and

rhodium coating, although palladium may be used. Basically, NSCR is the stationary application of the automotive three way catalyst system. Problems associated with using NSCR systems include catalytic poisoning from the engine's lubricant and inadequate fuel control systems. The cost of installing such a system is also very high as a result of the precious metals used in the catalyst, and the sophisticated control systems required.

A new technique of fuel and combustion monitoring, presently being developed by Lucas Engineering could help to eliminate some of the control problems associated with catalytic reduction. The technique is based on the use of an in-cylinder optical probe to provide combustion feedback to a closed loop control system. A recent paper by Nutton (24) describes the technique in detail. The system is said to be well suited to volume production and gives a more comprehensive combustion measure than present lambda oxygen sensors. The optical probe can be used to obtain the ignition delay and burn duration, and these parameters could then be maintained according to a mapped schedule by control of fuel and ignition systems. Information on cyclic variability and knock may also be obtained. The probe is small in size and could be incorporated into the spark plug. Adoption of this probe could make the use of catalytic converters for NOx reduction more attractive. More accurate control of the engine's equivalence ratio to within the required narrow band would allow the catalytic converter to operate at maximum efficiency and increase the working life of the catalyst.

Lean-Burn Combustion

Lean-burn combustion, as mentioned earlier, allows for substantial decreases in NOx emissions by increasing the air-fuel

ratio in order to reduce combustion temperature. The effect of adding excess air to the mixture is to reduce flame temperature by increasing the heat capacity of the cylinder charge per unit mass of fuel. This also has the effect of reducing flame speeds. Therefore to burn lean mixtures in an engine requires some method to increase flame speeds and possibly ignition energy. This is generally achieved by one of two methods: a swirl generating combustion chamber creating swirl which breaks down near TDC to produce turbulence, or by use of a high energy torch ignition prechamber, the method investigated in this thesis. The extra cost to the engine manufacturer can be modest, especially if the swirl generating method, such as the "Nebula" combustion chamber (20) discussed later in this chapter, is adopted. The main problems associated with the torch ignition system concern reduced spark plug life in the hot environment of the prechamber, and the difficulty of maintaining accurate fuel control to the prechamber under varying operating parameters.

Prestratified Charge Combustion

Prestratified charge combustion (PSC), described by Urban (36), is an after sales modification that has been applied to four stroke natural gas engines under 1500 kW. In this system controlled amounts of air are introduced into the intake manifold of the engine in a prearranged sequence and quantity. This stratification provides a flame-cooling effect, resulting in reduced formation of NOx. PSC has been applied to engines in California to meet current NOx emission requirements, and Urban (36) states that reductions of up to 90% have been reported without significant deterioration of fuel economy. Because PSC is a relatively simple system the costs of installation are relatively low. The main limitation is that this system can only

be applied to turbocharged gas engines, and not all engines will be readily adaptable to accommodate the increased air intake capacity that is required. A disadvantage of this system is the resulting reduction of maximum engine power.

Systems which have the potential for NOx reduction, but are not yet in wide commercial use include selective catalytic reduction (SCR) and exhaust gas recirculation (EGR). There are also some new chemical and electrochemical techiques undergoing initial evaluation.

Selective Catalytic Reduction

Selective catalytic reduction, again described by Urban (36), is applicable to engines running lean of stoichiometric hence containing significant quantities of oxygen in their exhausts. With this system, ammonia gas is injected into the exhaust prior to being passed over a metal catalyst. A number of base metal oxides are used in the catalyst, and the efficiency of NOx conversion is dependent on the exhaust gas temperature. In current SCR systems, a NOx analyser is used to measure the concentration of NOx in the exhaust, and from this ammonia is injected at the rate necessary to maintain maximum NOx conversion efficiency in the catalyst. This NOx analyser is a costly but necessary complication as the injection of excess ammonia will result in ammonia passing through the catalyst and being discharged to the atmosphere, while insufficient ammonia will result in low catalytic efficiency. Results from using this system have shown that NOx reductions of 80% can be achieved. Difficulties in operating this method of NOx reduction include fouling of the catalyst, and maintenance of catalyst temperature in the narrow band between 300 and 450 degrees C.

Exhaust Gas Recirculation

Recirculation of exhaust gases into the engine cylinder will have the effect of decreasing NOx emissions in two ways. The addition of exhaust gas diluent containing CO2 and H2O will increase the specific heat capacity of cylinder charge per unit mass of fuel. This will reduce flame temperatures and consequently reduce NOx formation rates. A secondary effect of recirculating exhaust gas is to reduce the quantity of excess oxygen passing through the engine, causing NOx formation to be more difficult. Figure 2.6 shows a typical response of NO emissions from a spark ignition engine to increasing exhaust gas recirculation (EGR).

Figure 2.7 (a) compares the effect of exhaust gas diluent on NO emissions with various other diluents. If the same data is plotted against diluent heat capacity (diluent mass flow rate × specific heat capacity) it collapses to the single curve shown in figure 2.7 (b). This demonstrates that it is the effect of the higher specific heat capacity of the exhaust gas which is the dominant factor in NO reduction.

Exhaust gas recirculation has been used by automotive manufacturers for over ten years and some testing has been done on stationary gas engines. Nominal reduction in NOx, while maintaining acceptable engine performance is limited to about 50% unless modifications to the combustion chamber are made. Disadvantages of this method are that maximum engine power is derated, engine life is reduced, and fuel consumption is increased.

Cyanuric Acid Reduction

Recently researched and reported by Caton (3), is a method of NOx removal that uses cyanuric acid as a reducing agent. At exhaust temperatures above 400 degrees C, the cyanuric acid breaks down to form free radicals which react with, and hence break down the NOx compounds. There appear to be a number of problems associated with this method of NOx reduction. The products of this reduction process can react with free radicals to form harmful compounds such as nitrous oxide and ammonia, or the cyanuric acid may pass through the exhaust unreacted, which is itself highly toxic. Any application of this method would therefore require considerable further development. Some experimental work using this technique has been done recently on a Diesel engine (3). Results have shown that NOx reductions of up to 98% are possible. Temperature of the exhaust reactor was found to be a critical parameter, and the system was most effective when the NOx levels in the exhaust were high.

Electrochemical Reduction

Also currently under evaluation is a method of electrochemical NOx reduction. This system uses an electrochemical reactor containing a solid electrolyte made from a high surface area ceramic ion such as zirconia or bismuth oxide. Electrochemical reduction of NO takes place in the region around the cathode electrode, yielding nitrogen and oxide ions. These oxide ions then dissolve into the solid electrode, and an equivalent number of oxygen ions are released as oxygen gas in the region of the anode . This method has been shown to work in the laboratory on gases containing no oxygen and engine applications have yet to be fully researched.

2.4 Prechamber gas engine development

In 1956, Thompson, Beadle and Blake (34) working for engine manufacturers Fairbanks Morse, initiated the development of the "jet ignition" gas engine to improve engine performance. Based on their successful dual fuel engines, the object was to reduce operating costs by eliminating the need for a pilot oil supply to provide the energy to ignite the gas/air mixture. Although, when operating a dual fuel engine, the quantity of oil required to ignite the main charge of natural gas constitutes only a few percent by mass, the cost at full load was quite a substantial proportion of the total operating cost.

Initial development work was carried out on a divorced cylinder of a large bore, normally aspirated, opposed piston dual fuel engine. This consisted of replacing the oil injection nozzle of this cylinder with a spark plug together with the necessary electrical system to produce a timed spark. Exploratory tests indicated that combustion was limited to a narrow operating band of manifold pressures, and hence air fuel ratios, outside of which detonation or misfire would occur (Exact values for these air fuel ratios were not given). Hence it was realised that there was a need for a new high energy ignition system, not as a means to reduce exhaust emissions, but merely to enable stable and safe operation of the engine over a wide range of loads and air-fuel ratios as an alternative to a complex and costly mechanical engine management system. If misfire occurred on a large natural gas engine, large quantities of unburnt hydrocarbons could enter the exhaust system and be potentially explosive. As a solution, a stratified charge jet or torch ignition system was developed to provide sufficient energy to ignite the charge in the main chamber

in the same way that the Diesel pilot fuel had with the dual fuel system.

The idea was to use a separate auxiliary combustion chamber, or prechamber, to surround the spark with a small quantity of enriched charge which could be readily ignited. The energy released from combustion of this localised charge was many times greater than that produced from the spark alone. The actual prechamber arrangement is given in figure 2.8.

The prechamber was fed by a separate supply of neat gas at constant pressure through a one way check valve. This allowed gas flow to the prechamber during exhaust and intake strokes, and in doing so, purging the prechamber of residuals remaining from the previous cycle. The gas was then leaned down to an ignitable mixture, ideally close to stoichiometric, during the compression stroke before being ignited by a spark. Once the stratified charge had been ignited, a high velocity jet of flame then propagated through a connecting orifice to the main chamber, thus readily igniting the leaner mixture. Figure 2.9 gives the firing range for air receiver or manifold pressures. The air receiver pressure was increased as a means of leaning the main combustion chamber air-fuel ratio. The dotted curve indicates the limit of stable combustion for a conventional open chamber gas engine. The results show that by use of jet ignition, the stable firing range can be increased so that the engine could be run from zero to full load with a fixed air manifold pressure of 127 mm Hg (5 in Hg).

This is basically the system being developed by Dorman Diesels with the SE series of gas engines and also by a number of other manufacturers of gas engines. The main difference is that

current development is centered around exploiting this system to reduce toxic exhaust emissions and improve engine performance. Some of the companies to have pursued the prechamber concept, apart from Dorman Diesels, include the American companies Waukesha, a subsidiary of Dresser Industries, Caterpillar and Superior Engines, a subsidiary of Cooper Industries.

Mayer of Waukesha (22) began prechamber gas engine development in 1982 by modifying their VHP model with a similar arrangement to the Dorman SE1 system, as can be seen in figure 2.10. Details of the fuel system are given in figure 2.11. By 1984 they had succeeded in putting an engine on field trial that was able to meet all legislated emissions. These included emission levels of 1.5 g/kWh (2g/bhph) for NOx and CO and 1 g/kWh (1.3g/bhph) unburnt hydrocarbons. Apart from reduced emissions, fuel economy was claimed to be improved by the order of 8 to 10 % over conventional open chamber engines at the time. With engines operating at compression ratios between 10:1 and 10.5:1 and with air-fuel ratios as lean as 29:1 the required low NOx emission levels were achieved. Their first prechamber gas engine to be commissioned was in 1984 at Red Oak, Oklahoma, a six cylinder unit driving a gas compressor. Since then, development has moved on to conversion of their recently introduced AT series of engines (4). Based on the Sulzer AT model, it incorporates modern design features such as four valves per cylinder, in common with most other engine manufacturers including Dorman Diesels.

Wadman (38), of Cooper Industries began prechamber gas engine development in 1981, and by 1985, 180 engines were in service. They found that by using a prechamber, as shown in figure 2.12,

and very lean air-fuel ratios, NOx emissions were reduced by 90 %, and smoother, stable combustion was achieved when compared with open chamber variants. Fuel consumption was also claimed to be reduced as well as improving knock margins. Some of the problems encountered with the prechamber system included reduced spark plug life and the need for an electronic engine management system. Spark plug life could, however, be greatly improved if the prechamber area received better cooling. To achieve accurate control of critical engine parameters, which was necessary if the required engine performance and emission levels were to be met, a pneumatic control system was designed. This was needed to hold a steady lean air-fuel ratio in the main chamber by controlling boosted air pressure in a closed loop that included crankshaft speed, boost and manifold pressures. Manual adjustments had to be made for fuel composition and gas temperature as well as for ambient conditions. Their engines did not use a carburettor as such, but simply introduced the gas into the inlet port with an obtruding vane to aid mixing. On site tests showed NOx emission levels down as low as 1 g/kWh.

Work by Snyder, Wright and Dexter (30) looked in more detail at the combustion processes that occur in a prechamber gas engine using high speed photography. The experiments were performed on a constant volume combustion rig that simulates the combustion processes. The rig itself, shown in figure 2.13, consisted of a 216 mm bore Ricardo engine fitted with quartz windows in both the prechamber and main combustion chamber, designed so that prechamber geometry could be easily modified. To simulate engine processes, a valve was used which could be closed to separate the two chambers during the charging process, and then opened to allow a prechamber gas inflow, similar to that which occurs during the

engine compression stroke. Extra oxygen was also added to increase the heat release rate to that of a real engine. Their results showed flame propagation from the prechamber for various key parameters such as prechamber volume, throat area and number of communicating orifices. Results from the photography showed that having several angled throats gave better penetration of the main chamber and a faster combustion rate than if just one was used. Peak pressure in the prechamber is also increased. It seemed that actual size of the prechamber had very little effect on main chamber combustion. It was noticed, however, that cycle to cycle variation of combustion was quite large. This was believed to be due to fluctuations in turbulence at the spark plug gap at the time of ignition. It should however be noted that their test rig obviously did not have all the variables present in a real engine, and so turbulence by itself may not be the most significant cause. Mixing on a very small scale may be a more significant factor.

The effect of torch jet direction from the prechamber into the main chamber on combustion performance has also been investigated by Ryu, Chitsu and Asanuma (26). The effects of torch nozzle direction, dimensions and prechamber volume on combustion characteristics and engine performance were examined experimentally on a gasoline engine. The conclusions that were drawn from their results were as follows. Spark ignition engines using a prechamber torch ignition system are capable of more rapid combustion than a conventional open chamber. With a vertical prechamber nozzle combustion is more rapid resulting in a steeper heat release rate than with other torch directions due to violent turbulence caused by the torch jet impingement vertically onto the piston head. It was concluded, therefore, that an engine with a

vertical prechamber nozzle will have a superior bmep and bsfc than with other arrangements, but emissions of NOx will be greater due to increased peak cylinder temperatures if air-fuel ratio is not increased.

2.5 Ignition Requirements for Lean Burn Gas Engines

Ignition requirements for lean burn gas engines are much greater than for conventional stoichiometric engines as mixture flamability limits are aproached. The energy produced from a spark alone may be insufficient to reliably ignite these lean mixtures. A prechamber igniter used instead can deliver greater ignition energy to the lean charge. Comparisons can be made between the effective ignition energy produced by a prechamber igniter and that of the spark it replaces. Heywood (15) desribes in detail the process of spark ignition. Three distinct stages may occur during the spark. The first stage is referred to as the breakdown stage, having extremely short duration, during which ionizing streamers pass from one electrode to the other, creating a conductive path and reducing the impedence of the gap. In the second stage, the arc phase, the initial plasma expands due to heat conduction and diffusion and the exothermic reactions begin which lead to flame propagation. This may be followed by a final glow discharge phase, depending on the design of the ignition system, in which the ignition system will discharge the remainder of it's energy into the ignition circuit.

During the arc stage, the cylindrical arc plasma increases in size as a result of heat conduction and mass diffusion to approximately 2mm diameter. As a result of these energy transfers, gas temperatures within the arc are limited to about

6000 K. During the initial breakdown stage, almost all the electrical energy is transmitted to the plasma, although the total energy supplied is very small. Less than 50 % of the total electrical energy is transferred to the plasma during the arc and glow discharge phases, the remainder is lost as heat transfer to the electrodes. The total energy transferred to the gas during these later stages is greatest, however, as a result of the long discharge times.

Heywood (15) suggests that to ignite a quiescent stoichiometric fuel air mixture at normal engine conditions requires approximately 0.2 mJ of spark energy. For leaner mixtures or where there is flow past the electrodes, a much greater magnitude of energy would be required ($\geq$ 3mJ). Conventional ignition systems deliver approximately 30 to 50 mJ of energy to the spark, but for reasons discussed above, only a fraction of this energy is transmitted to the gas mixture. There are practical reasons limiting the quantity of electrical energy that can be discharged in a spark. If the current is increased during the arc and glow discharge phases, energy losses will increase and heavy electrode erosion will result. Also, increase of ignition current will increase discharge time, which may not be acceptable at high engine speeds.

In comparison, the quantity of energy released by combustion of the fuel mixture within the prechamber is substantially greater. If we consider a prechamber of 10 cc volume being supplied with a fuel air mixture, the energy released would be in the order of 200 to 600 J. Less than 50% of this total energy will be transmitted to the main chamber as ignition energy via turbulent flame jets, the remainder lost by heat transfer to the

coolant. These flame jets which penetrate into the main combustion chamber will have substantially greater surface area than a spark, and ignite lean mixtures in a more repeatable manner. Temperatures within the flame front are of the order of 1600 to 2500 C. The ignition temperature of natural gas is approximately 650 C. The number and size of orifices connecting the prechamber to the main chamber will have a significant effect on flame propagation. Larger prechamber volumes and orifice areas result in slower jet velocities and hence in slower burning of the main chamber mixture. Increasing the number of connecting orifices will significantly reduce flame propagation times by reducing the average distance each flame front has to travel. For example, for one orifice the average distance the flame front would have to travel is 0.5 D, where D is the cylinder bore. However if four orifices are used, angled towards the cylinder walls, the average distance the flame front has to travel would be reduced to about 0.2 D, a reduction of 60%, thereby increasing overall burning rates.

2.6 Control Systems for Prechamber Gas Engines

For the prechamber gas engine concept to work effectively, accurate control of the air-fuel ratio delivered to the combustion chambers is essential. This usually requires the use of a closed loop air-fuel ratio control system that uses feedback from an air-fuel ratio sensing device to make corrections. A carburettor or a gas mixer alone is inadequate as this is merely a volume flow device and hence insensitive to fuel heating value, fuel and air temperatures or ambient pressure.

Eckard and Servé (11) have examined various ways of

achieving this control, in particular, methods of measuring the air-fuel ratio reliably. Initially a pneumatic controller was tried which adjusted air manifold pressure based on gas pressure and engine speed. This proved relatively successful, but was limited by the fact that it could not compensate for fuel heating value changes and required external adjustments to air and gas manifold pressures. Direct measurement of the oxygen content of the exhaust was considered as a potential control variable, but eventually it was determined that measurement of turbine inlet temperature was preferable. A thermocouple based controller using preturbine temperature was found to be a cheaper and less complex solution, providing equivalent or superior control. The relationship between air-fuel ratio and pre-turbine temperature is close to linear if other operating parameters such as ignition timing remain constant. Corrections are then made for fuel calorific value and ambient temperature.

2.7 Advances in Open Chamber Gas Engines

Several engine manufacturers have produced lean burn gas engines which do not use prechambers. These open chamber engines produce high levels of turbulence to increase flame speeds. Caterpillar first launched the 3500 range of lean burn open chamber gas engines in 1986. The 3500 series engine is a lean burn gas engine designed to operate above peak NOx air fuel ratios.

Wilson (39) reports that to operate satisfactorily in the lean burn operating range, between misfire and detonation limits, turbulence levels were increased. The 3500 series engines use high squish combustion chambers to increase turbulence and achieve

a fast burn. The excess air ratio λ is increased to 1.5, compared to 1.1 for the standard 3400 series engine. To eliminate temperature as a variable, the aftercooler was mounted upstream of the gas mixer so that intake temperature is maintained constant regardless of engine load. NOx emissions of 2.7 g/kWh (2 g/bhph) have been achieved with these engines.

Work has also been carried out by Macari (21) of Caterpillar on adapting a 3516 gas engine to run on low calorific value fuel such as 49 kJ/m³ digester gas (Compared to 89 kJ/m³ for natural gas), the composition of which consists of approximately 60 % methane and 40 % carbon dioxide. This engine used the Impco "vari-fuel" gas mixer which incorporates stepper motor controlled gas valves in order that orifice size and metering valve contour could be determined. Emissions of NOx were reported to be in the range of 2 to 4 g/kWh. Efforts were made to extend misfire limits and tests showed that both increasing gas supply pressure and advancing ignition timing improved these.

Recent work has been reported by Kingston, Jones and Heaton (20) on a new combustion chamber design that allows stable combustion of mixtures with air-fuel ratios as lean as 26.5:1 without the need for a prechamber. The new combustion chamber is based on the conversion of a swirling direct injection diesel engine and has been named the "Nebula" combustion chamber. Swirl by itself has not been found to be helpful in achieving regular ignition and fast burn in lean mixtures, however turbulence, and mixture homogeneity together with effective scavenging of the spark plug region have been found to be important factors.

The principle of the Nebula combustion chamber is to provide

optimum conditions for ignition and fast burn by destroying swirl and converting it into turbulence at the time of ignition. This is achieved by constraining the swirl in the piston bowl to form colliding air flows which interact, as shown in figure 2.14, creating intense turbulence and a fast burn capability.

Results obtained so far have been very promising, and have shown that even the most stringent Swiss and West German NOx limits could be met with good brake thermal efficiency using this design of chamber. Loads up to 12 bar bmep have also been obtained without knock, while brake thermal efficiencies of just under 40 % have been recorded.

2.8 Applications For Lean Burn Gas Engines

Lean burn gas engines have a wide range of applications. Apart from the more traditional uses, previously discussed, some more recent applications are discussed here.

Research has been carried out by Vinyard (37) at the Southwest Research Institute into alternative applications of lean burn gas engines. This included the possibility of fitting them into commercial vehicles and combined heat and power (CHP) as a means of meeting proposed standards for reduced emission levels. Lean burn natural gas engines have the potential to meet these standards for applications such as city buses or local delivery vans. Safety should not prove a problem as high pressure gas fuel tanks can be made at least as safe as petrol or diesel fuel tanks. Compressed natural gas (CNG) is already commonly used in Canada and New Zealand.

Combined heat and power, when two or more types of useful energy are produced concurrently, is an attractive application for a gas engine. Such a system may include an engine driving a generator set to produce electricity, while waste heat energy is used to provide hot water for space or process heating. These systems offer increased fuel efficiency and have been used for many years in large installations such as hospitals. High maintenance and short working life have proved to be the greatest obstacles for application on a smaller scale. However, recent work has shown that both of these problems can be ameliorated. Valve seat wear is a particular durability problem which for a gas engine can be five to ten times greater than on a leaded petrol engine. This is due to the relative sliding movement between the valve and the seat as the exhaust valve closes. Whereas lead deposits from petrol act as a lubricant between the two surfaces, in a gas engine, metal to metal contact occurs resulting in far greater seat wear. This wear can however, be reduced if a lubricous oxide is provided on the surfaces.

2.9 High Speed Hydrocarbon Measurement

In 1988 Collings (9) reported on a new technique for resolving in-cycle hydrocarbon concentration in a running engine. There has previously been very little literature on real time hydrocarbon measurement during the engine cycle. Some work on laser spectroscopy has been done, but this requires substantial modification to the engine.

Measurements were made using a novel high frequency flame ionisation detector from within the spark plug gap to investigate the correlation of local mixture strength at ignition with

subsequent pressure development. The method described allows the mixture strength to be measured directly at any suitable sampling point in a relatively unmodified engine.

The engine used in the tests was a Ricardo E6 research engine running with a compression ratio of 8:1 and at a fixed speed of 900 rev/min. A fixed choke carburettor operating at wide open throttle provided petrol air mixture.

The high speed FID, is similar to a conventional FID, and operates on the same principle, but the sample transfer system has been modified to improve the frequency response. Referring to figure 2.15, this had been achieved by using a very short sample tube which issues directly into the FID flame, rather than being premixed with the hydrogen supply as is the case with a conventional FID. When used to sample at atmospheric pressure, the FID chamber was operated at sub-atmospheric pressure in order to draw the sample in. Therefore the sample flow could not be controlled as accurately as in a conventional FID system, but for this real time application, the emphasis was on comparative rather than absolute values, so this was not considered important. The sampling system used by Collings (9) had a sample tube (which had an inside diameter of 0.12 mm and a length of 45mm) which passed through the spark plug centre electrode. The very small diameter of the sample tube was required in order that the sample flow did not interfere with the ignition process, and also to attempt to produce laminar flow in the sample tube, as this reduces mixing of the sample and hence reduces the time constant.

Behaviour of the sampling system under steady state conditions had been investigated by pressurising the spark plug

head with a mixture of 1.1% propane in air with varying levels of FID vacuum. Results of these tests are given in figure 2.16, after being scaled to have a common starting point at atmospheric supply pressure so that the system gain effects, due to the various vacuum levels, are eliminated. It was clearly seen that the supply pressure was significantly affecting the FID signal, and this was greatest at the lower level of FID vacuum. An intermediate vacuum of 15 mm Hg was however used, as the larger vacuum caused FID flame instability problems due to the larger sample flows into the flame. The sample flows in each section of the sampling system were estimated at the time of ignition, assuming laminar flow, in order to determine the theoretical time constant for the system. The total time constant was estimated to be 6 ms, and this value agreed well with the experimentally observed value. By increasing the sample flow rate and reducing sample tube lengths, it was believed that this time constant could be greatly reduced.

Some attempt to determine the frequency response experimentally, which was noted to be dependent on sample pressure, had also been made. This consisted of oscillating a jet of hydrocarbon gas across the sample tube end. The oscillations were increased in frequency until no further increase in response time was observed, and at this point, the time constant for the system was found. The results from this experiment, figure 2.17, show that the time constant for these particular conditions is about 1 ms.

Transit time, the time taken for the sample to travel from the sampling point to the FID flame is also identified as being a function of sample pressure. Collings (9), considered that the

sample tubes be kept as short as possible in order that the sample of interest is able to reach the FID and be measured before there is any significant pressure rise due to combustion. In this way the observed signal should be independent of the subsequent pressure development.

Results by Collings (9) for consecutive fired and misfired cycles are given in figures 2.18. The signals have not been corrected for transit time. The FID signal is shown to be zero for much of the induction stroke, and it was believed that this was as a result of the low cylinder pressure causing low velocities in the sample pipes. Hence a significant period of time was required before the air in the sample system would have been purged, and sample gas from the cylinder would have reached the FID. Between the two phases there is a transition period when the diffusion process in the cross flow direction in the sample pipes actually takes a finite time before the air is totally eliminated from the sample gas. The later part of the hydrocarbon signal during compression and firing strokes was believed to characterise the actual cylinder gas. The time delay between the time of ignition and the falling off of the signal was seen to be approximately 7 ms, and this correlates well with the earlier theoretical estimate for transit time under these conditions. Figure 2.19 shows an HC trace for two fired cycles with a higher amplifier gain setting. Occasional "blips" were now seen to occur in the signal. A possible explanation was that these were the result of crevice hydrocarbons being convected across the spark gap.

Similar work was continued by Sleightholme (29) also using the Cambustion high speed FID. Work was done to investigate

mixture inhomogeneity in a spark ignition engine. Propane and air were used as fuel for the engine, either completely premixed during a control experiment, or in varying degrees of homogeneity, including injection into the manifold to simulate petrol fuel injection. The Ricardo E6 research engine was again used, and the objective had been to investigate the effects of charge inhomogeneity on cyclic variability.

The same fast response FID system was used, except that the sample was taken from the cylinder via a special sample plug which screwed into a spare spark plug hole, instead of going through the spark plug itself. The sample plug is shown in figure 2.20. It consists of a 0.15 mm sample tube leading from the cylinder into a surge chamber of greater volume. This was achieved by using hypodermic needles of increasing size. This surge, or constant pressure chamber, was kept at a constant pressure of 200 mm hg vacuum during the tests in order that there was always a pressure drop across the sample tube, and hence sample flow to the surge chamber, as cylinder pressure is near atmospheric during the intake and exhaust strokes. At the point where the sample tube enters the surge chamber, a tube was placed that carries the FID head. This sample flow to the FID must be kept constant if HC concentration only, and not quantity, was to be measured. This was achieved by maintaining a constant vacuum in the FID chamber 100 mm hg below that of the surge chamber. The surge chamber is used to accommodate the fluctuations in sample flow entering the sample plug, generated by the greatly varying cylinder pressures.

Propane was used as the fuel, as it avoided fouling of the spark plug and sampling system. Engine tests were performed at 1000 rpm and at wide open throttle with an excess air ratio λ of

1.3. Response of the FID was found to be linear to mixture strength and independent of cylinder pressure. This was found by changing engine compression ratio, and mixture strength as shown in figures 2.21 and 2.22. A diagram showing the various injection positions and the location of the sampling plug are given in figure 2.23.

Results of in-cylinder measurements using the FID for these injection positions with an engine speed of 1800 rpm are shown in figures 2.24 for both fired and motored cycles. They show that the charge is inhomogeneous as it enters the cylinder for each of the injection positions. However, reduction in the inhomogeneity appears to take place in the cylinder to the extent that at the time of ignition a well mixed charge has been formed. Cyclic variations of both the incoming charge and the in cylinder mixing appear to be shown. Variations in the time at which the FID signal falls away as the flame reaches the sampling plug could indicate that either flame speeds or flow patterns may be changing.

It was observed that for well mixed charges there was a linear relationship between cyclic variability of combustion and cycle to cycle variations in mixture strength. However the effect of charge inhomogeneity on cyclic variability is unclear due to the overriding effect of cyclic variability of mixture strength.

Heywood (16) also reports on the use of the Cambustion fast-response FID for in-cylinder measurement of hydrocarbon concentration throughout the engine cycle. The work was performed on a Ricardo Hydra MK 2 single cylinder, two valve, naturally aspirated spark ignition engine running on a premixed propane/air

mixture. The sampling system consisted of the Cambustion HFR 200 sampling head, the details of which have been previously described. Referring to figure 2.25, the contents of the cylinder were sampled via a hypodermic type transfer tube of 0.2 mm diameter. The sample mass flow rate along this transfer tube fluctuates greatly with respect to time. The pressure at the end of the transfer tube therefore also fluctuates greatly. Heywood (16) had used a system which isolated these pressure changes from the sample head. Referring again to figure 2.25, this had been achieved by first expanding the flow from tube A into an expansion tube B, and then to the constant pressure chamber (ballast chamber) D. The sample flow to the FID was taken by the connecting tube C at the exit of the expansion tube B, where the pressure is the same as that within the constant pressure chamber.

Heywood (16) had found that to avoid back flow from the constant pressure chamber to the FID at times during the intake stroke and at low loads, it had been necessary to maintain a pressure within the constant pressure chamber below that of the lowest cylinder pressure by use of a high capacity vacuum pump. During engine tests, this pressure had varied between 0.4 bar and 0.67 bar depending on engine load. The sample flow at high loads being greater, and consequently, due to the finite capacity of the vacuum pump, smaller vacuums were achieved. However, fortunately, at higher engine loads the lowest cylinder pressures were greater so the reduced vacuum had been sufficient.

When operating the sampling system, Heywood (16) had found it necessary to install a water trap in the exhaust line of the FID so that condensed water did not block the vacuum line. This

condensate was produced as a result of burning the hydrogen fuel and the water vapour present in the sample. Calibration of the sampling system had been performed during bench tests by sampling mixtures of known concentration from a pressurized vessel, as well as in-cylinder sampling of a homogeneous mixture of propane and air during motoring of the engine.

During engine tests by Heywood (16), the sample inlet was located in the ground shell of the spark plug as shown in figure 2.26. Also shown in figure 2.26 is a typical pressure trace, and several typical FID signal traces, converted to propane concentration, for both firing and motoring engine cycles. The motored trace shows the sampling system to be independent of the fluctuating cylinder pressure, and the measured concentration corresponds well with the metered intake propane concentration.

In analysing the FID signal from the fired engine, allowance for the finite transit time for the sample to reach the FID from the sampling inlet had been made by Heywood (16). This transit time, a function of cylinder pressure, had been estimated by using a theoretical flow model developed by Collings (9). This transit time was found to be quite small after TDC when the cylinder pressure was high . (Typically less than 5 degrees CA)

Referring to the results by Heywood (16) in figure 2.26 showing the FID signal from the fired engine, the gradual rise in the signal was believed by Heywood to be showing the mixing of fresh charge with the burned residuals in the cylinder and transfer tube during the early part of the engine cycle. The dip in the signal at around 50 deg btdc was believed to be an anomalous aerodynamic effect in the sampling system due to the

sonic transition at the exit of the transfer tube while the high frequency noise at 20 degrees btdc was thought to be due to ignition system interference.

Heywood suggests that meaningful interpretation of the FID signal can not be made until the signal had reached a plateau value, as seen in figure 2.26, due to the finite response time of the system. The sharp fall of the signal to zero indicated the flame arrival at the sampling inlet, after which only residuals were sampled. Because the time for the flame to traverse the sampling inlet was small (approx 50 μs), the rate of fall was a useful measure of the response time of the instrument. Referring to figure 2.26, the molar residual gas fraction is equal to the ratio of (a/b) , where (b) is the motored HC level, and (a) is the fired HC level.

At high engine speeds and low load, the fired FID hydrocarbon signal, when firing, did not reach a plateau value before the arrival of the flame front due to the increased time constant, as shown in figure 2.27, unless there was a slow burning cycle. To obtain a signal which had a definite plateau region, a technique of skip firing one out of every ten cycles had been used. The FID signal was then used to determine HC concentration.

Heywood (16) also reported on the use of the FID to investigate decay and fluctuation of the residual gas fraction. The decay time was measured as a function of the number of engine cycles after the ignition system was switched off. A baseline case was carried out by artificially introducing residual gas into the uniformly mixed intake and firing the engine only after the in-cylinder residual gas of the previous fired cycle had been

flushed out by a number of motored cycles. It was shown that at low load, a significant number of cycles are required to scavenge the cylinder of residual gas. The effects of intake pressure and valve overlap on decay time were investigated.

Collings and Hands (10) report use of the Cambustion HFR 300 high speed hydrocarbon analyser to investigate the effects of misfire across a three way catalyst. The HFR 300 model used for this work, Cambustion's latest analyser, is of the same basic design as the previous HFR 100 and 200 series analysers. Two sampling heads were used, positioned before and after the catalytic converter. Dimensions of the sampling tubes and set up of the constant pressure system were not given. Before each test had commenced, the two sampling heads had been calibrated by flooding the exhaust system with a propane span gas of similar concentration to that expected. Misfire was introduced into one of the cylinders by reducing the fuel injected to it by half. The technique proved successful, and showed the complex way in which the catalyst responds to a misfire.

2.10 Prechamber Modelling Using Computational Fluid Dynamics

Moore (23) reports on his research at Bath University, in which he used a CFD program, PHOENICS to model the flow and mixing of gas and air in the prechamber of the SE1 engine. Initially a 2 dimensional piston and prechamber model was used, mainly for familiarisation, but the mesh was necessarily coarse and required a great deal of computing time to run. A subsequent 3 dimensional model consisting of the prechamber alone was adopted which allowed the prechamber geometry to be modelled in greater detail and with a finer mesh, and with reduced computer time. The mesh is shown

in figure 2.28. The version of PHOENICS which had been used for this work was a relatively early one and did not incorporate a body-fitted mesh. The effects of turbulence had been incorporated using the energy dissipation model, K-ε. A brief study was undertaken to determine the influence of the turbulence parameters at the nozzle boundary on the mixing process within the prechamber. Two cases had been considered, in the first, the values of K and ε had been set constant at the start of each time step. In the second case the turbulence parameters had been interpolated at each time step using values taken from the nozzle region of the earlier piston and prechamber model. The resulting fields of both turbulence energy and afr were found to be identical for the two cases.

Results by Moore (23) are shown in figures 2.29 and 2.30. Figure 2.29 shows velocity field vectors at a number of points during induction and compression strokes. Figure 2.30 shows contours of air/fuel ratio (afr) at 96 deg and 12 deg btdc for two cases of pilot charge, pure gas and an afr of 2.3:1. The former case resulted in an overall afr at the time of ignition (12 deg btdc) of 6.1:1 and the second case resulted in an overall afr of 14.5:1 at this point.

Work reported by Johns (19), also describes the application of CFD to the flow and mixing in a prechamber natural gas engine. The modelling was done for an engine for which experimental performance data was available. The study concentrated on operation of the engine near the lean limit of main chamber mixture strength, typically in the afr range 27:1 to 36:1. Both the prechamber and main chamber were modelled using a boundary fitted mesh, shown in figure 2.31. Calculations were made for

meshes containing 257, 774 and 1504 cells. The results presented were for the finest mesh and were considered to be both mesh density and time step independent. The size of the time step is not given. Only the compression stroke was modelled, and therefore, as the gas admission valve was excluded, an axisymmetric model was sufficient. Turbulence was incorporated via the energy-dissipation model.

Results by Johns (19) are shown as a series of plots in figure 2.32. Velocity fields and afr distribution are shown in 10 deg steps from 30 deg btdc to tdc for a main chamber afr of 32:1. The spark plug electrode is seen at the top of each plot. This series of plots show the strong jet from the main chamber impinging on the upper surface of the prechamber and producing regions of recirculating flow along the prechamber wall. By tdc the jet has diminished and a significant amount of radial diffusion has occurred causing spatial mixing. Variation in afr at the spark plug is shown clearly in figure 2.33 for three main chamber air-fuel ratios. Increasing main chamber afr was seen to have the effect of increasing the prechamber afr by a constant amount throughout the compression stroke. The richening of the mixture just before tdc was believed to result from the turbulent transport of the fuel after termination of the jet.

Comparisons were made by Johns (19) with phenomena observed during operation of the engine. It was found that for a particular main chamber afr, if the ignition timing was progressively retarded, a point would be reached when misfire occurred and stable operation of the engine was no longer possible. The onset of misfire was attributed to the prechamber charge being too lean to ignite, even when a pure gas pilot was

supplied to the prechamber. This is likely to be as a result of the connecting throat between the prechamber and main chamber being too large for the size of prechamber. The ratio of prechamber volume to throat area is 39:1. In comparison, the Dorman engine, which runs rich with a pure gas pilot has a ratio of 51:1. Comparisons between misfire limits determined by computation and experiment agreed favourably and are shown in figure 2.34.

Summary

A review of literature relating to exhaust emissions from gas engines, prechamber gas engine developement, in-cylinder hydrocarbon sampling and computational prechamber studies, has been made.

The parameters effecting exhaust emissions from gas engines, particularly of NOx and methods of their reduction have been discussed. Lean burn combustion is shown to be an effective method of reducing NOx emissions

Published work concerned with the design and control of prechamber gas engines has been reviewed. The important parameters and difficulties of this system have been identified.

A critical review of work relating to the application of a novel fast response FID to in-cylinder measurement of mixture strength has been made.

Results by other workers from prechamber modelling using computational fluid dynamics (CFD) has been discussed.

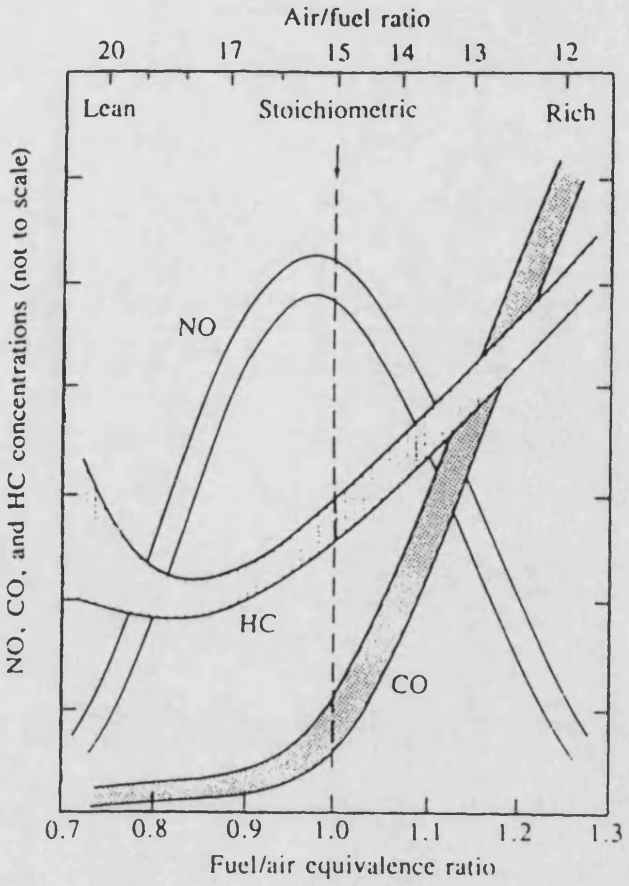

Figure 2.1 Effect of Fuel-Air Equivalence Ratio on Exhaust Emissions of NO, CO and HC for a Spark Ignition Engine

Reaction	Rate constant, $cm^3/mol \cdot s$	Temperature range, K	Uncertainty, factor of or %
(1) $O + N_2 \rightarrow NO + N$	$7.6 \times 10^{13} \exp[-38{,}000/T]$	2000–5000	2
(−1) $N + NO \rightarrow N_2 + O$	1.6×10^{13}	300–5000	±20% at 300 K 2 at 2000–5000 K
(2) $N + O_2 \rightarrow NO + O$	$6.4 \times 10^{9}\ T \exp[-3150/T]$	300–3000	±30% 300–1500 K 2 at 3000 K
(−2) $O + NO \rightarrow O_2 + N$	$1.5 \times 10^{9}\ T \exp[-19{,}500/T]$	1000–3000	±30% at 1000 K 2 at 3000 K
(3) $N + OH \rightarrow NO + H$	4.1×10^{13}	300–2500	±80%
(−3) $H + NO \rightarrow OH + N$	$2.0 \times 10^{14} \exp[-23{,}650/T]$	2200–4500	2

Figure 2.2 Recommended Forward and Reverse Rate Constants for NO Formation

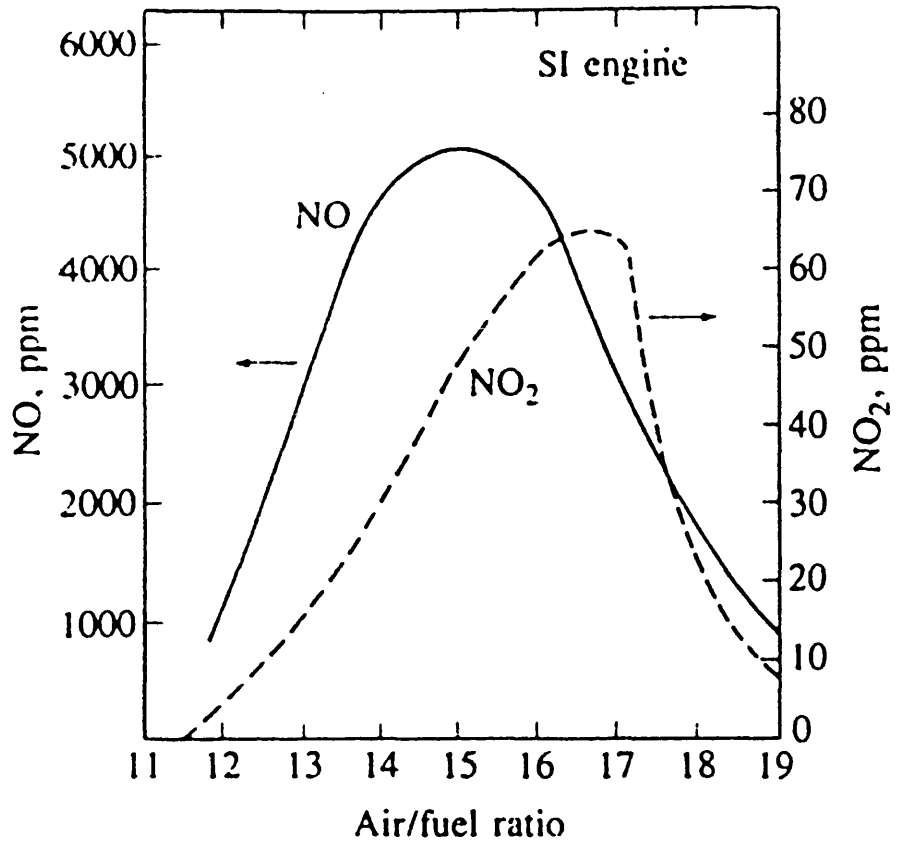

Figure 2.3 Effect of Air-Fuel Ratio on Emissions of NO and NO2

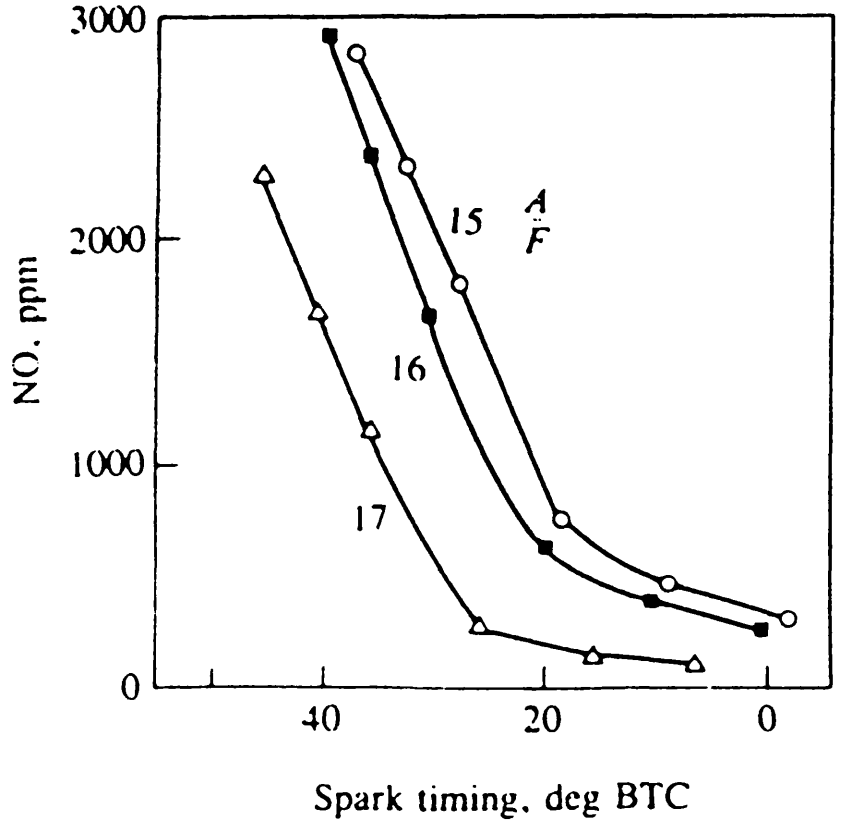

Figure 2.4 Effect of Ignition Timing on NO Emissions for Different Air-Fuel Ratios

Control method	Status	Nominal reduction	Potential engine applications
Nonselective catalytic reduction [4]	Commercial	90%	4-cycle
Lean-combustion [8]	Commercial	80 to 90%	2- and 4-cycle
Prestratified charge combustion [9]	Commercial	80 to 90%	Some 4-cycle
Selective catalytic reduction [4]	Potential[b]	80%	2- and 4-cycle[c]
Exhaust gas recirculation [10]	Potential[b]	50%	2- and 4-cycle
Parameter optimization [11, 12]	Potential[b]	30%	2- and 4-cycle
Cyanuric acid ($RAPRENO_x$)	Research	Unknown	Unknown
Electrochemical cell	Research	Unknown	Unknown
Thermal $DeNO_x$	Boilers[d]	–	None apparent
Urea (NO_xOUT)	Boilers[d]	–	None apparent

[a]Reference(s) of primary information source(s).
[b]Potential is used where potential application has been demonstrated.
[c]And some turbocharged four-cycle engines.
[d]Currently applicable only to boilers.

Figure 2.5 Methods of NOx Reduction and Their Application

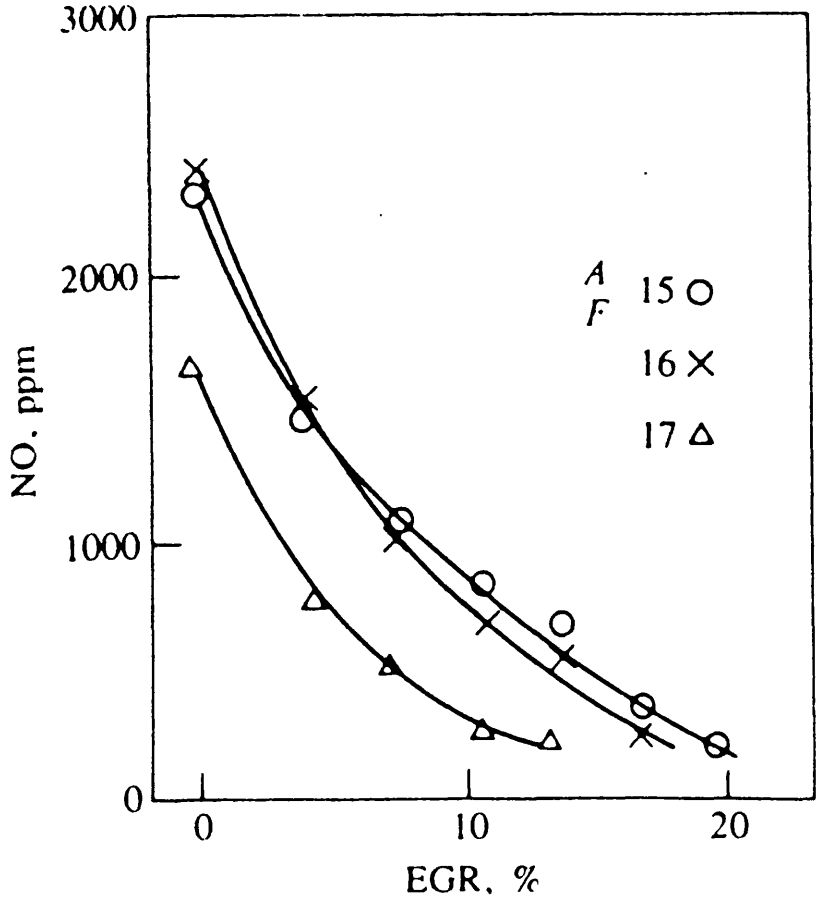

Figure 2.6 Variation of NO Emissions with Recycled Exhaust Gas (EGR) for Different Air-Fuel Ratios

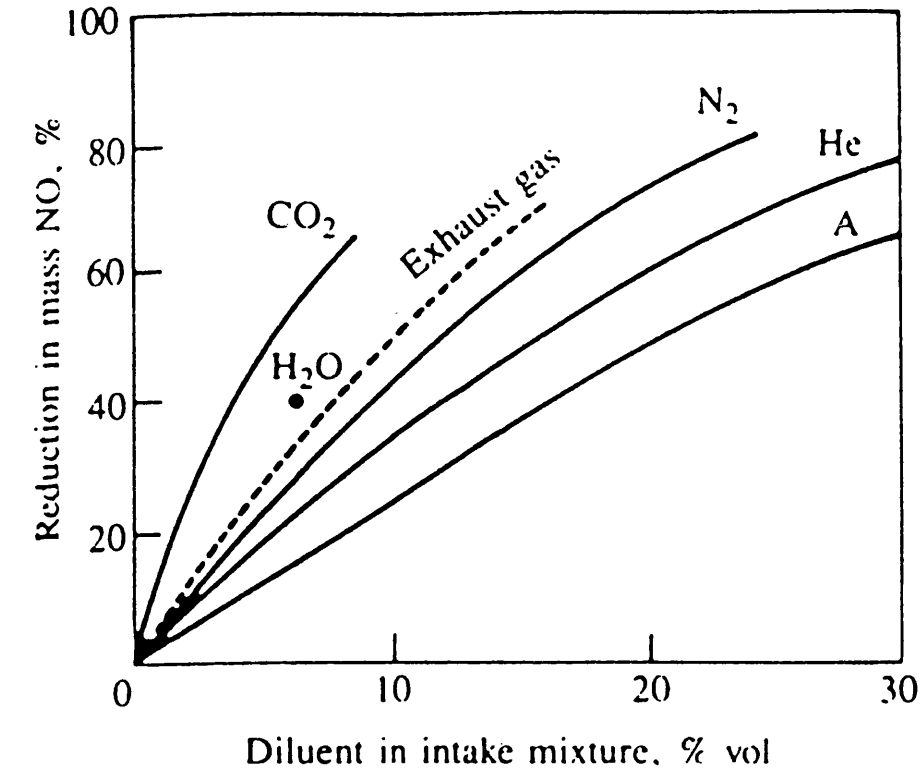

(*a*)

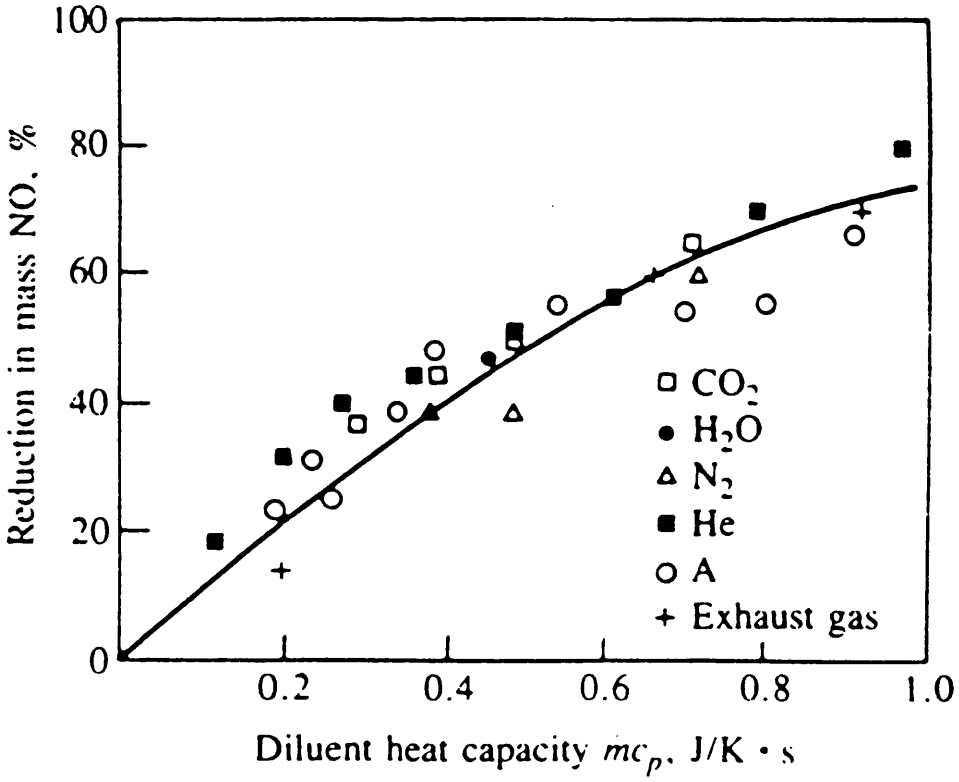

(*b*)

Figure 2.7 (a) Percentage Reduction by Mass of NO Emissions with Various Diluents; (b) Correlation of NO Reduction with Diluent Heat Capacity

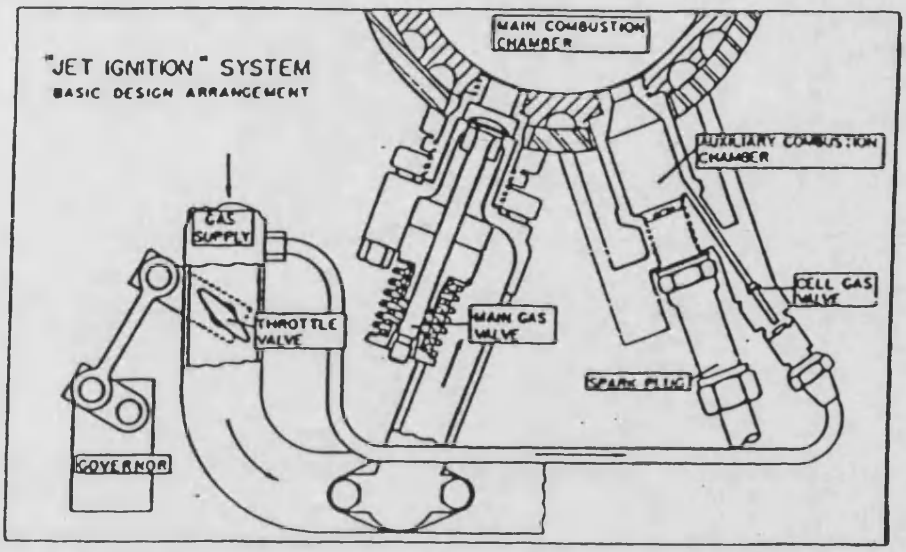

Figure 2.8 Prechamber Arrangement Used by Fairbanks Morse

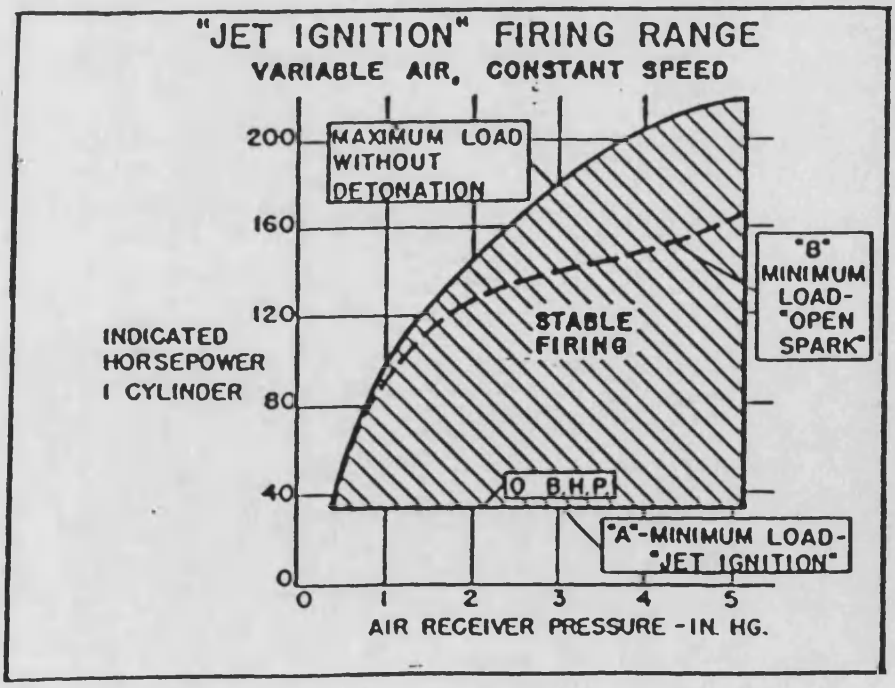

Figure 2.9 Jet-Ignition Firing Range

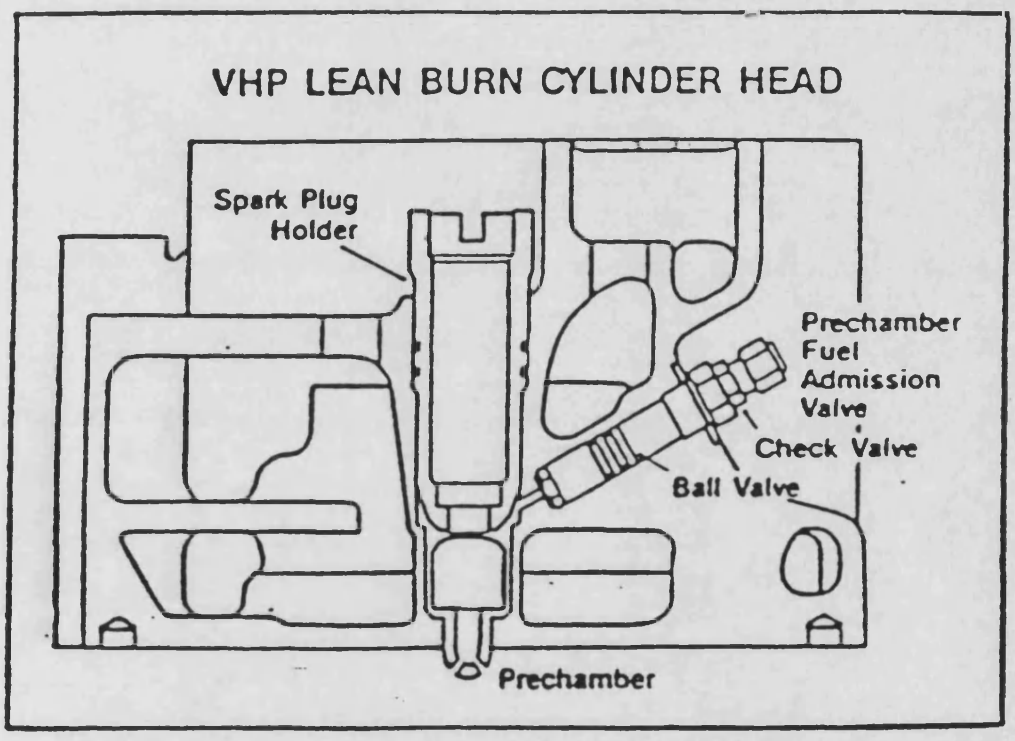

Figure 2.10 Waukesha VHP Cylinder Head and Prechamber Assembly

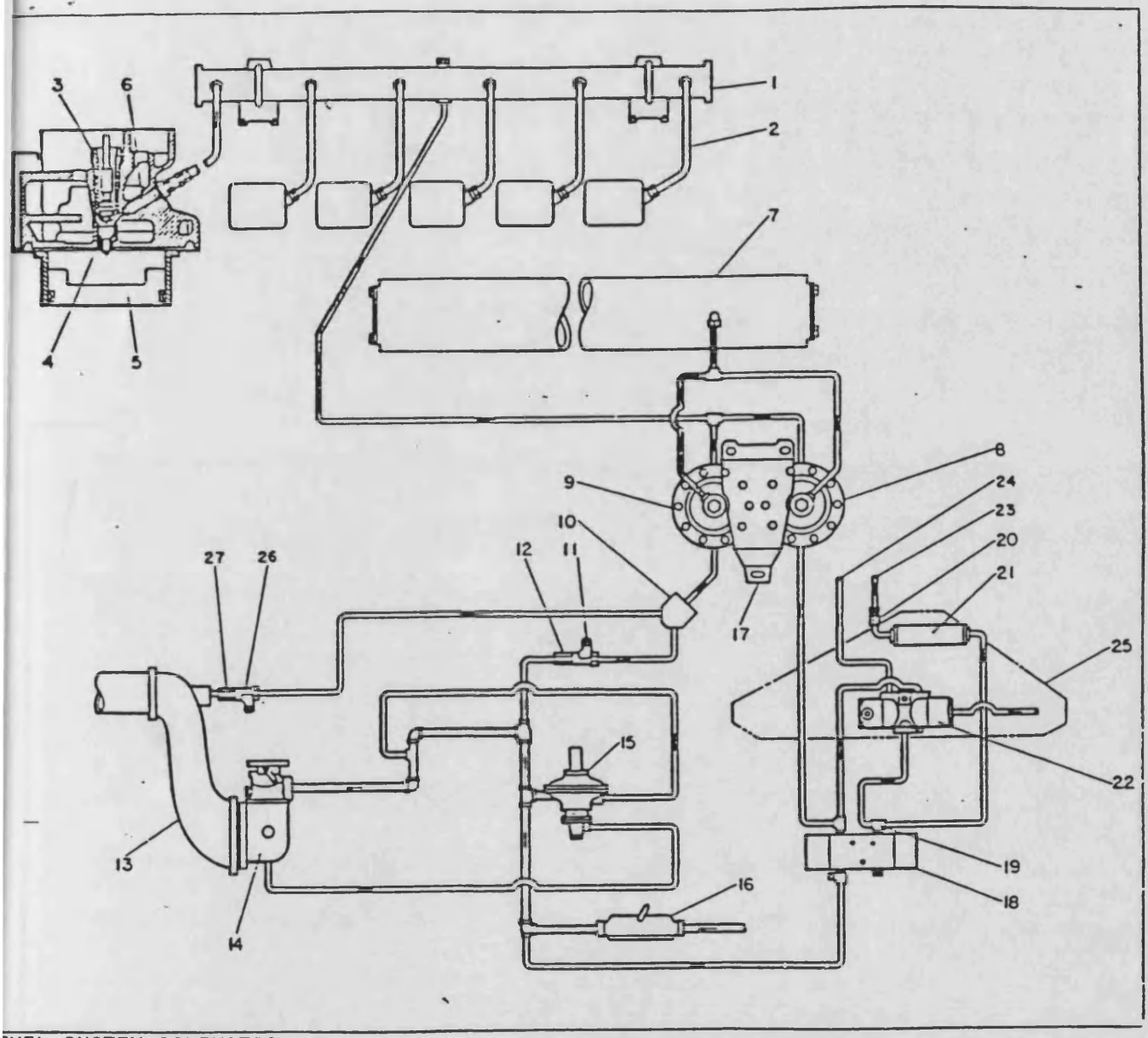

FUEL SYSTEM SCHEMATIC

Item	Description	Item	Description
1	Manifold Prechamber	15	Regulator, Gas
2	Tube Prechamber Inlet	16	Valve Gas Shut Off
3	Carrier Spark Plug	17	Bracket Press Diff Regulator
4	Prechamber Cylinder Head	18	Valve, Air
5	Piston 9.375 Dia.	19	Valve Shuttle
6	Valve Assm. Admission	20	Valve Orifice Check
7	Manifold Intake	21	Plenum, Air Gas
8	Fuel Regulator Prechamber	22	Valve Pilot Actuated
9	Fuel Air Regulator Prechamber	23	Tube Plenum Inlet
10	Connection Y Assm.	24	Tube Vent
11	Fuel Control Valve	25	Bracket Gas Valve Mounting
12	Fuel Check Valve	26	Air Flow Control Valve
13	Air Inlet Connection	27	Air Check Valve
14	Carburetor 6" Updraft		

Figure 2.11 Waukesha Fuel Supply System used on VHP Engine

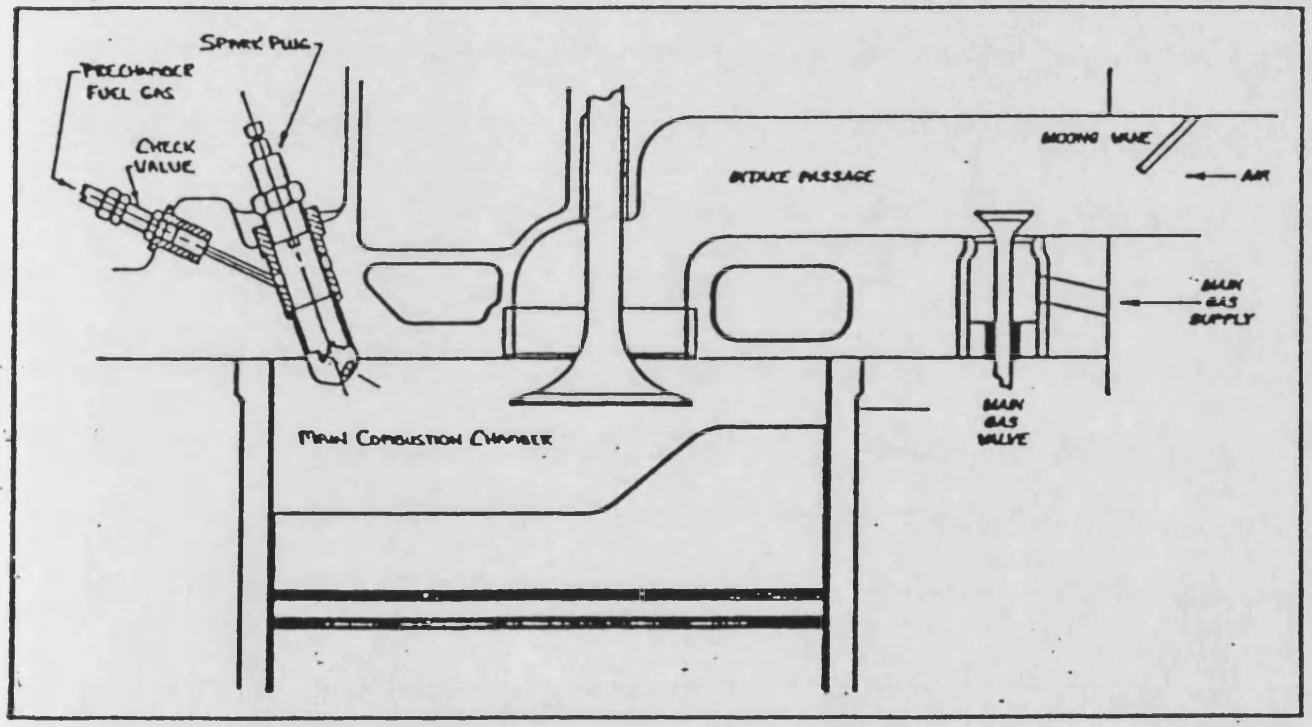

Figure 2.12 Superior Clean Burn Cylinder Head and Prechamber

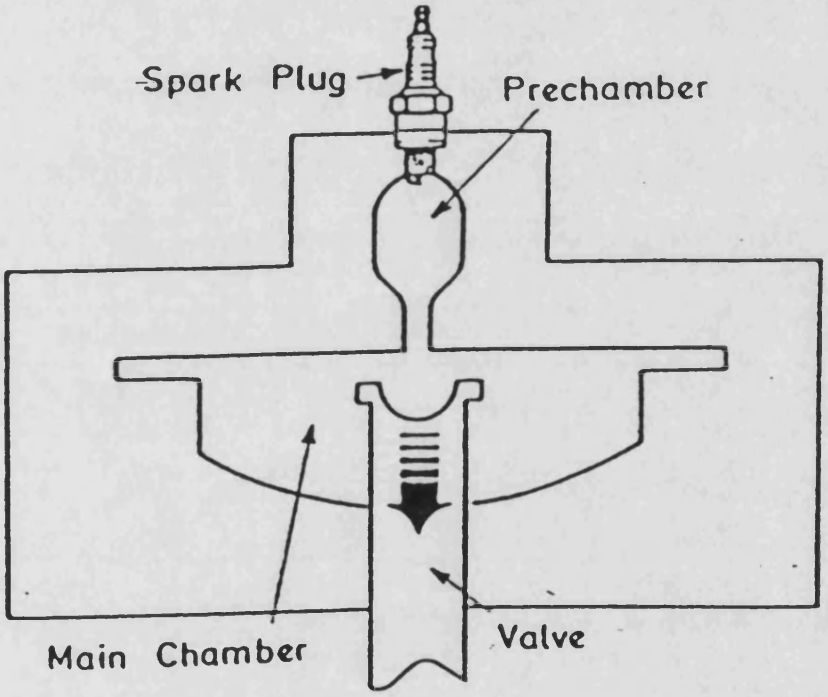

Figure 2.13 Simplified Section of CVC Rig

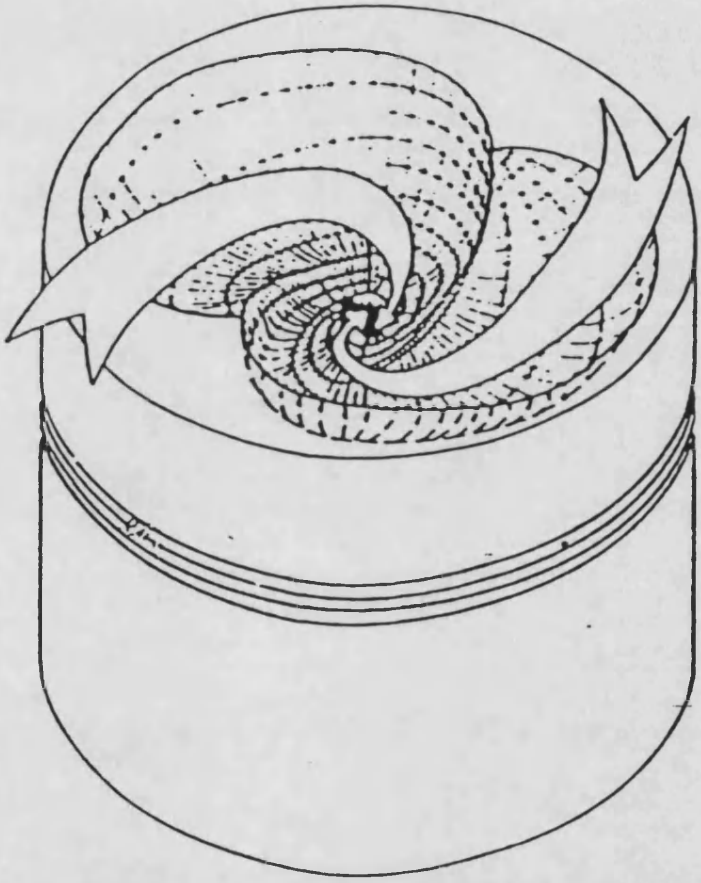

Figure 2.14 Principal of Operation of the Nebula Combustion Chamber

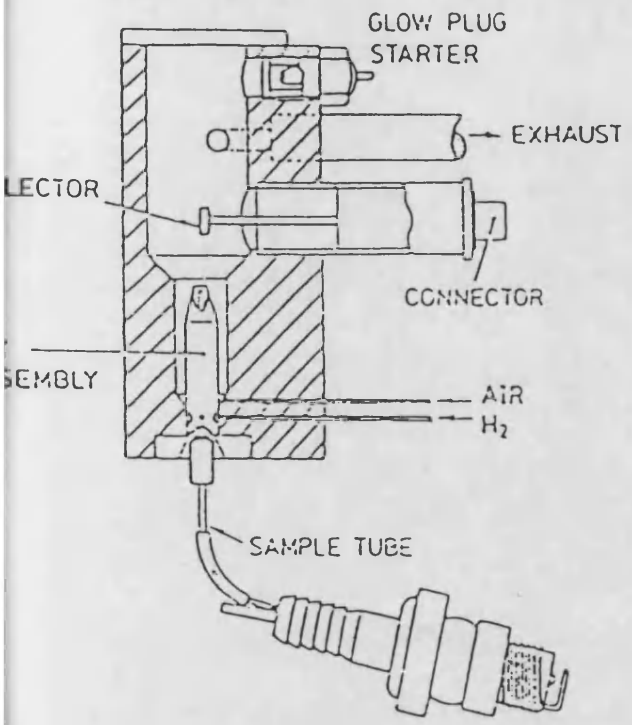

Figure 2.15 HFR FID and Sample Arrangement

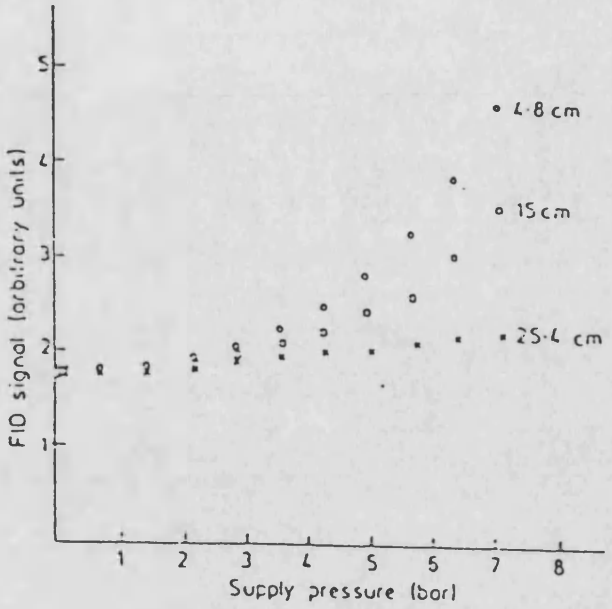

Figure 2.16 Effect of Supply Pressure on Fid Signal at three Values of FID Vacuum

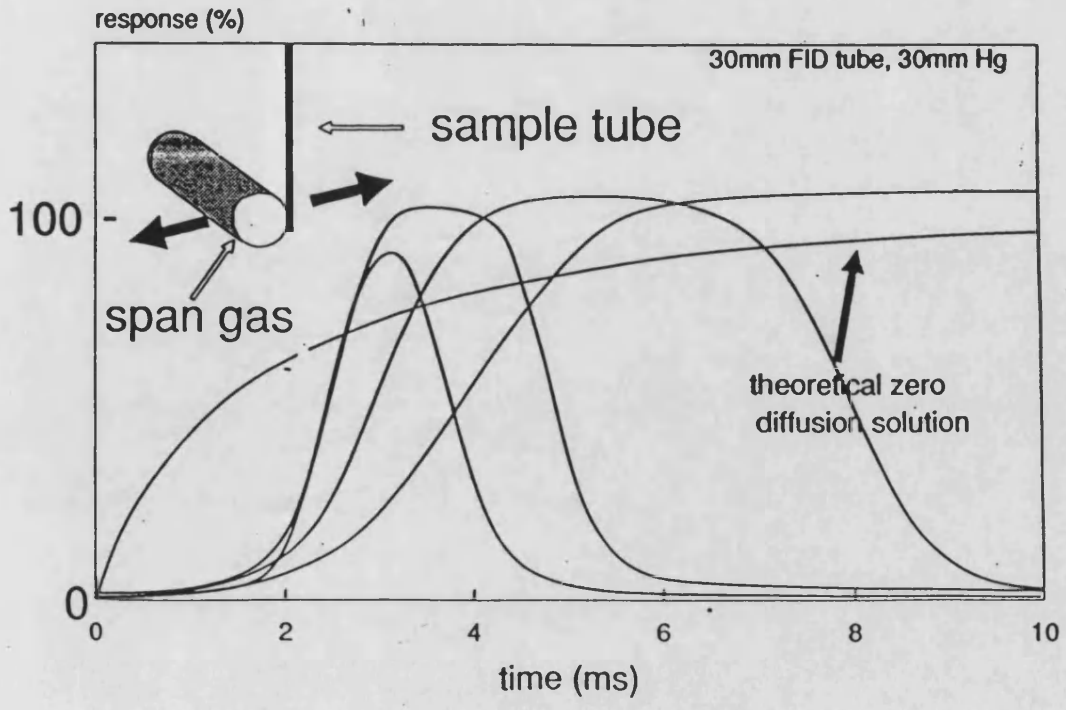

Figure 2.17 FID Frequency Response Characteristics

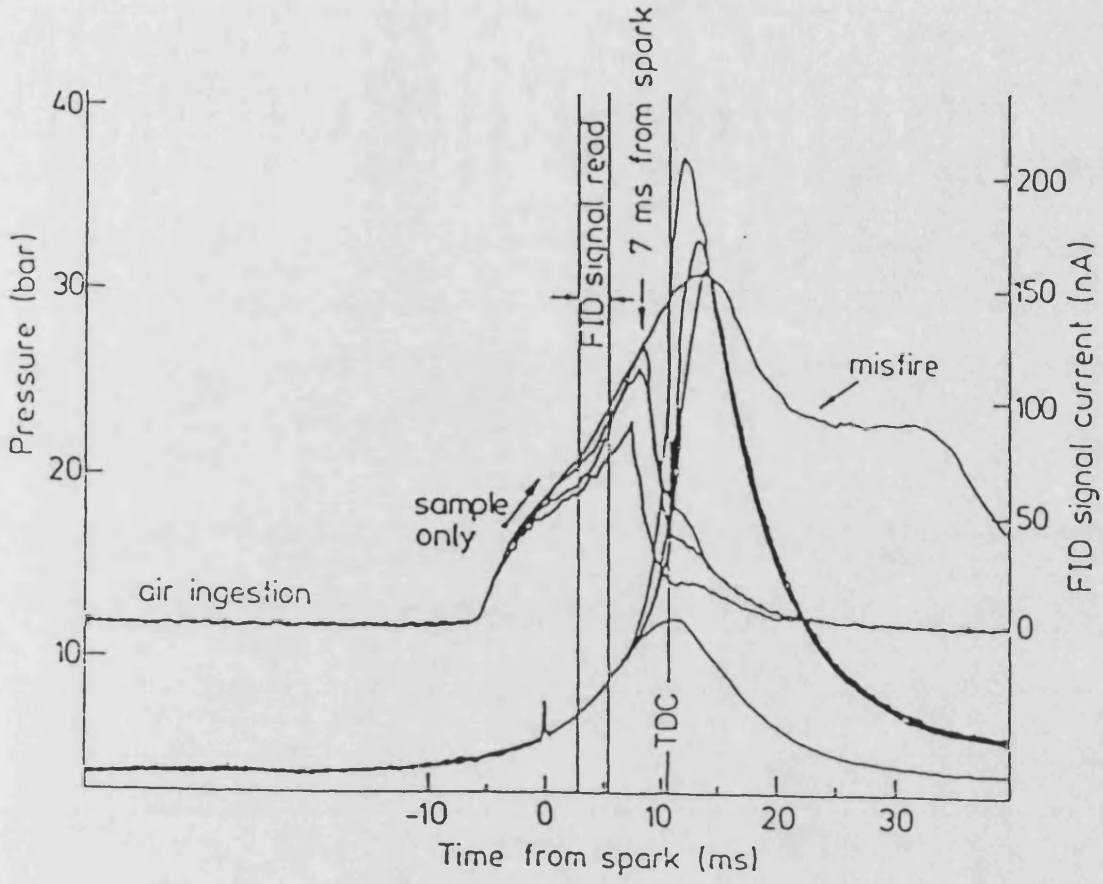

Figure 2.18 Consecutive Fired and Misfired FID and Pressure Signals

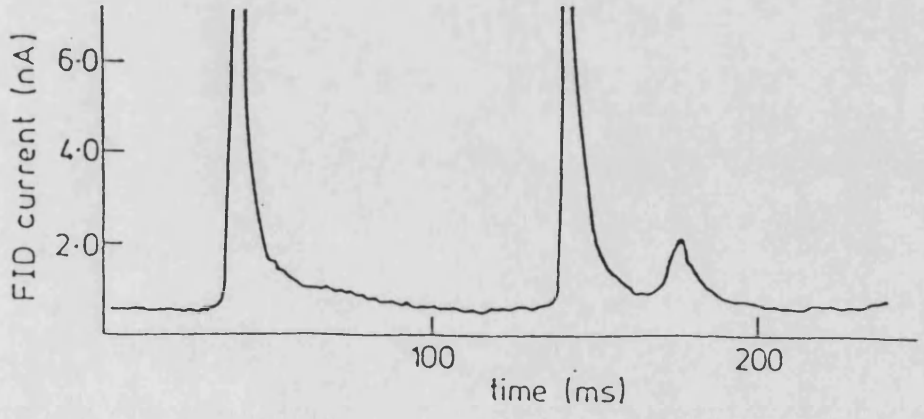

Figure 2.19 Fid Output at Higher Gain Setting

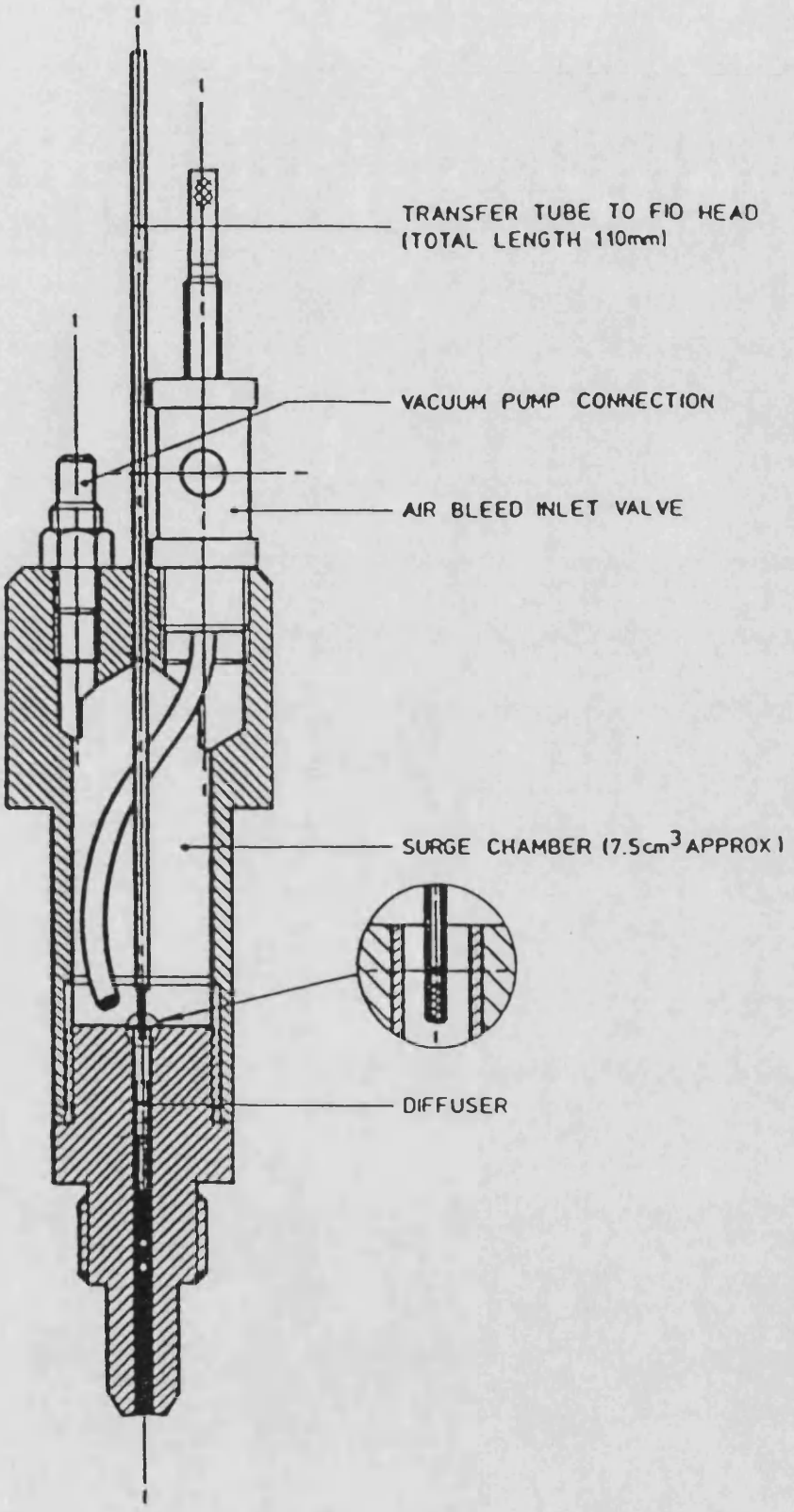

Figure 2.20 Cross-section of Cylinder Gas Sampling Plug

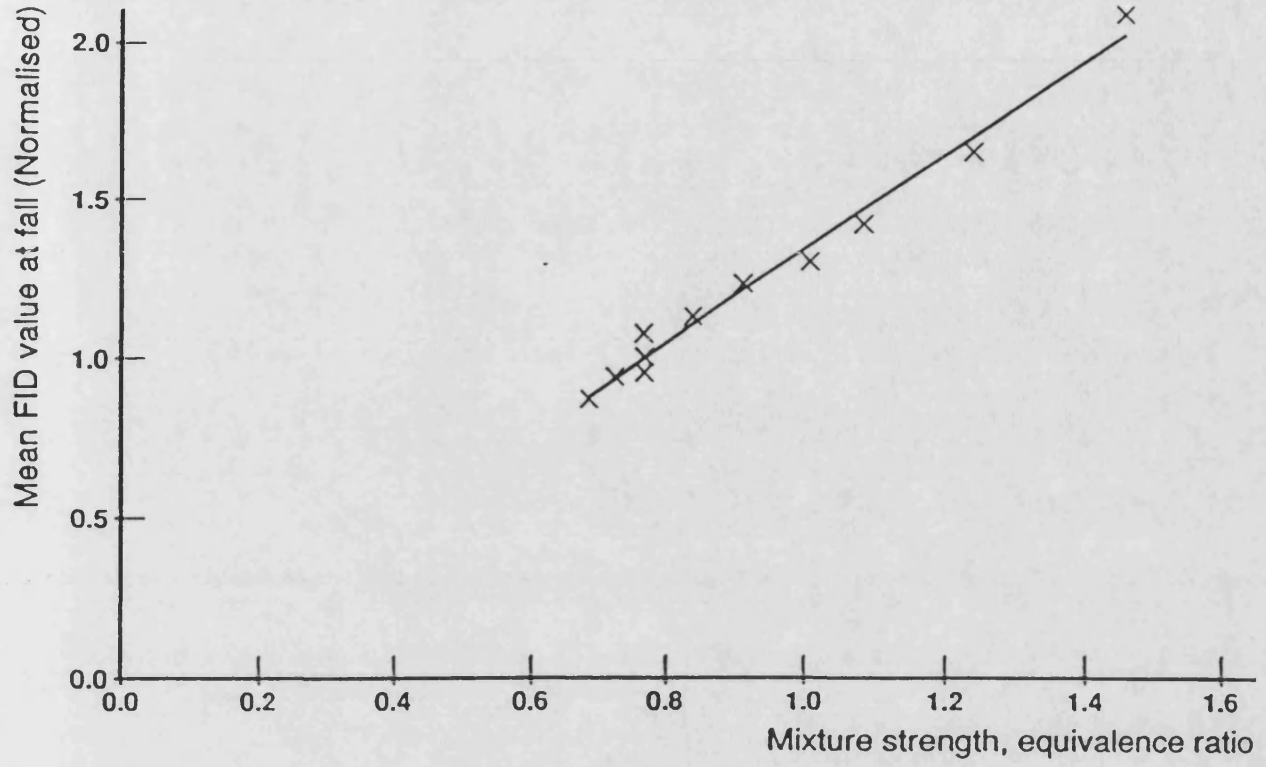

Figure 2.21 Linearly of FID Response to Mixture Strength

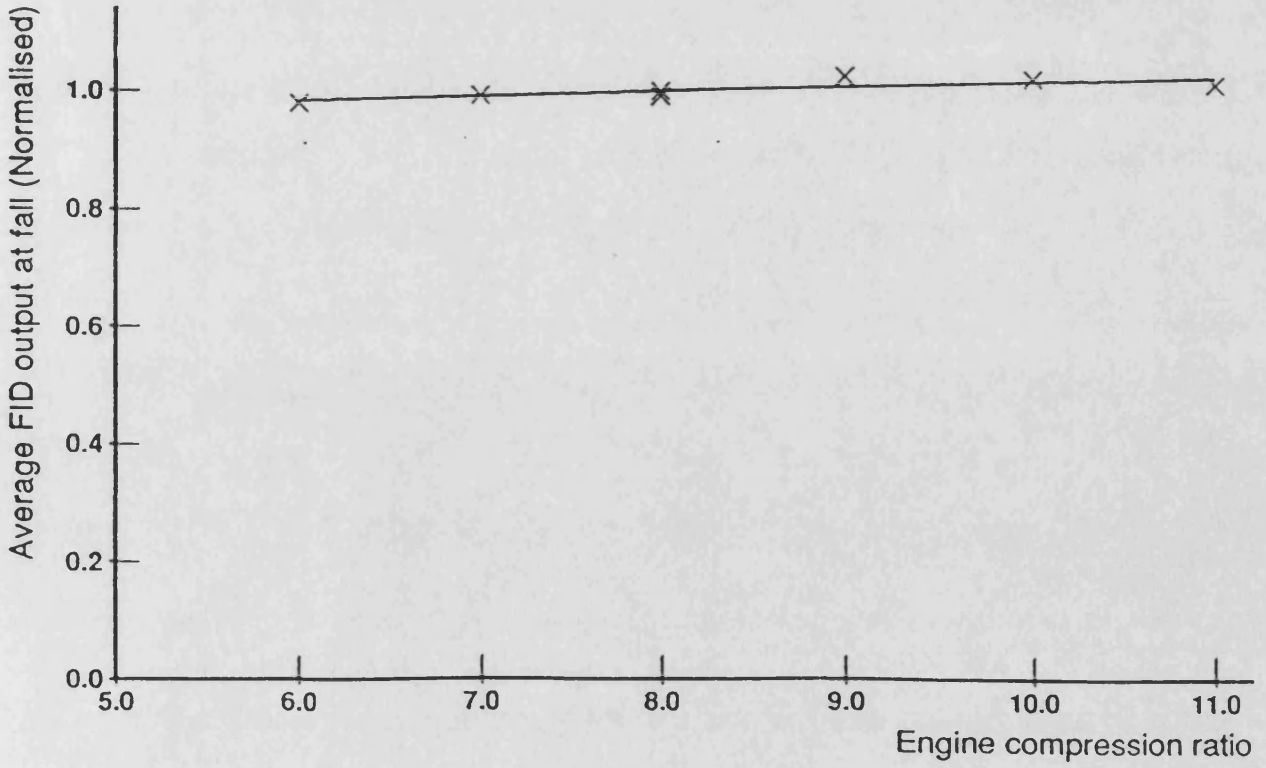

Figure 2.22 Response of FID Output to Compression Ratio

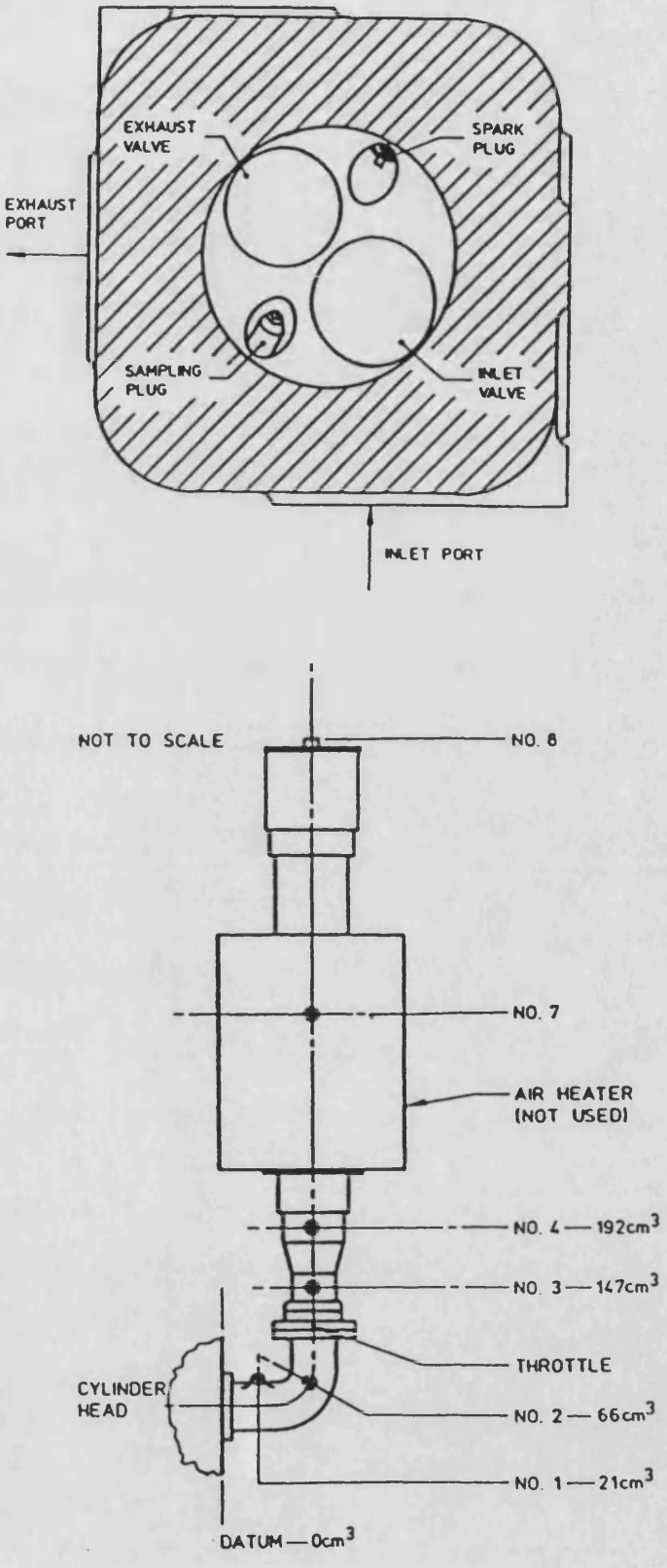

Figure 2.23 Positions of Sampling Plug in Cylinder Head and Propane Injection Ports in the Inlet Tract

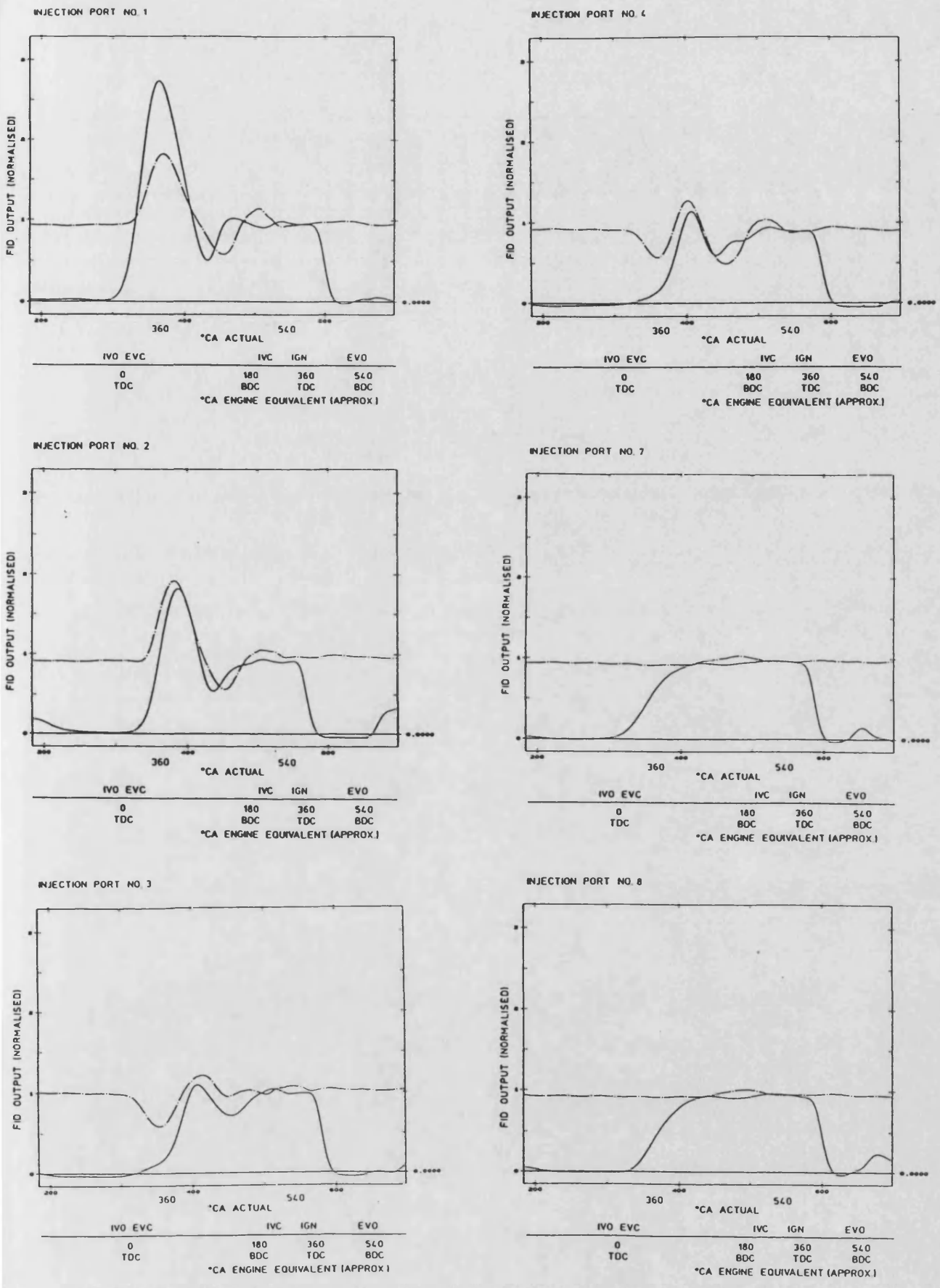

Figure 2.24 FID Traces Corresponding to Injection at Different Ports for Fired Engine (Solid Lines) and Motored Engine (Broken Lines)

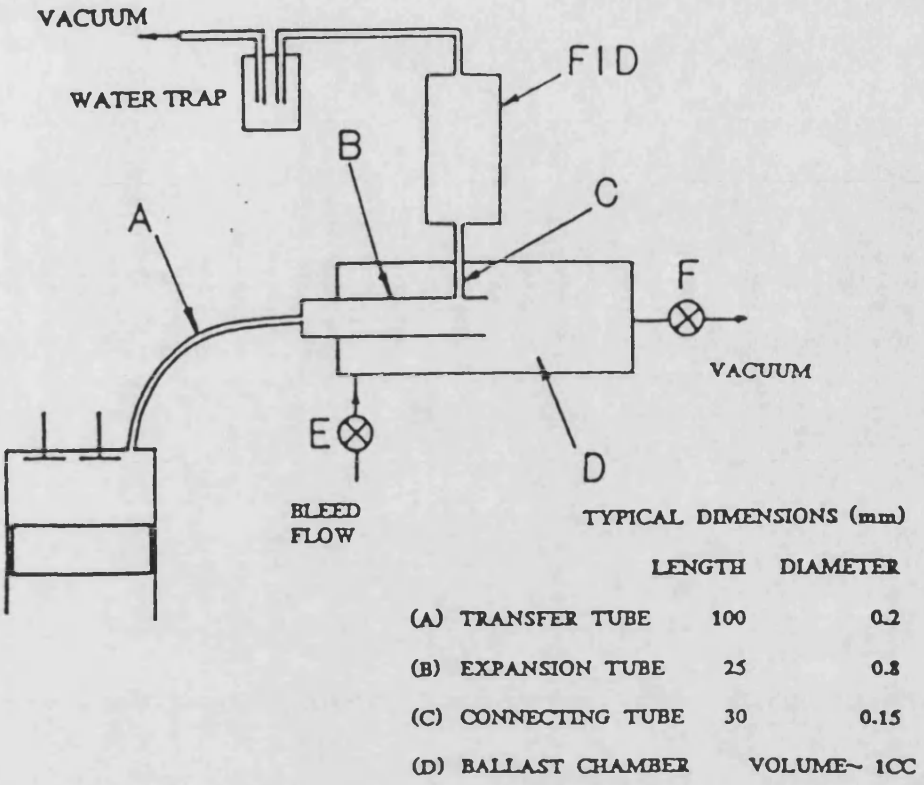

Figure 2.25 Constant Pressure Sampling System for the Fast Response FID used by Heywood

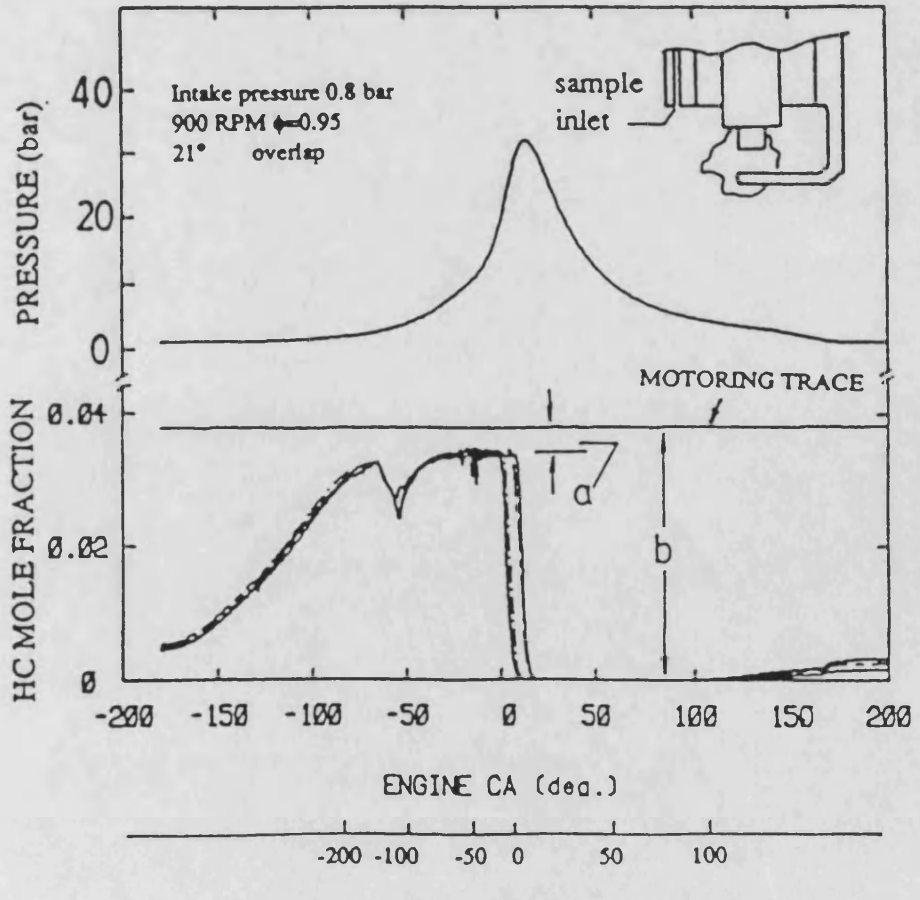

Figure 2.26 Typical Pressure and FID Signals at 900 rpm

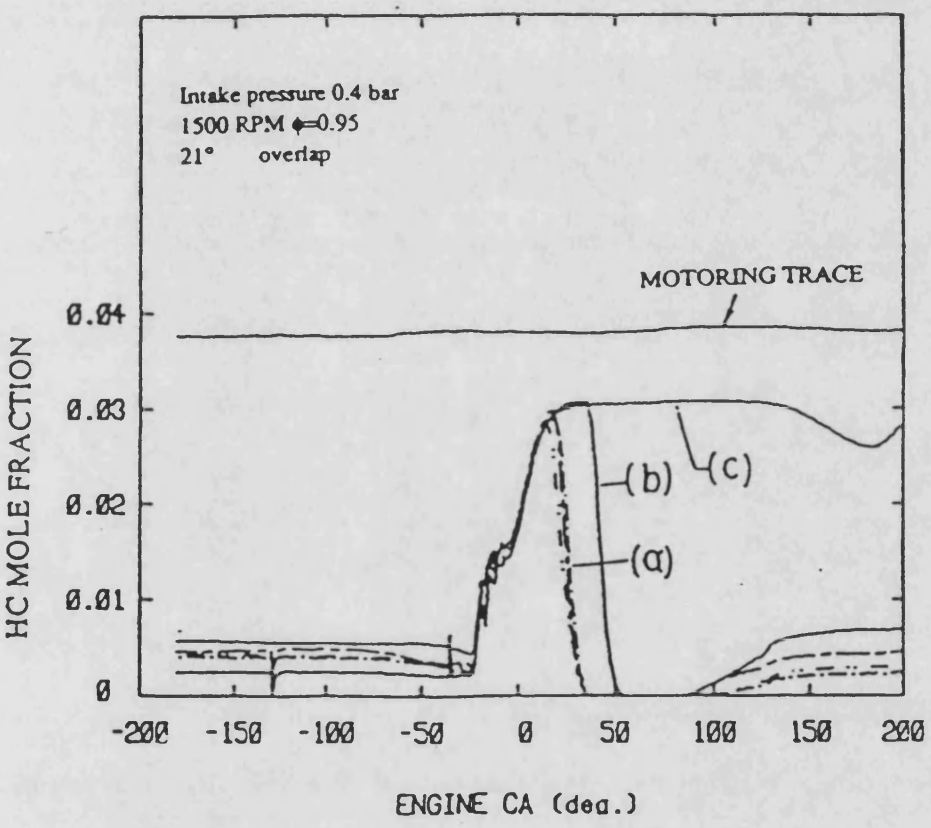

Figure 2.27 Typical FID Signals (a) at low load and 1500 rpm, (b) misfired cycle, (c) skip fired cycle

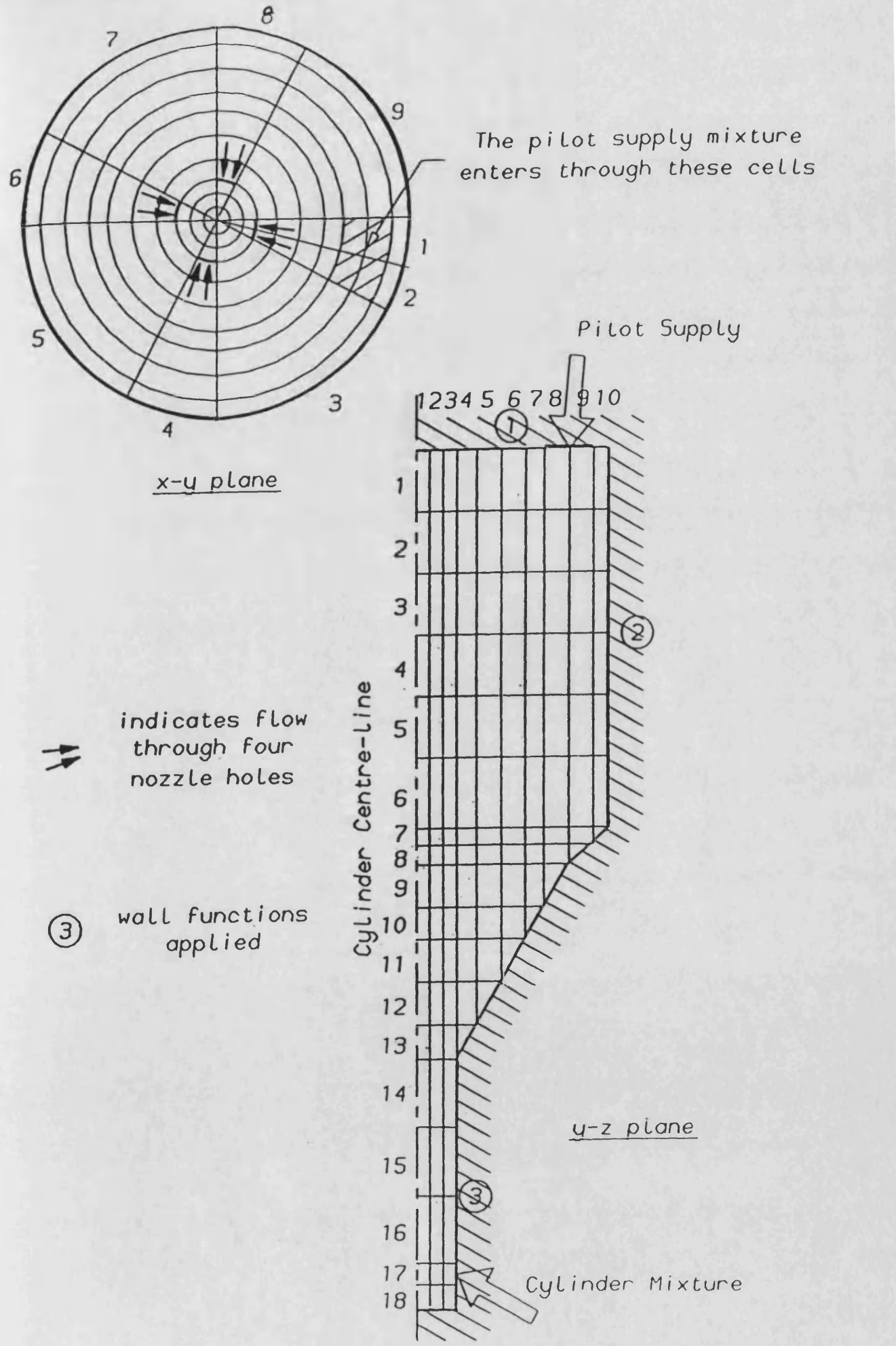

Figure 2.28 Three-dimensional Finite Difference Grid for Pre-chamber Model

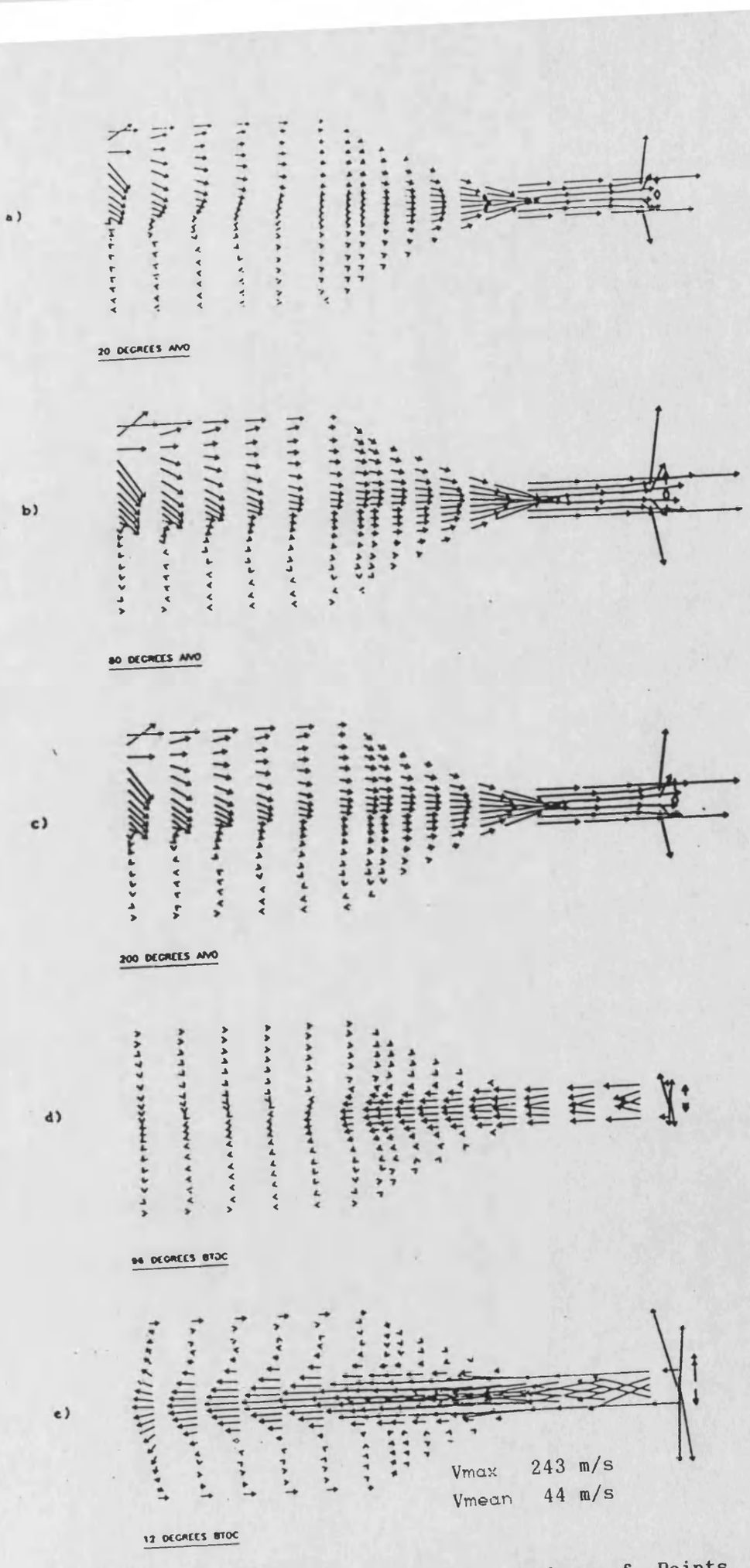

Figure 2.29 Velocity Vector Fields at a Number of Points during Induction and Compression

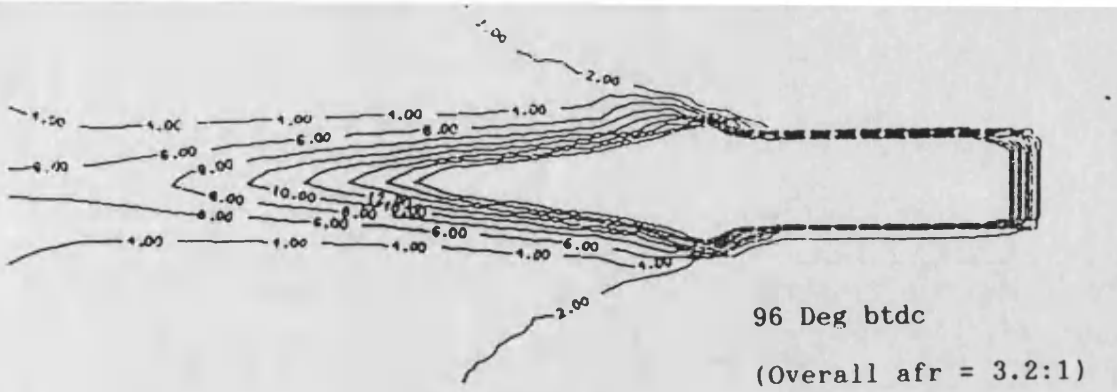

96 Deg btdc

(Overall afr = 3.2:1)

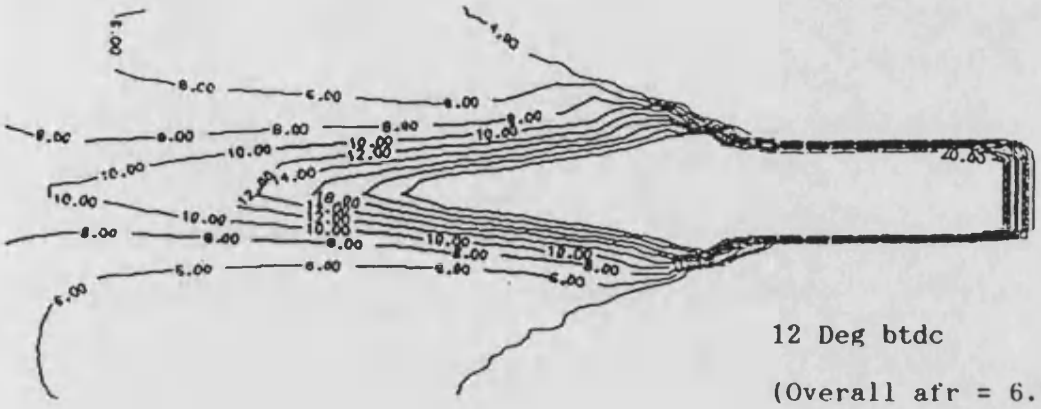

12 Deg btdc

(Overall afr = 6.1:1)

a) Pilot Air-Fuel Ratio = 0.0

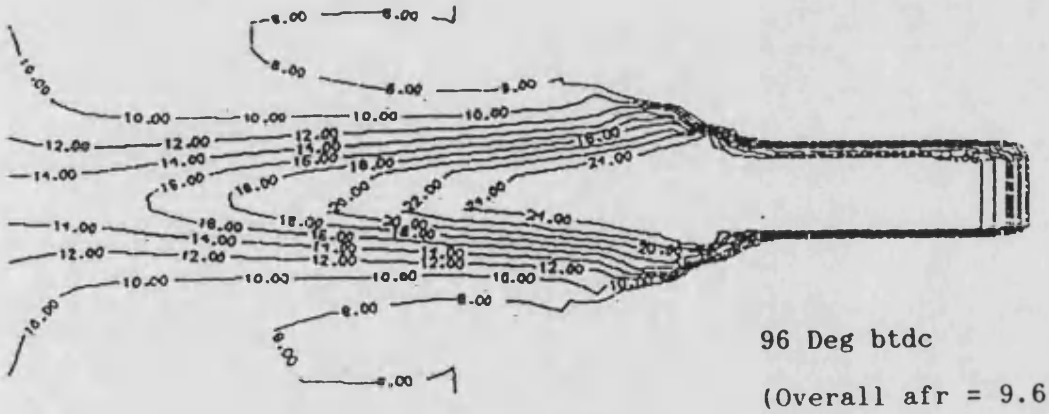

96 Deg btdc

(Overall afr = 9.6:1)

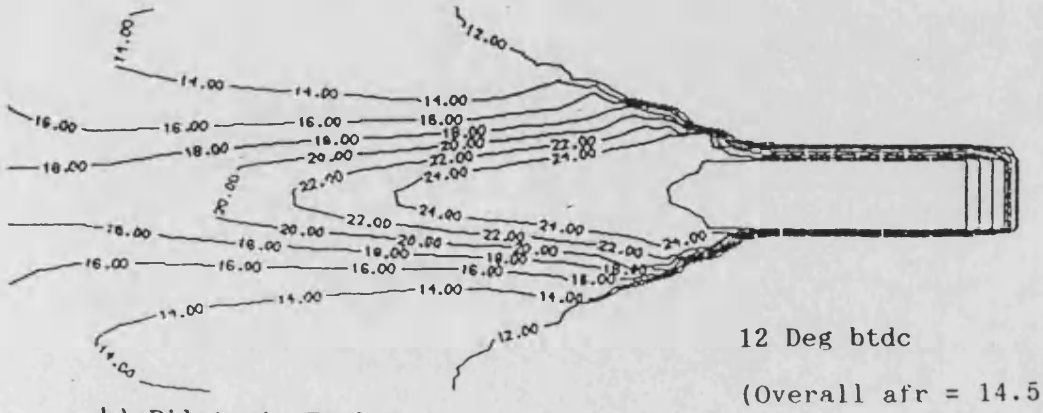

12 Deg btdc

(Overall afr = 14.5:1)

b) Pilot Air-Fuel Ratio = 2.3

Figure 2.30 Contours of Air-Fuel Ratio Obtained using PHOENICS CFD for a Pure Gas Pilot mixture (a) and an Air Fuel Ratio of 2.3:1 (b)

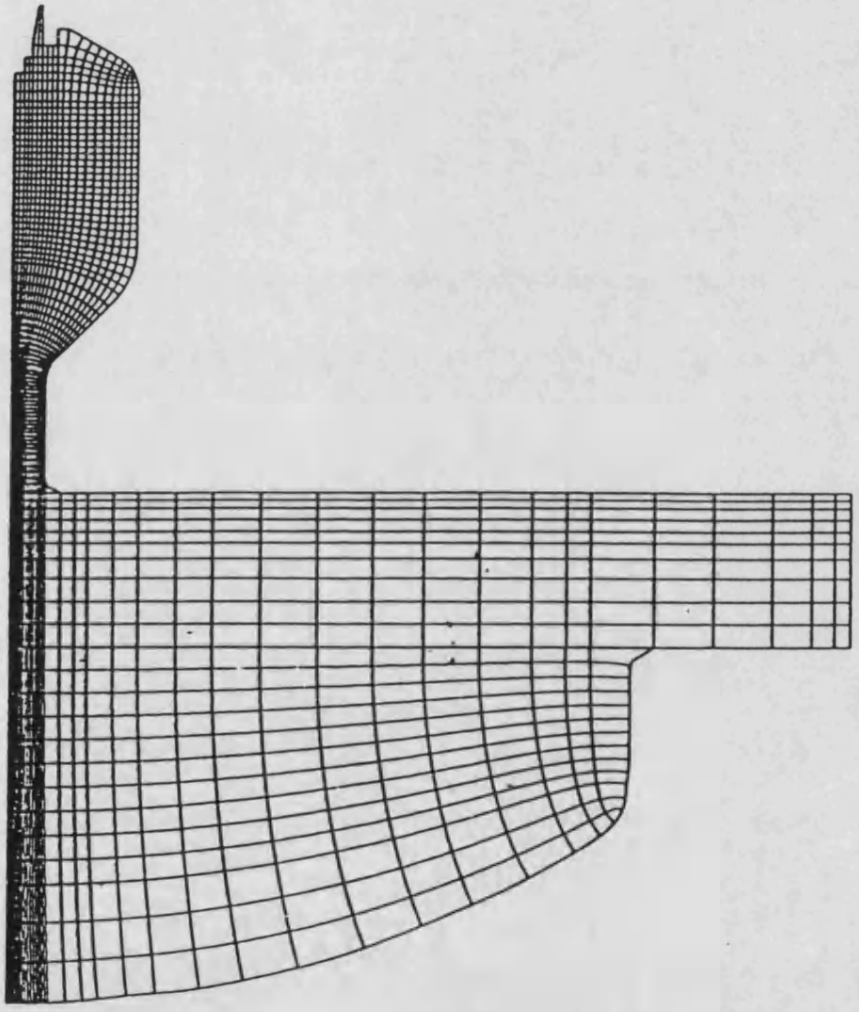

Figure 2.31 Computational Mesh Used For flow Calculations

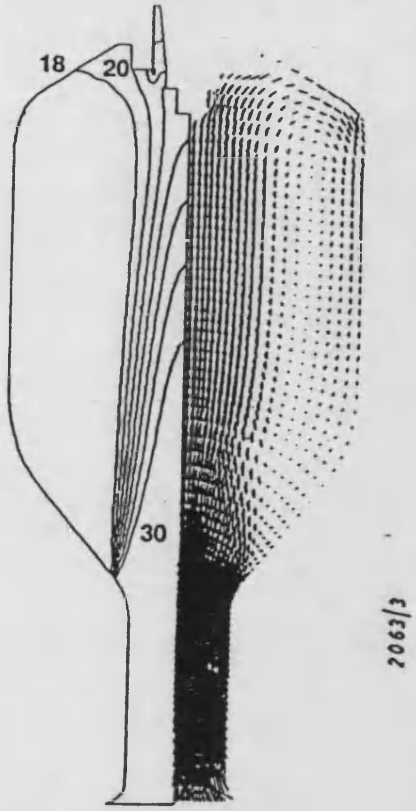

Velocity Field and Air-Fuel Ratio Distribution at 30°BTDC

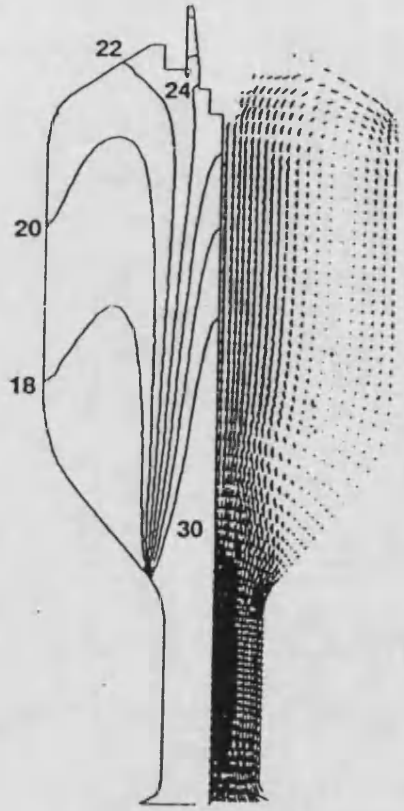

Velocity Field and Air-Fuel Ratio Distribution at 10°BTDC

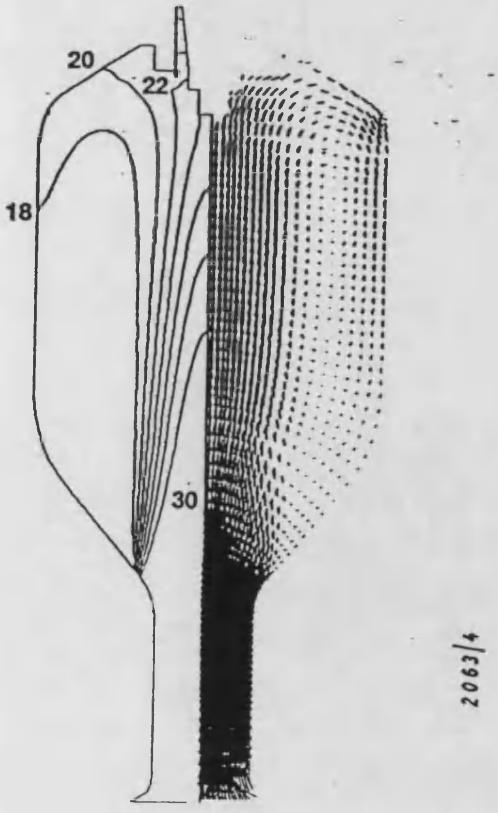

Velocity Field and Air-Fuel Ratio Distribution at 20°BTDC

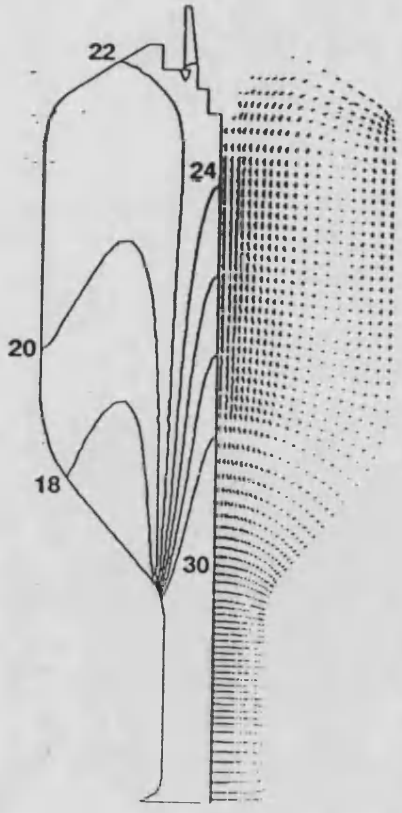

Velocity Field and Air-Fuel Ratio Distribution at TDC

Figure 2.32 Results from CFD Modelling

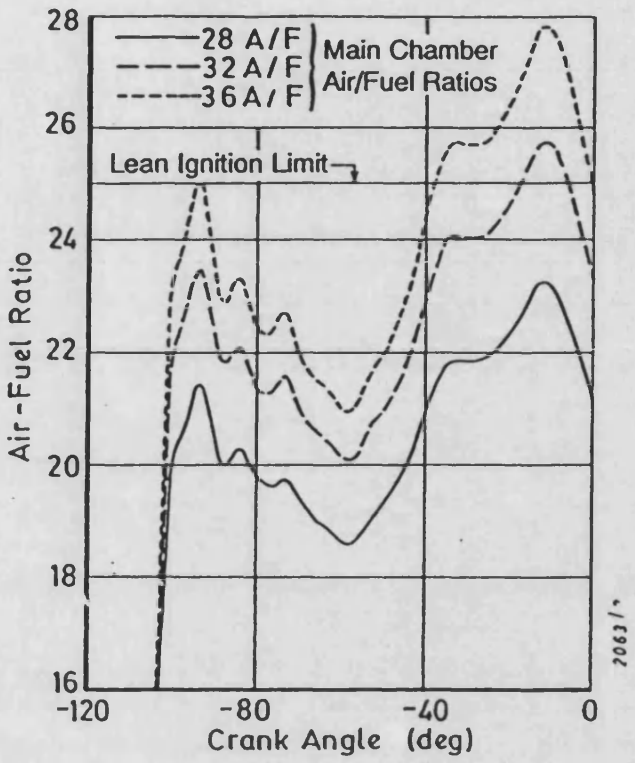

Figure 2.33 Variation of Air-Fuel Ratio at the Spark Plug During Compression

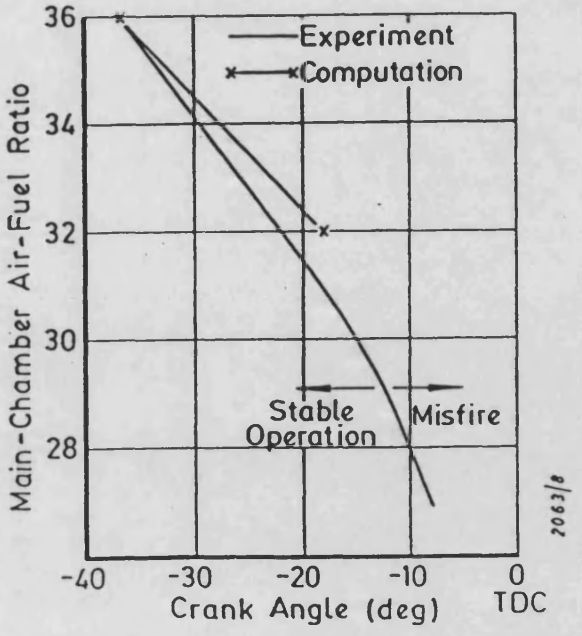

Figure 2.34 Variation of Spark Timing with Main-Chamber Air-Fuel Ratio for Stable Operation

Chapter 3

3. Experimental Engine Test Rig

3.1 Introduction

This chapter desribes a single cylinder gas engine research rig, it's instrumentation, and the commissioning of the rig. Further details of the engine and it's design can be found in Moore (23).

The objective was to commission a fully instrumented prechamber gas engine rig enabling control of all main operating parameters. The engine itself, shown in figure 1.1, is a single cylinder research engine designed by Moore (23) in collaboration with Dorman Diesels Ltd. The engine, developed solely for research purposes, is a variant of the Dorman "SE" engine range. This range is produced in various builds, including straight 6, 8 and V12 configurations for diesel or gas applications. Features of the "SE" range include four valve cylinder heads and oil cooled pistons. The single cylinder "SE1" variant reported in this thesis incorporates counter rotating balance shafts for reduced vibration, and an artificial turbocharging system allowing independent control of turbocharging parameters. Details of the engine are given in Appendix B. Advantages of using the single cylinder SE1 engine for research, instead of a production multi-cylinder engine, include reduction of running costs, elimination of cylinder to cylinder variabilities, and improved access for instrumentation. Loading of the SE1 engine is achieved by connection to a Froude G4 dynamometer. Fuel supplied to the engine was mains natural gas (see Appendix B) delivered to the engine fuel system at a pressure of approximately 3 bar via a gas compressor. The engine installation is shown in plates 3 and 4.

In the design and development of the fuel supply systems, there were three necessary objectives. Firstly, it was required to develop a control system which allowed the necessary independent control of all fuelling parameters at given engine operating conditions. Equally important, was to maintain a degree of inherent control by retaining dependency of key fuelling parameters on the particular operating conditions in order that the engine could be easily managed, particularly during start up and load changes. Finally, accurate measurement of fuel and air flows to both combustion chambers was required, which included pressure and temperature corrections. As a result of fulfilling these conditions, the fuelling system proved necessarily complex and time consuming to commission. The final arrangement of the fuel supply system is shown in figure 3.1.

3.2 Development of the Fuel System

Initial testing of the SE1 gas engine was started using an in house designed and manufactured fixed venturi gas mixer as shown in figure 3.2. Gas flow being controlled by use of a stepper motor operated metering valve. The metering valve consisted of a cone that is lifted in and out of the gas jet to vary the flow area. This was to allow the operator to have independent control of the air-fuel ratio delivered to the intake manifold. However this system proved unsatisfactory for two reasons. It had very poor self regulation characteristics which meant that constant adjustments were necessary with any change in engine operating parameters. Because of this, load acceptance was a difficult and delicate operation as both boost pressure and metering valve lift had to be adjusted simultaneously to maintain correct air-fuel

ratio as dynamometer load was applied. It was also soon realised that at full rated load, the engine would demand more gas than the mixer could cater for. This was a problem that could not easily be resolved as there was little margin for increasing mixer specification without remanufacture.

It was decided, therefore, to adapt an existing proprietary gas mixer to suit the requirements of the SE1 engine and test program. This would provide the engine with a certain amount of self regulation so that start up and load changes could be managed more easily. This is particularly important in a lean burn engine as it is inherently unstable towards the lean limit. The mixer chosen for this application was an Impco 200 series variable venturi gas mixer, shown in adapted form in figure 3.3. This mixer is in widespread use in the gas engine industry. It was selected as its capacity is sufficient to accomodate the 70 % or so extra air flow required for lean burn combustion when compared to that for stoichiometric, but at the same time, not so large that part load control becomes difficult.

The principle of operation is that of a variable venturi carburettor. The flow of fuel gas through the mixer is regulated by the lifting of a shaped cone positioned in the exit plane of the fuel nozzle, the lift of which is governed by the pressure within the venturi. The precise profile of this cone governs fuel concentrations throughout the engine load range. For this reason, the fuel cone had to be specifically shaped for our application. This was aided by performing a series of tests on the gas mixer with the addition of a perspex window in the mixer body to monitor valve lift. The standard Impco cone and the new modified cone are shown in figure 3.4. Figure 3.5 shows variations of afr for both

the new cone valve and the standard cone valve. The standard valve began very rich at low load, but rapidly leaned off as the load was increased, limiting maximum power to a dynamometer load of 33 kW (6.9 bar bmep). The new cone profile maintained the afr close to a constant value as the load was increased, leaning off only as maximum load was approached.

Further modification of the gas mixer, shown in figure 3.3, included the addition of a valve spring tension adjuster for fine adjustments of afr and a gas enrichment facility for start up and high loads. Coarser variations in afr throughout the load range were achieved by adjustment of the gas delivery pressure to the mixer by using an adapted pressure regulator, connected as shown in figure 3.1. This regulator used boost pressure as a reference pressure to enable the gas delivery pressure to the mixer to be greater than boost pressure, essential for correct operation of the mixer. A similar pressure regulator was used in the gas supply to the prechamber, again to provide a suitable "overpressure" to the prechamber mixer. This caused the gas supply to the prechamber to increase with load and provide a degree of self regulation. Overall manual control of the gas supply was governed by a multi-turn needle valve. The fuel mixer in the case of the prechamber fuel system was that of a fixed venturi type junction. Air flow to the prechamber mixer was governed by a manually controlled pressure regulator and needle valve combination and could be closed off altogether.

Gas and air flows to the prechamber were measured by dual rotameter flow meters (small and large), installed with two way valves as shown in figure 3.1, in both gas and air supplies to the prechamber. This was to widen the measurable flow range of the

gases by switching between the two flow meters. These were calibrated for the appropriate gas, and corrected for pressure and temperature during data reduction. Gas flow to the main combustion chamber was measured in the same manner by a single rotameter, together with a high accuracy positive displacement "Rootes" flow meter measuring the total gas consumption for the engine. Excellent agreement between the two types of flow meters was observed to within 2%. Air flow to the main chamber was measured with a sharp edged orifice plate constructed to BS 1042 standards.

The high pressure natural gas required by the engine was supplied by a single stage compressor. The output pressure from the compressor being approximately 3 bar at low loads, but reducing slightly at higher loads as fuel demands increase. The compressed gas is cooled using a water cooled heat exchanger. Excess gas not required by the engine at low loads is recirculated. An initial problem encountered with the fuelling system was contamination by oil of the high pressure gas delivered to the engine. This was found to be caused by the gas compressor, the existing oil traps supplied with the unit being inadequate. An ultra fine oil trap capable of removing the fine oil spray, installed downstream of the compressor, eliminated this problem.

Several important safety features have been incorporated into the engine and fuel system as the dangers of compressed natural gas and air mixtures must be stressed. A serious problem associated with natural gas burning engines is the possibility of ignition of the intake manifold contents due to flash back from the engine. For this reason, a bursting disc was fitted to the manifold, so that pressure could be safely released without

causing the manifold to rupture. This proved to be an essential requirement, as during engine testing, this occurred on a number of occasions when temporarily operating the engine "off-design". In accordance with British Gas regulations, two pressure operated shut down solenoid valves are incorporated into the fuel supply system. One is activated should the mains pressure fall significantly in the supply line due to compressor demand, which could lead to air entering the line, forming an explosive mixture. The other switch would be activated should a high pressure build up downstream of the compressor.

3.3 Simulated Turbocharger System

An artificial turbocharging system was used on the single cylinder SE1 test engine as it is not practical to use a real turbocharger for several reasons. It is not possible to match a turbocharger to a single cylinder engine due to the nature of the exhaust flow. Long periods of little or no flow mean that a pulse pressure turbocharger would not operate efficiently. Also, there would not be the option of independent adjustment of boost and turbine back pressures, which is a highly desirable feature on a research engine.

The artificial turbocharging system developed for this application is shown schematically in figure 3.6. This is equivalent to the real turbocharger model shown in figure 3.7. The inlet, exhaust and ambient pressures and temperatures are shown for the two systems. The system consists of a high capacity Bellis air compressor (specification given in Appendix A) with the components needed to provide a controllable steady pressure at the desired intercooler temperature. Total air flow is measured by

means of an orifice plate to B.S.1042 specification, and heating of the air is achieved by an 18 kW electric element in a feedback control loop. This allows selection and control of a wide range of inlet temperatures, and in effect means that the "apparent" ambient temperature can also be varied.

Appropriate exhaust back pressure to maintain a fixed overall turbocharger efficiency is achieved by use of a gate valve in the exhaust pipe. A by-pass safety valve is incorporated which uses a pressure sensitive bursting disc which ruptures should a dangerous pressure build up in the exhaust occur. The simulation of the turbine is described by Moore (23).

3.4 Instrumentation

The brake output of the engine is absorbed and measured by a Froude G4 hydraulic dynamometer, which was completely reconditioned for this project. Crankshaft speed is measured by use of a photo-electric cell and a flag attached to the flywheel, and displayed in revolutions per minute by a digital counter. Control of the crankshaft speed is achieved using a Heinzmann electronic governor operating on the throttle butterfly valve, and set to the desired speed with a multi-turn potentiometer.

All pressures are recorded manually, using either water or mercury filled manometers. Thermocouples are used to measure all temperatures except those across the engine coolant heat exchanger. More accurate platinum resistance thermometers are used for this purpose as the temperature difference across this component can be small.

In-cylinder measurement of pressure is made by a Kistler type 6121 piezo electric pressure transducer. This enters the main combustion chamber through the top face of the cylinder head, and is recessed from the chamber surface for protection from thermal shock. The signal from this, and in later tests from the FID as well, is recorded using the high speed data acquisition system, Computerscope. The system consists of an analogue to digital converter with a 64 kByte memory buffer. The card is controlled from an IBM compatible PC by driver software. Computerscope has the ability to sample at a rate of up to 1MHz or may be multiplexed to provide up to 16 channels at reduced frequencies. The sampling rate of Computerscope can be controlled by an internal clock, or in our application, by pulses from an optical encoder attached to the crankshaft to give one degree time increments.

Measurement of NOx emissions from the exhaust is achieved using a Signal model 4000 chemiluminescent NOx analyser, the details of which are described in the following section.

3.5 Measurement of Exhaust NOx

Oxides of nitrogen emitted from the exhaust are measured using a chemiluminescent gas analyser in accordance with the recommendations set down in the United Nations Agreement, Regulation 49, (35) concerning gaseous pollutants from stationary gas engines. The analyser has an additional pre-filter unit and heated sample lines to avoid condensation occurring between the sampling point and analyser. This would distort the measured value as oxides of nitrogen are water soluble.

The principle of measurement of a chemiluminescent analyser is based upon the gas phase reaction which occurs between ozone and nitric oxide to produce, apart from nitrogen dioxide and oxygen, light emission.

$$NO + O_3 \Rightarrow NO_2 + O_2 + \text{LIGHT EMISSION}$$

The light emission occurs because approximately 10 % of the nitrogen dioxide produced is in an electrically excited state and hence the transition from this high level to equilibrium, as molecules lose their energy, produces light emission. This light emission ranges in wavelength between 0.3 and 0.6 micrometers, with an intensity that is in direct proportion to the mass flow rate of the nitric oxide into the reaction chamber. The light emission is measured by means of a photo multiplier tube and associated electronics.

As previously stated, only a small proportion of the total energy loss from the nitrogen dioxide falling to a lower energy level produces light emission. The majority of the energy is translated into heat. The heat loss is pressure dependent, since the number of collisions per second varies in direct proportion to the pressure. Therefore maintenance of a low pressure in the reaction chamber will favour energy loss by light emission.

Low pressure in the reaction chamber also minimises the interference effects from other gases, such as carbon dioxide and water vapour, which are known to be very efficient at deactivating excited nitrogen dioxide. This deactivation process is known as quenching and can cause a significant error in NOx measurement if

low pressure is not used.

The sample lines and internals of the analyser are heated to a temperature of 180 degC to avoid the possibility of water condensation forming. This allows measurement to be made on a "wet" basis as approved in U.N.A. Reg. 49. Alternatively, all water condensation would have to be removed and measurement performed on a dry basis. An appropriate correction factor must then be included to give the true "wet" measurement. A detailed layout of the analyser internals and sample line are shown in figure 3.8.

The analyser is merely a comparator. In order to obtain an absolute value for NOx emission, the analyser must first be calibrated. This is done by sampling two gases. Pure air is sampled to obtain a zero reading, followed by a gas containing a known concentration of NOx of the same order as the exhaust gas sample. Calibration of the analyser is repeated at regular intervals during engine testing. In this work we used a β standard calibration gas. The β standard gas was in turn calibrated against more expensive, higher grade α standard gas. The analyser's response is assumed to be linear across this range. The linearity can, however, be checked by use of a gas divider, a device which allows various known concentrations of NOx to be sampled by the analyser.

To comply entirely with the recommendations in Reg. 49, the humidity of the air at inlet to the engine should be measured so that appropriate correction can be made. Because the SE1 engine uses a simulated turbocharger arrangement, this measurement is not easily possible. However, the error associated is small, and for

these tests has been neglected. The correction equation for humidity is given in Appendix C.

Summary

A single cylinder gas engine test rig, consisting of a Dorman SE1 divided chamber gas engine, fuel supply systems, artificial turbocharger, and comprehensive instrumentation has been installed and commissioned. The installation allows independent control of all significant fuelling parameters and can simulate the running of a multi-cylinder "SE" engine.

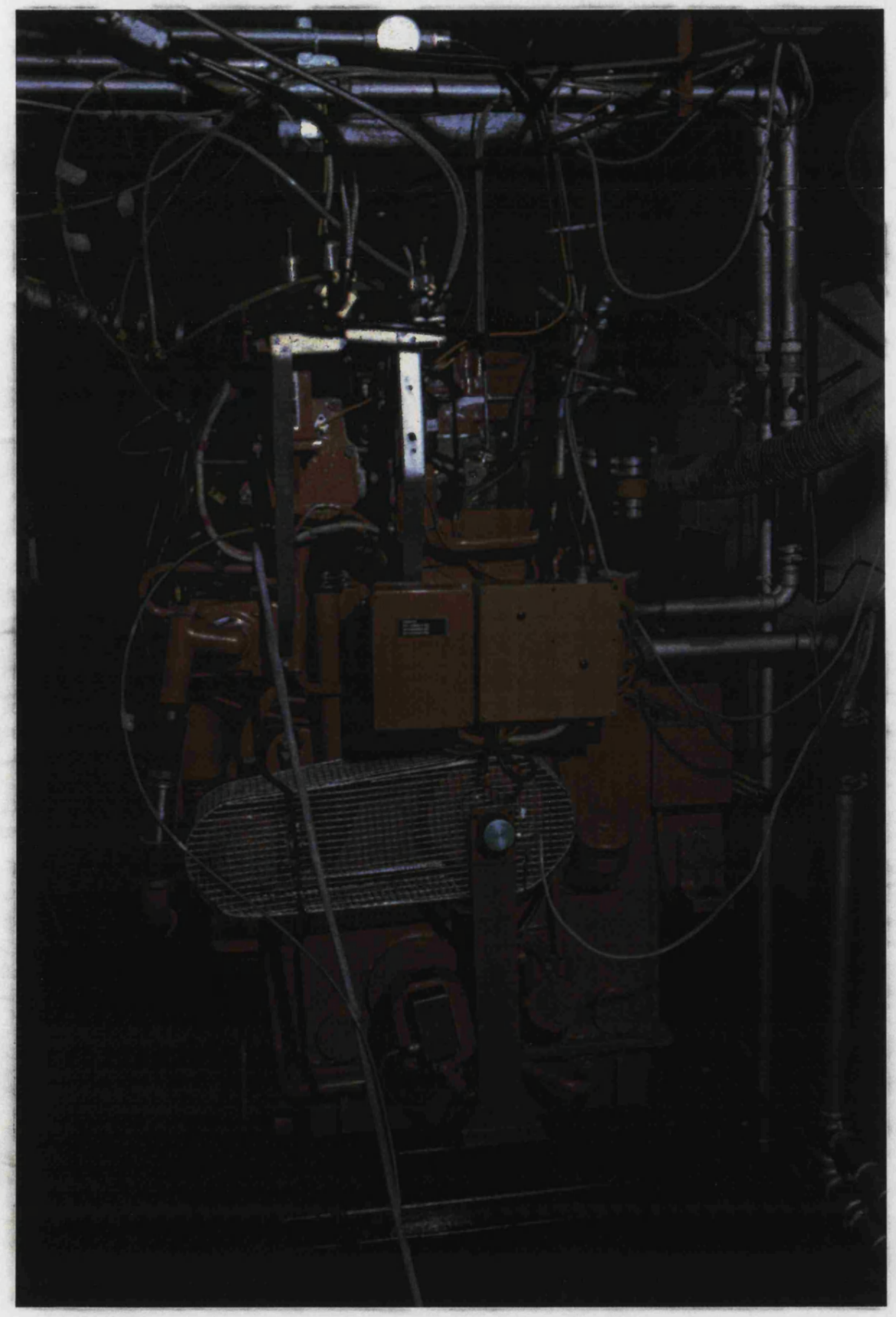

Plate 3. Front View of SE1 Engine Installation

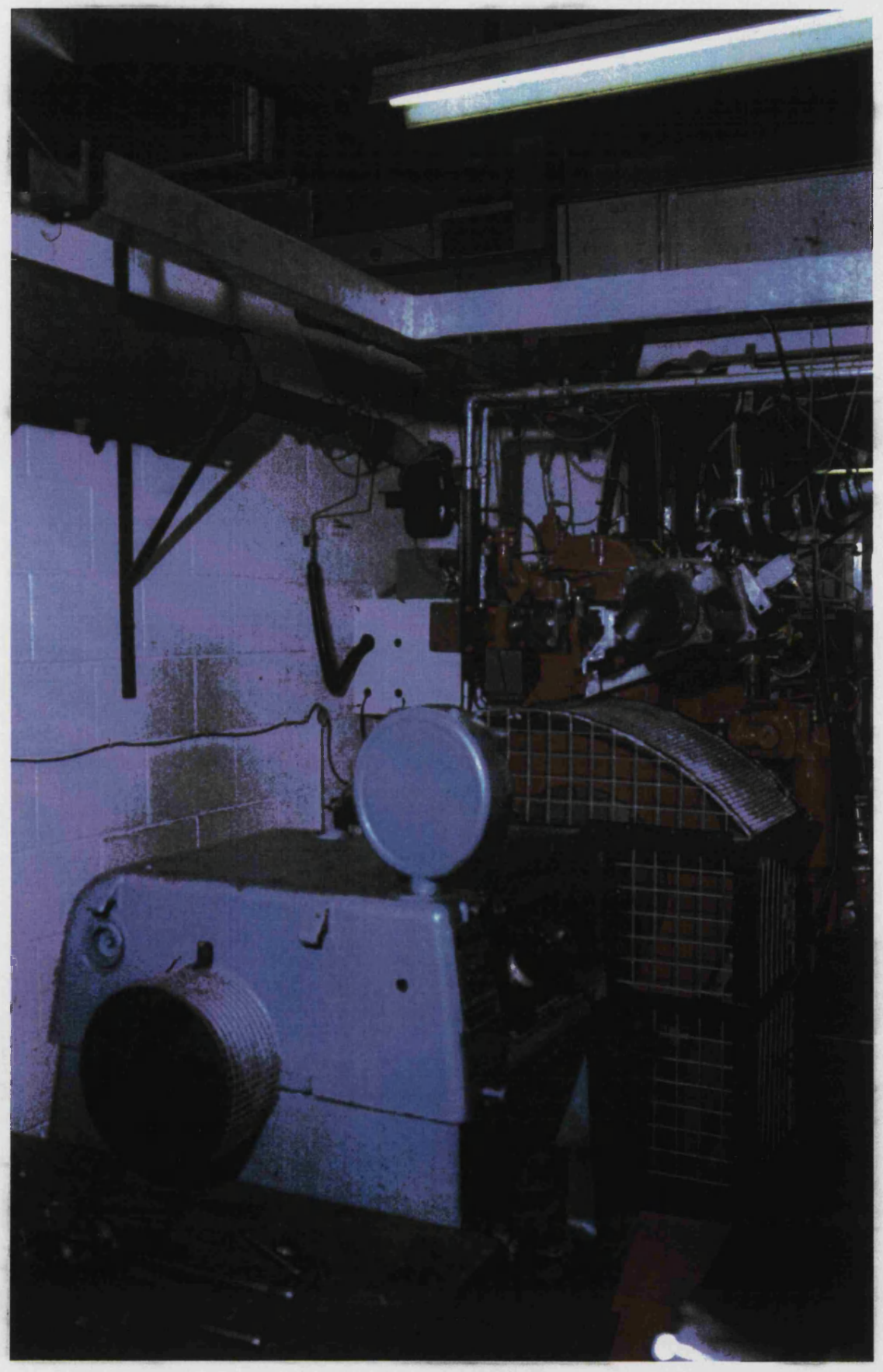

Plate 4. Rear View of SE1 Engine Installation

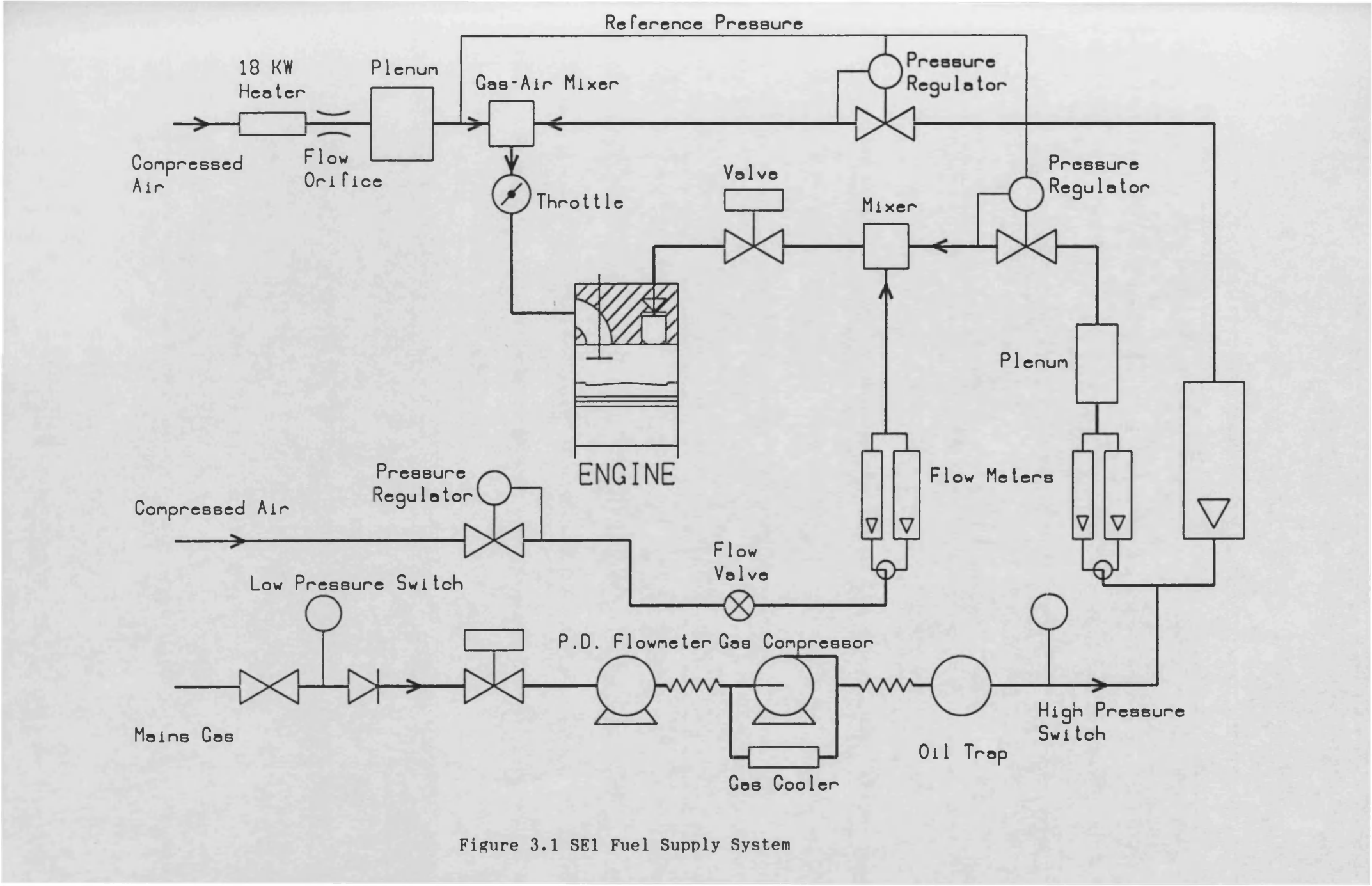

Figure 3.1 SE1 Fuel Supply System

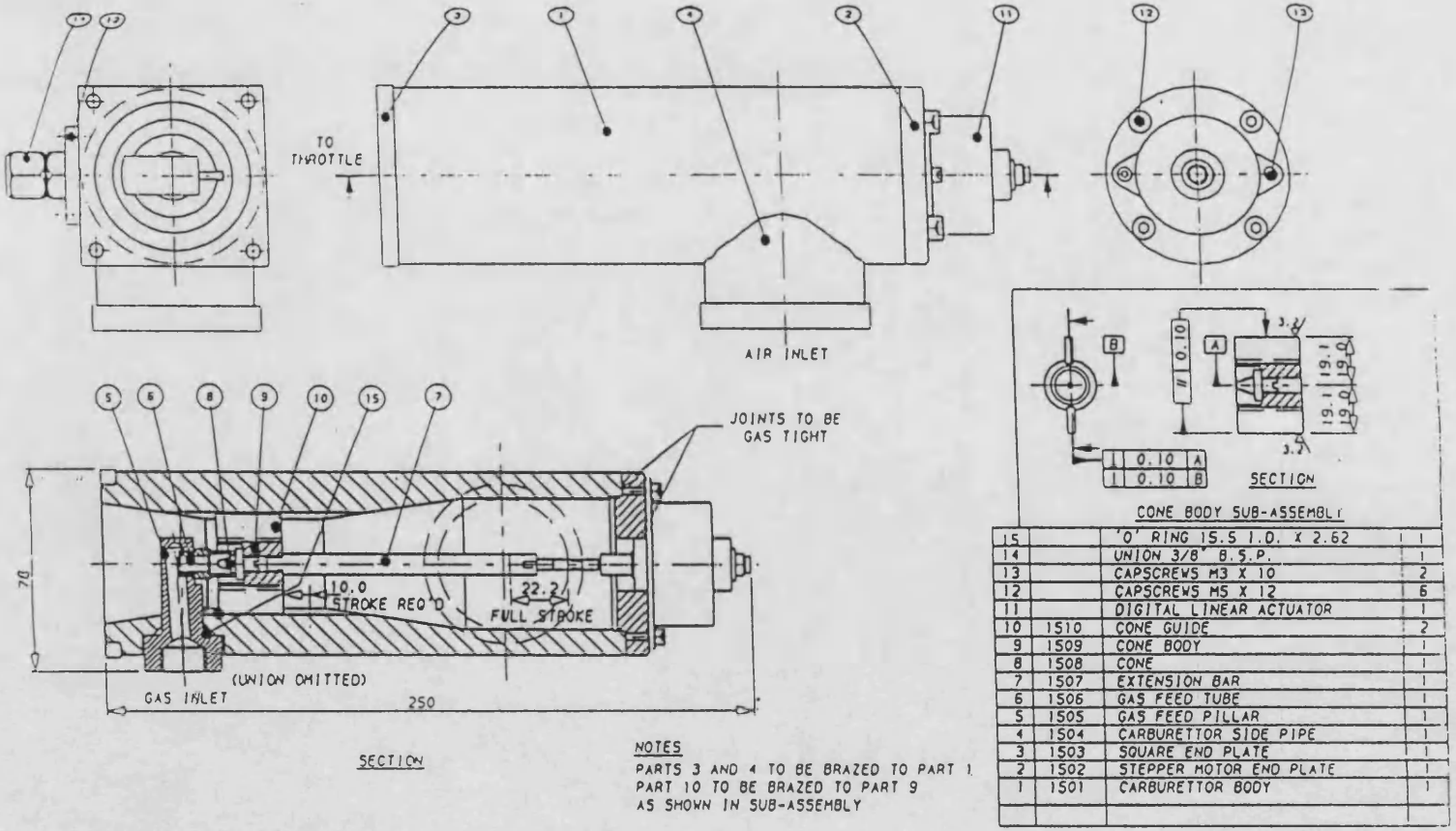

15		'O' RING 15.5 I.D. X 2.62	1
14		UNION 3/8" B.S.P.	1
13		CAPSCREWS M3 X 10	2
12		CAPSCREWS M5 X 12	6
11		DIGITAL LINEAR ACTUATOR	1
10	1510	CONE GUIDE	2
9	1509	CONE BODY	1
8	1508	CONE	1
7	1507	EXTENSION BAR	1
6	1506	GAS FEED TUBE	1
5	1505	GAS FEED PILLAR	1
4	1504	CARBURETTOR SIDE PIPE	1
3	1503	SQUARE END PLATE	1
2	1502	STEPPER MOTOR END PLATE	1
1	1501	CARBURETTOR BODY	1

Figure 3.2 Experimental Gas Mixer

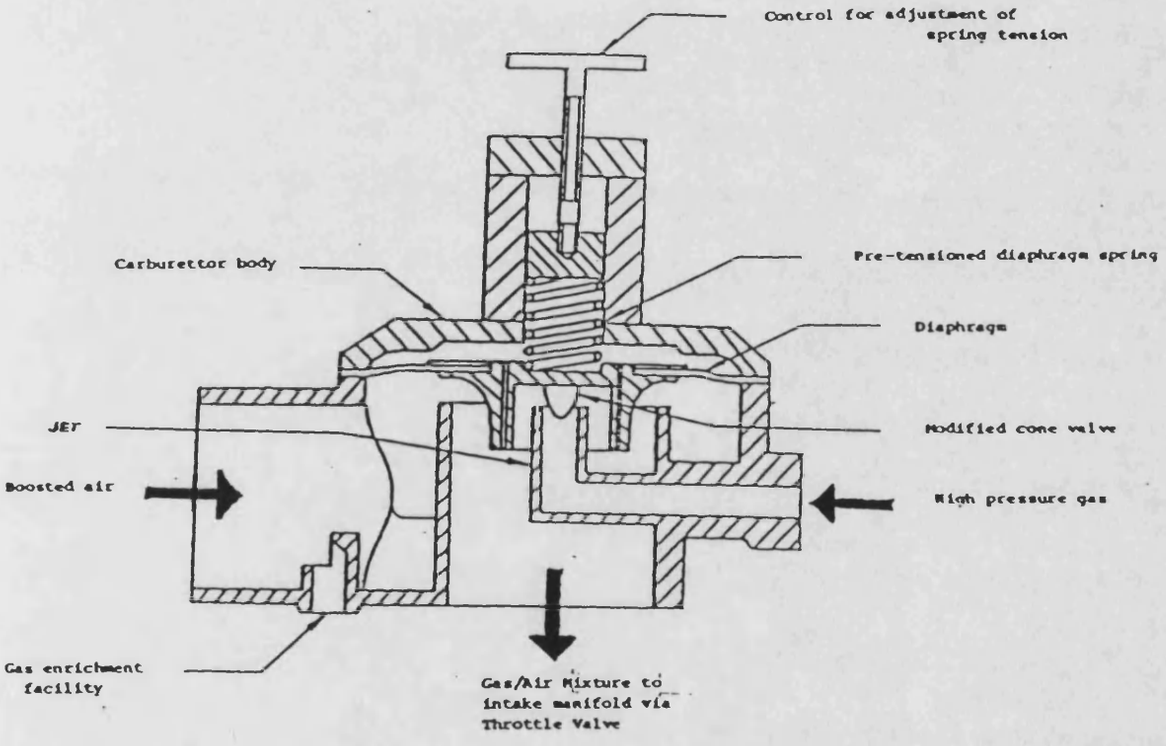

Figure 3.3 Modified Impco 200 Series Gas Mixer

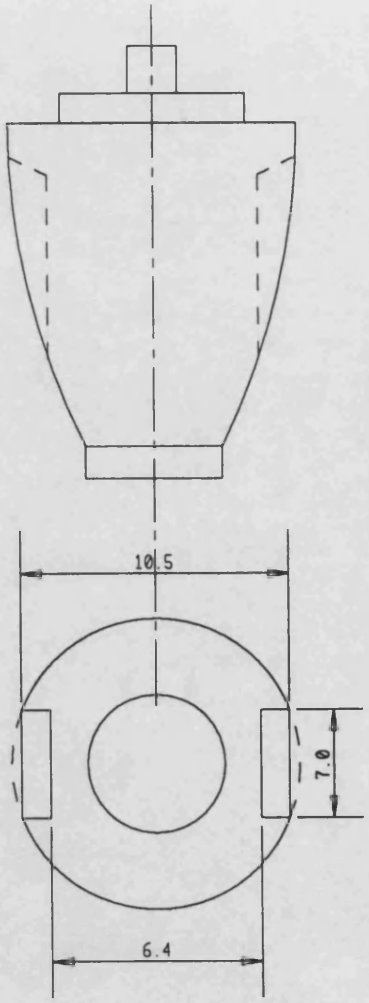

STANDARD IMPCO METERING CONE

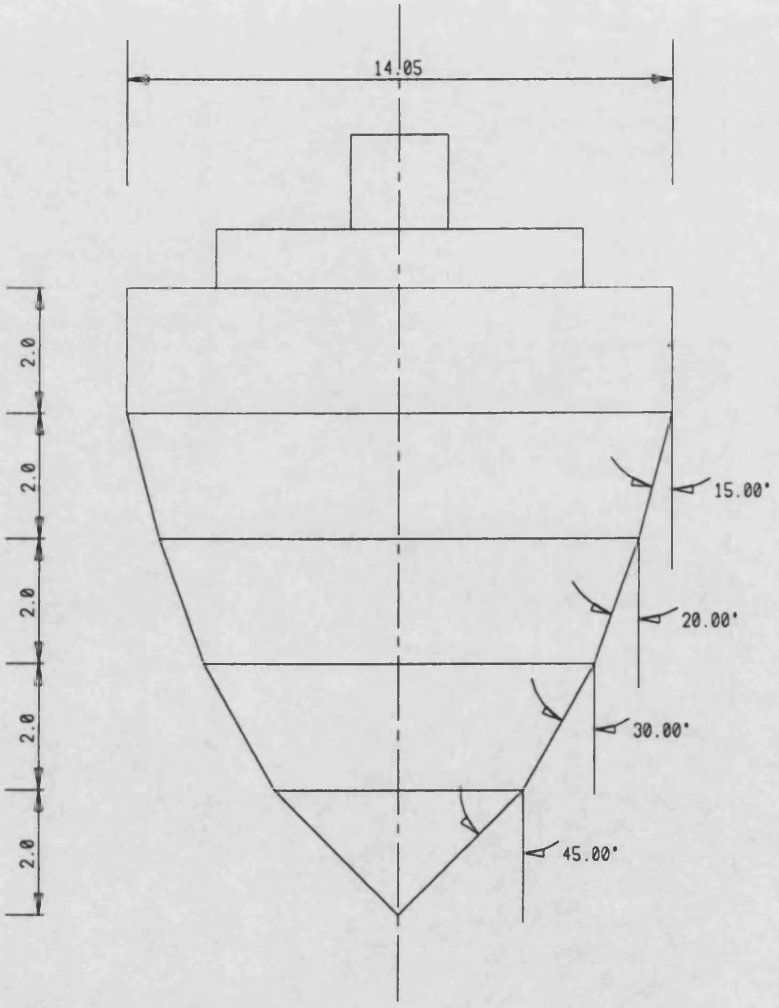

MODIFIED METERING CONE FOR SE1 GAS ENGINE

Figure 3.4 Standard and Modified Gas Metering Cones

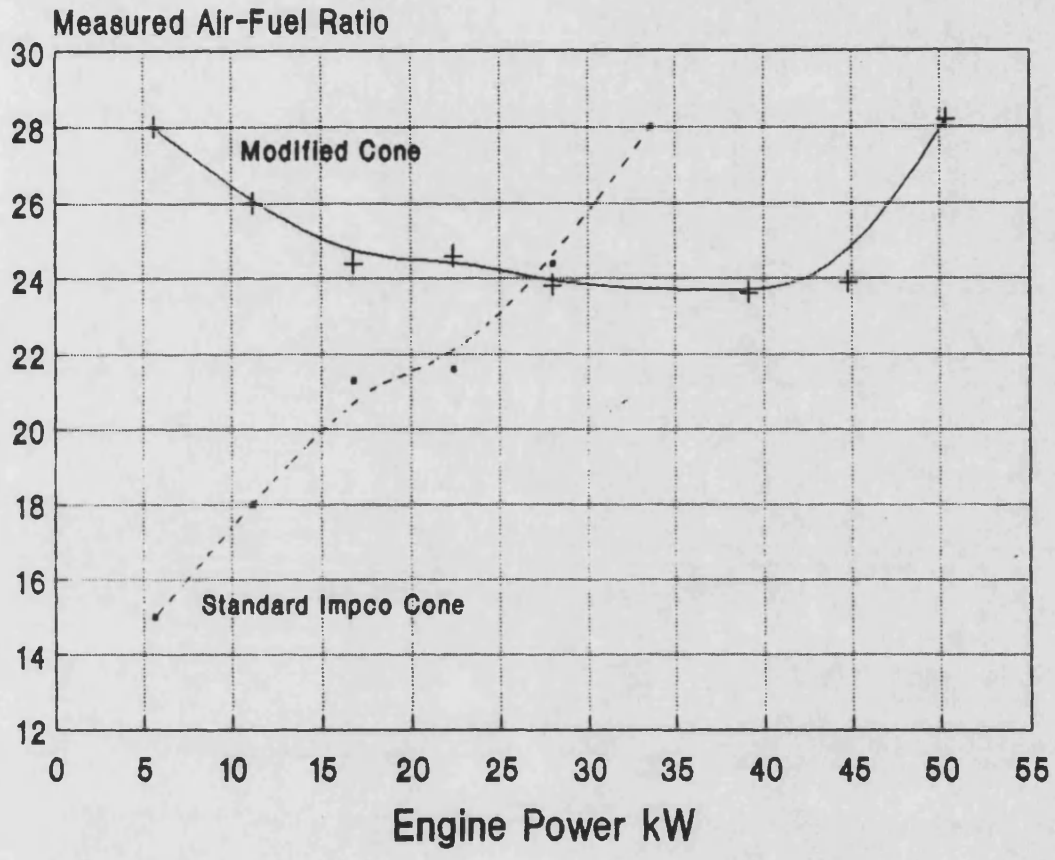

Figure 3.5 Gas Mixer Performance

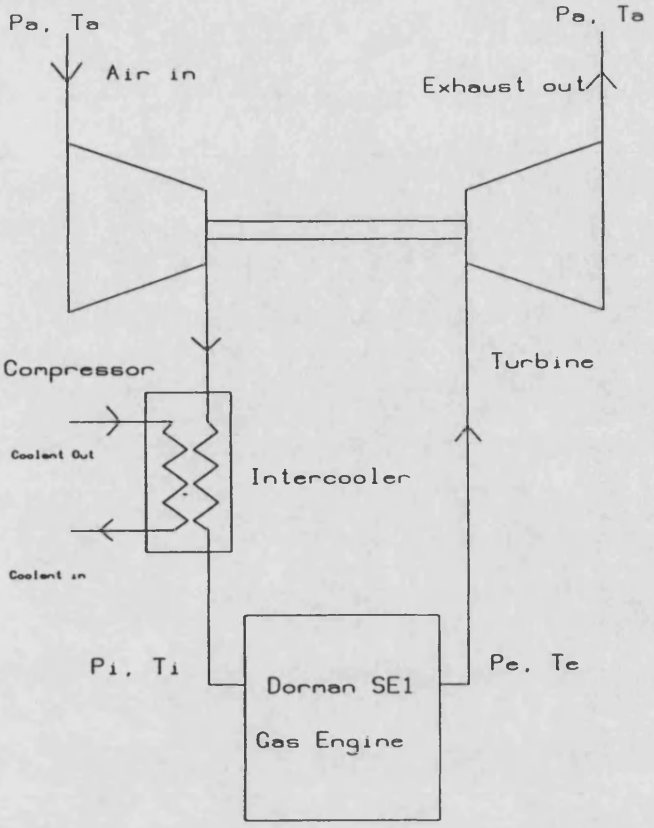

Figure 3.7 Theoretical Turbocharger System

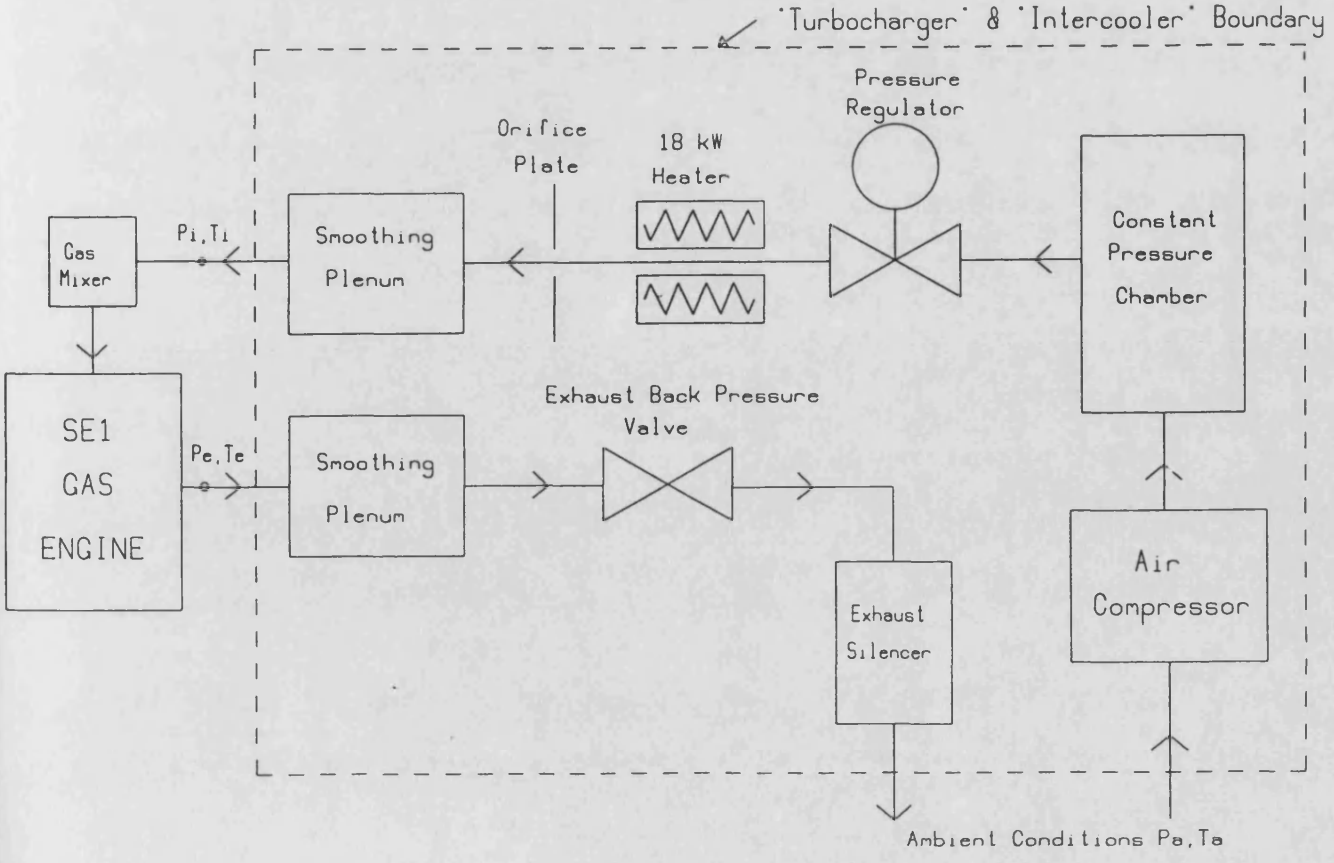

Figure 3.6 Artificial Turbocharger System

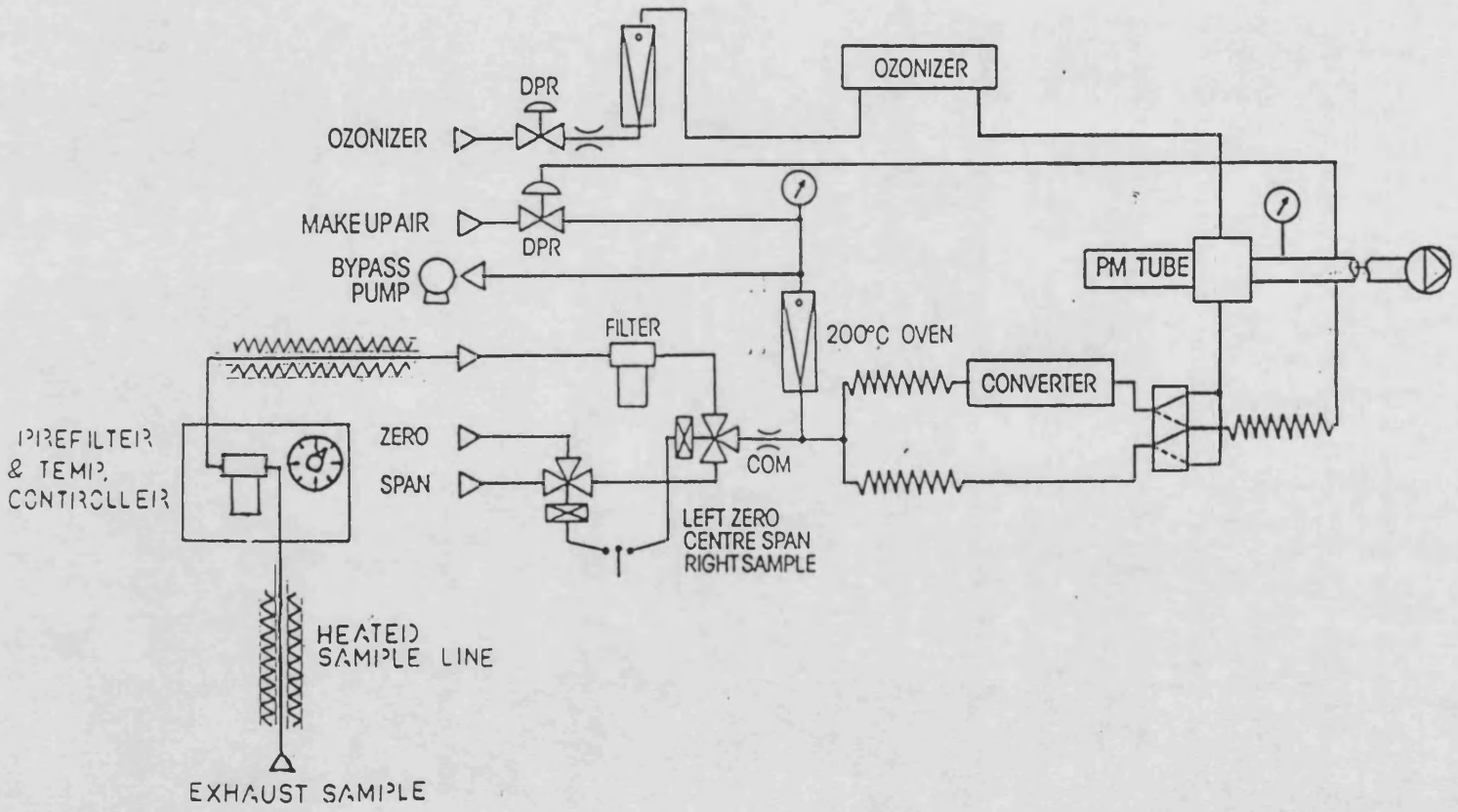

Figure 3.8 Schematic Diagram of Signal Chemiluminescent Analyser

Chapter 4

4. Engine Parametric study

4.1 Introduction

The objectives were to vary the main parameters of the combustion system and to examine their effects on engine performance and exhaust emissions, particularly of NOx. The parameters which were varied included main chamber afr, prechamber volume, prechamber fuel quantity and afr, ignition timing, and ambient temperature. These were chosen as they could be varied practically and are likely to significantly effect combustion. As explained in chapter 2, the formation of NOx is dependent on peak combustion temperature and duration, therefore parameters which affect combustion will have an effect on emissions of NOx. Other parameters such as compression ratio, prechamber geometry etc would also effect combustion, but it was not within our scope to vary these.

4.2 Experimental Procedure

As a starting point for the engine tests, values for each of the operating parameters were taken from data obtained by Dorman Diesels during earlier tests on a six cylinder 6SE prechamber engine. This included the turbocharger boost pressure and back pressure schedules which were adhered to throughout all the tests. These schedules are shown in figure 4.1. Parametric studies were performed at two load conditions, 6.9 bar and 10.3 bar bmep.

Before any testing was performed, the SE1 engine was started and run until a coolant temperature of approximately 80 degrees centigrade was reached by applying partial load. The NOx analyser was allowed to warm up before any measurements were taken in order

that the prefilter unit, sample lines and analyser could reach thermal equilibrium conditions. For each load and speed condition the "turbocharger" was set up to provide appropriate boost and back pressure conditions. This consisted of setting compressor boost pressure and corresponding intercooler outlet temperature to measured values from earlier tests performed by Dorman Diesels on their multi-cylinder engines. The exhaust back pressure was set to a calculated value to maintain an overall quasi-steady turbocharger efficiency of 55%. It was also assumed that the effectiveness of the Dorman air to air intercooler was 75%, and that the datum ambient temperature was 25 degrees centigrade.

All engine data apart from the high speed data, was entered into a data reduction program to process and format the data and provide permanent storage onto disc. This data could be recalled into the program later should further processing be required. A listing of this software is given in Appendix F. This software is also used in setting the correct turbocharger backpressure and intercooler exit temperature for given engine operating conditions.

4.3 Ignition Timing Study

Ignition timing was varied over the range 9 deg to 20 deg btdc. Figure 4.2 shows the result of timing variation on engine performance and NOx emission for three different main chamber mixture strengths. It shows that specific fuel consumption seems to vary very little over the range. NOx emission, however, increases as the timing is advanced. This is as expected since advancing ignition timing produces greater peak cylinder pressures and temperatures and hence increased NOx production. It should be

noted that the rate of increase of NOx emission with respect to ignition advance is significantly greater the richer the main chamber mixture is. This means that at lean main chamber air-fuel ratios, greater than 28:1, the effect of ignition timing on NOx emission is small.

An important variable which is not shown in figure 4.2 is engine knock. The knock that was detected was very light and since it did not appear on the main chamber pressure trace, was believed to be occurring in the prechamber. This prechamber knock appeared to be very much ignition timing dependent, but not as expected. As ignition timing was advanced, instead of the prechamber knock increasing as would be expected in a conventional spark ignition engine, due to increased cylinder pressure and temperature, it actually deminished. This was a surprising observation, but can, however, be explained by the relatively small volume of the prechamber, and hence the time taken for all the mixture to be burnt is very short. Combustion in the prechamber may be complete before the maximum compression pressure is reached. Hence if ignition timing is advanced, pressure and temperature during combustion in the prechamber are reduced, as is the tendency for knock.

4.4 Prechamber Study

The initial test program began with an investigation into the fundamental prechamber variables around one prechamber geometry. There are two important variables to be considered, the air-fuel ratio of the mixture supplied to the prechamber (quality) and the amount of mixture supplied per cycle (quantity).

When considering the first, air-fuel ratio, one must remember that this is merely the air-fuel ratio supplied to the prechamber, and that during the compression stroke this will be greatly diluted as it is mixed with the very lean charge of the main combustion chamber. An illustration showing the three stages of this process is shown in figure 4.3. In the first stage, during the induction stroke, a rich gas mixture (3:1 or richer) enters the prechamber through the admission valve, filling the prechamber and purging it of the residual gas from the previous cycle. Any excess mixture will pass into the main chamber through the connecting nozzle. At the second stage, shown in figure 4.3, a high velocity jet of leaner mixture (approx 25 - 30:1) is forced into the prechamber through the connecting nozzle during the compression stroke. This jet of lean mixture entering the prechamber mixes with the rich mixture, leaning it down, until at the final stage just before ignition, a mixture close to stoichiometric (17:1) is established in the vicinity of the spark plug.

The second of the two parameters, the quantity of mixture, needs to be more carefully defined if meaningful and consistent results are to be obtained. One logical way of considering the flow of gas is to define a filling ratio, λ, to show the extent to which the prechamber is filled. This is defined as follows:

$$\lambda = \frac{\text{Volume of Prechamber Charge at Manifold Pressure}}{\text{Volume of Prechamber}}$$

As gas flow rate by volume is obviously pressure and temperature dependent, for consistent, comparable results, the delivered gas flow rate must be corrected. It is therefore

corrected to manifold conditions for pressure and temperature, since this is approximately the state prevailing in the cylinder during induction.

An initial parametric map for the 10 cc prechamber, shown in figure 4.4, was produced. The map for prechamber mixture quality against prechamber mixture quantity is shown in figure 4.5. An overall air-fuel ratio of approximately 24:1 was maintained during the tests and load was kept constant at 6.9 bar, just over half load. All other parameters were kept constant, so far as possible. Although many of the parameters were set at unfavourable values as far as engine performance and emissions were concerned, the map clearly shows the effect of the two prechamber parameters on NOx emissions.

The operating envelope of the map was found to be enclosed by three boundaries. A lean limit boundary across which misfire of the main charge occurs either bacause the prechamber mixture itself is too lean to be ignited by the spark, or because the flame front contains insufficient energy to ignite the lean main charge. As the engine is known to stall completely at this boundary, it suggests that the first of these theories is more likely. A rich limit boundary across which unstable combustion occurs makes up another side of the operating envelope. At this point the mixture in the prechamber is so rich that it can not be reliably ignited by the spark, and severe prechamber knock occurs. Finally, the remaining boundary of the window consists of a physical limit to the maximum quantity of charge that can be supplied to the prechamber with the present components. This boundary could be moved if modifications were made to the fuel supply system, particularly to the prechamber disc valve, although

it will ultimately be limited by choking of the supply system.

From this map, several deductions can be made regarding the influence of the prechamber on exhaust emissions of NOx. Firstly, and perhaps most importantly, it shows that the prechamber does indeed play a significant part in NOx emissions, despite the fact that its volume is less than 3 % of the clearance volume in the main chamber. This is due to the high temperatures associated with stoichiometric combustion in the prechamber which cause production of NOx. Substantial reductions can therefore be made by optimising the two prechamber parameters, as is clearly shown. The map also shows that the engine can be operated quite satisfactorily with a pilot supply of neat gas only to the prechamber, albeit at very low filling ratios. The map shows that NOx emissions as low as 2 g/kWh can be achieved with gas only. However operating in this region does have disadvantages. Firstly, very accurate control of such small flow rates would be required as the operating range for low NOx emissions is greatly reduced, and secondly low filling ratios mean reduced scavenging leading to higher temperatures and reduced spark plug life. Also to be noted is the fact that the lean limit boundary runs close to parallel with the contours of constant NOx emission. This means that there is quite a wide range of values of filling and air-fuel ratio where minimum NOx can be obtained.

With the information gained from this initial prechamber map, further testing was performed to create the prechamber map shown in figure 4.6 . This was produced with the engine running close to the manufacturers maximum rated load (10.33 bar bmep), together with a more favourable air-fuel ratio, with respect to NOx emission, of approximately 27.5:1. Ignition timing had, however

been advanced to 14 degrees btdc from the previous value of 9 degrees btdc as the result of the ignition timing study, in order to reduce prechamber knock to a more acceptable level. This earlier timing is, however, slightly less favourable with regard to NOx emission.

This second map, as would be expected, takes the same shape as the first, except for the fact that it appears slightly truncated in comparison. This was to be expected, as this second map was obtained at a higher load, and hence higher boost pressure. Therefore the pressure drop across the prechamber disc valve will be reduced during the induction stroke as prechamber conditions will be similar to manifold conditions during this period. Another theory is that a flow to the prechamber can occur during the exhaust stroke if the back pressure is not too great. This may occur at low loads when "turbine" back pressure is low, but is less likely at high loads when back pressure is greater.

The important point to note about this map is that the target NOx emission level of 2 g/kWh at full rated load can be achieved if the prechamber is operated close to the lean misfire limit. Typically, a gas engine running close to stoichiometric conditions would produce NOx emission levels of perhaps ten times this amount.

Having mapped the two prechamber variables, air-fuel ratio and filling ratio at two engine operating points for the initial 10 cc prechamber, the prechamber itself was changed. The second prechamber, see figure 4.4, was of the same design as the first. The only difference was that its volume had been increased from 10 cc to 15 cc by increasing the chamber height. Similar prechamber

maps were then obtained for this larger volume. The object was to assess the effect of prechamber volume on NOx emission. If a large proportion of the NOx is produced in the prechamber, it would be expected that NOx emissions would be greater for this second prechamber.

Figures 4.7 and 4.8 show prechamber maps for the 15 cc prechamber at the two loads previously mapped for the 10 cc prechamber. Unfortunately the map at half load cannot be directly compared with the earlier map as it was obtained for a much leaner main chamber air-fuel ratio of approximately 28.5:1. However it does show the potential NOx emission reduction, albeit at half load. At the optimum region of the map, close to the lean misfire limit, its lowest value is 0.5 g/kWh .

For the map at the high load, however, the data was recorded with identical engine operating parameters to allow a direct comparison between the two prechamber volumes to be made. However, as can be seen, there appears to be very little difference between the two maps. Values for the prechamber filling ratio are much lower. This is due to the fact that its volume is 50 % greater, but the size of the gas admission valve and the delivery pressure of the pilot mixture had not been changed.

4.5 Main Chamber Study

An investigation was made into the effect of main chamber parameters on engine performance and emissions. Prechamber parameters were set at favourable but stable values, close but not too close to the lean misfire operating limit. Filling ratio was maintained at unity and prechamber air-fuel ratio at 3:1 for all

the main chamber testing. These were chosen as they could be maintained at both full and half load conditions.

As far as ignition timing was concerned, a compromise setting had to be made. Retarding the ignition meant reduced NOx emissions, but however, this caused prechamber knock to worsen, as explained earlier. An ignition timing of 12 degrees btdc was chosen.

Testing was done at various engine loads and main chamber air-fuel ratios while all other engine operating parameters were maintained constant with the exception of those necessary to maintain correct turbocharger performance as given by the schedule. The results of this exercise are best shown as a load versus air-fuel ratio map, as can be seen in figure 4.9.

The range of main chamber air-fuel ratio was from 23.5:1 to slightly more than 28:1 under full load conditions. During the engine tests, it was observed that richer mixtures are required at lower loads to avoid engine misfire. This may be explained by the fact that the ignition timing is not automatically varied with engine load. At low loads, a more advanced ignition timing is required for maximum thermal efficiency. The range of loads were from 3.5 bar bmep to approximately 10.5 bar bmep, just below the original target full load. Testing at higher loads was only prevented by a "tailing off" of main chamber air-fuel ratio caused by reduced boosted gas pressure limited by gas compressor capacity.

Contours for variables of interest have been shown on this map. As is to be expected, NOx emission increases rapidly as main

chamber air-fuel ratio is enriched, from 1 g/kWh at 28:1 to 10 g/kWh at 24:1 at a load of 6 bar bmep. Correspondingly exhaust temperature is seen to decrease over this range from 600 C to 540 C. It is shown that for a given load, exhaust temperature can provide a reasonable indication of the main chamber air-fuel ratio. From this map the brake thermal efficiency appears to hold constant as mixture is leaned off. One might have expected a slight loss of efficiency as very lean mixtures are reached due to reduced flame speeds.

It should be noted that the values for thermal efficiency are not totally realistic as this is a single cylinder engine and so has proportionately higher frictional and cooling losses than a multi-cylinder engine. Realistically, 2 or 3 % could be added to these values to bring them in to line with a multi-cylinder engine. This compensation can be determined experimentally by plotting the Willans line, fuel consumption versus load, for both the single and multi-cylinder engines. By comparing these, the proportional extra frictional forces for the single cylinder engine can be determined. A Willens line for the SE1 engine has been produced and is shown in figure 4.10. The frictional mean effective pressure (fmep) is shown to be approximately 2 bar.

4.6 Ambient Temperature Study

The effect of ambient temperature cannot be studied on a multi-cylinder production engine with a real turbocharger, unless a special enviromental cell is avaliable. However, as the SE1 engine uses a simulated turbocharger system as described in chapter 3, there is an ability to vary the effective ambient temperature. The effect of ambient temperature is important as an

engine may be required to operate in a variety of environments with fluctuations due to both day and night operation and seasonal variations.

Figure 4.11 shows the response of the engine to variation in simulated ambient temperature over the range 5 - 40 deg C. The turbocharger efficiency, boost pressure and intercooler effectiveness were held constant during the tests. It can be seen that, as a result, main chamber air-fuel ratio decreased slightly with increasing ambient temperature. This is due to reduction in the air density entering the engine. This effect combined with increasing charge temperature causes the emission of NOx to increase by a factor of 4, from 0.6 to 2.3 g/kWh.

4.7 Summary

A parametric study of the SE1 prechamber gas engine has been performed. Operating envelopes of prechamber fuelling parameters for two sizes of prechamber and at two loads have been established in which stable running of the engine can be maintained. Within these envelopes, areas of optimum engine performance and emissions have been identified.

Ignition timing was shown to have a significant effect on engine performance, emissions of NOx and engine knock. Advancing the ignition timing increased thermal efficiency but also increased exhaust emissions of NOx. Interestingly, retarding the ignition was found to increase prechamber knock. This was believed to be as a consequence of the extremely short duration of burning in the prechamber, completion occurring before peak cylinder pressure has been reached. An ignition timing of 12 deg

btdc was considered as a satisfactory compromise for thermal efficiency, NOx emission and prechamber knock.

A study of main chamber air-fuel ratio showed this parameter to have a first order effect on the exhaust emissions of NOx. The lowest levels of NOx coinciding to the leanest values of air-fuel ratio. The extent to which the air-fuel ratio could be increased was limited by the misfire limit. This was found to be approximately 28:1 at high loads. No measureable reduction in the thermal efficiency of the engine was noted as the air-fuel ratio was increased to this limit.

An experiment to investigate the effect of ambient temperature proved to be difficult as this parameter has a second order effect on air-fuel ratio. It appears that an increase in ambient temperature will significantly increase NOx emission.

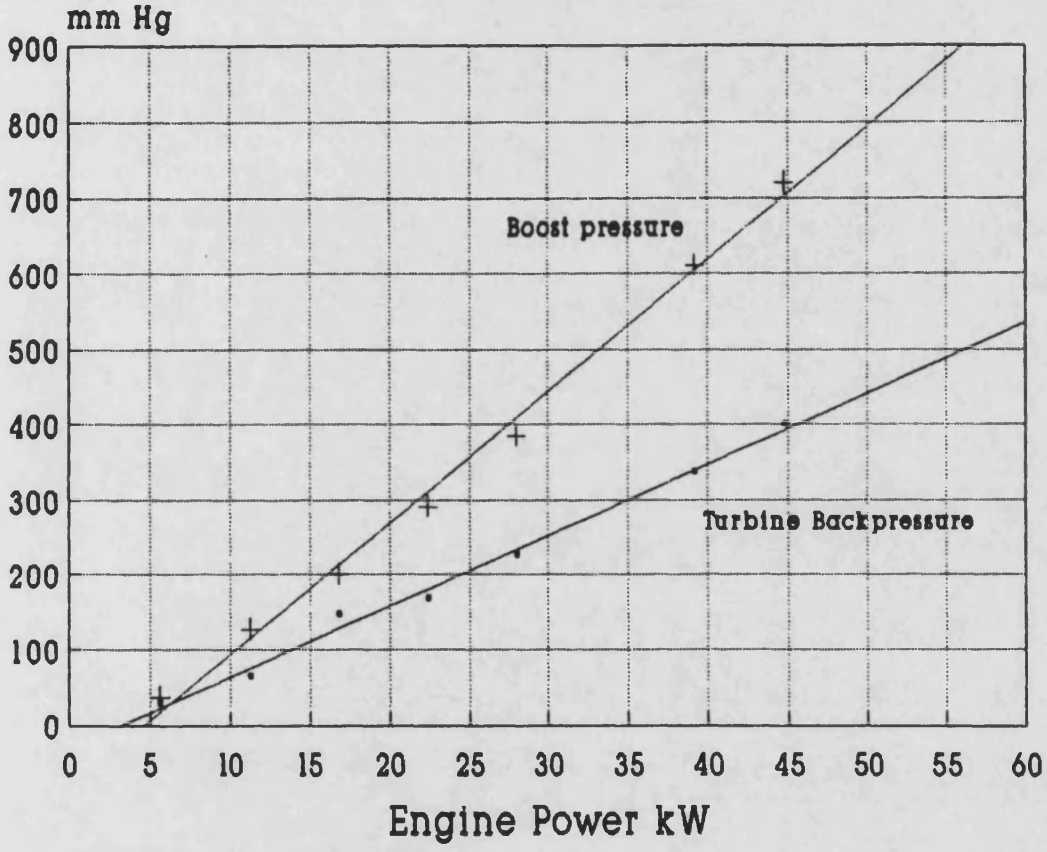

AT 1500 RPM FOR TURBO EFFICIENCY OF 55%

Figure 4.1 Turbocharger Boost and Back Pressure Schedule

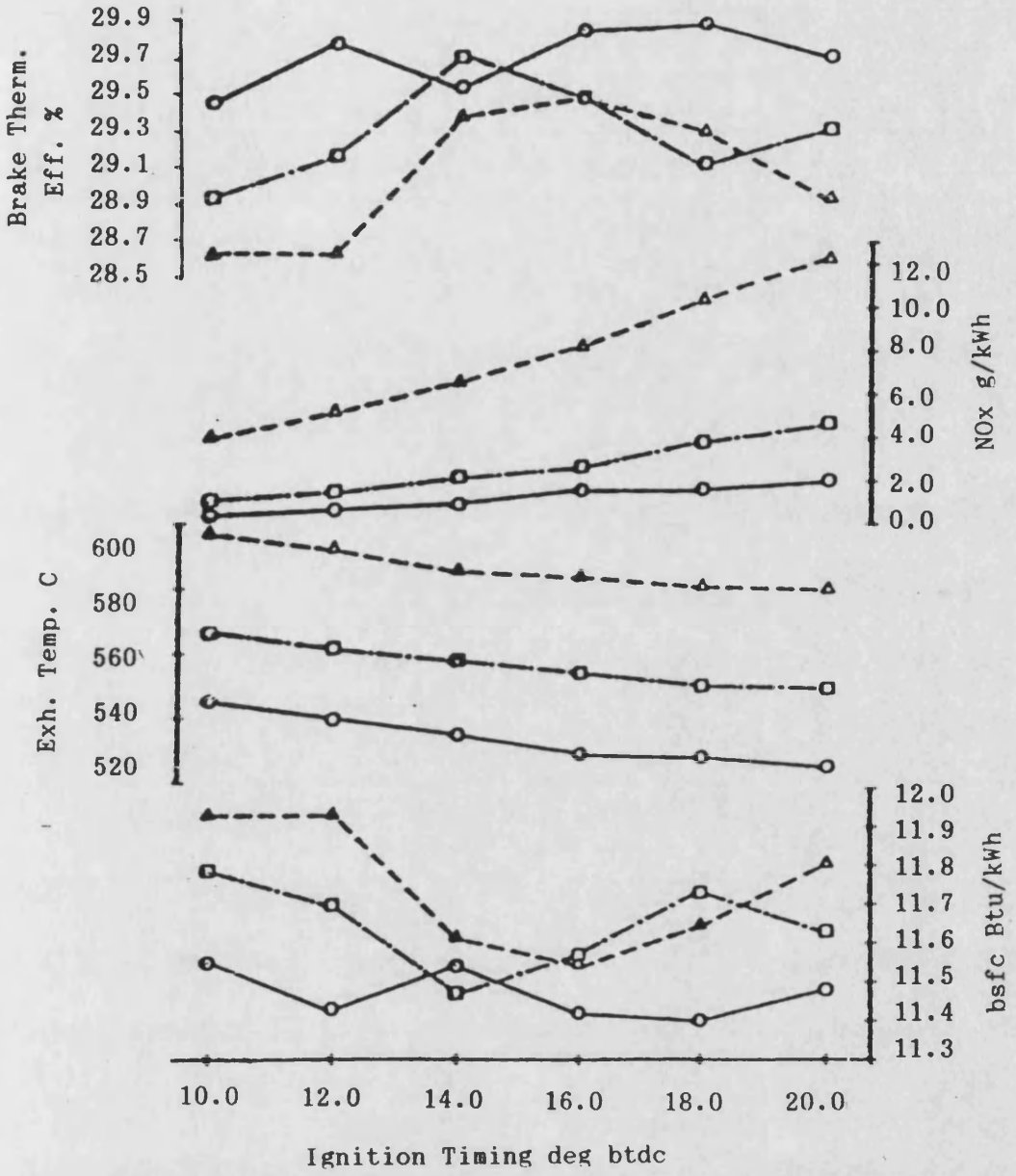

Figure 4.2 Response of Engine to Variation in Ignition Timing

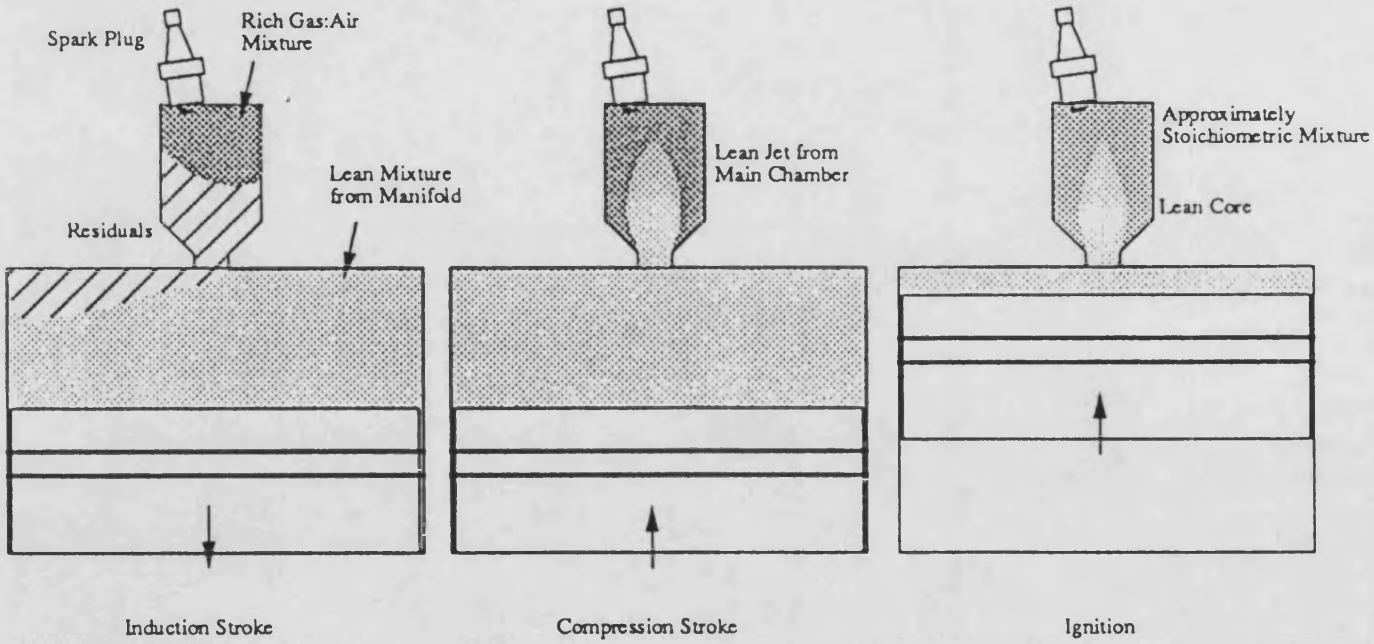

Figure 4.3 Mixture Preparation in a Prechamber Gas Engine

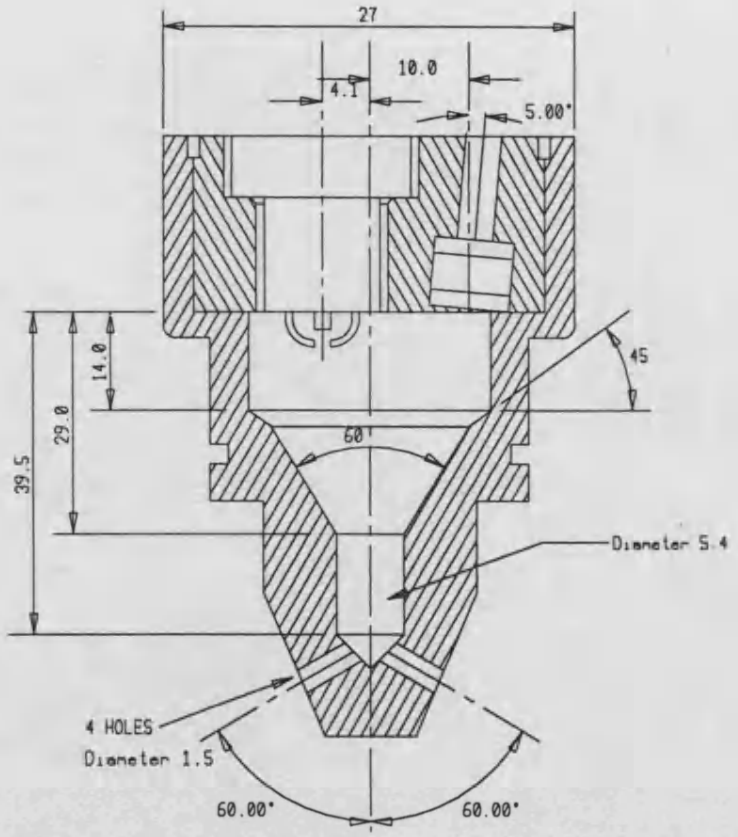

SECTIONAL VIEW OF 10cc PRECHAMBER

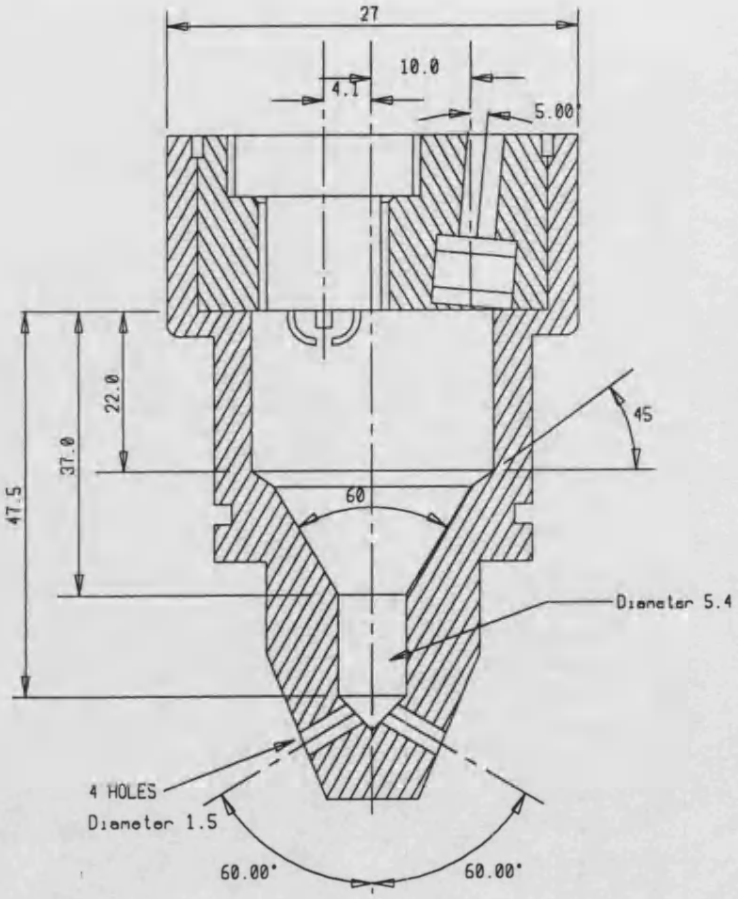

SECTIONAL VIEW OF 15cc PRECHAMBER

Figure 4.4 10cc and 15cc Prechamber Geometries

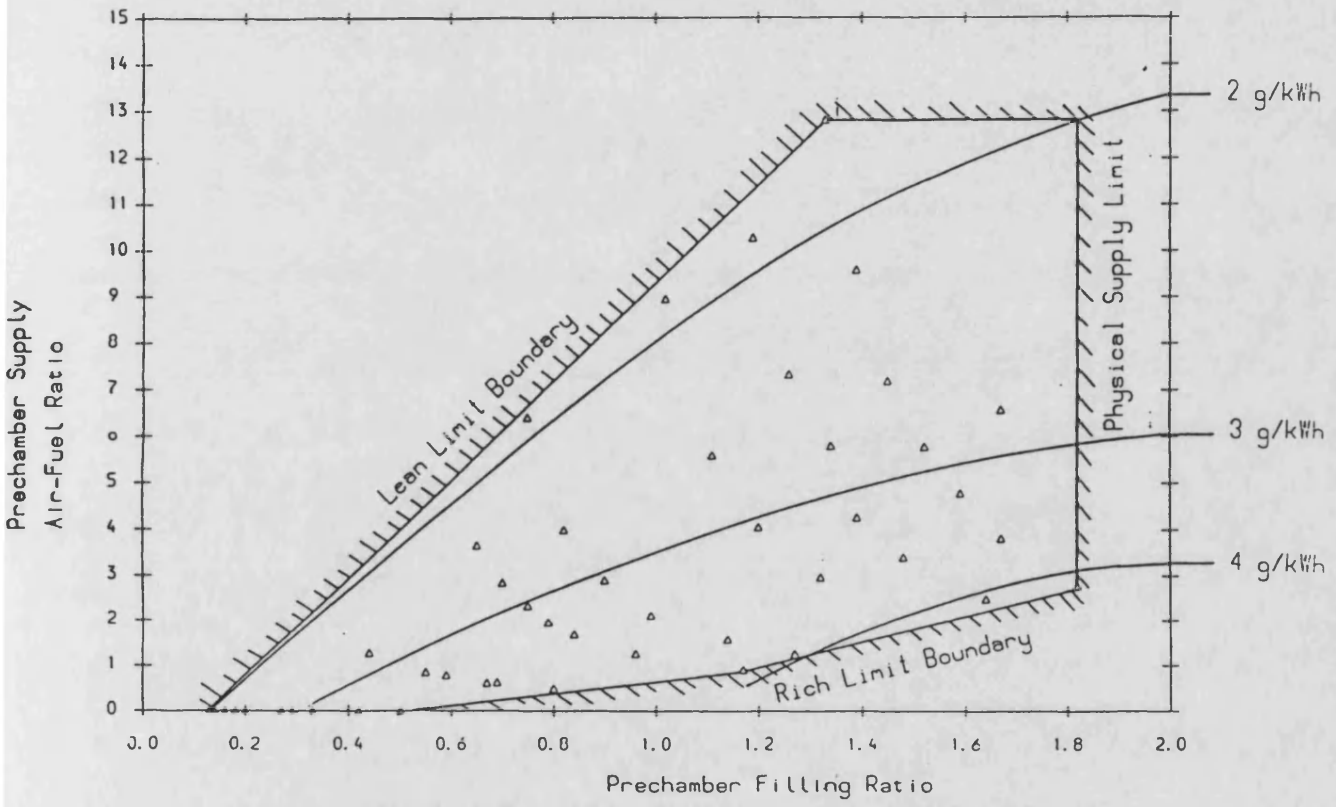

Schedule

Speed	1500 rpm
bmep	6.9 bar
afr (Overall)	24:1
Turbo eff.	55%
I/cooler eff.	75%
Intake Temp.	37C
Ign. Timing	9 btdc
Prechamber Vol	10cc

Figure 4.5 10cc Prechamber Fueling Map at 6.9 bar bmep showing the feasible operating region and contours of NOx production.

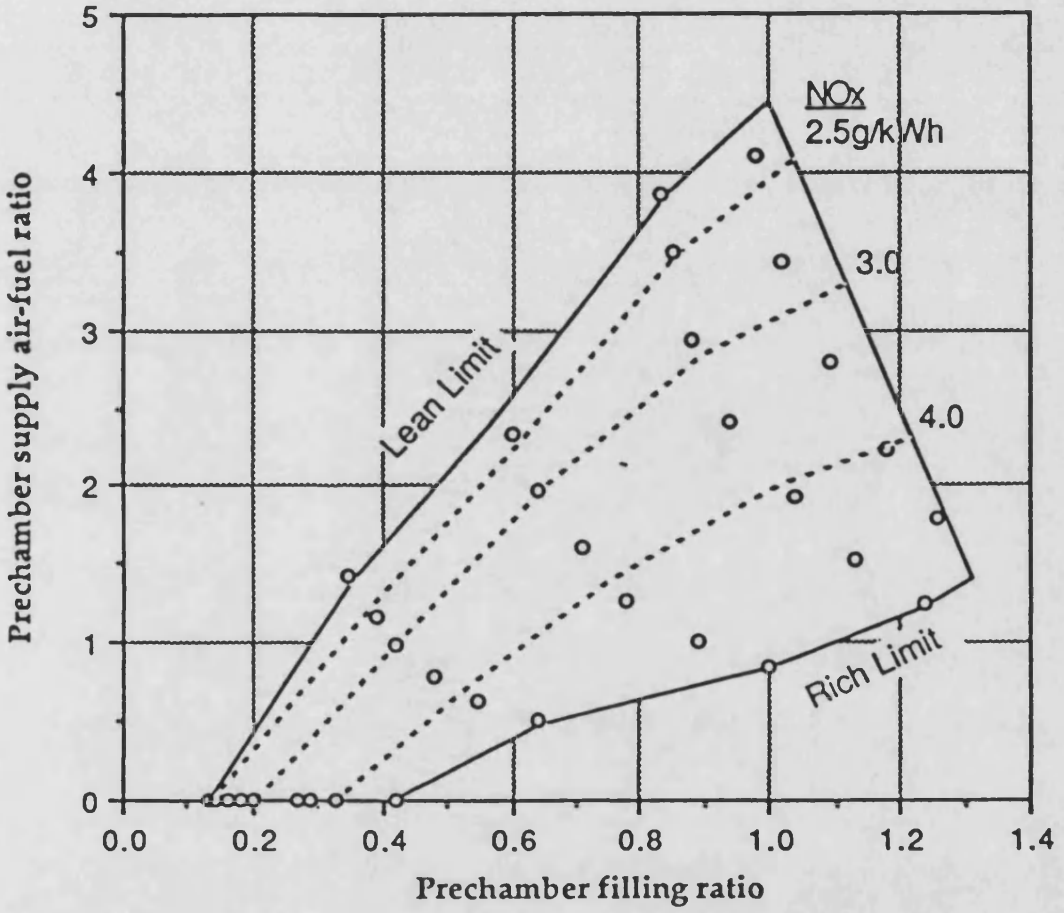

Schedule

Speed	1500 rpm
bmep	10.33 bar
afr (Overall)	27.5:1
Turbo eff.	55%
I/cooler eff.	75%
Intake Temp.	42C
Ign. Timing	14btdc
Prechamber Vol	10cc

Figure 4.6 10cc Prechamber Fueling Map at 10.33 bar bmep showing the feasible operating region and contours of NOx production.

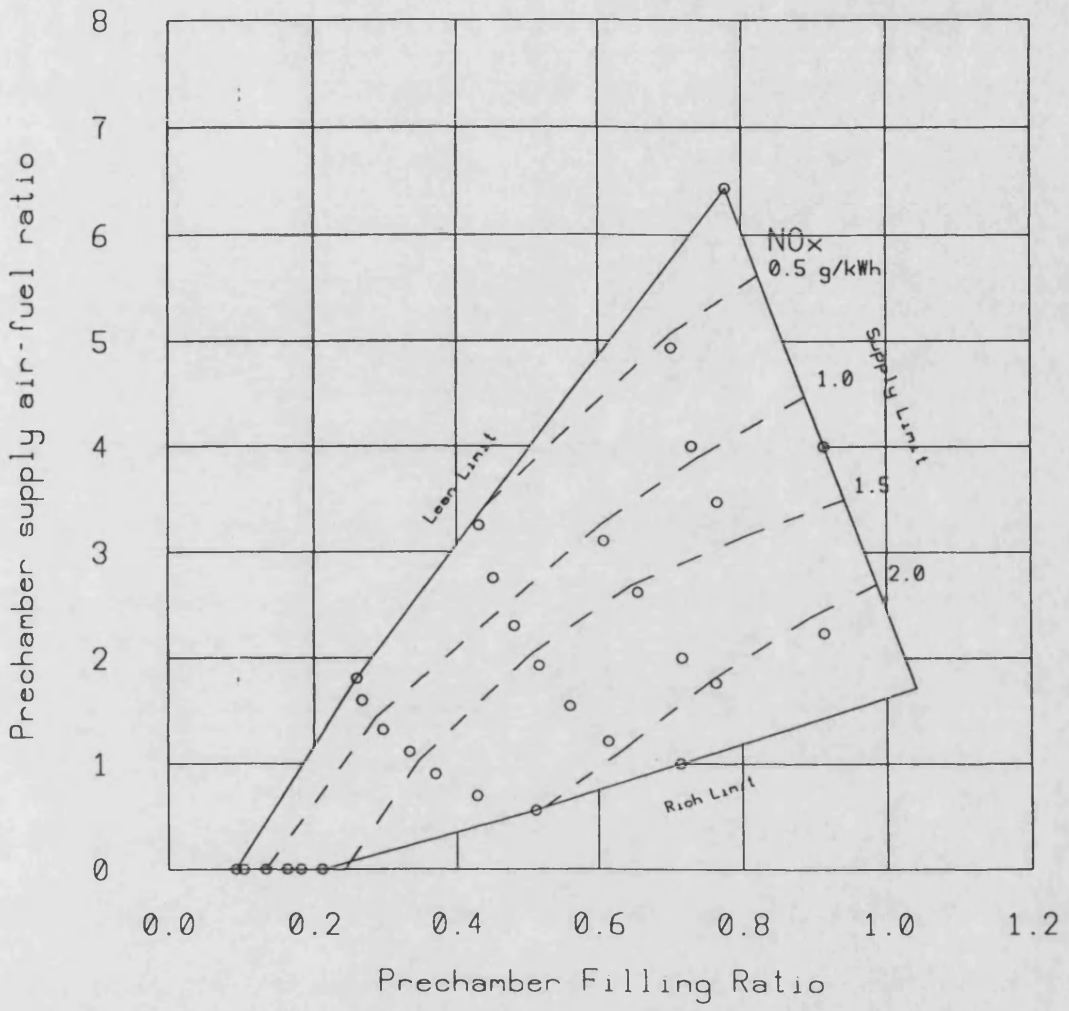

Schedule

Speed	1500 rpm
bmep	6.9 bar
afr (Overall)	28.5:1
Turbo eff.	55%
I/cooler eff.	75%
Intake Temp.	42C
Ign. Timing	14 btdc
Prechamber Vol	15cc

Figure 4.7 15cc Prechamber Fueling Map at 6.9 bar bmep showing the feasible operating region and contours of NOx production.

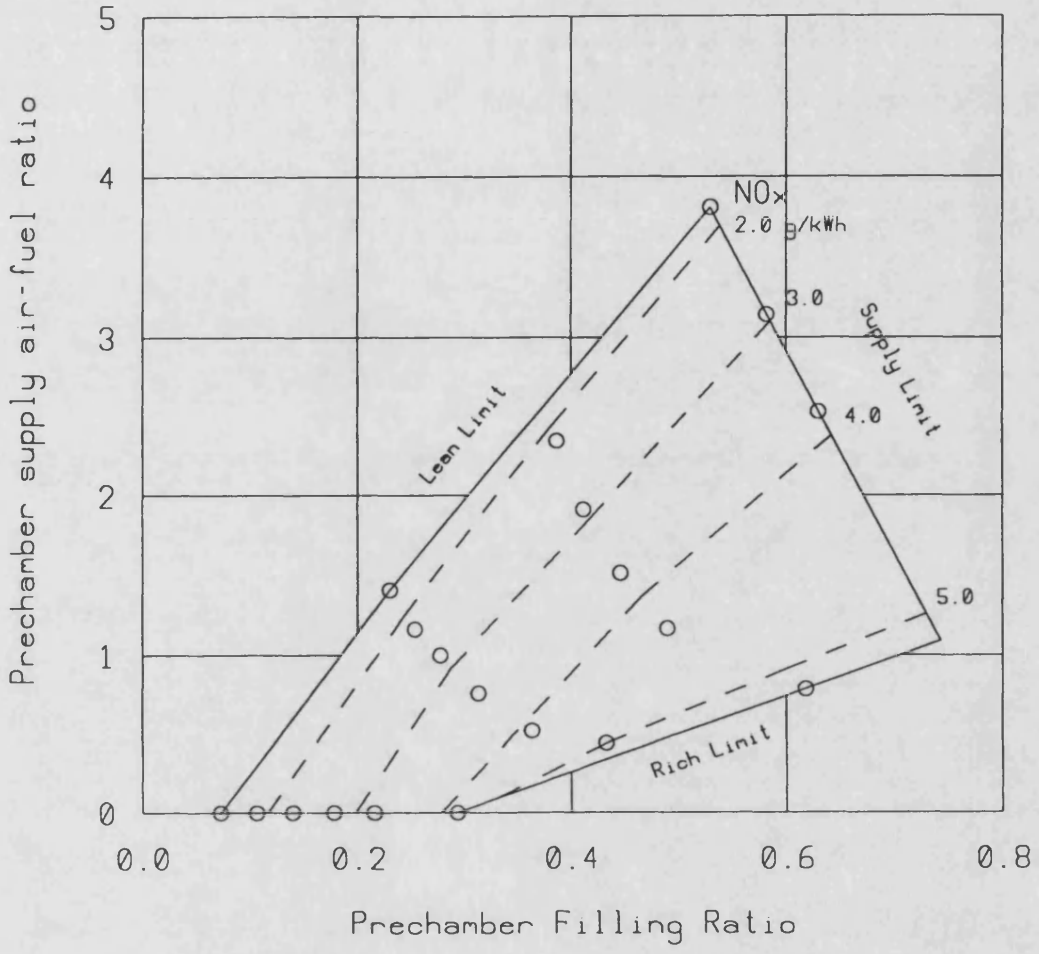

Schedule

Speed	1500 rpm
bmep	10.33 bar
afr (Overall)	28:1
Turbo eff.	55%
I/cooler eff.	75%
Intake Temp.	42C
Ign. Timing	14 btdc
Prechamber Vol	15cc

Figure 4.8 15cc Prechamber Fueling Map at 10.33 bar bmep showing the feasible operating region and contours of NOx production.

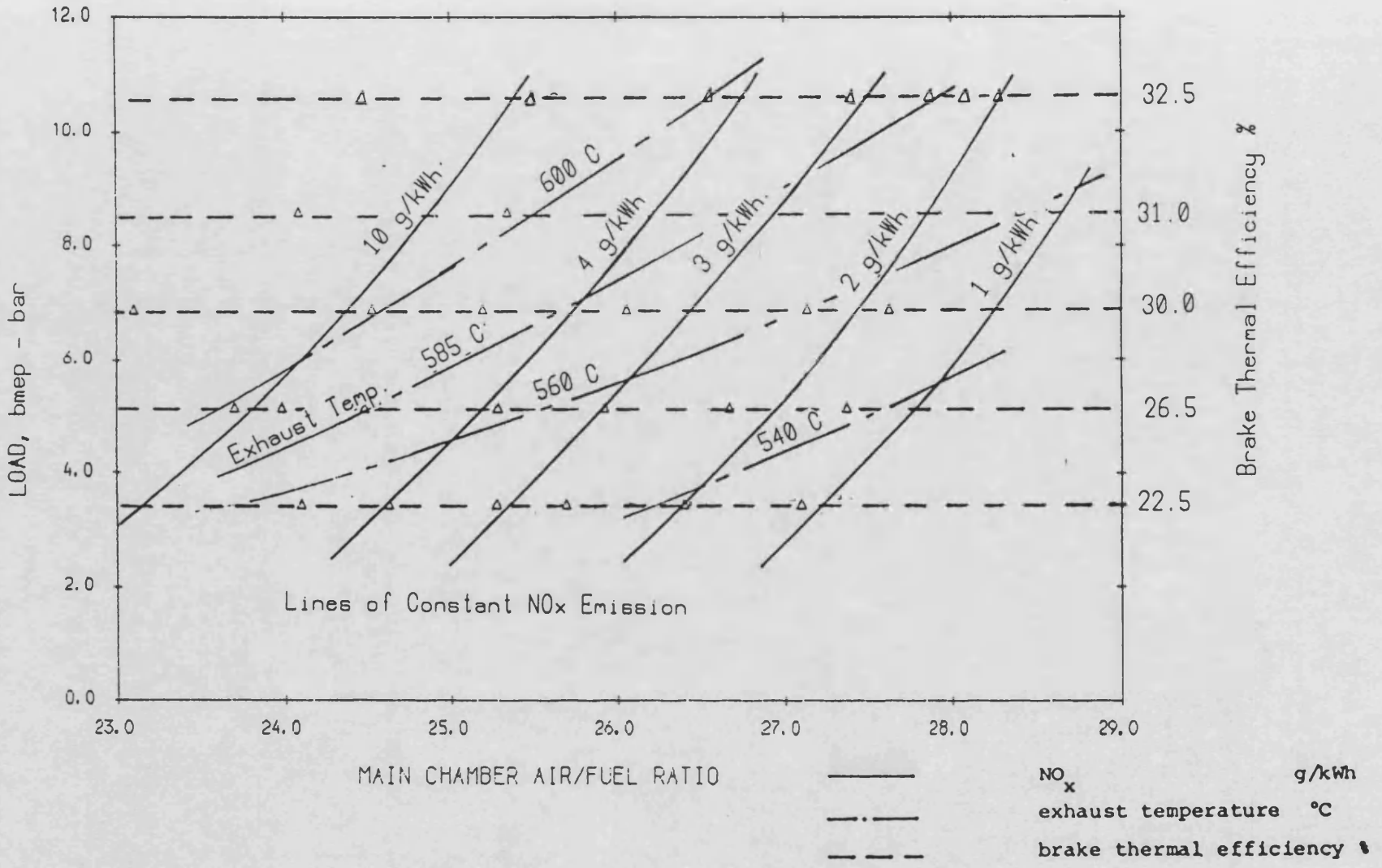

Figure 4.9 Main chamber performance map showing contours of brake thermal efficiency, exhaust temperature and NOx.
(Prechamber conditions were held constant)

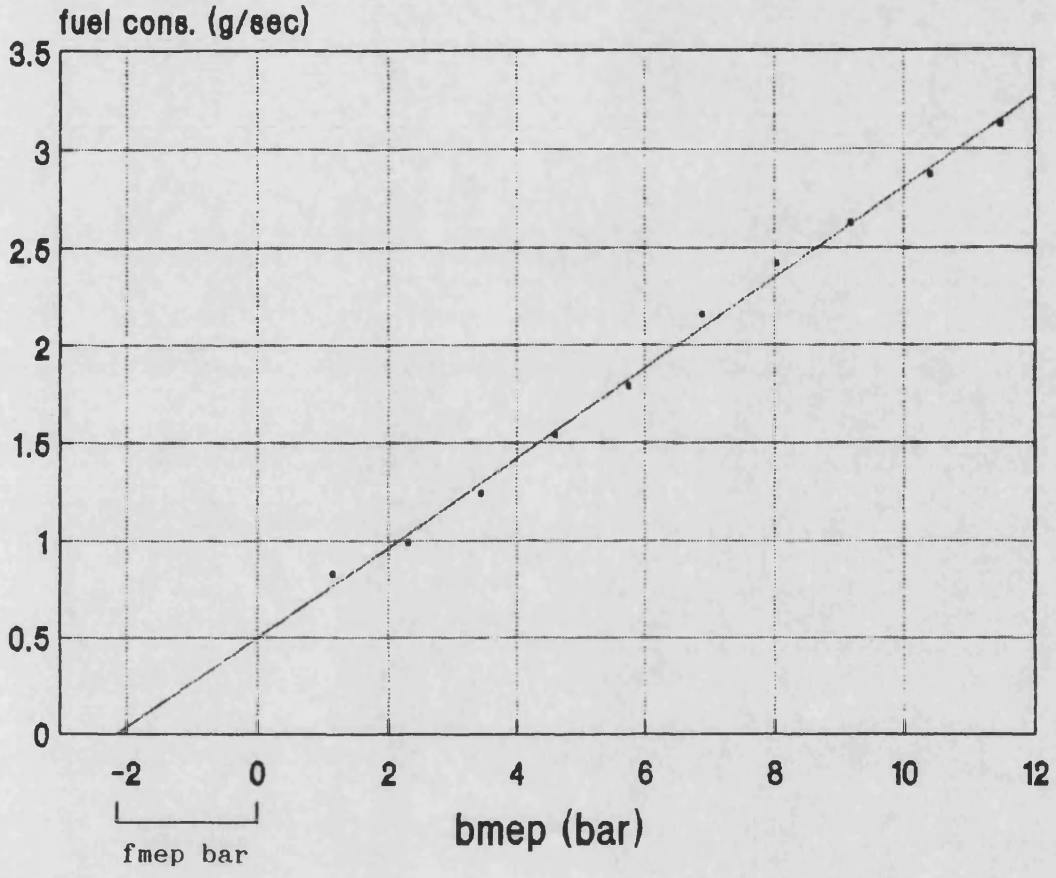

Figure 4.10 Willans Line for SE1 Gas Engine

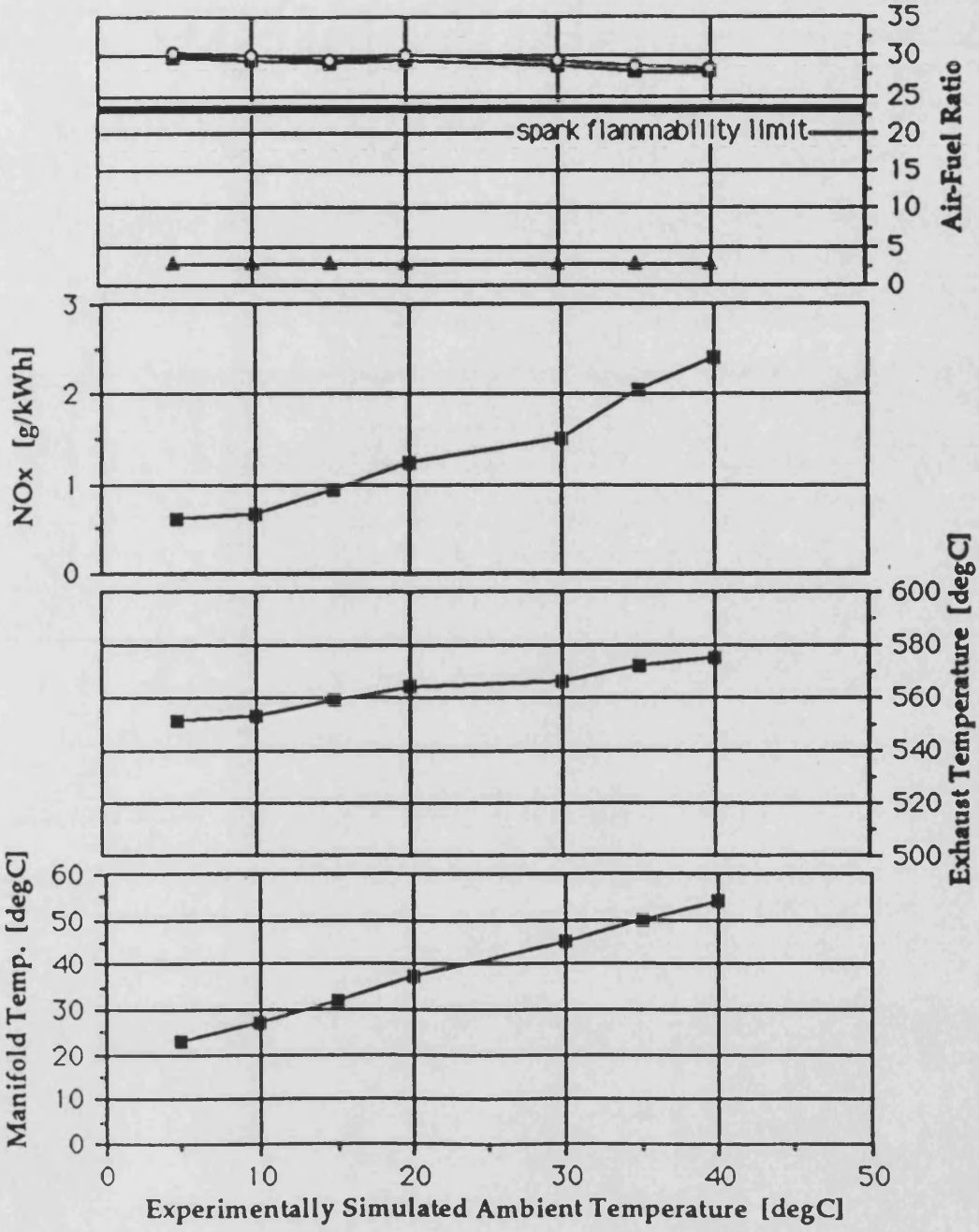

Figure 4.11 Response to Variation of Ambient Temperature

Chapter 5

5. Verification of the STAR CFD Computer Program

5.1 Introduction

This chapter is concerned with the description and validation of a computational fluid dynamics (CFD) program used to study mixing in the prechamber. The object was to use the program to model a well documented fluid flow problem and make comparisons between measured and computed results. This study included the effects of changing key elements of the model on program performance. Subsequently, the program was used to model the SE1 prechamber with greater confidence and understanding. The program used for this initial study was an early version which did not have the facility for transient flows.

5.2 Introduction to the STAR CFD Computer Code

STAR is a computer software program produced by Computational Dynamics for the simulation of multi-dimensional fluid flows, heat and mass transfer and to some extent, chemical reactions. STAR uses a numerical finite-volume procedure for solving the governing partial-differential conservation equations of mass, momentum, and energy for laminar or turbulent flows. These basic conservation equations are given in general form in appendix E. Several other computational fluid dynamics (CFD) programs, for example PHOENICS, use finite volume methods. A minority of programs use the finite element technique. Finite Volume methods have been found to be superior when modelling fluids, whereas finite element methods are ideally suited to the modelling of solids.

5.3 Creating a CFD Model using STAR

Creating the model for STAR consists of three processes. Firstly, a geometic model made up of individual cells is created. Secondly, boundary regions are defined and conditions at each of these are prescribed. If the these boundary conditions are time dependent (STAR version 2.1 only), a transient history file containing boundary conditions at defined time intervals must be created. Finally the control data which control the solution algorithms must be set. These values will effect the stability and convergence of the solution.

5.3.1 Creating a Geometric Model

Producing the mesh is the most difficult and time consuming part of the modelling process. Many factors must be considered during its construction if the model is to produce satisfactory results. Models created using other programs such as ANSYS and PATRAN can also be imported into STAR. An outline of the procedure for creating a geometric model for STAR is given as follows:-

1. Consider the best approach to model the problem so that the least number of cells will be required. (eg. look for symmetry in the model)
2. Define the outline of the geometry by giving coordinates of vertices. (Cartesian, cylindrical and spherical coordinates systems may be used)
3. Insert further cell vertices between these to produce sufficient cell density using mesh generation commands. (Cell density should be greatest in regions of interest such as those with high pressure or velocity gradients.)

4. Define the first reference cell using a set sequence required by STAR
5. Generate further cells based on the definition of the first cell until mesh structure is complete.
6. Renumber and reorder vertices and cells to the STAR format using the sequence command.
7. An obstruction, such as a baffle plate, can be easily added by changing the definition of the appropriate cells. The obstruction may be made solid by defining the cells as being inactive that is, not allowing fluid transfer across cell boundaries, or porus by allowing limited transfer across cell boundaries.

5.3.2 Factors of Cell Design Affecting Convergence and Solution Accuracy

When producing a mesh, the following features of cell geometry must be considered to avoid instability caused by cell distortion.

Aspect Ratio

This is a ratio between leading cell dimensions, such as the length/width ratio. This should be kept below a value of 10 or solution accuracy will deteriorate. Cells close to an impermeable surface such as a wall are less affected by large aspect ratio.

Included Angle

The angle subtended between the cell surfaces should not deviate from 90 degrees by more than 45 degrees. Again this is less critical for cells close to impermeable surfaces.

Mesh Density

An important parameter which effects both the ability of the solution to converge and the accuracy of the results. Mesh density needs to be greatest where velocity or pressure gradients are highest. There will always have to be a compromise between mesh density and computer run time. Several trials may be needed to achieve the best compromise.

Time Step (For Transient Problems)

This is an important parameter for transient problems where boundary conditions vary with time (Star Version 2.1). If time steps are too large the solution may become unstable and diverge. Again a compromise must be reached between computer run time and solution accuracy. The optimum time step size is related to both cell dimensions and flow velocity by an index known as the Courant Number, C, defined as;

$$C = \frac{V_s \times \delta t}{\delta l}$$

where V_s is the velocity of sound, δt is the time step interval and δl is the cell dimension in the direction of flow. Ideally this index should be close to unity, however in practice, values in the range of 5 to 20 will still produce stable converged solutions.

5.3.3 Applying Boundary and Flow Conditions

Once the mesh has been successfully constructed and sequenced, boundary and flow conditions must be applied to the model. STAR allows a number of different boundary types to be

defined. These are; wall condition, prescribed inlet, outlet, prescribed pressure, axis of symmetry, plane of symmetry, and cyclic. The steps in defining the boundary conditions are:

1. Identify and index all boundary surfaces of the mesh.
2. Define the boundary type at each of the surfaces. (By default all boundaries are defined as walls.)
3. Enter conditions at each of the boundaries, as required.
4. Define properties of the fluid such as viscosity, density etc
5. For turbulent flows, the K-ε model, incorporated in the program, may be used.

When applying an outlet condition to a boundary, the user must consider the possibility of recirculating flow, which would give flow in both directions at the outlet boundary. Under these circumstances, the program will ignore any incoming flow, creating a subsequent error. To avoid this, a pressure boundary condition may be used instead, which permits flow in both outgoing and incoming directions to be modelled.

5.3.4 Control Data

The final data to be entered is that which controls the solution procedure. This includes the values given to the relaxation factors for each variable, controlling the stability of the solution, and the speed at which it converges. Also to be specified is the convergence criterion, a measure of whether satisfactory convergence has been met together with the number of iterations to be made should this criterion not be met. Control can be exercised over the solution data, for example in

determining which data sets are to be displayed or stored during individual iterations, or in final converged form. Initial field values for each variable may be entered as starting values for each iteration, in order to speed up convergence, or alternatively, data from previous iterations may be used.

5.3.5 Running STAR

When running STAR, convergence or divergence of the variables being solved will occur. Convergence depends on the residual values between each successive iteration falling below a predetermined value. This can also be observed from the values for the field variables at specified monitoring locations within the model which are printed out while running STAR interactively.

If divergence of the solution occurs, the user must return to PREPSTAR and change some of the control parameters for the numerical solution. This includes increasing the number of sweeps per iteration and reducing the relaxation factors of the divergent variables.

5.3.6 Processing of the Results from STAR

The results from STAR can be accessed using the post-processor within STAR, or written to ASCII files for processing by the user. The post-processor can produce vector and contour plots of the desired variable for any plane through the model. Field values for each variable can also be displayed for each cell or vertex.

5.4 Validation Tests:

Modeling the Flow of Air Through a Sharp Edged Orifice Plate

5.4.1 Objectives

To model the air flow through a sharp edged orifice plate designed to British Standards 1042 (2) using the STAR computer program and to compare the results with those given by BS 1042. This is a tough cfd problem as there are regions of recirculating flow and sharp gradients of velocity where the jet emerges downstream of the orifice plate. In particular, model refinement and solution technique are to be investigated in order to establish their effects on convergence and accuracy of solution.

The overall objective is to achieve some verification of STAR's flow modelling capabilities and gain confidence in the program as a whole. Further use of STAR to solve unknown flow problems such as the flow and mixing in the prechamber of a stratified charge gas engine can then be considered.

5.4.2 The Orifice Plate Problem

A sharp edged orifice plate was chosen as it is a well tested and understood fluid flow device and much empirical data is available for comparison. This problem is also similar to the prechamber problem which also has an orifice or throat and regions of recirculating flow. The orifice plate to be modelled was produced to the geometry and recommendations given in BS 1042. Figure 5.1 shows the orifice to be modelled. Pressure tappings are taken at the corners between the orifice plate and pipe wall. Values of pressure were taken at these positions in the results

produced by the CFD model. BS 1042 also allows for pressures to be taken 1 diameter upstream and 1/2 diameter downstream, however the corner pressure tappings are preferred as the effects of pipe wall friction do not need to be allowed for.

The flow conditions for the problem are given below.

Flow	Axisymmetric steady state
Pipe diameter	0.2 m
Orifice diameter	0.1 m
Fluid	air at 293 K
Density	Assumed constant at 1.205 kg/m3
Viscosity	1.82 E-5 kg/m s at 293 K
Upstream velocity	mean value of 1.0 m/s at 1m upstream of orifice plate
Reynolds Number	13,200 at 1m upstream of orifice plate (Turbulent)
Mass flow	3.786 E-02 Kg/s

5.4.3 Expected Flow Through an Orifice Plate

As fluid flows through an orifice plate, the section of most interest is the one of minimum cross sectional area of flow. This is not at the orifice itself, as the cross section of the stream continues to decrease for some distance downstream. This is as a result of the inward radial component of velocity gained by the fluid as it converges upstream of the orifice. Figure 5.2 (12) shows the expected flow through an orifice with relative pressure variation below. In strict analogy to the venturi tube, the area of minimum jet section, the vena contracta, which corresponds to

the throat of a venturi tube, should be used in the flow equation. However no satisfactory method of actually measuring this minimum jet area is known, whereas measurement of the orifice area is a relatively simple operation. A correction factor, the contraction coefficient, is therefore included in the total discharge coefficient for convenience. By experiment, the amount of contraction has been found to depend primarily on the diameter ratio, β, and the properties of the fluid; hence, the discharge coefficient will also vary with these factors when it includes the effects of jet contraction.

All studies of the static-pressure changes close to a sharp edged orifice have shown that on the inlet side, within the last 0.1 D, the static pressure increases slightly to a maximum at the corner of the plate and pipe wall, as seen in figure 5.2. On the outlet side, the static pressure rapidly decreases until a minimum is reached between 1/4 D and 1/2 D, at the vena contracta. For any one orifice, the distance from the plane of the inlet side to the vena contracta is a function of the orifice-to-pipe diameter ratio β, becoming less as β increases. Numerous experiments by different investigators over a wide range of pipe sizes have shown that the relation between the position of the vena contracta and the diameter ratio β, is independent of the actual pipe sizes for pipe diameters greater than 50 mm. The average maximum and minimum distances between the orifice and the vena contracta, as reported by different experiments, are shown in figure 5.3.

From the above given parameters and orifice plate geometry, the unknown coefficient of discharge can be obtained from BS 1042 for various positions of pressure tappings. This is based on the Stolz equation in Appendix D. If the orifice and pipe geometries

and Reynold's number are assumed to be known without error, then the uncertainty of discharge coefficient is within 0.5% for this example.

5.4.4 The STAR Orifice Plate Model

A model was constructed to the dimensions given by BS 1042. The lengths of pipe upstream and downstream of the model were 10 and 15 times orifice diameter respectively. As the orifice plate problem is axisymmetric, the whole orifice need not be modelled for a full solution as it is in effect only two dimensional. Therefore, a 5 degree segment of the orifice was used. When constructing the initial model, parameters were included so that the mesh density could be varied to produce further models identical to the first, except for the number of cells. The relative distribution of the cells was also kept approximately constant so that the effect of mesh density by itself could be investigated. Seven models were produced, with cell numbers ranging from 36 cells to 770 cells.

As the flow through the orifice was turbulent (Re - 13200) the K-ε turbulence model incorporated in STAR was used to simulate the effects of turbulence.

5.4.5 Running the Orifice Models

When running the STAR models, a number of problems were encountered before converged solutions were obtained. The first problem was concerned with the recirculation region immediately downstream of the orifice plate. As would be expected, recirculation was predicted by STAR, however this region appeared

to extend unusually far downstream (To the order of 50 times pipe diameter downstream). This caused errors in the solution as the outlet boundary condition, used initially, would not allow for a recirculating flow across the boundary. This problem could be overcome by extending the downstream pipe by a very large amount, until all recirculation had ceased. However this was an undesirable solution as CPU time for the longer model was obviously much greater.

It was found that a better solution was to define the pipe outlet as having a pressure boundary condition as this would allow for fluid flow in both directions across the boundary.

5.4.6 Results for the Orifice Plate models

It was found that the number of iterations required for a converged solution to the desired degree of accuracy was independent of the number of cells used in the model's construction. However the time required to achieve this was proportional to the total number of cells in each model.

The converged solutions for each of the orifice models were examined using the Poststar graphics package. Plots of velocity vectors and pressure contours for each of the models were made and these are shown in Figures 5.4 to 5.10 .

The recirculation zones can be clearly seen in all of the models. A small anomalous flow is seen to cross the axis of symmetry. However, the velocity vectors shown on the plots are the mean resultant velocities taken at the centre of each cell, and hence do not exactly represent the velocity at the axis of

symmetry, which would be parallel to the symmetry plane.

For each of the orifice models, coefficients of discharge were calculated using equation 2 given in Appendix D, based on Bernoulli's analysis. These are shown graphically in Figure 5.11. For the 288 cell model, the pressure and velocity variations were plotted along the axis of the model. These are shown in Figures 5.12 and 5.13. The velocity profile immediately upstream of the orifice was also plotted for this model, and is shown in Figure 5.14.

Continuity of flow for each of the models was checked using equation 3 given in Appendix D. Mean inlet and outlet velocities were calculated. The densities and areas at inlet and outlet to the model are constant, as defined in the problem. It was found that for all models, conservation of mass was maintained.

5.5 Comparison of STAR Predicted Flow with Expected Results

The velocity vector plots in Figures 5.4 to 5.10 show flow patterns as would be expected. Figure 5.14 shows the velocity profile immediately upstream of the orifice plate for the 288 cell model. The flow is an almost fully developed turbulent pipe flow, similar to that shown in Figure 5.2.

Values for coefficient of discharge agree closely with those given by BS 1042 , and at best, with a cell number of 770, the predicted coefficient of discharge is within 2% of it. Figure 5.11 shows that for this model, approximately 300 cells are required to predict a Cd within 5% of the BS 1042 value.

Figure 5.12 shows pressure variation along the centre line through the orifice. The pressure drops sharply across the orifice plate, as would be expected, however the pressure recovery further down stream of the orifice is only small. This should be much greater than predicted by STAR. Referring to figure 5.12, pressure should have recovered by the order of 50% after a distance of 5 pipe diameters downstream.

From Figure 5.13, the high velocity downstream jet created by the orifice has decayed very little by the same distance downstream of the orifice, whereas in practice, due to the effects of diffusion, would have decayed substantially after this distance.

5.6 Discussion and Conclusions

Qualitatively, STAR appears to produce realistic flow patterns through the orifice plate itself, but seems to run into difficulty downstream. The jet produced by the orifice extends further downstream than experimental data would suggest (2).

Considering the STAR flow predictions quantitatively, the program appears to have been very successful. Conservation of mass through the models was maintained in all the tests, and excellent predictions for the coefficient of discharge have been made.

5.7 Summary

A new CFD program, STAR, has been used to model a well documented orifice flow problem constructed in accordance with BS 1042. Comparisons of the results have been made with those given by BS 1042 and other sources which show excellent quantitative agreement. The effects of mesh density on solution accuracy have shown that approximately 300 cells are required to accurately model this problem.

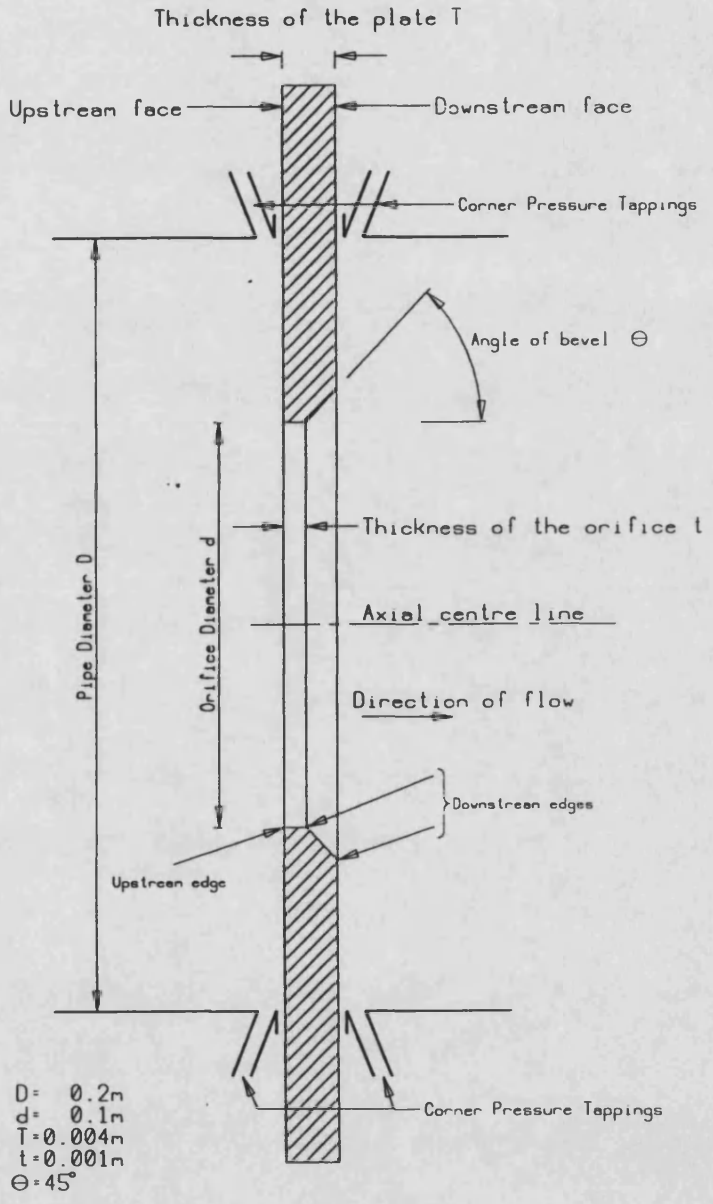

Figure 5.1 Orifice Plate to BS1042 used for CFD model

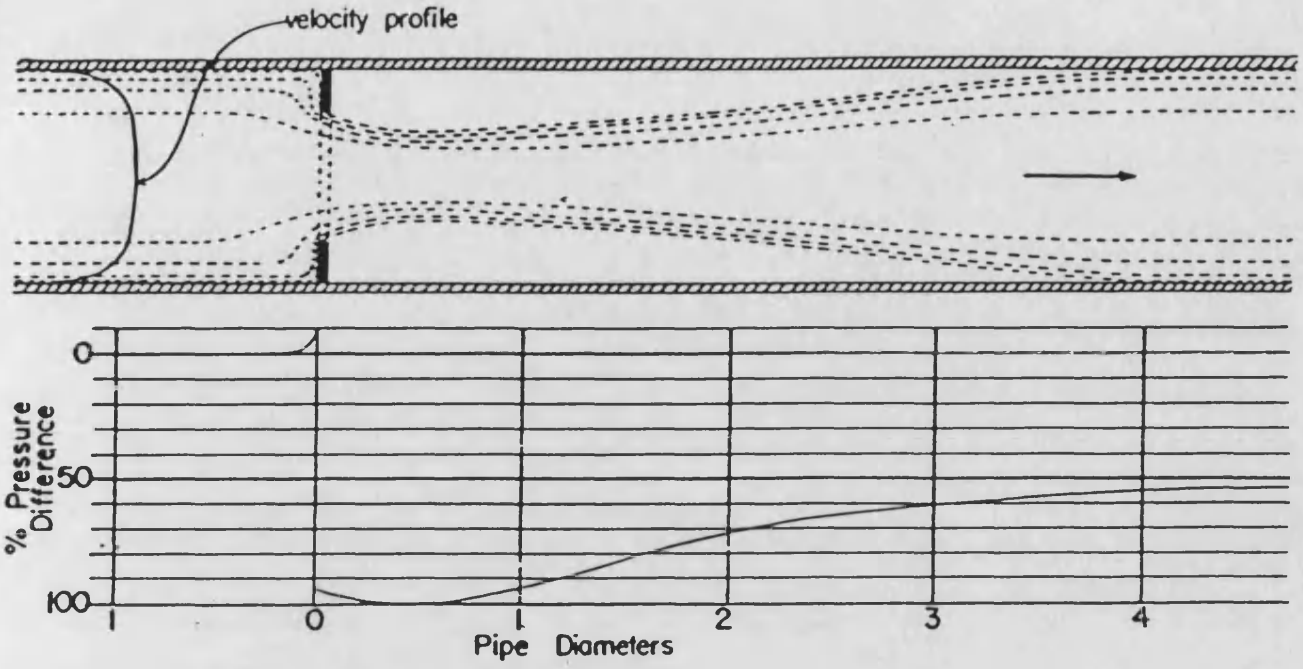

Figure 5.2 Diagramatic Representation of Fluid Flowing Through a Thin-Plate Sharp-Edged Orifice and Relative Pressure Changes

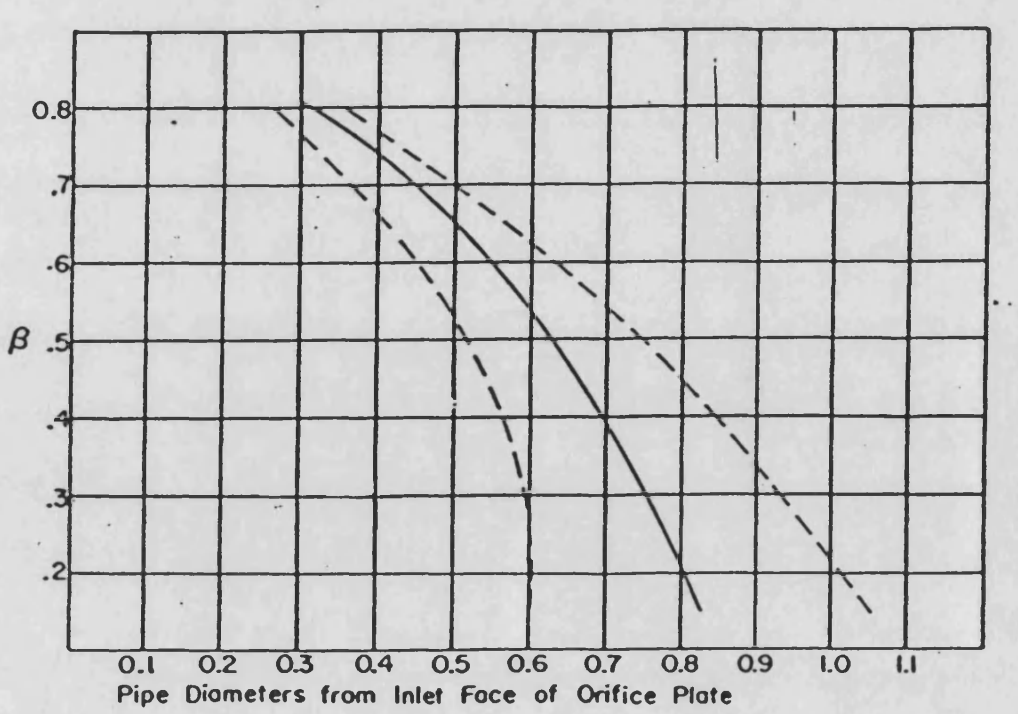

Figure 5.3 Location of Vena Contracta for a Sharp-Edged Orifice (Broken Lines Show Maximum Variation Limits)

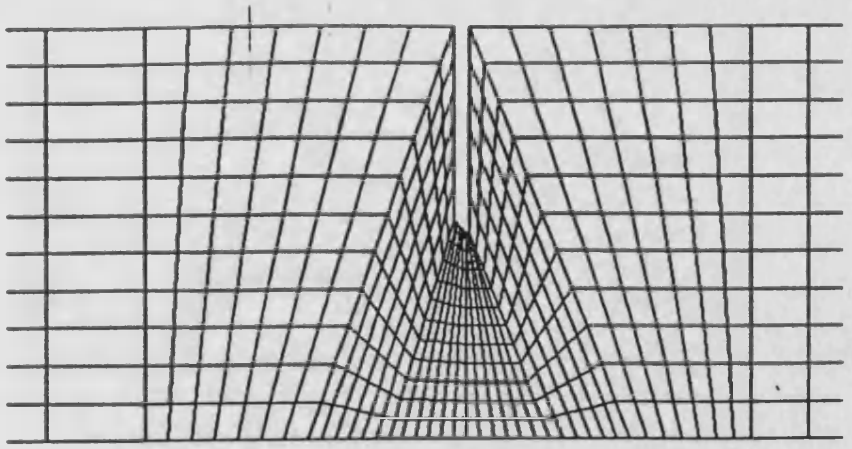

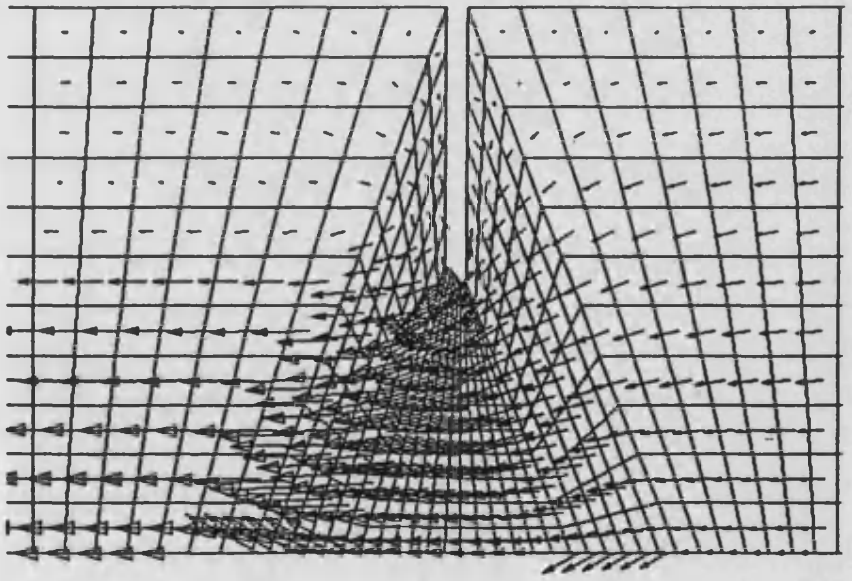

VELOCITY
COMPONENT W
M/SEC

MAX 0.584252
MIN -.611731E-01

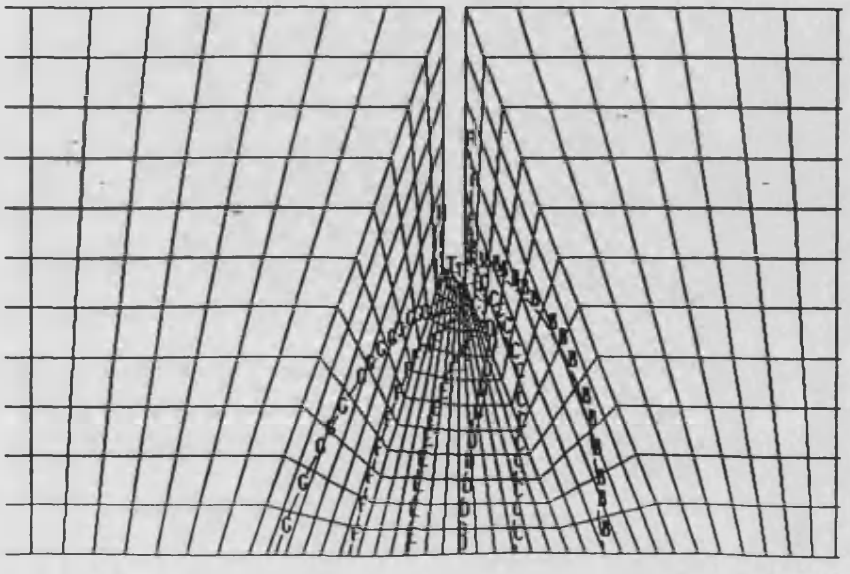

PRESSURE

N/M**2

MAX 0.200848
MIN -.156823

A	0.1937
B	0.1625
C	0.1313
D	0.1001
E	0.6884E-01
F	0.3762E-01
G	0.6405E-02
H	-.2481E-01
I	-.5602E-01
J	-.8724E-01
K	-.1185
L	-.1497

Figure 5.4 Results for 770 Cell Orifice Model Using STAR CFD

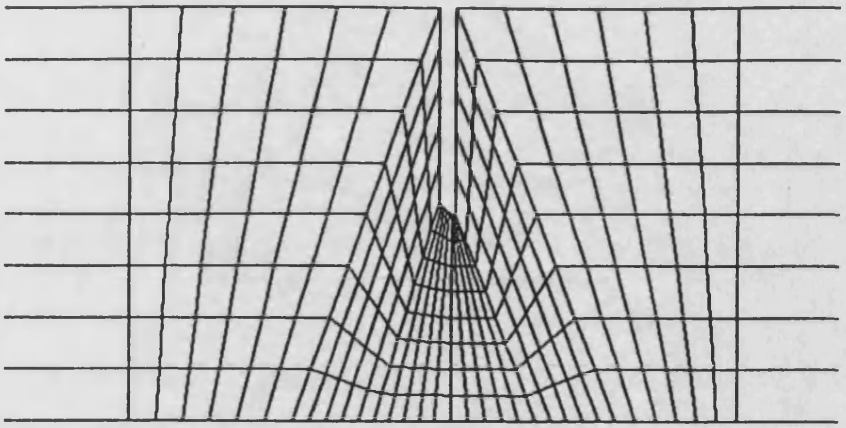

VELOCITY
COMPONENT W
M/SEC

MAX 0.553255
MIN -.574830E-01

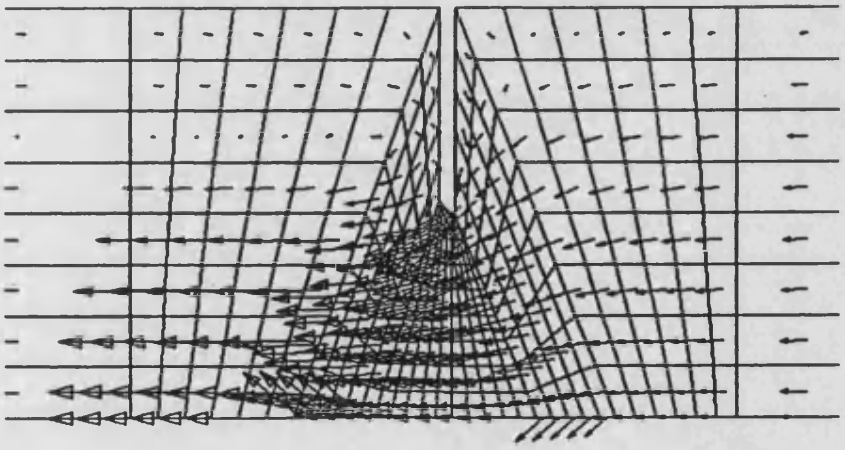

PRESSURE

N/M**2

MAX 0.190526
MIN -.144618

A	0.1838
B	0.1546
C	0.1253
D	0.9608E-01
E	0.6683E-01
F	0.3758E-01
G	0.8330E-02
H	-.2092E-01
I	-.5017E-01
J	-.7942E-01
K	-.1087
L	-.1379

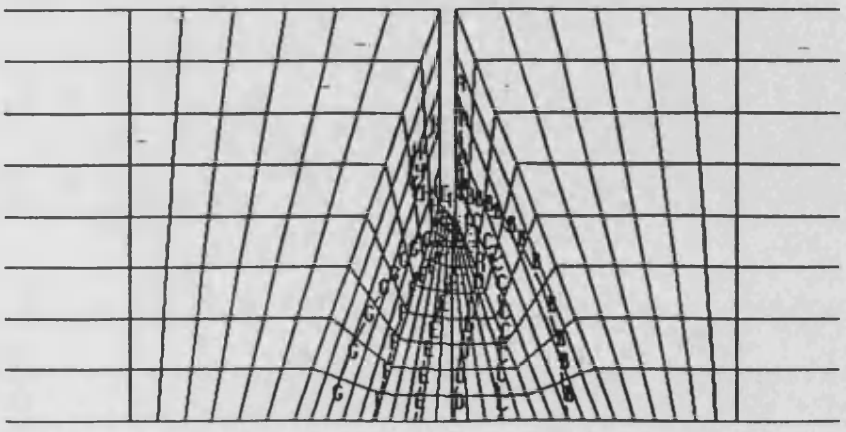

Figure 5.5 Results for 432 Cell Orifice Model Using STAR CFD

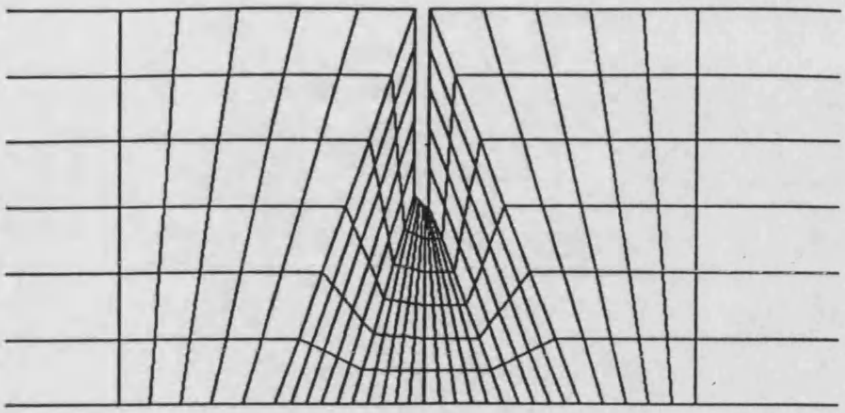

VELOCITY
COMPONENT W
M/SEC

MAX 0.514301
MIN -.618141E-01

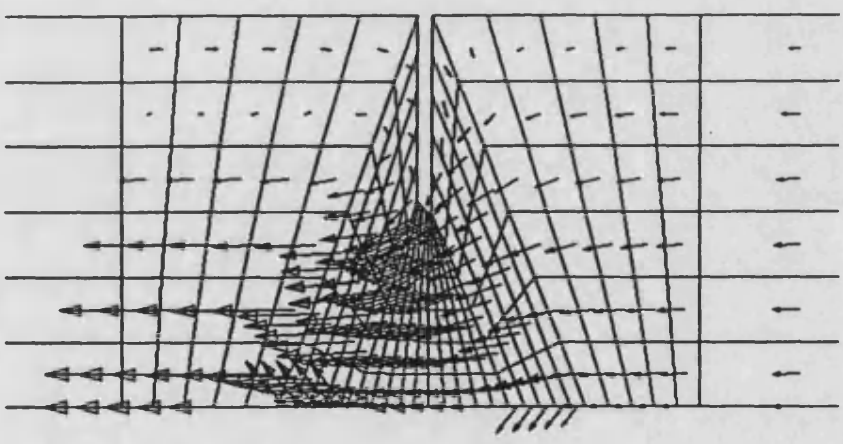

PRESSURE

N/M**2

MAX 0.176116
MIN -.130790

A	0.1700
B	0.1432
C	0.1164
D	0.8962E-01
E	0.6284E-01
F	0.3606E-01
G	0.9271E-02
H	-.1751E-01
I	-.4430E-01
J	-.7108E-01
K	-.9787E-01
L	-.1247

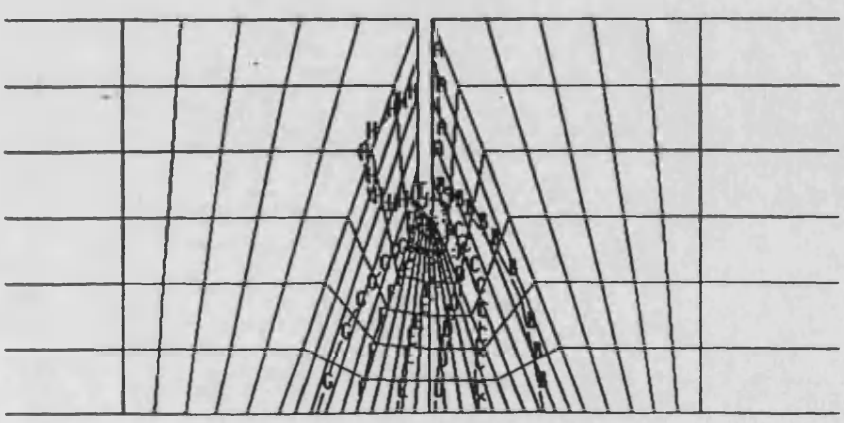

Figure 5.6 Results for 286 Cell Orifice Model Using STAR CFD

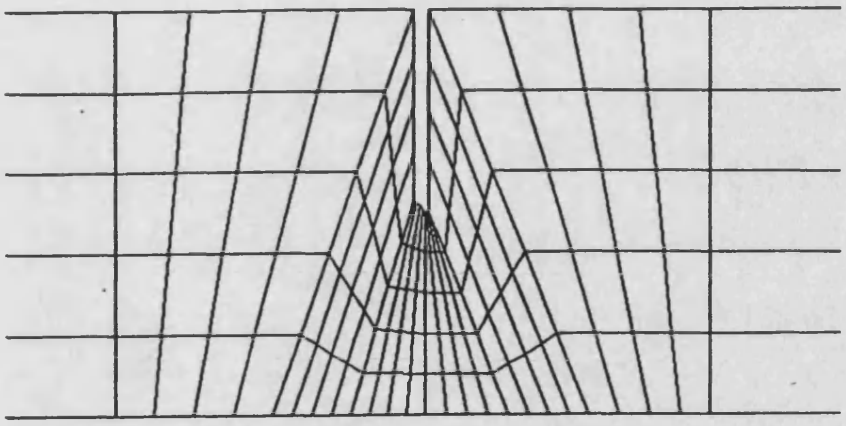

VELOCITY
COMPONENT W
M/SEC

MAX 0.486775
MIN -.658669E-01

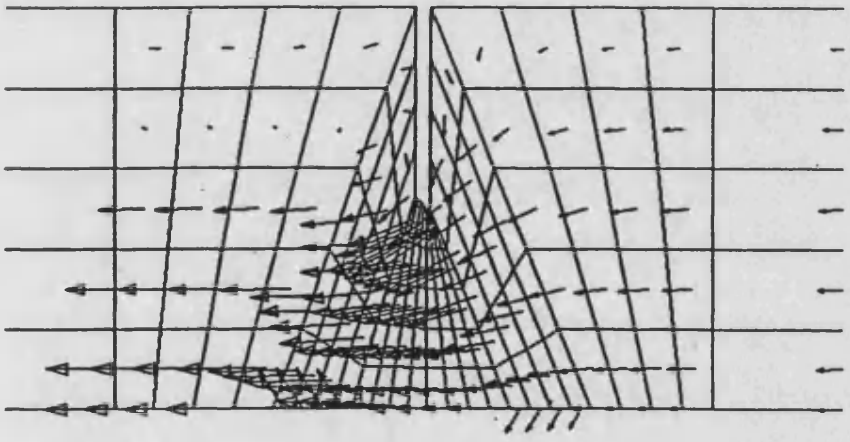

PRESSURE

N/MM**2

MAX 0.171843
MIN -.122933

A	0.1659
B	0.1402
C	0.1145
D	0.8877E-01
E	0.6304E-01
F	0.3732E-01
G	0.1159E-01
H	-.1413E-01
I	-.3986E-01
J	-.6559E-01
K	-.9131E-01
L	-.1170

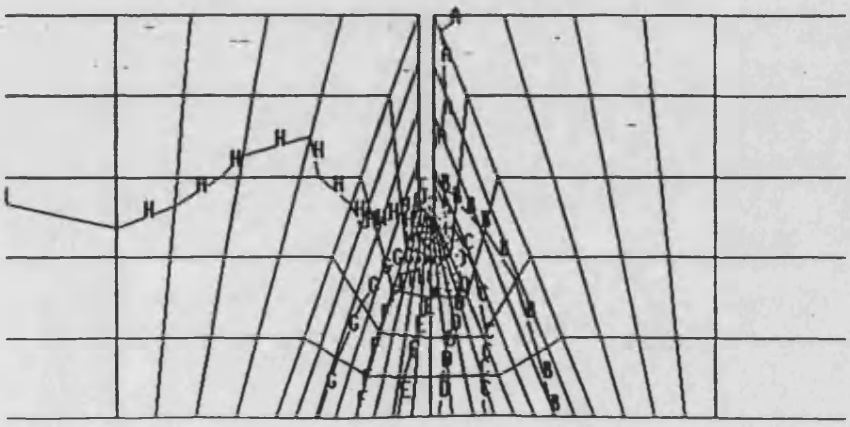

Figure 5.7 Results for 200 Cell Orifice Model Using STAR CFD

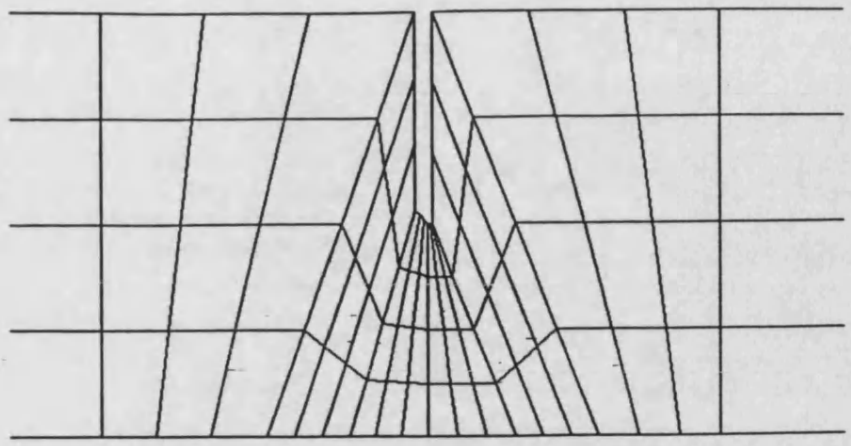

VELOCITY
COMPONENT W
M/SEC

MAX 0.456296
MIN -.750136E-01

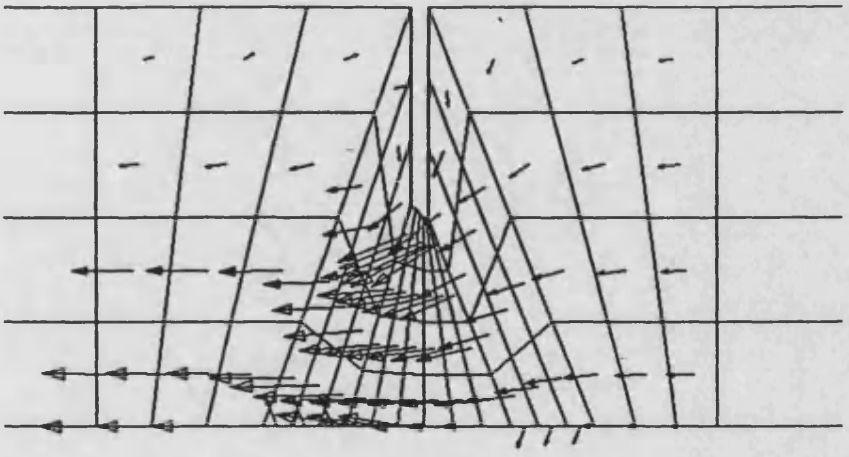

PRESSURE

N/M**2

MAX 0.167056
MIN -.112657

A	0.1615
B	0.1370
C	0.1126
D	0.8823E-01
E	0.6382E-01
F	0.3940E-01
G	0.1499E-01
H	-.9418E-02
I	-.3383E-01
J	-.5824E-01
K	-.8265E-01
L	-.1071

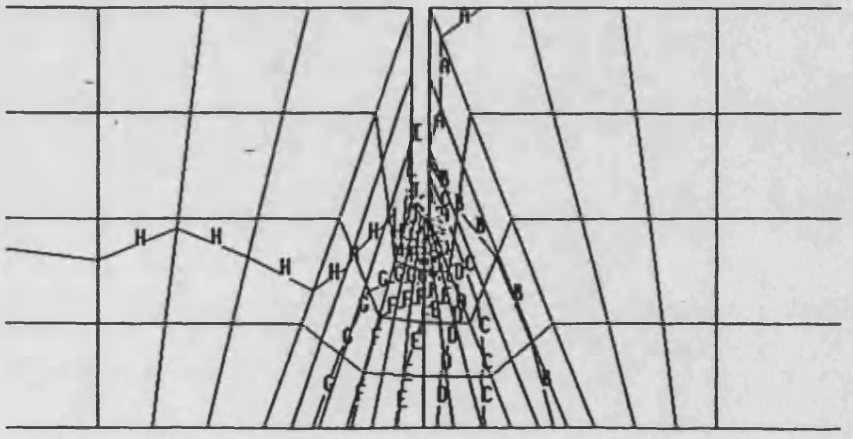

Figure 5.8 Results for 120 Cell Orifice Model Using STAR CFD

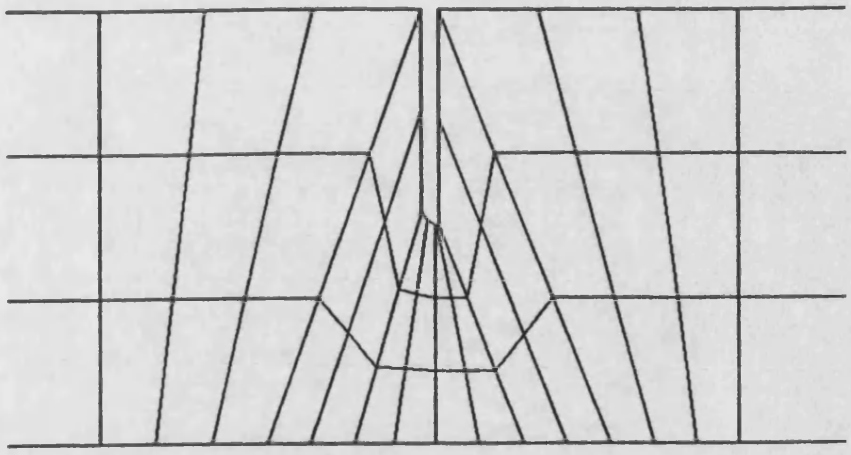

VELOCITY
COMPONENT W
M/SEC

MAX 0.442527
MIN -.562686E-01

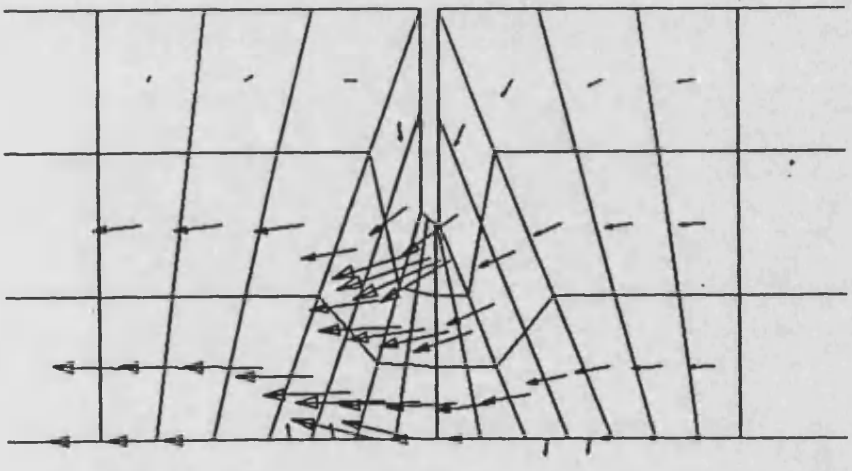

PRESSURE

N/MM**2

MAX 0.160784
MIN -.952597E-01

A 0.1557
B 0.1333
C 0.1110
D 0.8863E-01
E 0.6628E-01
F 0.4393E-01
G 0.2159E-01
H -.7565E-03
I -.2310E-01
J -.4545E-01
K -.6779E-01
L -.9014E-01

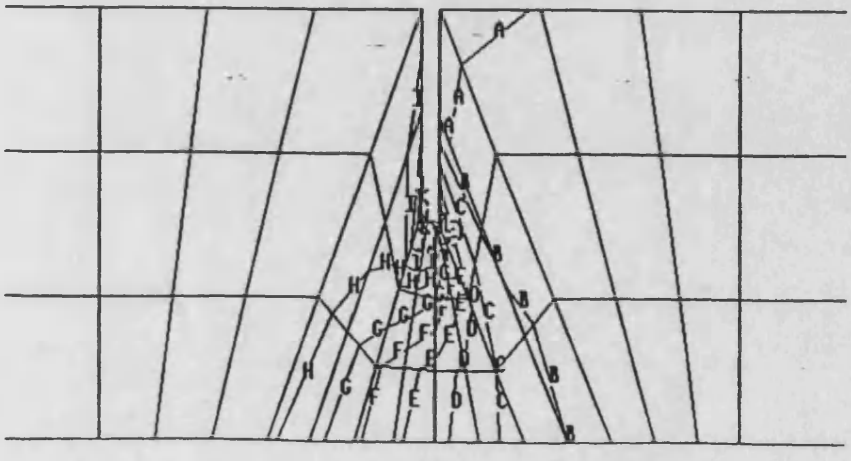

Figure 5.9 Results for 66 Cell Orifice Model Using STAR CFD

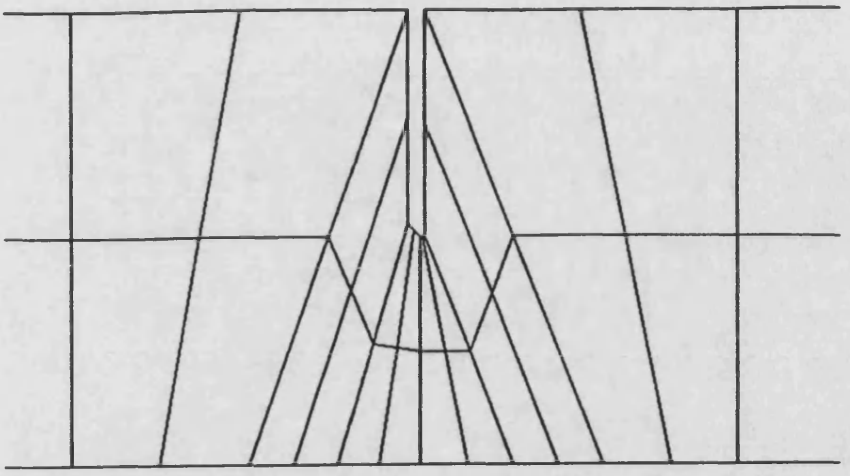

VELOCITY
COMPONENT W
M/SEC

MAX 0.427948
MIN 0.000000

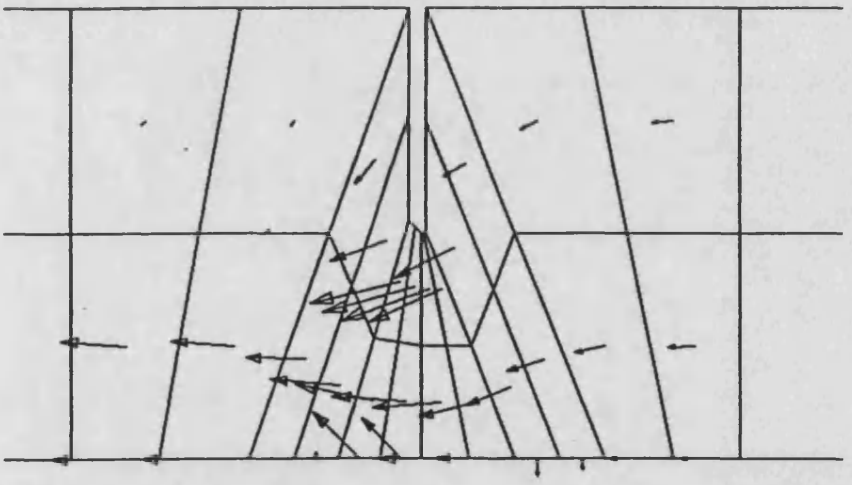

PRESSURE

N/M**2

MAX 0.129723
MIN -.688751E-01

A	0.1258
B	0.1084
C	0.9109E-01
D	0.7375E-01
E	0.5642E-01
F	0.3909E-01
G	0.2176E-01
H	0.4426E-02
I	-.1291E-01
J	-.3024E-01
K	-.4757E-01
L	-.6490E-01

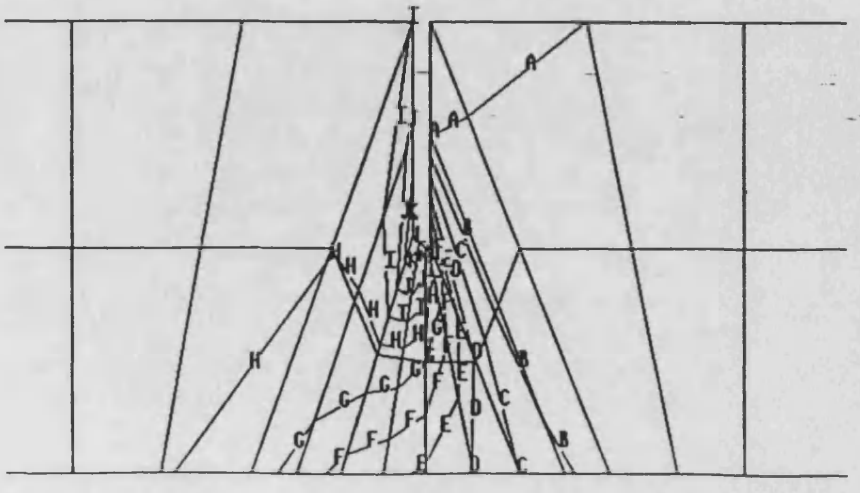

Figure 5.10 Results for 36 Cell Orifice Model Using STAR CFD

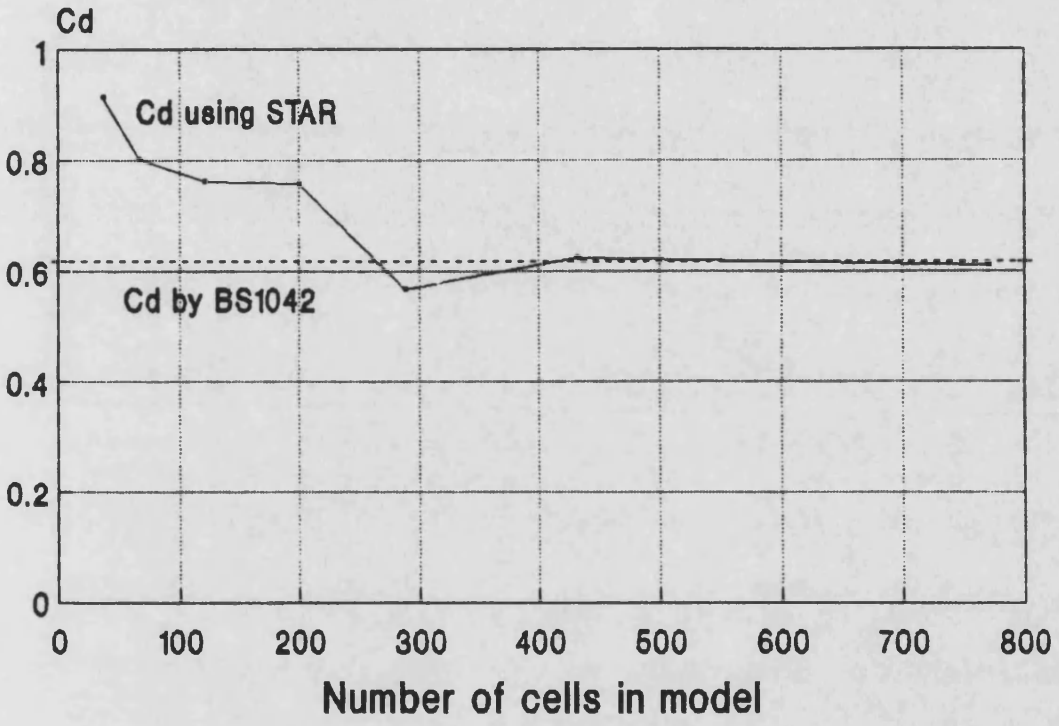

Figure 5.11 Change in Coefficient of Discharge with Increasing Number of Cells in Model Mesh

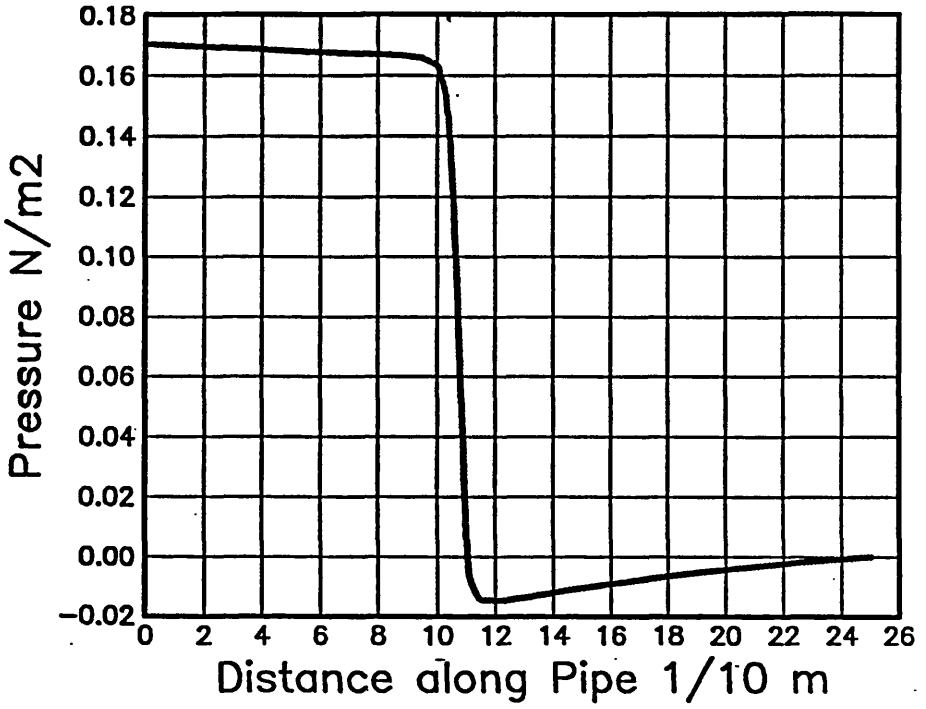

Figure 5.12 Pressure Variation along Pipe Axis Through Orifice Plate, Predicted by STAR CFD

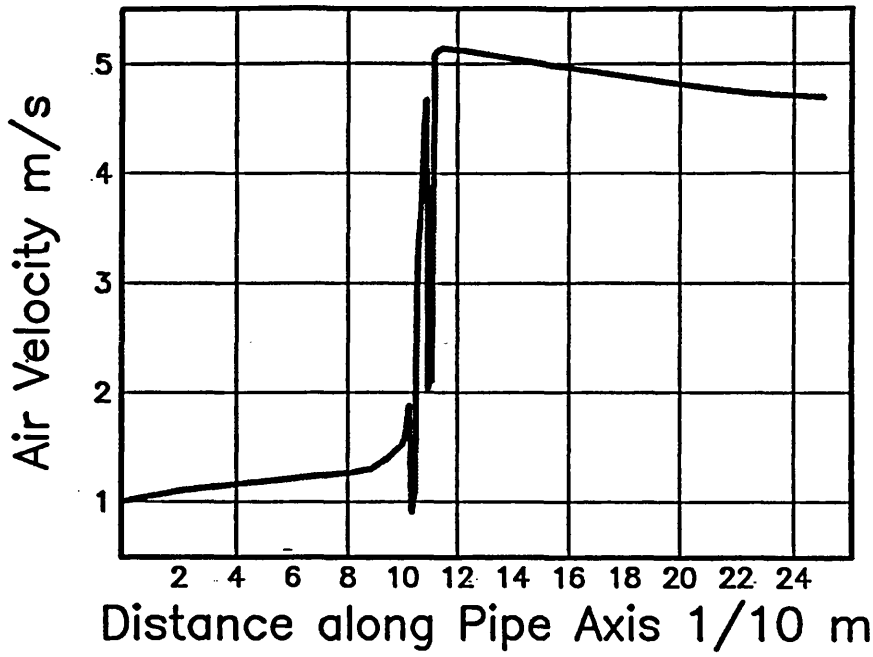

Figure 5.13 Velocity Variation along Pipe Axis Through Orifice Plate, Predicted by STAR CFD

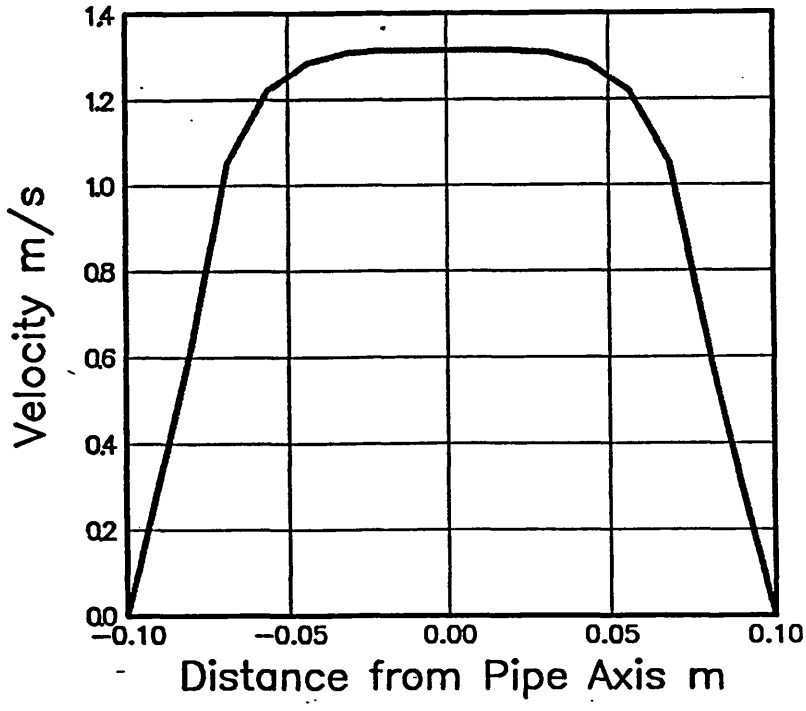

Figure 5.14 Velocity Profile Immediately Upstream of Orifice

Chapter 6

6. Testing and Validation of a Novel High Frequency FID

6.1 Introduction

This chapter describes a novel high frequency flame ionisation detector (FID), and its validatation for pressure independence for subsequent application to in-cylinder measurement of mixture concentration. The instrument has been designed to overcome the restictions of slow response times associated with conventional FIDs to the extent that in-cylinder, real time measurement of fuel concentration may be possible for at least part of the engine's cycle. However, due to the difficult nature of in-cylinder sampling, it is necessary that the instrument and sampling system be tailored to this application and thoroughly tested and validated by a series of bench tests before any measurements on the engine can be made.

6.2 Description of the Cambustion High Speed FID

The basic principle by which any flame ionisation detector (FID) operates is that when a hydrocarbon is burnt, significant quantities of ions are formed. The number of ions produced being proportional to the number of carbon atoms burnt in hydrocarbon form. This physical effect is not yet fully understood, but it is known that the process of ion generation occurs as a result of a non-equilibrium effect known as chemi-ionisation as opposed to thermal or equilibrium ionisation, since the latter produces negligible ionisation at normal flame temperature. In flames not involving hydrocarbons such as hydrogen and carbon monoxide flames, ion generation is limited to equilibrium values and hence insignificant. If however, a hydrocarbon sample is introduced into such a flame, significant ionisation will immediately occur.

A conventional FID arrangement is shown in figure 6.1. The flow of fuel gas, air and sample to the FID are carefully controlled by the use of capillary tubes and pressure regulators. This allows the FID to work extremely well under steady state conditions but as a consequence causes the frequency response to be very poor. The high frequency response FID (HFR FID) developed by Cambustion is shown schematically in figure 6.2 . The fundamental difference between this design and a conventional FID is that the sample gas is not mixed with the fuel gas prior to being burned, but instead passes directly into the flame. It is this design feature that enables the FID to have a high frequency response, since dispersion effects between the sample and fuel gases are eliminated. The frequency response is now only limited to dispersion effects within the sample tube itself. Clearly a short sample tube is desirable for good frequency response, and this is also a critical parameter in determining the transit time or time delay between the sample gas entering at the sampling point, and being detected at the FID. Both of these variables are considered in depth later.

Plates 5 and 6 show the FID sampling head and the control unit. A schematic layout of the HFR FID and control system is given in figure 6.3. Negative ions generated in the flame are collected by a collector electrode positioned immediately above the flame and maintained at +180 volts with respect to the body of the FID. The electrical signal produced is then amplified and conditioned. The output signal thus produced is proportional to the total mass flow of the hydrocarbons entering the FID, and therefore great care must be taken in setting up the sample flow and calibration of the instrument to make accurate interpretation

of the signal possible. This aspect of the HFR FID makes the system difficult to use since it is the concentration of hydrocarbons that we desire to measure, and not mass flow rates. Therefore it is critical that the sample flow rate into the FID is maintained constant in order to isolate the signal from this variable, and much of the work reported in chapter 6 is devoted to this aim.

Details of the HFR FID sampling head are shown in figure 6.4. The sample gas is drawn into the FID chamber by maintaining it's pressure below that of the sample source. This pressure difference between the sample source and the FID chamber is the governing parameter for controlling the sample mass flow rate to the FID. A vacuum pump is connected to the FID chamber, and this is used both to maintain low pressure in the FID and to scavenge the exhaust products from the chamber. As the exhaust products contain water vapor, a condensate collection bowl is placed in this vacuum line to enable removal. Initial ignition of the hydrogen flame is achieved by an electrical glowplug. To prevent the dangerous build up of hydrogen fuel in the FID chamber, should the flame become extinguished, a thermocouple which detects the heat from the flame is used to operate a solenoid disconnecting the fuel supply.

The sample has been shown in figure 6.4 to be entering the FID directly via a sample tube. For most practical applications of the HFR FID however, this method is unsuitable as the pressure at the sampling point would have to be both constant and within a narrow range. Constant sample pressure would be required because, as mentioned earlier, the FID responds to both hydrocarbon concentration in the sample gas and sample mass flow rate. Since

sample flow rate is a function of the pressure difference (Δp) between the sampling source and the FID chamber, clearly a change in sample pressure would result in a change in sample flow to the FID, and hence FID output. The magnitude of the sample pressure would have to be such that Δp would provide sufficient, but not excessive sample flow to the FID. Larger sample flows into the FID may result in the instability or extinction of the FID flame.

To overcome these limitations a method of isolating the pressure at the sampling point from the pressure which is fed into the FID chamber has been developed by Collings (9). Figure 6.5 shows a system that will accommodate large fluctuating pressures at the sampling point but provide a constant controlled sample flow to the FID. The sample first enters the transfer tube, the diameter of which should be matched to the range of sample pressures and the length of which should be kept to a minimum for reasons discussed later. Pressure drop occurs along the length of this transfer tube before the sample is passed into an expansion tube of much greater diameter where a large pressure drop occurs. The length of this expansion tube is relatively short (23 mm) and it exhausts either to atmosphere or to a constant pressure chamber. Immediately before the open end of the expansion tube, where the pressure is theoretically constant, a constant flow of sample gas is drawn up a smaller sample tube to the FID. The dimensions of all these pipes controls not only the sample flow rates, but also the frequency response and transit time for the sampling system and hence they need to be optimised for particular sampling conditions. To do this a theoretical analysis of the sample flow within the system is required.

6.3 Analysis of the Flow Through the HFR FID Sampling System

In analysing the flow through the sample system, the two quantities of greatest interest are the dispersion time and the transit time. Dispersion refers to the spreading out of the concentration profile along the sample tubes due to an effective longitudinal diffusion referred to as Taylor diffusion (32,33). The dispersion time is defined as the characteristic diffusion length divided by the convection velocity. If the dispersion time is larger than the response time for the FID, then the dispersion time becomes the overall response time of the instrument. The transit time refers to the finite time taken for a unit of sample to pass through the sampling system to the FID and be measured. These two quantities are shown to be closely coupled. Longitudinal sample diffusion has been studied by Taylor for both laminar (32) and turbulent (33) flows.

Analysis of the flow through the sampling system when considering in-cylinder measurement has been studied in detail by Collings (9), and is discussed here. Referring to figure 6.6, the mass flow rate of sample through the transfer tube when inserted into the combustion chamber of an IC engine will be a function of time due to the fluctuating cylinder pressure. The velocity of the sample gas along this tube will be very great, reaching sonic conditions at higher sample pressures. The diameter of this transfer tube is necessarily small (typically 0.2mm) to minimise sample flow, and hence reduce interference to the gases in the combustion chamber being sampled. The sample gas passes from the transfer tube into the constant pressure chamber via an expansion tube. The purpose of this expansion tube is to avoid the mixing

of the incoming sample with the gas already present in the chamber.

In practice, the constant pressure chamber may be the atmosphere. However this limits the application of the sampling system to higher cylinder pressures since a significant pressure drop across the transfer tube is required to maintain a minimum flow. To enable sampling during low pressure periods of the cycle, such as intake and exhaust strokes, a constant pressure chamber in which a partial vacuum can be created may be required depending on the engine installation and operating conditions. This requirement is greatest if the engine is normally aspirated and running with a closed throttle as opposed to a turbocharged engine operating with a wide open throttle for which minimum cylinder pressures are much greater.

When a constant pressure chamber is used instead of the atmosphere, as shown in figure 6.5, the pressure in it is determined by the average sample flow rate through the transfer tube, the flow to the FID, the vacuum suction controlled by valve F, and the amount of bleed flow through valve E. To maintain approximately constant pressure in the chamber, the bleed flow must be many times greater than the sample flow, and the vacuum supply must be sufficient for there to be a positive sample flow into the chamber at all times.

The junction between the transfer tube and the expansion tube should ideally be a diffuser in order to minimise eddy mixing at this point. However due to the small dimensions of these two tubes this is not practical and a step change which will produce some back mixing has to be accepted. An estimate of the effect of

this back mixing has been made by Collings (9), from the turbulent diffusion time τv across the corner eddy, which has the size $1/2(\emptyset_B - \emptyset_A)$. If we use a conservative estimate of the eddy diffusivity of ;

$$(0.1\ \emptyset_A \mathbb{U}_A)$$

then ;

$$\tau v = \frac{(\emptyset_B - \emptyset_A)^2}{(0.1\ \emptyset_A \mathbb{U}_A)}$$

Using the dimensions from figure 6.5, and a transfer tube exit velocity, $\mathbb{U}_A$, of 100 m/s then ;

$$\tau v \approx 200\ \mu s$$

When a fluid flows in a tube, the presence of a radial velocity profile means that different stream tubes have different convection velocities. If the fluid contains a sample of varying concentration this results in a smearing out of the concentration profile as the fluid travels along the tube. However, if the tube is of very small diameter, this differential convection is to some extent counter balanced by radial diffusion. The effect of radial diffusion on flow through a capillary pipe can be seen in figure 6.6. This resultant effective diffusion is given by Taylor:

$$k = \frac{d^2 \mathbb{U}^2}{(192\ D)} \qquad \text{for laminar flows} \quad (1)$$

and; $$k = 5.05\ dv^* \qquad \text{for turbulent flows} \quad (2)$$

where d is the tube diameter, $\bar{U}$ is the mean velocity, D is the laminar mass diffusivity and v^* is the frictional velocity defined by:

$$v^* = \sqrt{(\tau_w/\rho)}$$

where τ_w is the wall shear stress.

The dispersion time is shown to be linked to the transit time (Lagrangian transit time) for steady flows by;

$$t_p = \frac{\sqrt{(k\ t_s)}}{Vc} \qquad (3)$$

where t_s is the transit time for steady flows and Vc is the velocity of the sample entering the FID. The FID itself has a finite integration or response time during which a unit of sample is averaged. If the transit time was constant, this unit of sample gas would be the same as the unit of sample gas that originally entered the sampling system. The transit time for in-cylinder sampling is however highly unsteady due to the fluctuating cylinder pressure. As a result, the sample gas within the sampling tubes is in effect being either stretched or compressed like a length of elastic, so that for a given interval of time, the averaged sample concentration entering the sampling system will differ from that averaged over the same time interval when it reaches the FID t_s seconds later.

If the integration time for the FID is τ, then Collings (9) shows that;

$$C_m(t) = \frac{1}{\tau} \int_t^{t+\tau} C(t' - t_s(t'))dt' \qquad (4)$$

where $C_m(t)$ is the sample concentration measured by the FID at time t, and C is the concentration at the entrance to the transfer tube. This shows therefore that it is desirable that the transit time t_s is either constant or small.

In calculating the transit time, Collings (9) used one dimensional flow analysis. The velocity profiles in the sampling system are first determined. Because the tube diameters are very small, the thermal entrance length is small compared to the tube length, so that isothermal flow could be assumed. Therefore:

$$\frac{\partial \rho}{\partial t} = - \frac{\partial}{\partial x}(\rho v) \qquad (5)$$

and,

$$\frac{\partial v}{\partial t} = - \frac{RT}{\rho} \frac{\partial \rho}{\partial x} - \frac{f v^2}{2d} - v \frac{\partial v}{\partial x} \qquad (6)$$

Where R is the gas constant, d is the tube diameter, T the temperature, and f the Moody friction factor.

The time for pressure equilibrium in the sampling is of a similar order to that of the cylinder pressure rise time when the engine is running at over 1000 rev/min. Therefore, unsteady flow equations are used for analysis of the transfer and expansion tubes, while steady flow equations are used for the sample tube into the FID as this is exposed to a constant pressure difference.

As the cylinder pressure rises during compression and combustion strokes, the sample gases in the transfer and expansion tubes are accelerated by the increasing pressure force. At some point in time the velocity at exit from the transfer tube becomes sonic and the flow is choked. This is not a problem since the

pressure at the exit to the expansion tube is equal to that of the CP chamber or atmosphere. However, depending on tube dimensions, it may be possible, as the cylinder pressure continues to rise, for the flow at exit from the expansion tube to become choked as well. If this happens, the pressure just inside the end of the expansion tube is no longer equal to that of the atmosphere or the CP chamber, but adjusts according to inlet conditions. The expansion tube would become pressurised and the exit to the transfer tube would eventually become unchoked. Under these conditions there would no longer be a constant pressure difference between the end of the expansion tube and the FID, and the sampling system would have failed.

Since choking at the exit of the expansion tube usually occurs when the whole velocity profile in both the transfer tube and expansion tube are increasing (i.e. the left hand side of equation 6 is positive), a conservative estimate of the inlet pressure at which this occurs is estimated from solving the steady state version of equations 5 and 6. This yields ;

$$\frac{dx}{dv} = \frac{2d}{f}\left(\frac{RT-v^2}{v^3}\right) \qquad (7)$$

When the exit to the expansion tube just chokes, the pressure at the exit is equal to that of the CP chamber, and the velocity is the isothermal speed of sound, $\sqrt{(\gamma RT)}$. The exit of the transfer tube is also choked. Equation (7) is integrated analytically using these boundary conditions, from the expansion tube exit to the transfer tube entrance.

Calculated critical cylinder pressures at which choking of the expansion tube exit occurs are shown in figure 6.7. As can be

seen, it is almost linearly proportional to CP chamber pressure. It is not exactly proportional as the friction factor for the two tubes is dependent on CP chamber pressure.

6.4 Validation Test Rig for the HFR FID

Before any in-cylinder hydrocarbon measurements were made, validation tests under known and controlled conditions were carried out to determine the performance of the FID and sampling system and to allow any necessary modifications to be made. The primary purpose of these tests was to determine if the sampling system would be successful in isolating the FID itself from pressure changes occurring at the end of the sample probe. For the results of these tests to be meaningful for our application, great effort was made to simulate pressure changes expected in the engine. After successful completion of these preliminary tests, attention was then switched to calibration.

Validation tests were performed on a test rig employing the actual prechamber and cylinder head assembly that would later be used for the engine tests. The arrangement is shown in figure 6.8. Using actual engine components allowed the use of sample pressures of similar order to those found within the fired prechamber, and also meant that the integrity of the system could be checked for leakage before being installed on the engine.

The method of inserting the sample probe through the cylinder head and prechamber wall is common with that used during later engine tests and this is described in detail in chapter 7. Connecting nozzles from the prechamber through the cylinder head were blocked off, and a tap for discharging the prechamber

contents was connected to the disused spark plug hole. Sampling gases were fed to the prechamber via the gas admission valve, and an external manually operated gas valve was used to control the rate at which the prechamber was pressurised. Additional valves were used to switch between different sample gas sources. Pressure regulators were used to control delivery pressures. Measurement of the sample pressure within the prechamber, essential for the interpretation of the FID signal, was made by a piezo-resistive pressure transducer.

Output signals from both the FID and pressure transducer were collected using the high speed data acquisition system described earlier.

6.5 Validation Test Procedures

The objective of these tests was primarily to ensure that the HFR FID was pressure independent. To show this, it was necessary to supply the prechamber of the validation rig with a hydrocarbon gas at a number of different pressures. To prove the transient capabilities of the HFR FID, rapid rates of pressure change comparable to those found during the compression and firing strokes of the Dorman gas engine would need to be applied.

Initially a high pressure source of hydrocarbons was not available, so a method of compressing low pressure natural gas with a high pressure supply of nitrogen was used. The prechamber was initially filled with natural gas at a pressure of approximately 3 bar which was delivered via a line connected to the gas compressor installed on the Dorman rig. The prechamber was subsequently charged with a regulated supply of high pressure

nitrogen from a bottle. This both raised the pressure within the prechamber to a much greater level, and leaned off the pure natural gas to a level near to what might be expected at the time of ignition in the fired engine. Pressurisation was performed either slowly and in stages, to examine steady state FID response, or rapidly to investigate the more significant transient response of the FID. Charging the prechamber with pure natural gas and then rapidly compressing with nitrogen, to some extent represented the conditions in the prechamber during the induction and compression strokes of the fired Dorman engine.

One disadvantage of these two stage tests was that as two separate gases were used, a second variable, the mixture strength was introduced and may have given a distorted FID response. Subsequently, a source of premixed high pressure hydrocarbon sample gas (10% methane in nitrogen) was obtained and used in tests where sample pressure only was changed.

6.5 Validation Tests Results

Results from the validation tests initially proved disappointing until problems associated with the sampling system had been overcome. These first tests were done using two gases as previously described. Figure 6.9 shows results from a step pressure change accompanied by a rapid leaning of the mixture from pure natural gas to around 12 % natural gas in nitrogen. The top trace shows the sample pressure, while the lower shows the output from the FID. The FID signal, though apparently measuring correct hydrocarbon concentrations before and after this step change, fails during the transition, indicated by the abrupt spike seen as the pressure first starts to rise. Subsequent repetition of this

test showed that this signal spike reduced in magnitude as the rate of pressure change was reduced, confirming that the error was associated with the transient rather than steady state response of the FID.

It was thought that this temporarily increased sample flow to the FID might be caused by the transition to sonic velocity at the exit of the expansion tube resulting in an increased pressure drop to the FID. Close examination of the T-piece showed an obstruction at the end of the expansion tube which would account for the pressure fluctuations in the expansion tube with resulting changes in sample flow to the FID. This obstruction was removed, and subsequent tests showed the signal spike to be eliminated.

A second series of tests was then performed using a high pressure supply of 10% methane in nitrogen to show clearly if the HFR FID signal was independent of sample pressure. Referring to figure 6.10, a step pressure change was again performed, but with the sample concentration remaining constant. The FID signal, however, is seen to drop sharply as the pressure rises, followed by a gradual recovery of the signal to its original value after a number of seconds. Again, the transient response was at fault. This problem was associated with a temporary drop in the pressure difference between the exit of the expansion tube and the FID chamber. It was believed that this was caused by excessive sample flow into the FID chamber causing a temporary increase in pressure before the vacuum pump was able to regain the original level. The noise seen in the FID signal is believed to be caused by condensation produced by the hydrogen flame forming on the collector electrode.

The connecting sample tube to the FID was reduced in area by the insertion of an inner sleeve from 0.3mm Ø to 0.15 mm Ø , effectively reducing the sample flow by 75% . The previous tests were repeated, and FID signal deviation during a step pressure change was eliminated. Figure 6.11 shows firstly a step pressure increase with no measurable change in FID signal followed by a rapid pressure drop. The FID signal is seen to fall away as the sample pressure drops to below approximately 3 bar. This agrees reasonably well with the critical pressure predicted from the mathematical model for the sampling system without a vacuum CP chamber. Below this critical pressure the sample flow through the expansion tube is less than that demanded by the FID, and so a flow of gas from the CP chamber, or atmosphere as in this case, will occur. This critical pressure is shown more clearly in figure 6.12 when the pressure is increased gradually.

6.6 Summary

The testing and validation of a novel high frequency FID has been described using a sampling system suitable for in-cylinder measurements on an internal combustion engine. This was done by performing a number of controlled bench tests. After several modifications to the sampling system geometry, the instrument was shown to be independent of sample pressure over a range found within a typical spark ignition engine. The instrument was also found to respond linearly to mixture concentration.

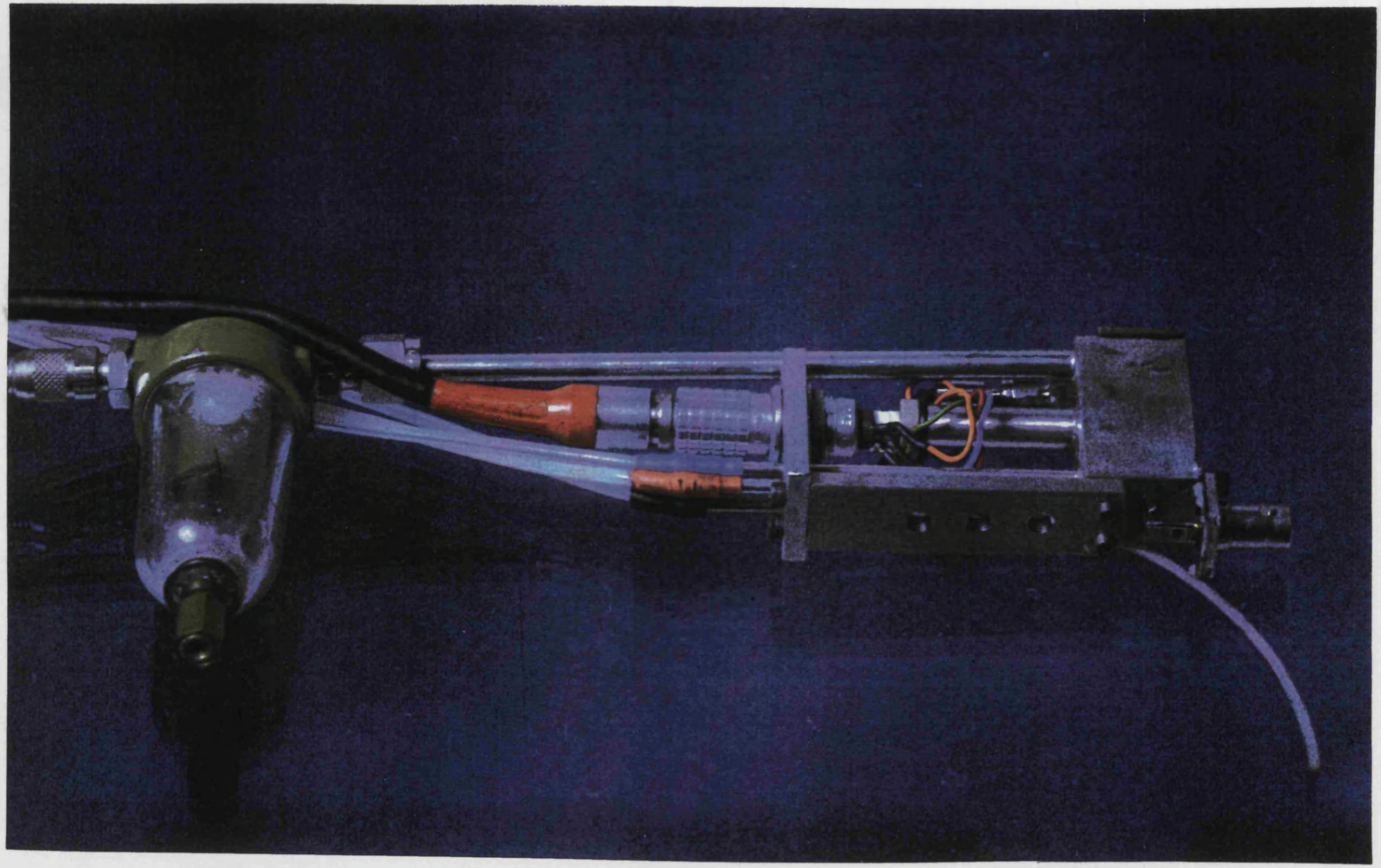

Plate 5. HFR FID Sampling Head

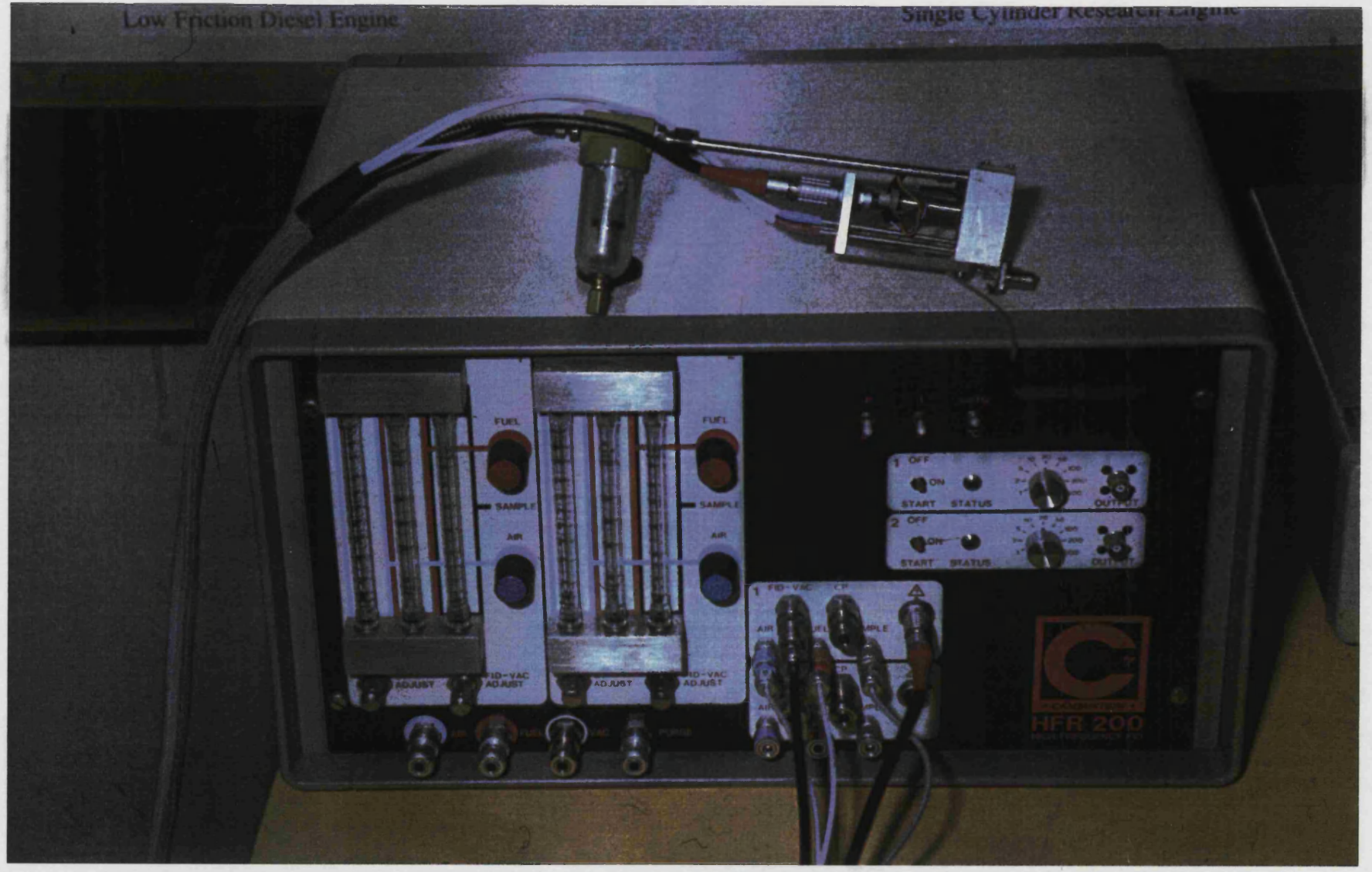

Plate 6. HFR FID Sampling Head and Control Unit

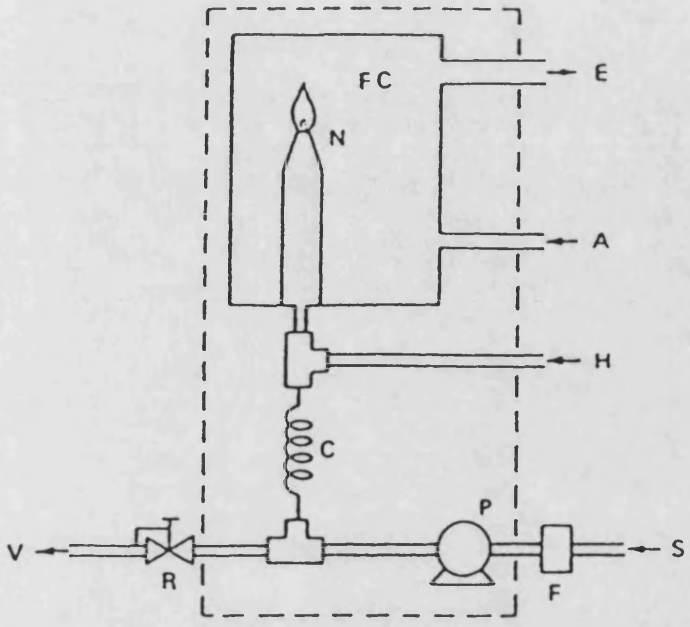

A Regulated air supply
E Exhaust
H Regulated fuel supply
S Sample
F Filter
P Pump
C Sample capillary
R Sample regulator
FC Flame chamber
N Nozzle
V Excess sample vent

Figure 6.1 Conventional FID Arrangement

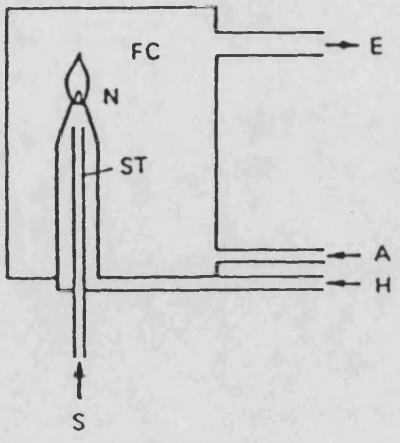

E Exhaust to regulated vacuum
A Regulated air supply
H Regulated fuel supply
N Nozzle
S Sample
ST Sample tube

Figure 6.2 Cambustion FID Arrangement

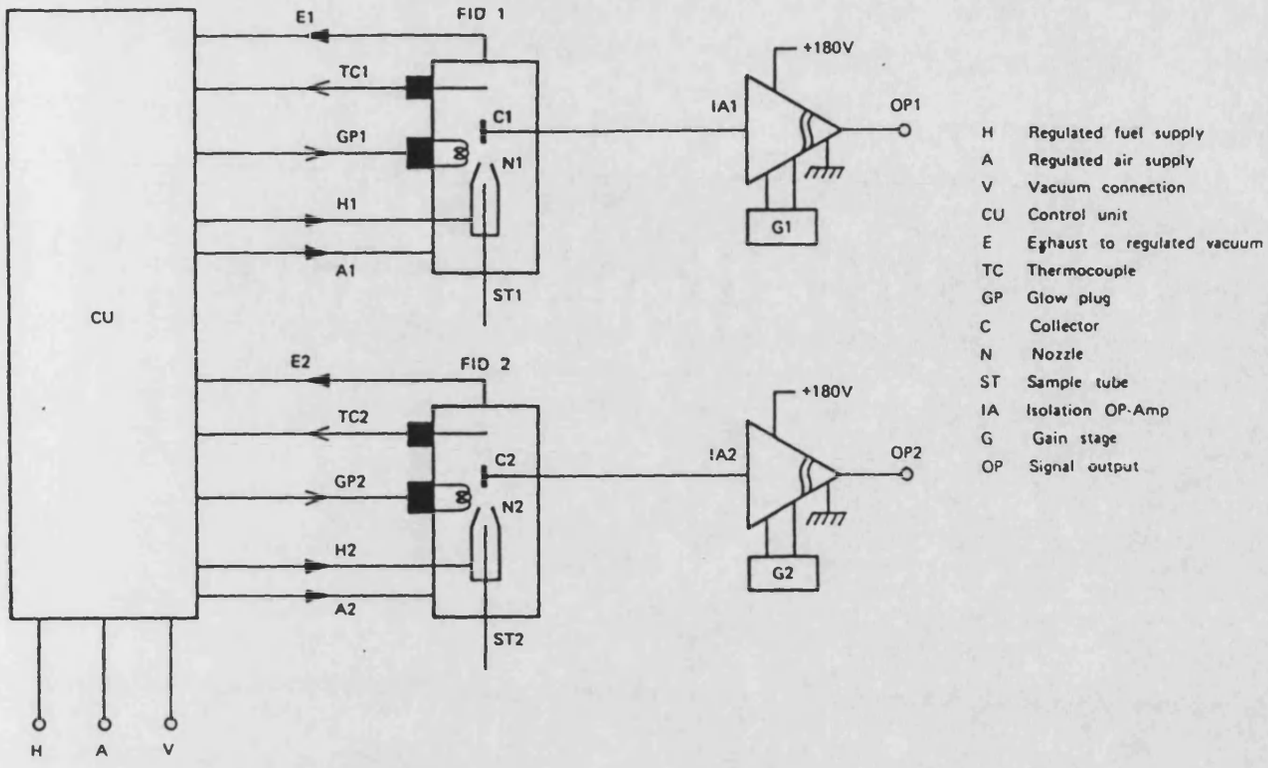

Figure 6.3 Schematic Layout of HFR FID and Control System

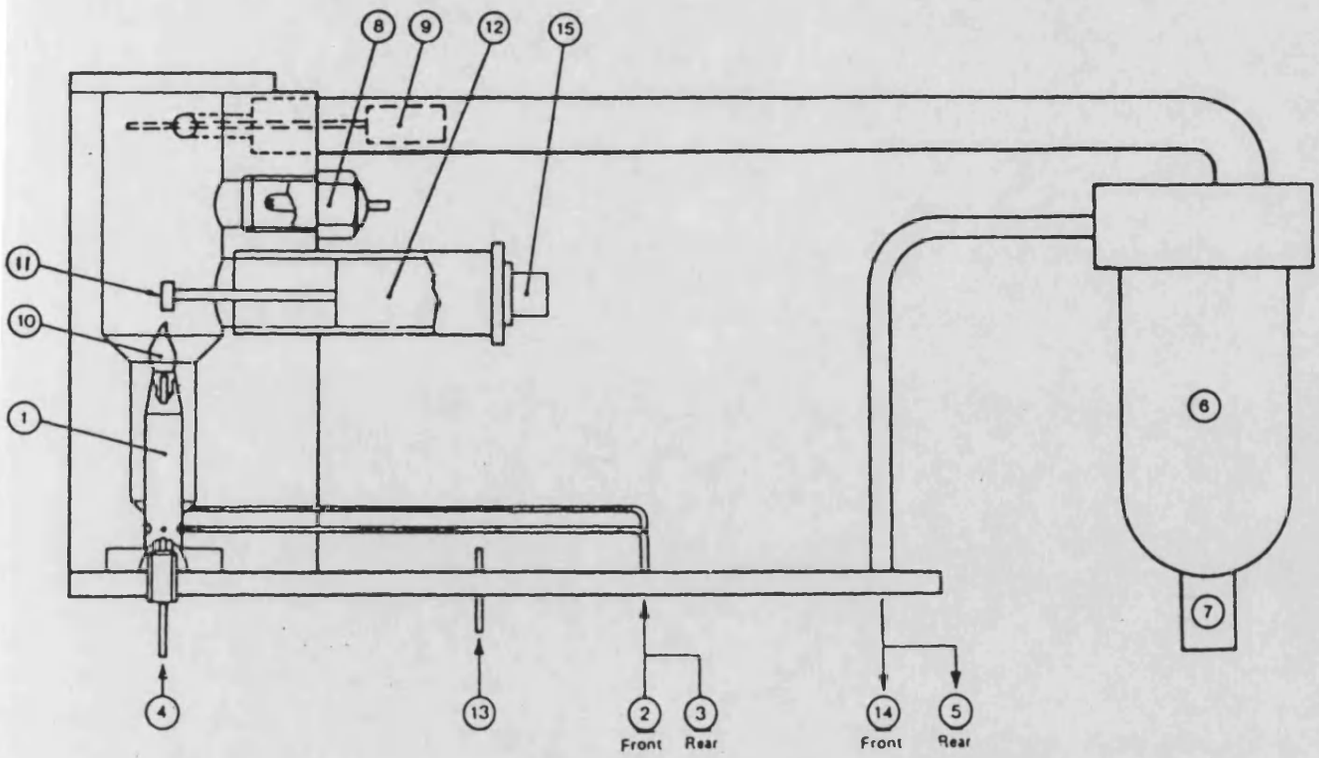

Figure 6.4 Details of HFR FID Sampling System

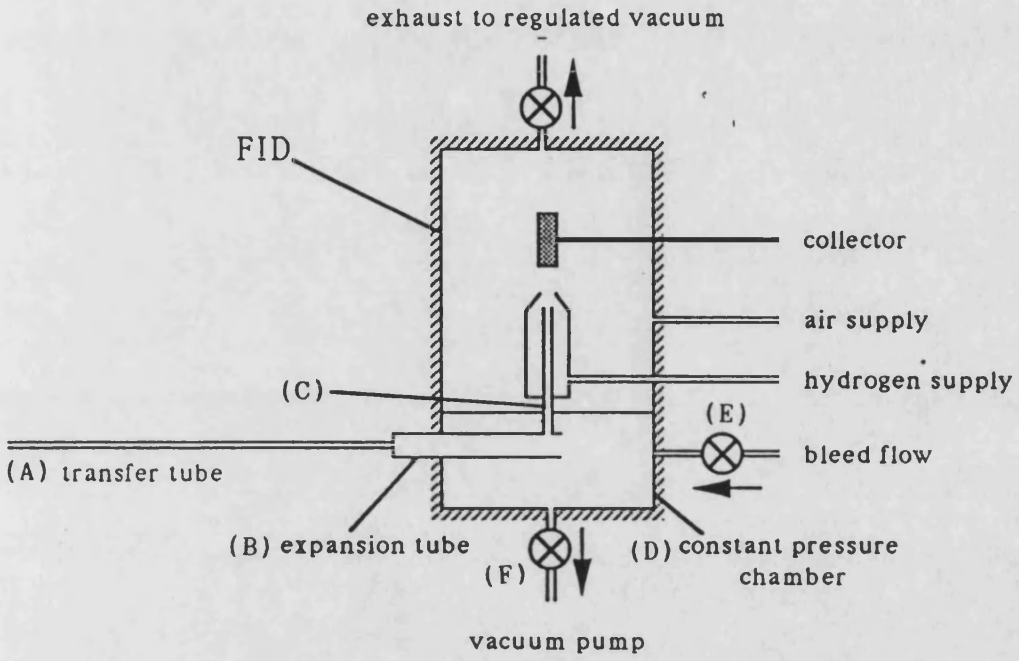

Typical Dimensions (mm):-

	Length	Diameter
(A) Transfer Tube	100	0.2
(B) Expansion Tube	25	0.8
(C) Connecting Tube	30	0.15

(D) Constant Pressure Chamber Volune - 1cc

Figure 6.5 Constant Pressure Sampling System

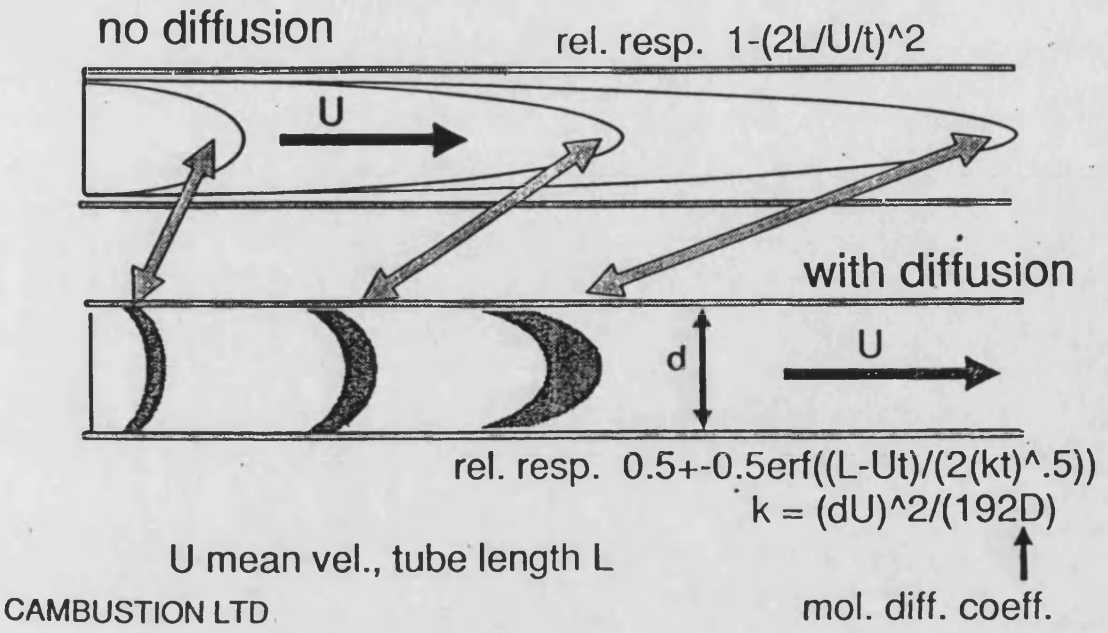

Figure 6.6 Effect of Radial Diffusion on Capillary Flow

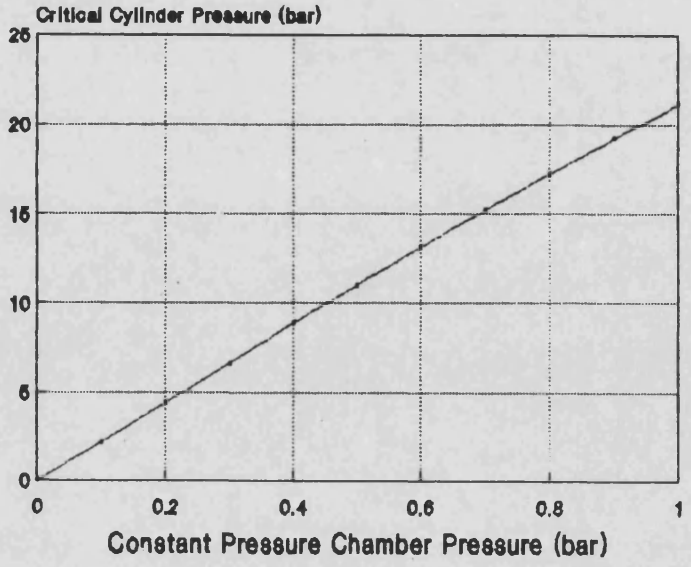

Figure 6.7 Critical Cylinder Pressures at which Choking Occurs at the Expansion Tube exit for the Sampling Unit given in figure 6.5

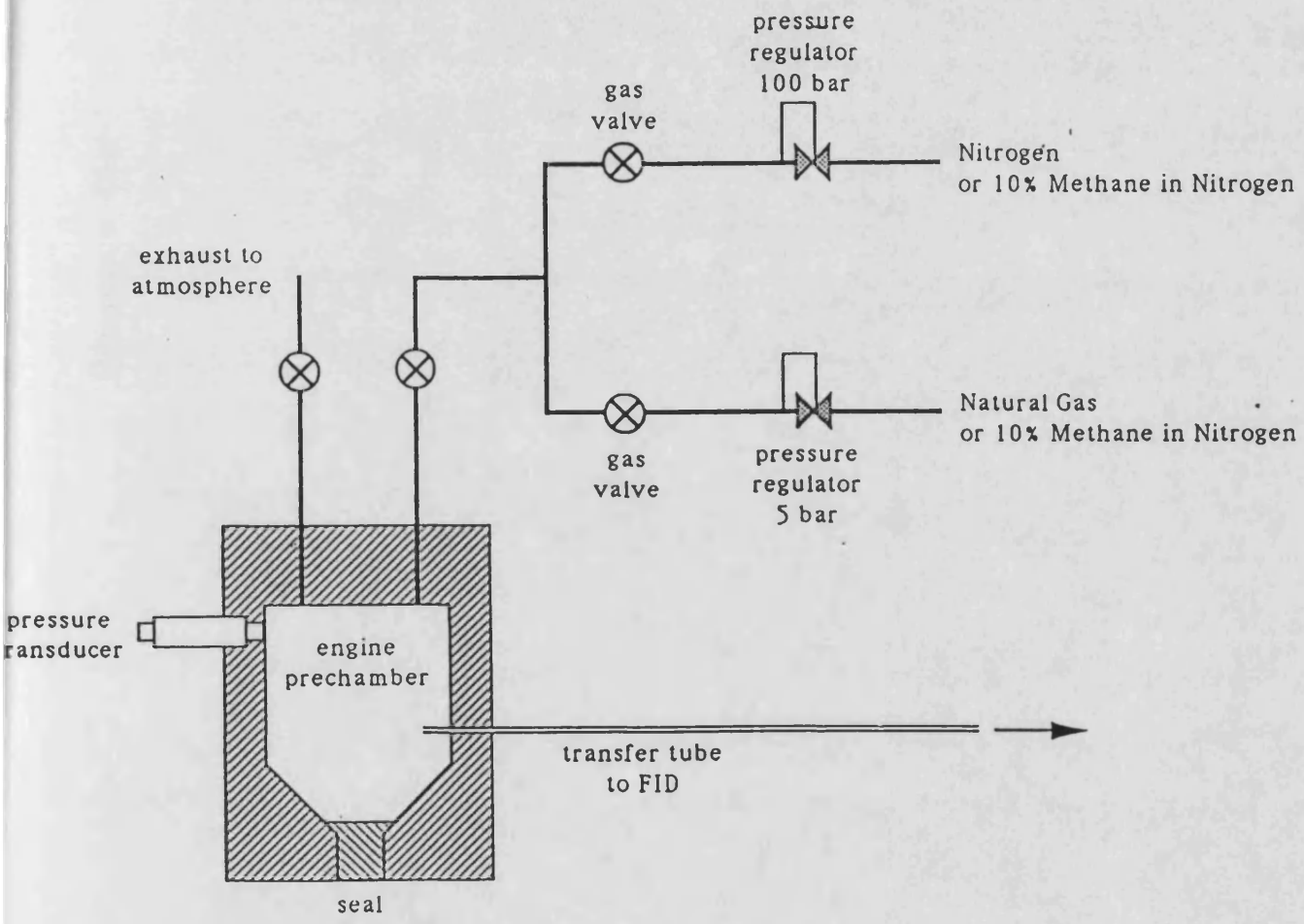

Figure 6.8 Arrangement used for FID Validation Tests

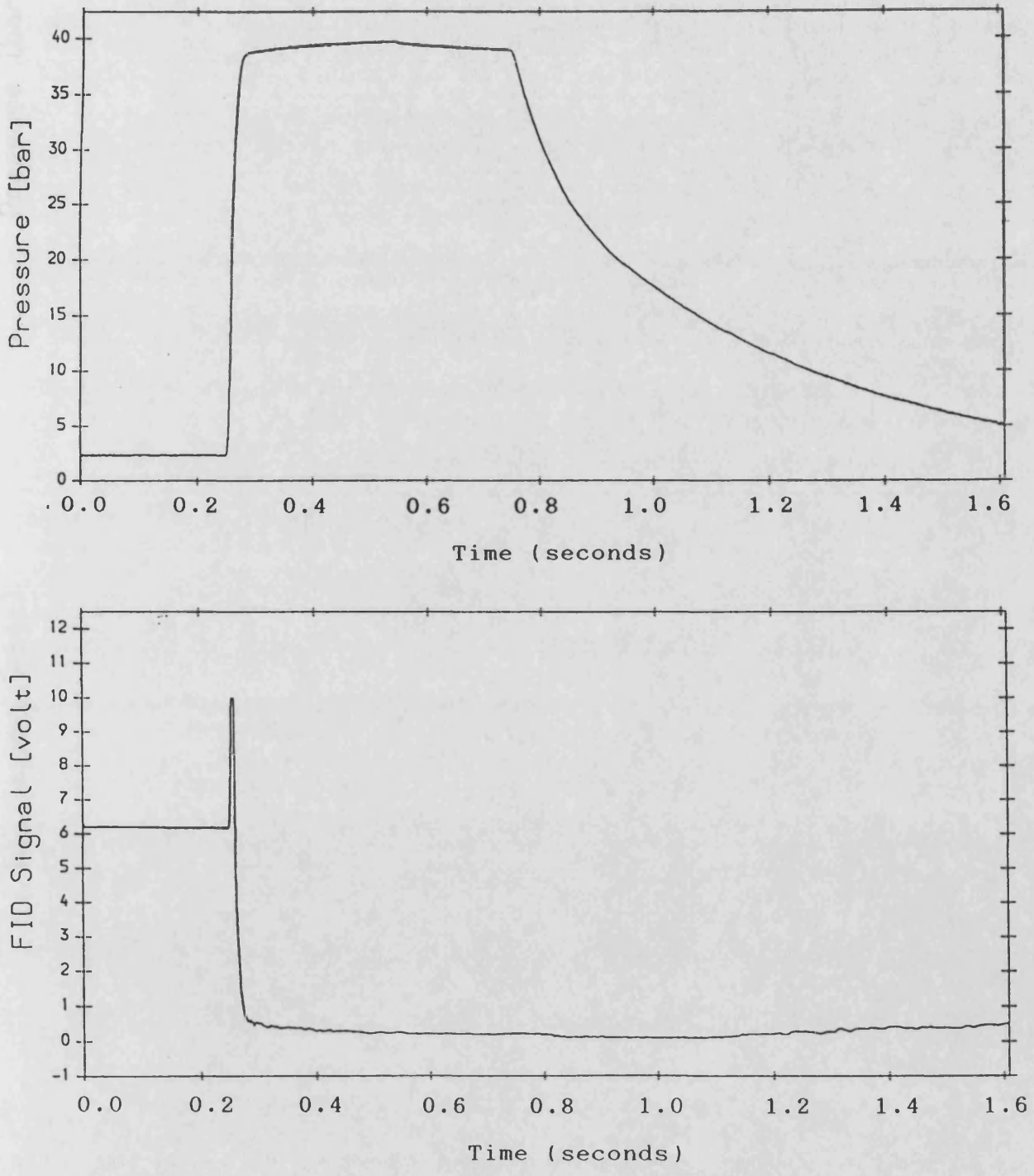

Figure 6.9 FID Signal for Step Pressure Change Accompanied by Rapid Leaning of Mixture

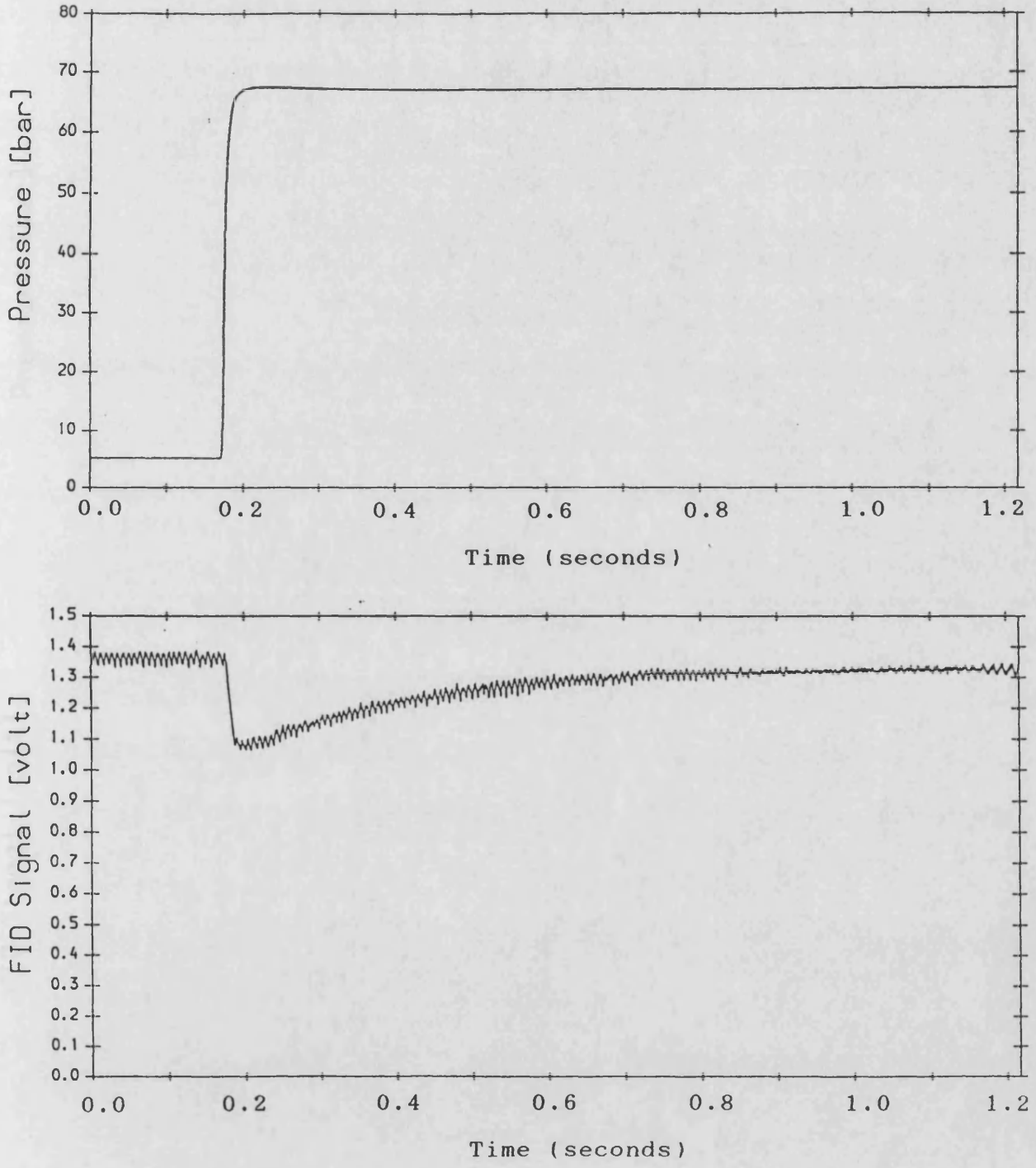

Figure 6.10 FID Signal for Step Pressure Change using 10% Methane in Nitrogen

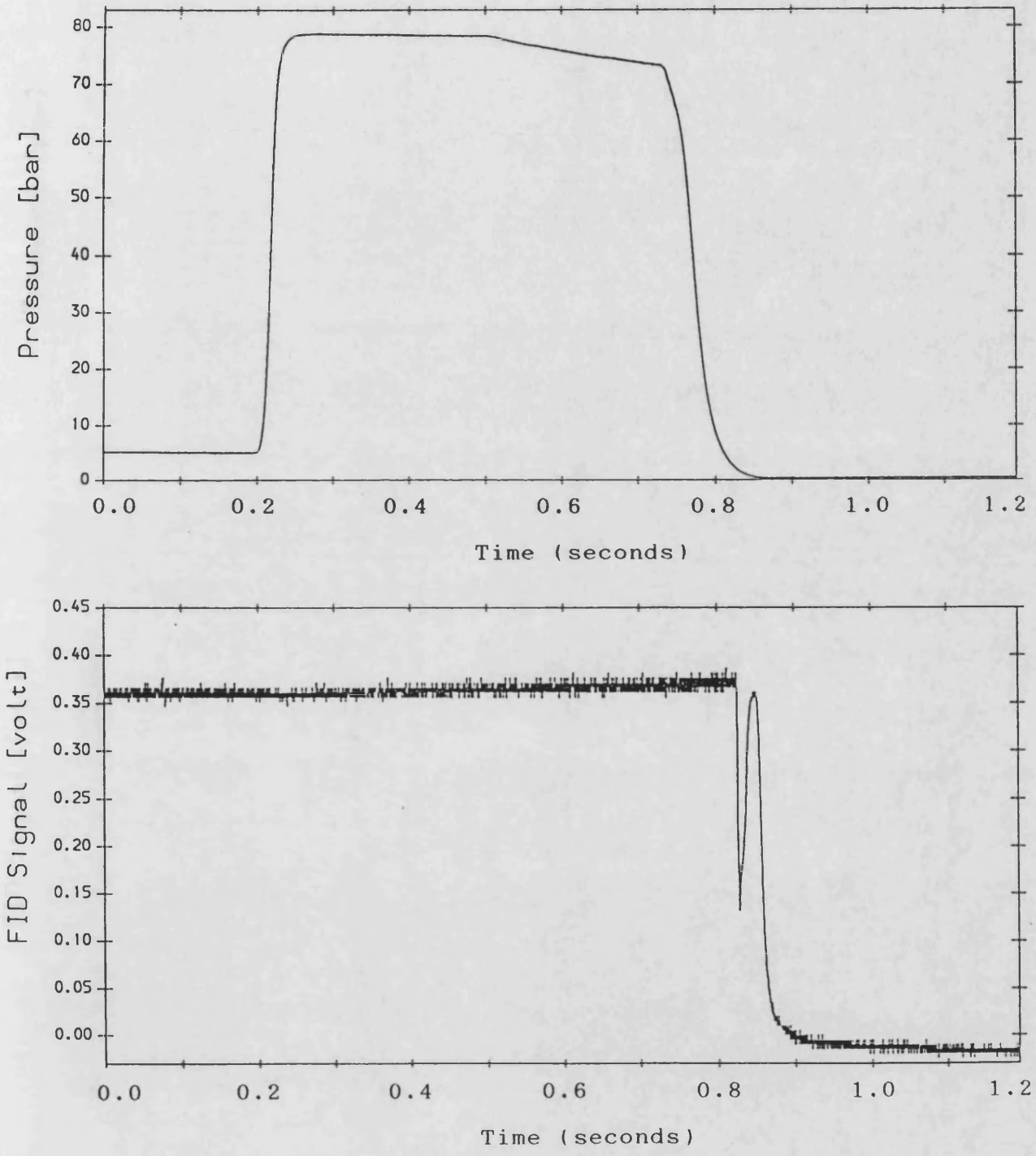

Figure 6.11 FID Signal for Step Pressure Increase Followed by Rapid Pressure Drop using 10% Methane in Nitrogen

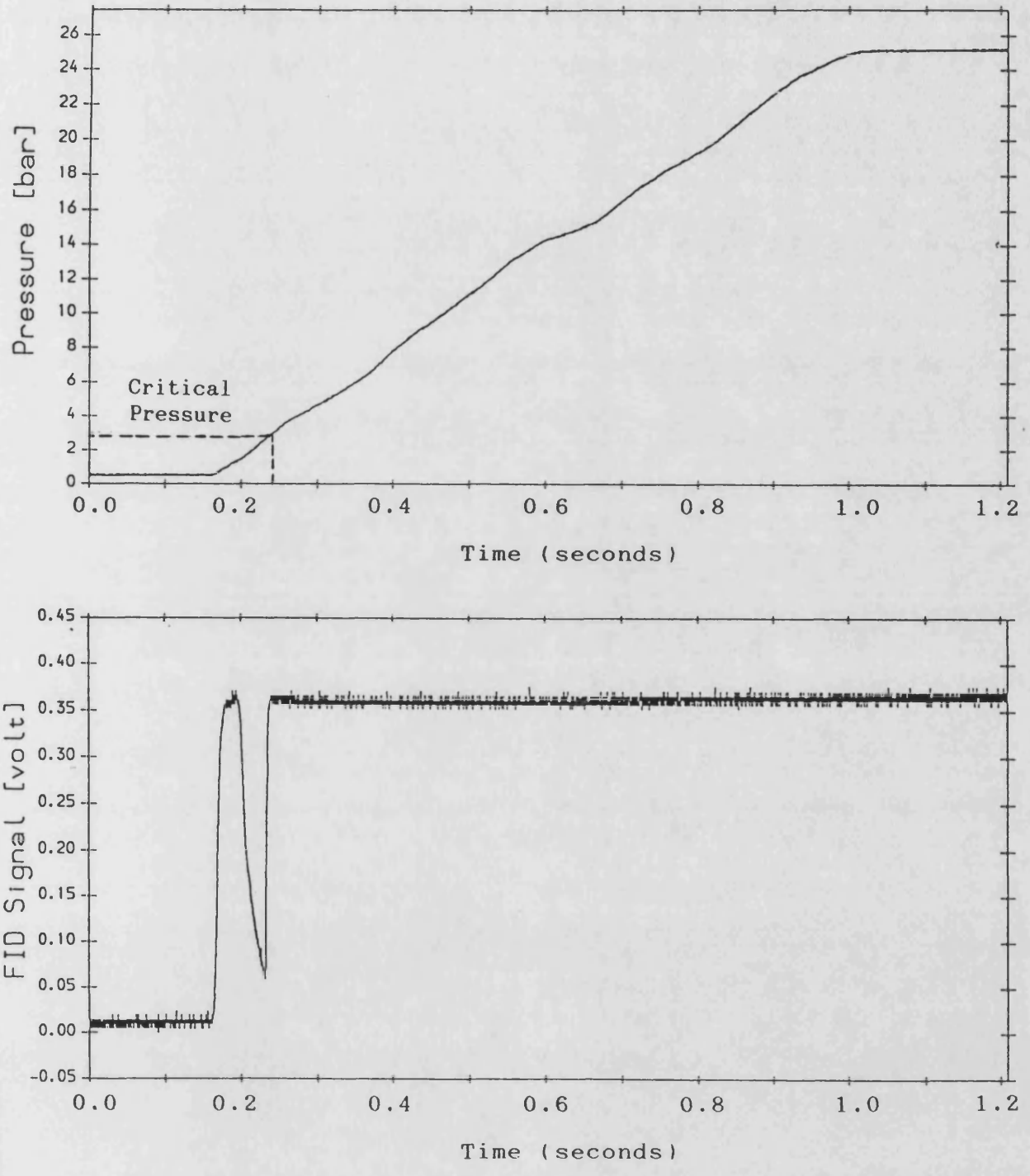

Figure 6.12 FID Signal for Gradual Pressure Rise using 10% Methane in Nitrogen

Chapter 7

7. Prechamber Hydrocarbon Sampling using the HFR FID

7.1 Introduction

This chapter describes the application of the HFR FID sampling system, described in chapter 6, to measure the instantaneous hydrocarbon concentration within the prechamber of the SE1 gas engine. This technique is relatively new, and untried on this type of engine. The object was to investigate the variation of mixture concentration with respect to time and space within the prechamber. The effect of changing certain engine operating parameters was also investigated.

7.2 Engine Installation of the HFR FID

The FID sampling system geometry used during these engine measurements was the same as previously used in the validation tests reported in chapter 6. They were originally derived from calculations using the flow model developed by Collings (9), and by the physical constraints of the engine.

For several reasons, the Dorman SE1 engine is particularly well suited to this technique of sampling. Firstly, as the engine is of a single cylinder design, the space around it allows greater freedom for inserting a sample probe through the cylinder head walls. Secondly, the fuel used is gaseous, and so there is not the possibility of fuel droplets blocking the small sample tubes to the FID as with liquid fuelled engines. Thirdly, the engine is designed to operate at relatively low crankshaft speeds, hence allowing more time for the FID to sample during the engine cycle. As the time constant for the HFR FID is both finite and independent of crankshaft speed, this means that more of the FID

signal will be meaningful. This point is illustrated clearly in work reported by Heywood (13) for an engine operating at different speeds. Finally, the SE1 engine is designed for turbocharged operation, therefore the lowest pressures within the cycle will be significantly higher than for a naturally aspirated engine. These higher cylinder pressures, as a consequence, will increase the period during the cycle when the instrument will operate.

The main difficulty of sampling from within the prechamber was in gaining access to the prechamber itself. The SE1 engine uses a four valve cylinder head, and the prechamber assembly is positioned in the centre of these valves. This means that sampling from the prechamber is more difficult than from the main combustion chamber, resulting in a longer sample tube with a corresponding reduction in instrument performance.

Work on in-cylinder measurement reported by Heywood (13) used a sampling system in which the sample tube was passed into the combustion chamber through a drilled spark plug. This method allows measurement of the mixture near to, or within the spark gap. Though obviously a very desirable method of sampling, it was thought to be unsuited for initial measurements on the SE1 engine. This was because the SE1 engine uses an unconventional platinum electrode spark plug and accurate drilling of it to accept a sample tube would prove difficult. Access to the spark plug on this engine is awkward and would result in a longer sample transfer tube to the FID compared to a method of direct entry through the cylinder head wall. This would result in reduced FID performance as a result of increased time constant and transit time for the sampling system.

It was decided that a method of passing a sample tube through the side wall of the cylinder head and into the prechamber would be adopted. As the cylinder head is a four valve design, space is limited, and much work was done in determining the most direct route to the prechamber through the cylinder head water jacket, while avoiding valves, ports and oil passageways. Details of the probe and its insertion into the prechamber are shown in figure 7.1. The hypodermic transfer tube is contained within a protective sleeve. This in turn is housed within a larger sample probe together with a thermocouple for measuring the prechamber wall temperature. The probe passes through the wall of the prechamber and finishes flush with the inner surface. A gas-tight seal between the probe and the prechamber is provided by a clamping force exerted from a bolt passing through the exterior cylinder head wall. The integrity of this seal was tested during the earlier validation tests described in chapter 6. Plate 7 shows the probe inserted into the prechamber, while plate 8 shows the sampling head installed on the engine. A schematic diagram showing the sampling arrangement is shown in figure 7.2.

Although the position of this probe was fixed relative to the cylinder head, the two piece symmetrical construction of the prechamber assembly did offer scope for movement of the sampling point in relation to prechamber geometry. Minor modifications enabled the upper section of the prechamber assembly which contained both the spark plug and gas admission valve to be rotated a full revolution with respect to the lower section through which the sample probe was fixed. This effectively allowed measurements to be taken at points around the prechamber perimeter on this fixed plane.

The possibility of sampling the gases away from the prechamber wall and towards the centre of the prechamber by extending the length of the sample tube also existed. Initial tests were done using a protruding sample tube, but as a result of its small size and the high combustion temperatures occurring within the prechamber, the protruding portion of the sample tube was unable to survive for any length of time and so the idea was not pursued. A larger, more robust sample tube would survive, but however, its effect on the flow of gases within the prechamber could become significant.

7.3 Calibration of HFR FID For Prechamber Measurements

Accurate calibration of the HFR FID is more difficult than for a conventional steady state FID as its performance is orientated more towards rapid response times than long term repeatability. Validation tests reported in chapter 6 demonstrated the sensitive nature of the HFR FID to its controlling parameters, and suggest that results are best judged qualatively rather than quantitively. A method of calibrating the FID was pursued, however, in order that quantitative interpretation of the in-cylinder results could be made.

Ideally, calibration of the HFR FID should be done under conditions as close to those found during the engine tests as possible. Calibrating the HFR FID with span gas, while connected to the engine, at regular intervals during the engine tests would be the most satisfactory solution as this would involve least disturbance to the sample system. This would involve flooding the combustion chambers with a combustible span gas and was considered both impractical and unsafe. Instead, calibration was done away

from the engine on a separate calibration rig.

Details of the calibration rig are shown in figure 7.3. The arrangement approximates to that used during the engine tests. This consists of a "dummy" transfer tube connecting the sampling head to a high pressure vessel supplied with a controlled span gas. This "dummy" transfer tube is of the same dimensions as the one installed in the cylinder head. The span gas is fed into the vessel via a pressure regulator from a high pressure source. It was believed important to calibrate the HFR FID at various high and low pressures so that the pressure independence of the instrument could be periodically checked. A piezo resistive pressure transducer was included so that accurate measurement of the span gas pressure within the vessel could be monitored.

Although the FID will respond to all hydrocarbon gases, its response will depend on the carbon to hydrogen ratio of the fuel. It is therefore important that the span gas should be the same as the gas to be sampled, and of similar concentration. Since it was intended to sample natural gas (94% methane), a span gas of known concentration of methane was used for calibration.

7.4 Preliminary Test Results

Initial prechamber tests were at a standard engine operating condition, details of which are listed in figure 7.4. The FID sampling system was operated with a vacuum of 600 mm Hg in the constant pressure chamber with the objective of measuring fuel concentration during the low pressure induction stroke as well as during compression and combustion strokes. The sampling position for these tests was fixed to one point on the perimeter of the

prechamber, approximately half way up and immediately opposite the gas admission valve.

The resulting FID signal from these tests indicated changes in methane concentration during the later part of the compression stroke. The signal was seen to be repeatable from cycle to cycle. Figure 7.5 shows a typical FID signal together with the pressure within the main cylinder. This FID signal is shown without any correction for transit time.

7.5 Interpretation of FID Signal

Correcting the FID signal for the transit time between events occurring within the prechamber to those at the FID required careful consideration. As discussed in chapter 6, this transit time is dependent on the sample pressure, it's value changing greatly between low and high pressures. This is also true of the frequency response and time constant of the instrument. The flow modelling computer program "Satflap" was used to determine changes in these quantities with respect to sample pressure for the sampling system.

Figure 7.6 shows the effect of cylinder pressure on transit time and frequency response for the sample system geometry used for the in-cylinder measurements. Transit time is shown to decrease as the sampling pressure increases. This relationship approximates to that of a rectangular hyperbola, and for sample pressures above 10 bar, the transit time tends to a constant value of 5 ms which equates to a crank angle of 45 degrees. This value was used to correct the FID signal for transit time by shifting it 45 degrees forward. Although the FID signal begins at sample

pressures below 10 bar, this period cannot be corrected for as the time constant for the sampling system at these low pressures is large and consequently the signal is believed to be showing the response characteristics of the instrument.

Frequency response is shown in figure 7.6 to increase with cylinder pressure as the velocities within the sample pipes increase. Two step increases in frequency response are shown to occur at approximately 5 bar and 35 bar cylinder pressure. These are as a result of the transition from laminar to turbulent flow in the sampling system. This occurs firstly in the transfer tube, and then in the expansion tube. The frequency response with turbulent flow is greater than with laminar flow as the turbulence reduces the effective diffusion within the sample pipe as discussed in chapter 6.

Figure 7.7 shows the FID signal after being corrected for a transit time of 5 ms and converted to hydrocarbon concentration by mass using results from calibration tests. Four distinct stages are apparent in the FID signal. These stages can be explained by the events known to be occurring within the prechamber, and the theoretical performance of the HFR FID.

The first part of the signal, shown from 25 to 90 degrees crank angle after btdc would actually have occurred much earlier during the induction stroke during which the sample pressure is very low and transit and response times would be very high. This portion of the signal is believed to be predominantly showing the response characteristics of the FID at these very low pressures, and not changes in mixture concentration. If the FID were able to respond to changes in mixture concentration during this period, we

would expect to have seen a leveling off of the prechamber mixture concentration during the later part of the induction stroke and early part of the compression stroke as the prechamber becomes full of fresh charge from the gas admission valve. This has been shown to be the case with results from CFD modelling, reported in chapter 8 of this thesis. There are signs of the mixture levelling off between 75 and 90 degrees, although it is not clear if this is real, or due to the poor response of the FID.

In work reported by Heywood (13) on a conventional engine, a plateau region of constant mixture concentration was seen during the compression stroke close to the point of ignition. With the prechamber engine design, this plateau region would be greatly reduced in size as the prechamber mixture would be rapidly leaned down during the later part of the compression stroke by the leaner mixture within the main cylinder being forced into the prechamber through the connecting nozzles. Consequently a method of skip firing the engine to allow the FID time to respond, such as employed by Heywood for higher engine speeds, would not enable this plateau concentration to be obtained.

From about 90 degrees after btdc, the FID signal begins to fall, which can only be as a result of a decrease in mixture concentration. This is the expected leaning down effect occurring during the compression stroke, although while the pressure is still below 10 bar, the signal will be distorted with respect to crank angle as the assumption of a 5 ms transit time would be inaccurate and the low frequency response of the instrument would essentially filter out the higher frequency components of the signal. As the pressure rises above 10 bar at approximately 130 deg abdc (50 deg btdc) the FID signal is effectively a real time

measurement of the mixture strength.

Confirmation that the assumption of a 5 ms transit time is realistic is indicated by the point at which the mixture at the sampling point is burnt. This is shown clearly by a sharp fall to zero of the FID signal at around 5 degrees btdc. This agrees well with the ignition timing of 12 degrees btdc shown in the trace below the FID signal when allowance is made for the fact that the point of sampling is some 20 mm in distance from the position of the spark.

The FID signal was found to be consistent from cycle to cycle. This is clearly shown in figure 7.8 where FID signals from 9 consecutive cycles are shown overlaid.

The FID response to the flame front passing the sampling point is a reliable means of measuring the time constant of the HFR FID. Since the flame speed is very high, and the sampling area is very small, there is effectively a step change occurring at the sampling point. Figure 7.9 shows more clearly the uncorrected FID signal, converted to mixture concentration by mass, at this time. A 90 % drop in signal is seen to occur in a period of approximately 10 degrees crank angle. This equates to a time constant for the instrument of approximately 1 ms. This compares with the value predicted by the flow model computer program SATFLAP of 0.6 ms. Also from figure 7.9 a measurement of transit time for the sampling system is clearly shown to be approximately 47 degrees crank angle.

Absolute values of measured mixture concentration by mass give good agreement to those expected. The peak concentration

measured is seen to be approximately 30 % natural gas which would have occurred earlier in the induction stoke. This is equivalent to an air-fuel ratio of 3.3:1. The delivery air-fuel ratio was actually 3:1 . At the time of ignition, the measured fuel concentration is seen to be approximately 6 % , or 17:1 air-fuel ratio by mass. This is very close to the stoichiometric air-fuel ratio which is the desired mixture strength in the prechamber at the time of ignition. However, it should be noted that this is actually the air-fuel ratio measured at one point at the prechamber perimeter, and is not representative of the overall prechamber air-fuel ratio which is known to be inhomogeneous.

7.6 The effect of Prechamber Fuel Flow on Measured Mixture Strength

With the engine operating at the standard operating condition given in figure 7.4, the air-fuel ratio of the pilot charge supplied to the prechamber was varied by changing the flow of natural gas. Figure 7.10 shows FID signals for four pilot air-fuel ratios and corresponding cylinder pressure traces. As expected, as the gas flow to the prechamber is increased, mixture concentration is seen to increase throughout the cycle. With higher gas flow to the prechamber the FID signal is seen to begin earlier. This is as a result of the higher gas supply pressures associated with increased flow causing the gas admission valve to open earlier in the induction stroke.

Richer air-fuel ratios supplied to the prechamber are shown to result in richer mixtures at the time of ignition. The signals for these richer mixtures are seen to be extinguished later as the flame front passes the sampling point. This would indicate that

flame speeds are reduced for mixtures rich of stoichiometric. Pressure within the main cylinder is shown to be greatly dependent on prechamber mixture concentration. This is perhaps not unexpected since the period of time for the flame front to pass through the prechamber and into the cylinder governs the effective ignition timing, and the flame speed is dependent on mixture concentration.

With maximum gas flow to the prechamber, total misfire of the engine was seen to occur. In figure 7.11, an example of a misfired cycle followed by a fired cycle is shown by the darker trace. The lighter trace superimposed on top shows two consecutive fired cycles for comparison. Cylinder pressure for each of these is shown above. In both cases, the hydrocarbon concentration during the compression stroke up to the point of ignition is shown to be the same. In the misfired cycle, the HFR FID continues to sample the mixture concentration during the power stroke showing initially a constant concentration followed by a gradual reduction.

The HFR FID also continues to sample into the exhaust stroke indicating a sharp increase in natural gas concentration at 450 degrees CA followed by a gradual decline. If we attempt to correct for transit time at these low pressures ($\approx$ 15 ms), this peak in mixture concentration is likely to occur at around 300 degrees CA. This occurence demonstrates two important points. Firstly, the HFR FID using a vacuum constant pressure system appears to be able to sample from within the prechamber during the low pressure periods of the engine cycle although precise interpretation of the signal may not be possible. Secondly, the peak in mixture concentration during the exhaust stroke confirms

the possibility of the gas admission valve opening during the exhaust stroke. During a misfired cycle, the pressure within the prechamber during the exhaust stroke is greatly reduced when compared to a fired stroke, as seen in figure 7.11. This may result in the pressure difference across the gas admission valve becoming positive instead of negative, since it is pressure operated, it will momentarily open.

7.7 The effect of Ignition Timing on FID Signal

Ignition timing for the engine was varied between 8 degrees btdc and 20 degrees btdc while all other operating parameters were maintained constant. Pilot air-fuel ratio to the prechamber was set at 3.0:1 with a filling ratio of 1.2. FID signal traces for ignition timings of 8,12,16 and 20 deg btdc are shown overlaid in figure 7.12. Cylinder pressures are also shown. As expected with a spark ignition engine, peak cylinder pressure is seen to increase as ignition timing is advanced. The main feature observed in the FID signals is that as the ignition timing is advanced from 8 deg btdc to 20 deg btdc, the point at which the flame front passes the sample probe (seen as a rapid fall in the signal around 180 deg CA) is advanced by the same number of deg CA. This indicates that flame speeds and flame initiation periods are unaltered by ignition timing.

7.8 Mixture Distribution around Prechamber Perimeter

Measurement of the mixture concentration around the perimeter of the prechamber was possible by rotation of the upper portion of the prechamber. As the design of the prechamber is symetrical about a vertical plane through the centre of the spark plug and

gas admission valve, only a rotation of 180 degrees is necessary to show the full distribution. Measurements were made at five points through the rotation, and for several pilot prechamber air-fuel ratios.

FID measurements were taken around the prechamber perimeter for pilot air-fuel ratios of 3.7:1, 3.0:1 and 2.3:1 under fixed load conditions. Figure 7.13 shows ensemble averaged measurements over 20 consecutive cycles at the five sampling positions for a pilot air-fuel ratio of 2.3:1, after correction for FID transit time. It is seen that some variation in measured mixture strength occurs around the prechamber perimeter, with a tendency for the mixture to be richest nearest to the pilot gas admission valve.

The results of these measurements are shown more clearly in figures 7.14 to 7.16 as polar plots of mixture concentration for each pilot air-fuel ratio at two points in the compression stroke, 45 deg btdc and 12 deg btdc. In the centre of these plots, a cross sectional representation of the prechamber showing spark plug and gas admission valve positions is included. The pilot air-fuel ratios for these plots are 3.7:1, 3.0:1 and 2.3:1. Fuel concentrations at each point are expressed as both percentage mass on the right side, and air-fuel ratio on the left.

Several features concerning mixture in these three plots are observed. As expected, fuel concentrations at both 45 deg btdc and 12 deg btdc increase at all positions around the perimeter as the pilot air-fuel ratio delivered to the prechamber is enrichened in the three plots. For each pilot air-fuel ratio, mixture distribution around the prechamber perimeter is seen to vary to differing extents at both 45 deg btdc and 12 deg btdc. In all

cases, the mixture concentration is richest on the side of the prechamber nearest the gas admission valve.

This tendency for the mixture concentration to be greatest near the gas admission valve is seen to be most significant earlier in the compression stroke at 45 deg btdc, and less so at the time of ignition. This indicates that during the compression stroke, the fuel mixture within the prechamber apart from being leaned down by the jet of leaner mixture from the main chamber, becomes better mixed around the perimeter of the prechamber. For the two leaner pilot air-fuel ratios, this mixture distribution is nearer to uniform around the prechamber, particularly at the time of ignition. This may be as a result of the quantity of mixture entering the prechamber (filling ratio) having been changed in order to achieve the increased air-fuel ratio. For the three pilot air-fuel ratios of 3.7:1, 3.0:1 and 2.3:1, the prechamber filling ratios are 1.1, 1.2, and 1.35 respectively.

7.9 Comparison with Results from CFD by Moore (18)

Comparisons of mixture distribution around the prechamber perimeter can be made with results produced using CFD modelling by Moore (18) . A CFD model had been produced using the computer code PHOENICS to model gas mixing within the prechamber during the intake and compression strokes up to the point of ignition. Figure 7.17 shows contours of air-fuel ratio over a section through the prechamber for similar engine operating conditions. The gas admission valve would be in the top left hand corner of the model. These results are for a pilot prechamber air-fuel ratio of 2.3:1 and at 12 degrees btdc and with a prechamber volume of 15 cc (experimental results obtained using 10 cc prechamber).

Comparisons can be also be made between measured mixture concentrations during the compression stroke at positions around the prechamber perimeter and computed values obtained using the PHOENICS CFD model. Figure 7.18 shows both transit time corrected FID measurements at positions around the prechamber perimeter and computer predicted values for the same pilot air-fuel ratio of 2.3:1. FID measured values shown here for the five positions around the prechamber are ensemble averaged over 20 consecutive cycles. It should be noted that the computed values of gas concentration are spatially averaged overall values, however the FID measurements are point measurements at specific positions around the prechamber perimeter. Measured mixture levels agree well with the overall computed values after approximately 65 degrees btdc (135 degrees crank angle). Before this point, the FID appears unable to operate, confirming earlier thoughts that the peak in the FID signal represents the time at which the FID begins to provide real hydrocarbon measurements. Before this point, it is believed that the large time constant of the instrument resulting from the lower cylinder pressures earlier in the compression stroke limit the operation of the FID.

The computed variation in mixture concentration during compression indicates how the FID signals are likely to have appeared had the instrument been working earlier in the compression stroke. Once the FID begins to respond to changes in mixture concentration within the prechamber, the trends correlate very well with computer predicted values. Measured FID values are, as already mentioned, point measurements at positions around the prechamber perimeter. However, mixture concentrations are likely to be higher at these positions around the prechamber

perimeter relative to the overall prechamber concentration as a result of the central jet of leaner charge entering the prechamber during the compression stroke. This effect can be seen clearly in figure 7.17, showing how the mixture concentration becomes leaner along a traverse from the prechamber perimeter to the centre. This suggests that absolute values of gas concentration would perhaps agree even more closely with predicted values when this difference is taken into account.

7.9 Summary

Mixture concentration has been sampled from within the prechamber of the SE1 gas engine during part of the engine's cycle. The HFR FID was found to begin working correctly from between 50 deg and 80 deg btdc during the compression stroke and to continue to do so during the power and exhaust strokes. Confirmation of the instrument's performance (time constant and transit time) determined using the Collings (9) computer model has been achieved by measuring the time and duration of the flame front passing the sampling point. During parametric tests, the following features were observed:

Increasing the pilot mixture concentration, above stoichiometric at the time of ignition, is seen to reduce flame speeds until eventually total misfire occurs. In the case of misfire, and as a result of the subsequent reduced pressures, the prechamber valve was found to open during the exhaust stroke.

Ignition timing has little or no effect on flame speeds or flame initiation period.

Mixture variation around the prechamber perimeter was found to vary by up to 50% during the compression stroke, the richer mixture being nearest the gas admission valve, but at the time of ignition was found to be almost uniform.

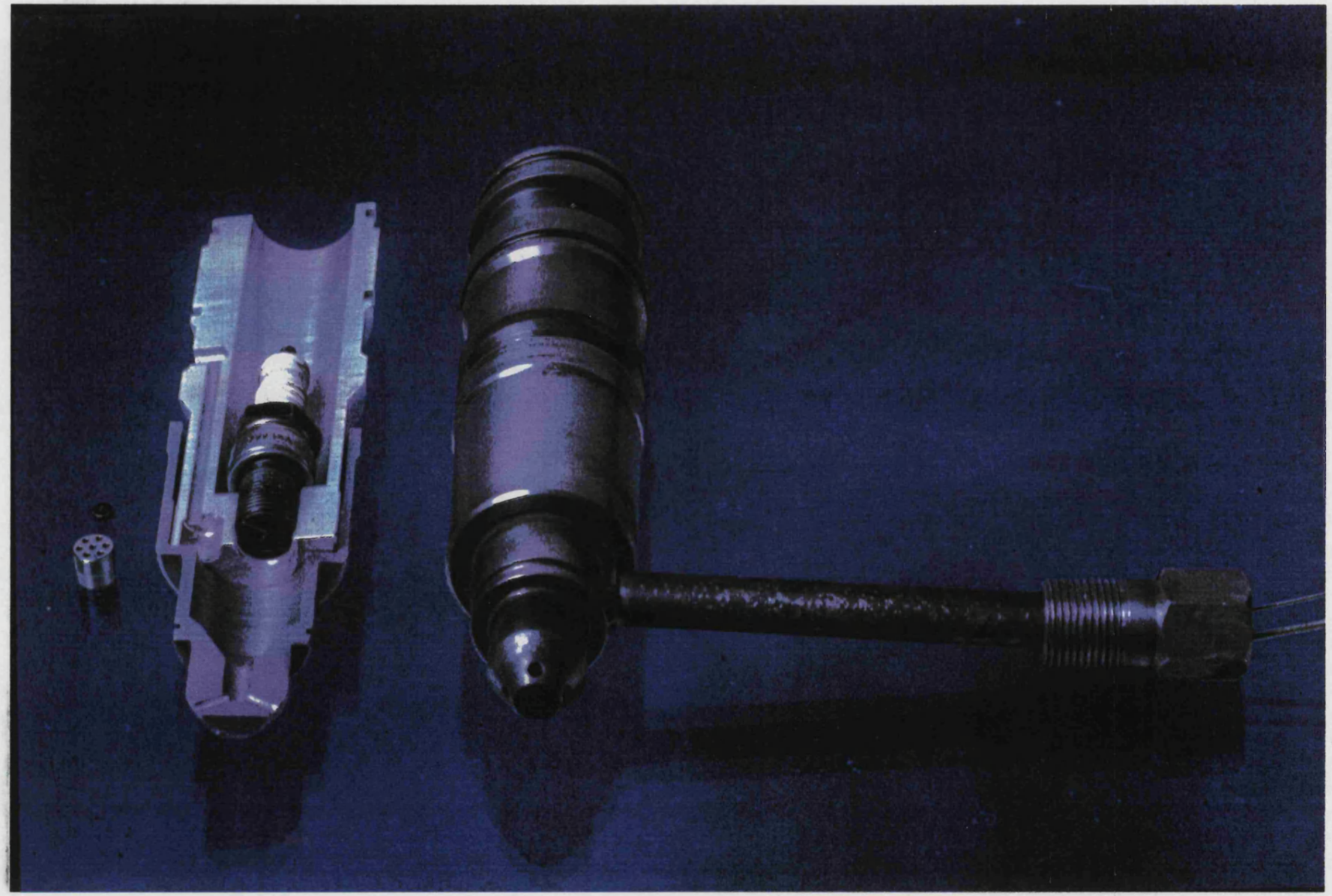

Plate 7. Installation of HFR FID Probe into Prechamber

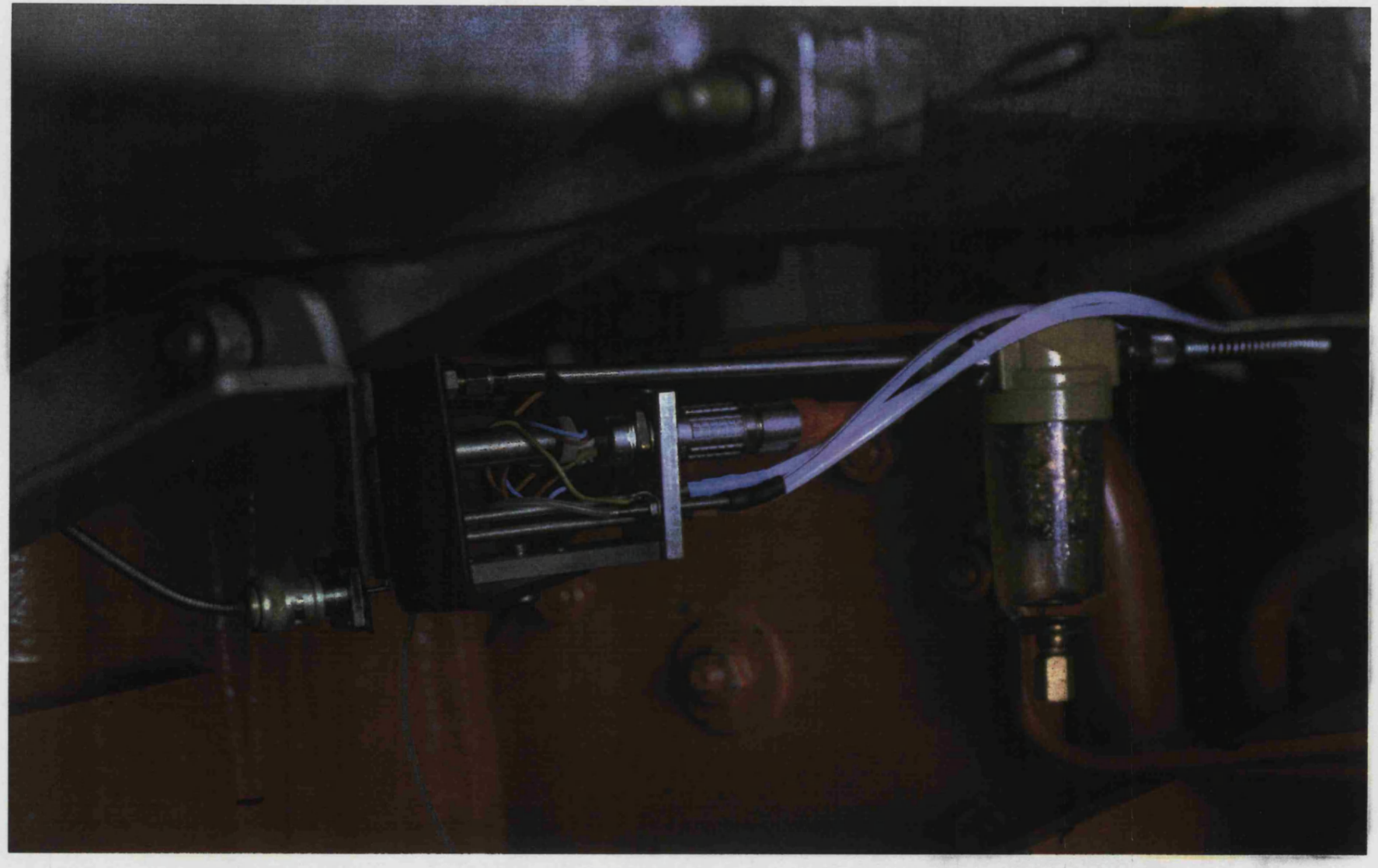

Plate 8. HFR FID Sampling Head Installed on Engine

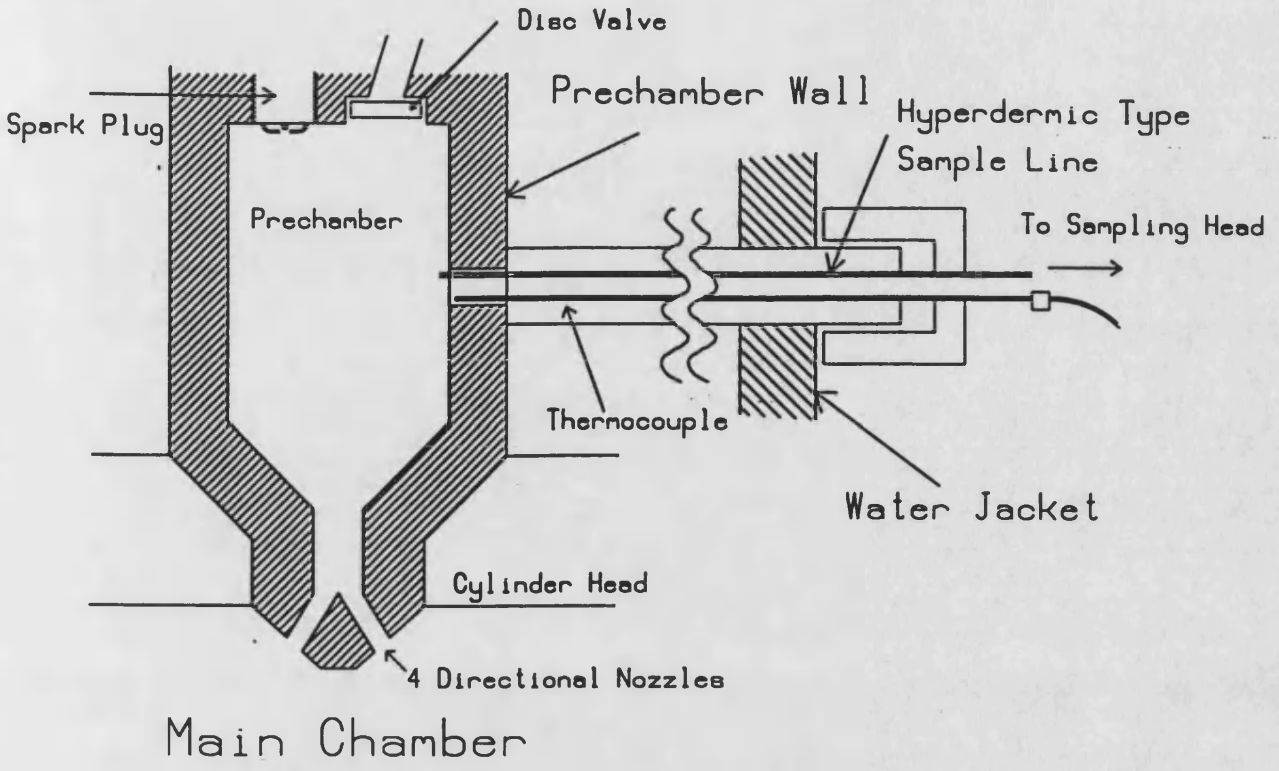

Figure 7.1 Detail of FID Sample Probe Insertion into Prechamber

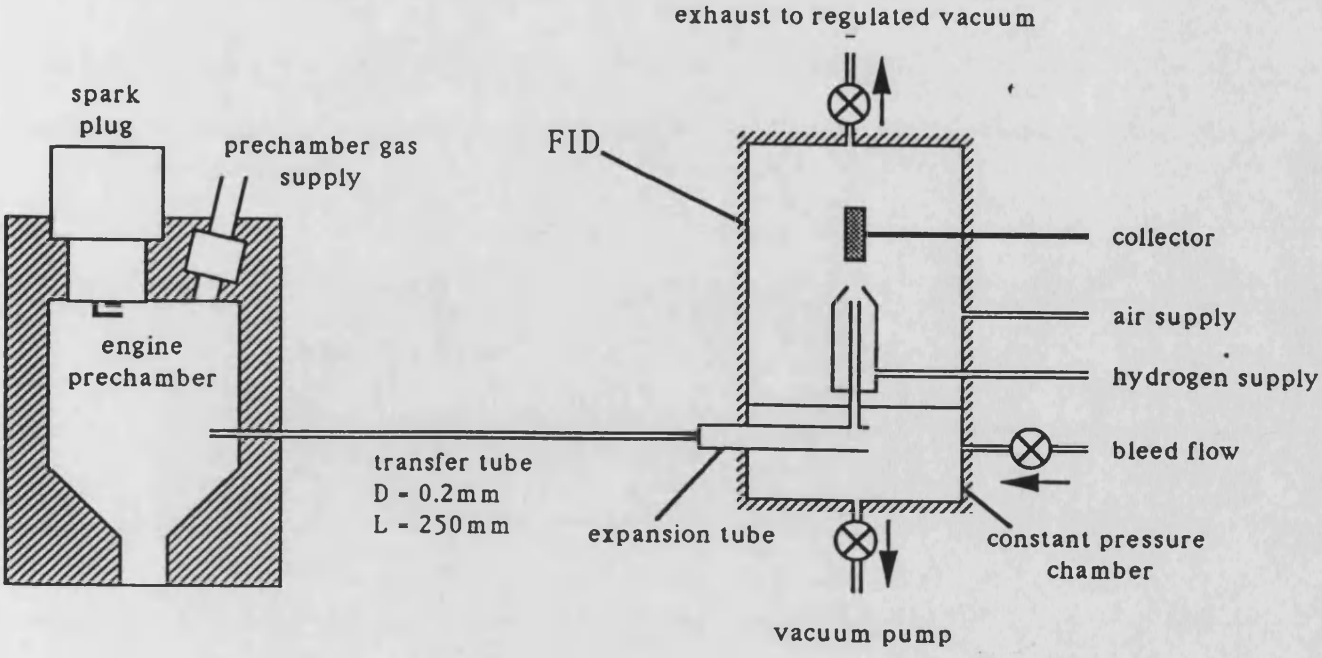

Figure 7.2 Schematic Diagram of Prechamber Sampling Arrangement

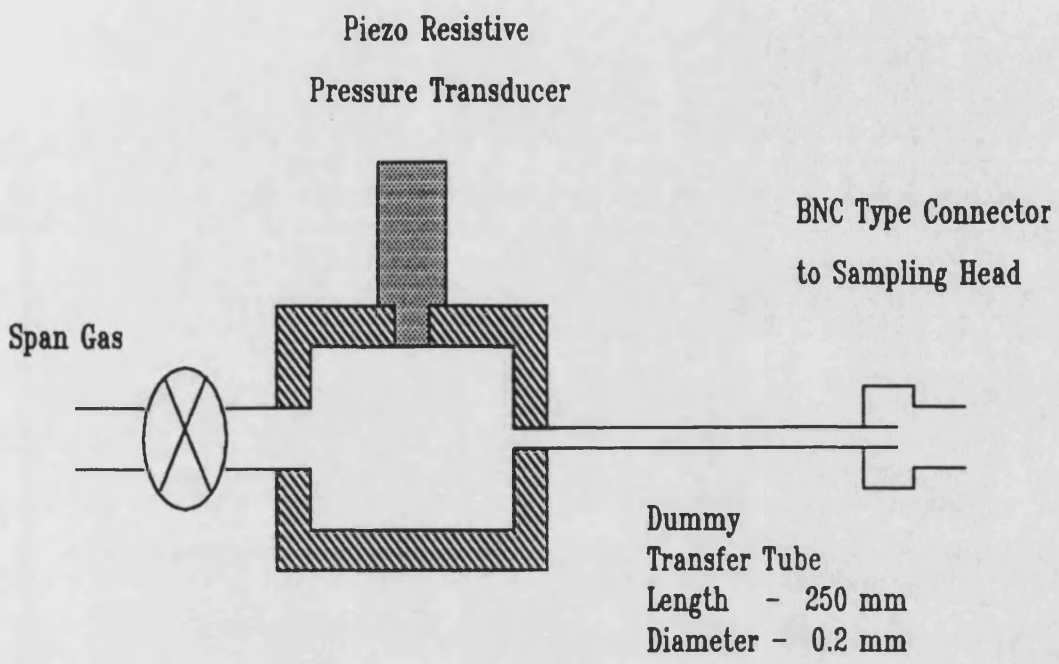

Figure 7.3 HFR FID Calibration Arrangement

Engine Operating Conditions

compression ratio	10:1	
prechamber volume	0.01	litres
ambient temperature	25	degC
speed	1500	rev/min
ignition timing	12	deg btdc
main chamber afr	26:1	
datum prechamber afr	3:1	
datum filling ratio	1.12	
'turbocharger efficiency'	55	%
boost pressure	1.48	bar
bmep	6.89	bar

Figure 7.4 Standard Engine Operating Conditions used for FID Sampling

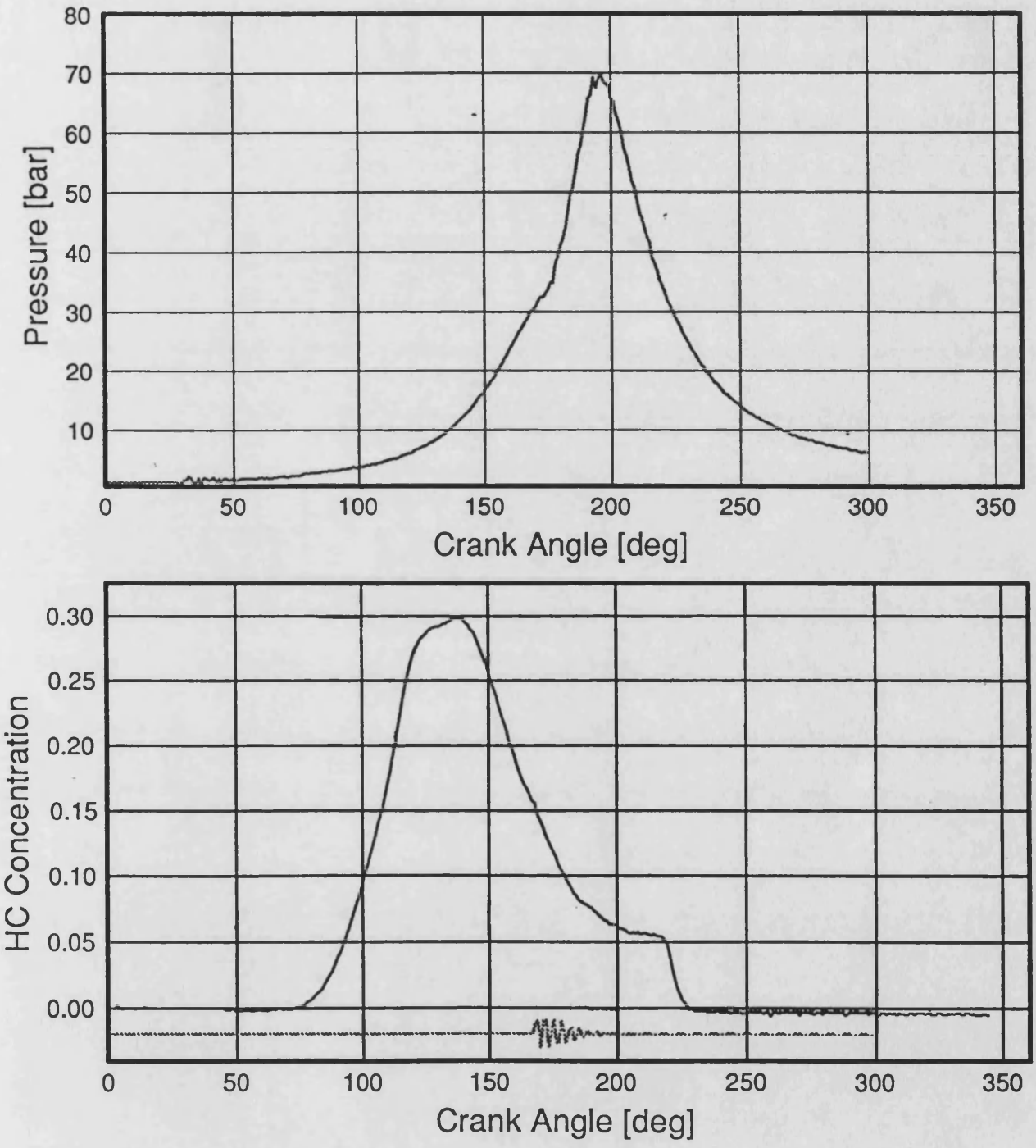

Figure 7.5 Typical FID and Main Chamber Pressure Signals Without Correction for Transit Time

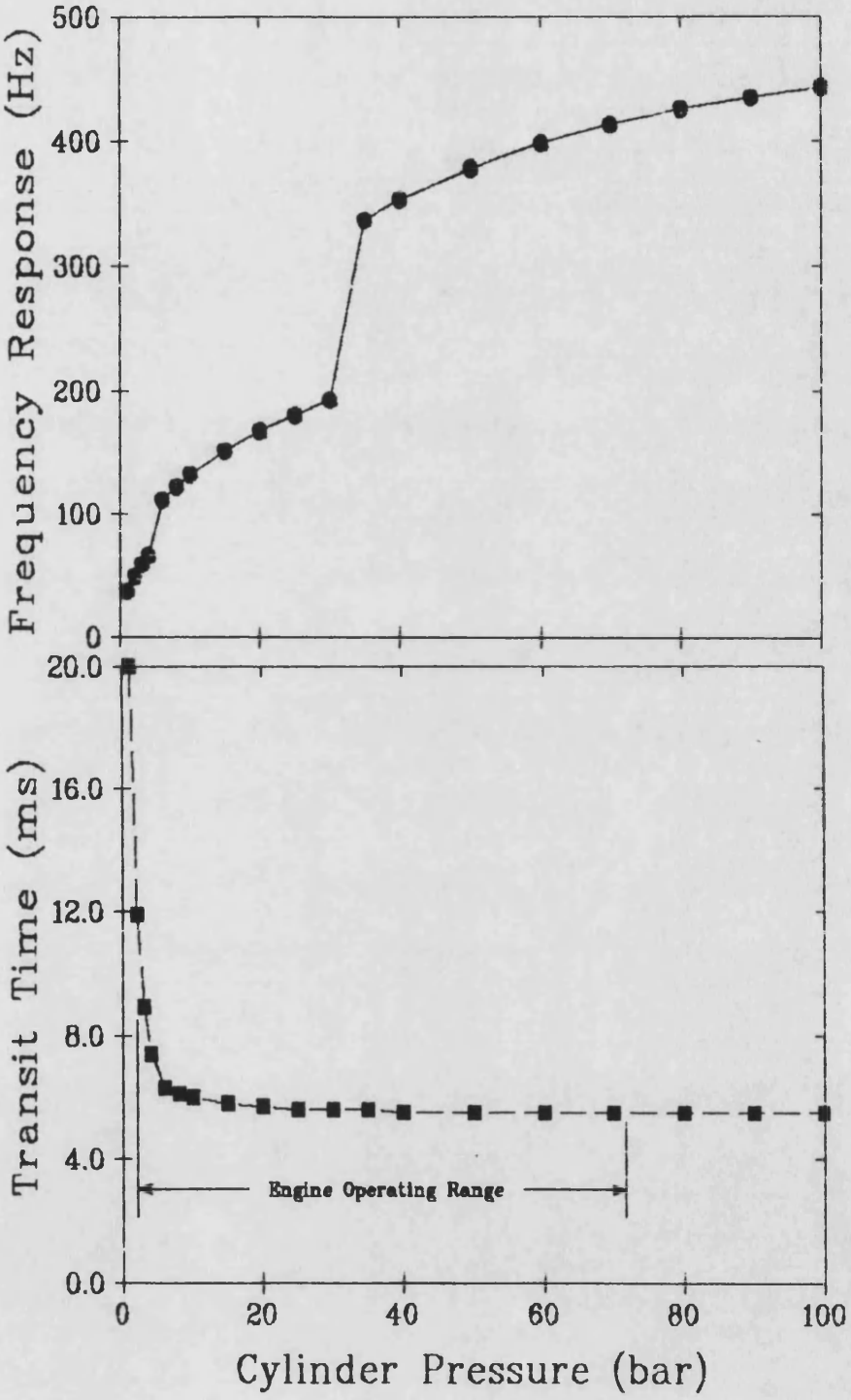

Figure 7.6 Effect of Sample Pressure on Transit Time and Frequency Response

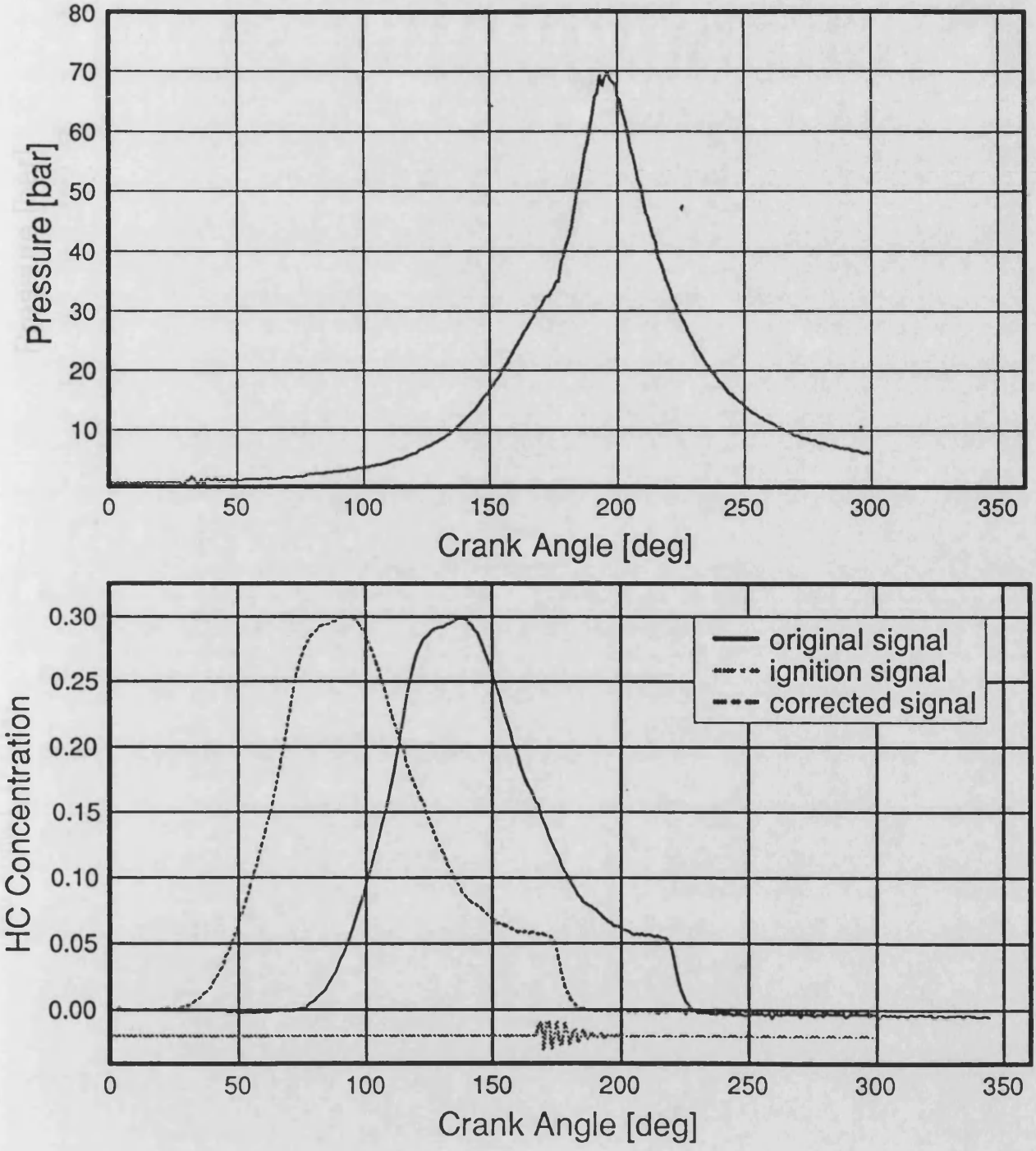

Figure 7.7 Main Chamber Pressure and FID Signal Corrected for Transit Time

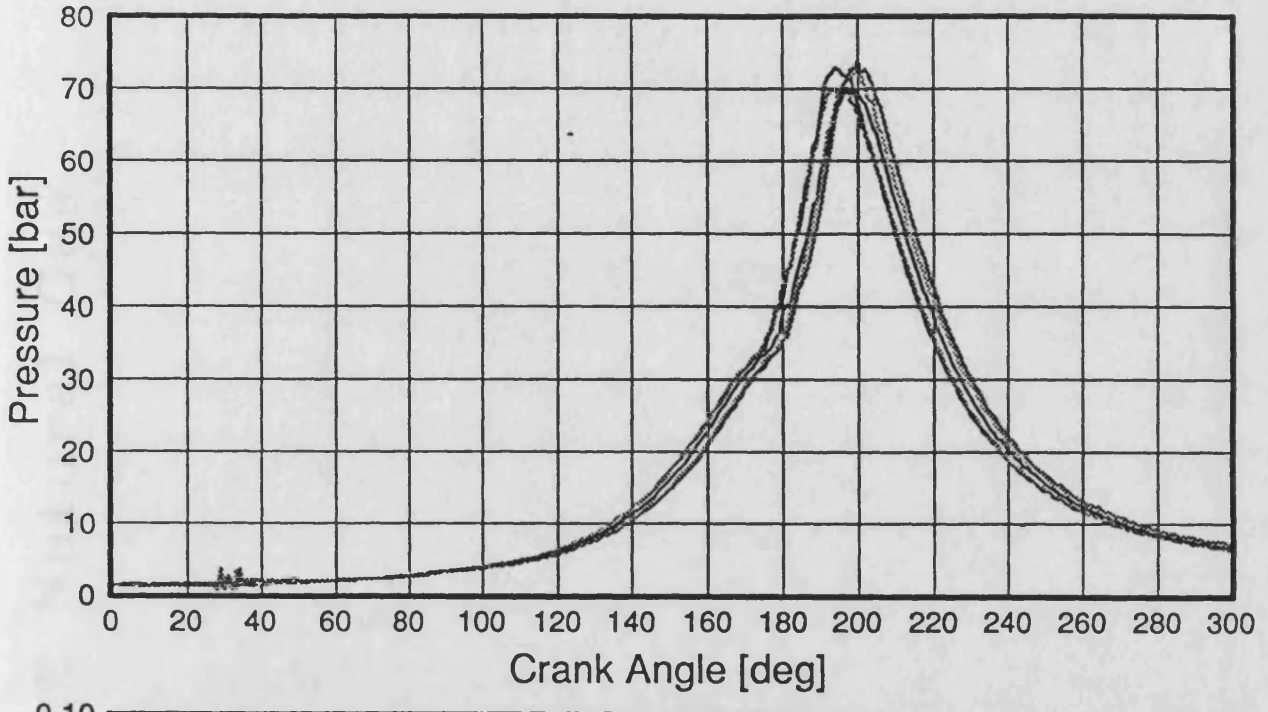

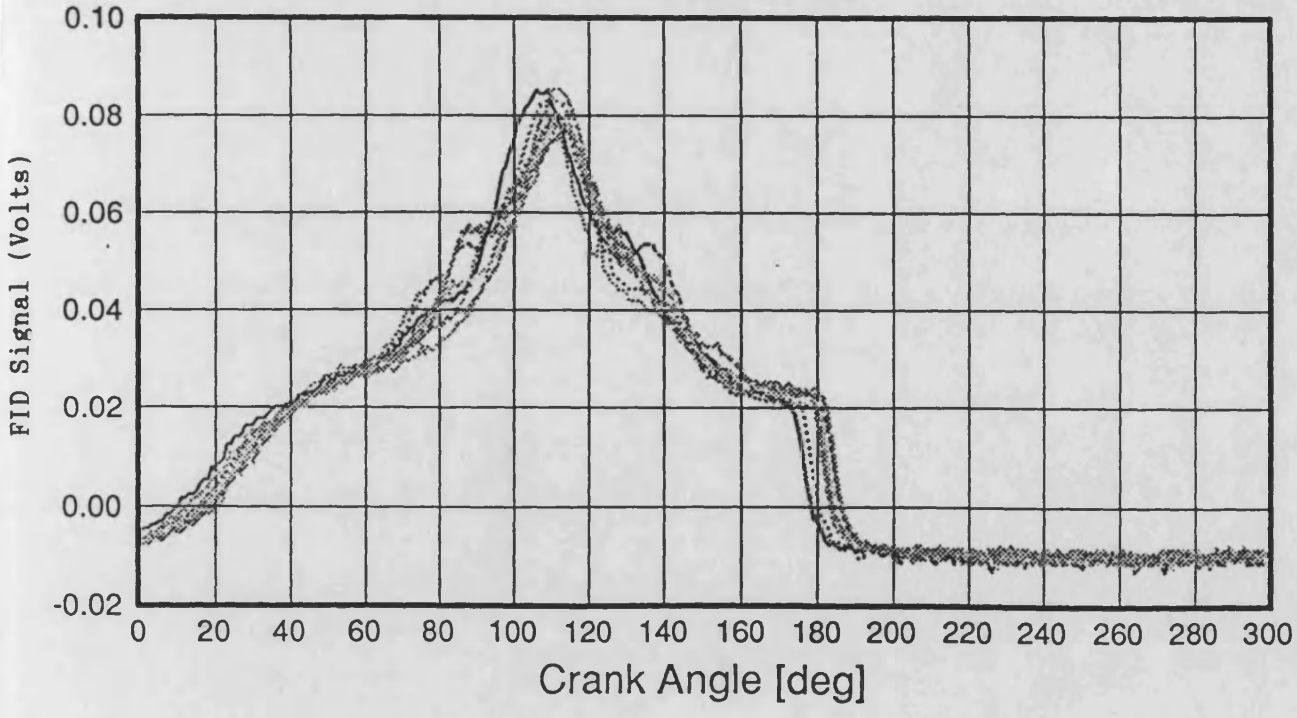

Figure 7.8 Cyclic Variation of FID and Pressure Signals for 9 Consecutive Cycles

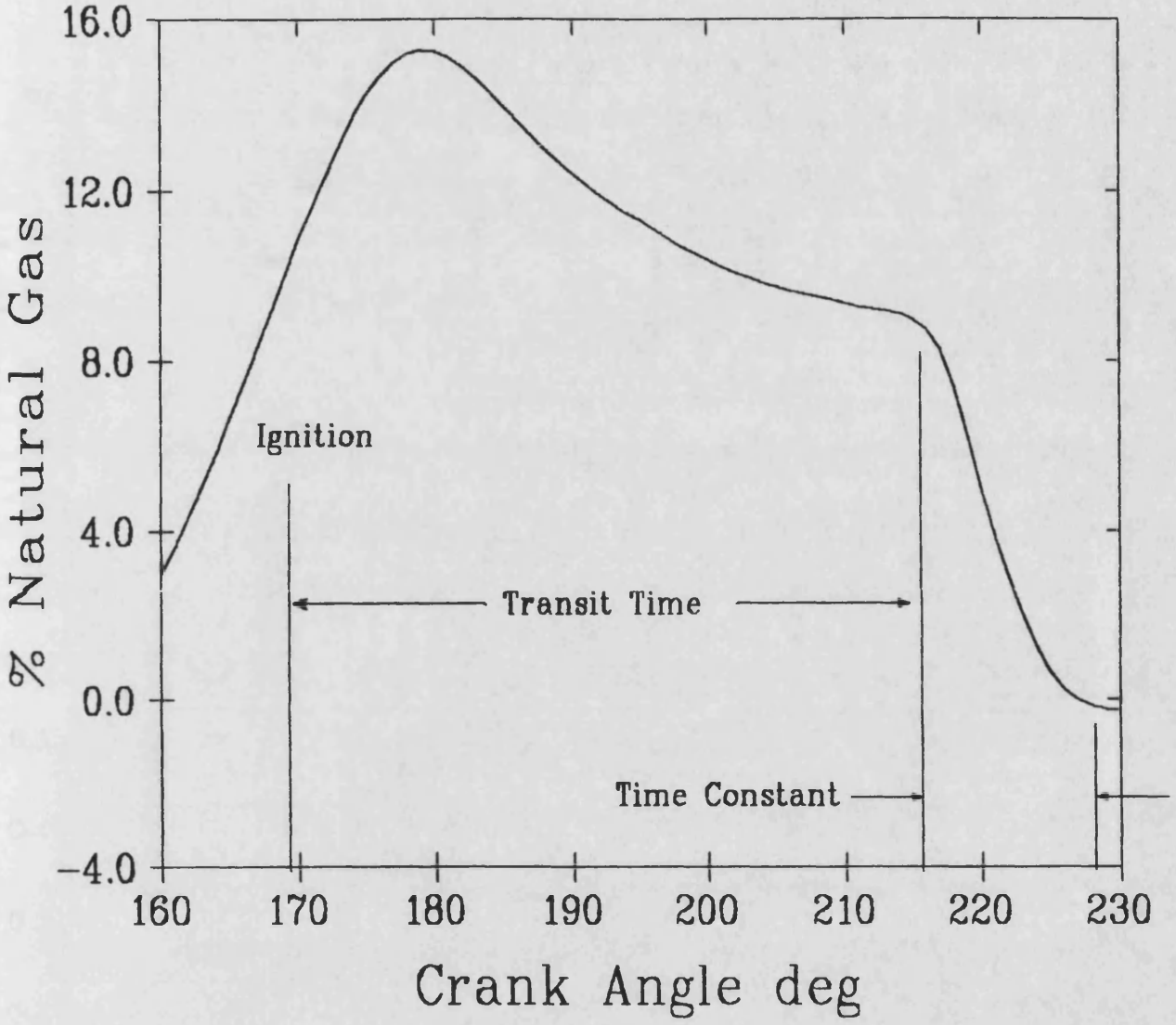

Figure 7.9 Estimation of Transit Time and Time Constant from Flame Front Passing Sampling point

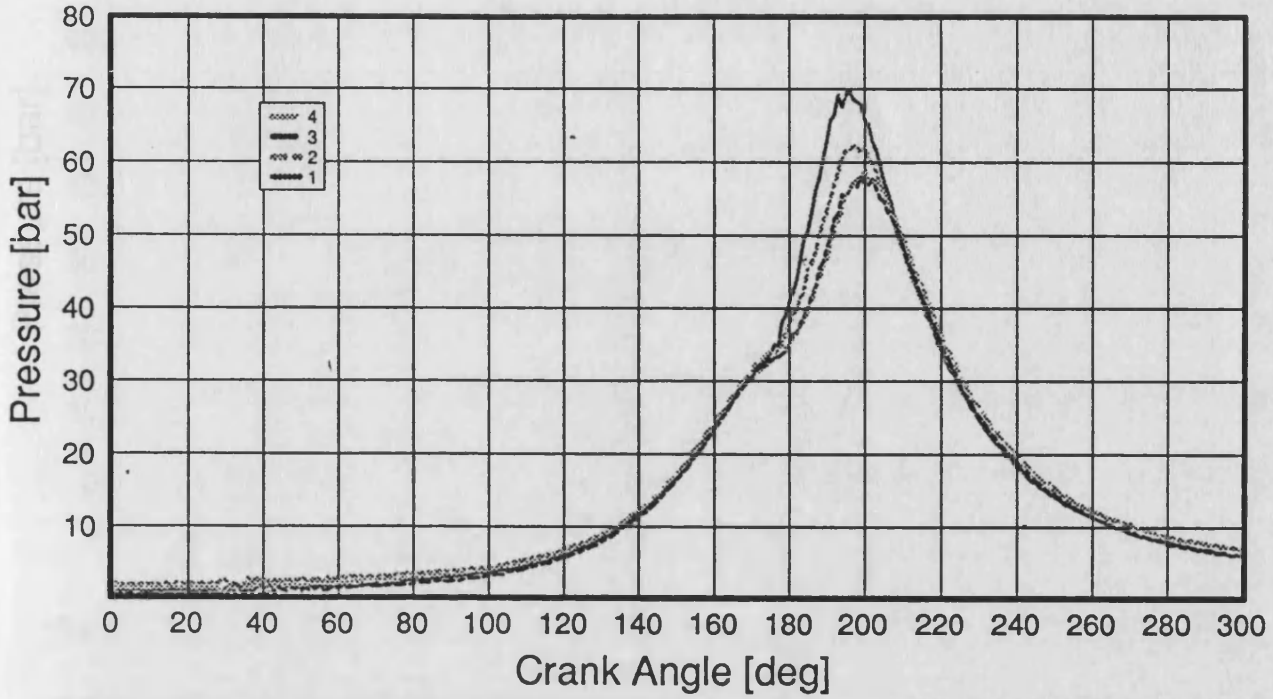

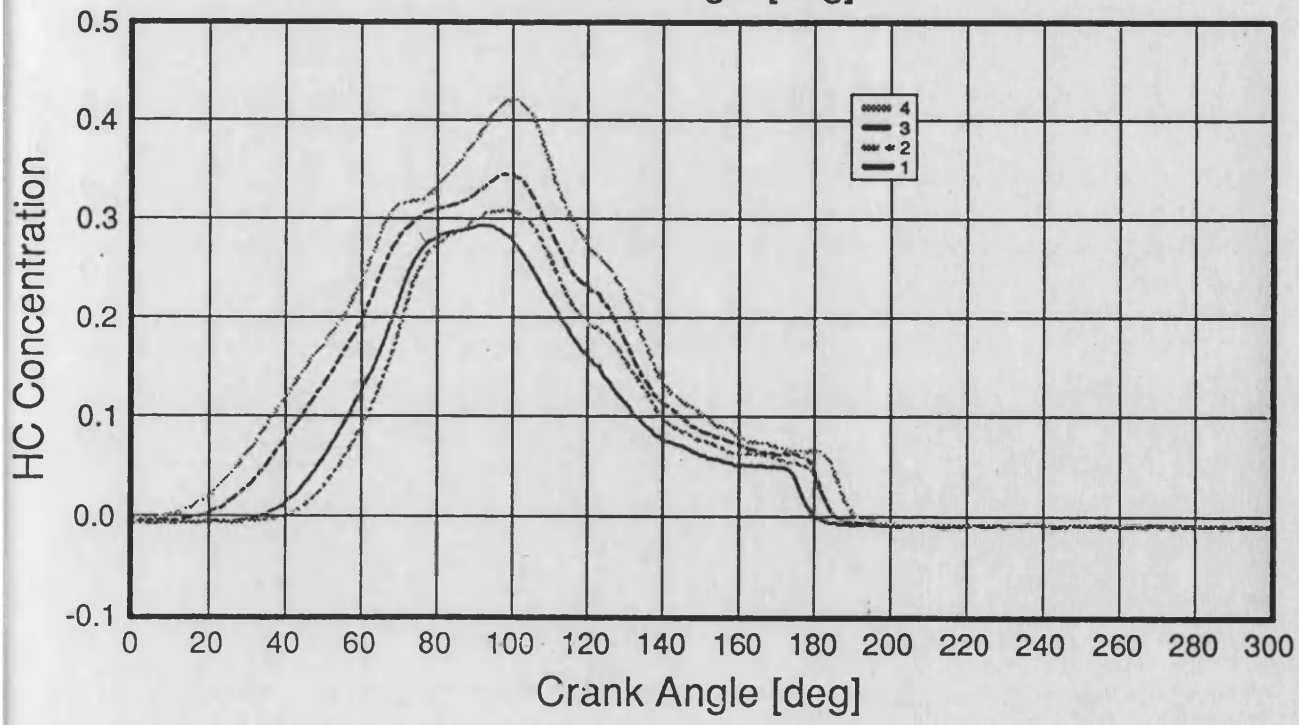

1 - 25% 2 - 30% 3 - 40% 4 - 50%

Figure 7.10 Effect on FID Signal For Increasing Pilot Mixture Strength

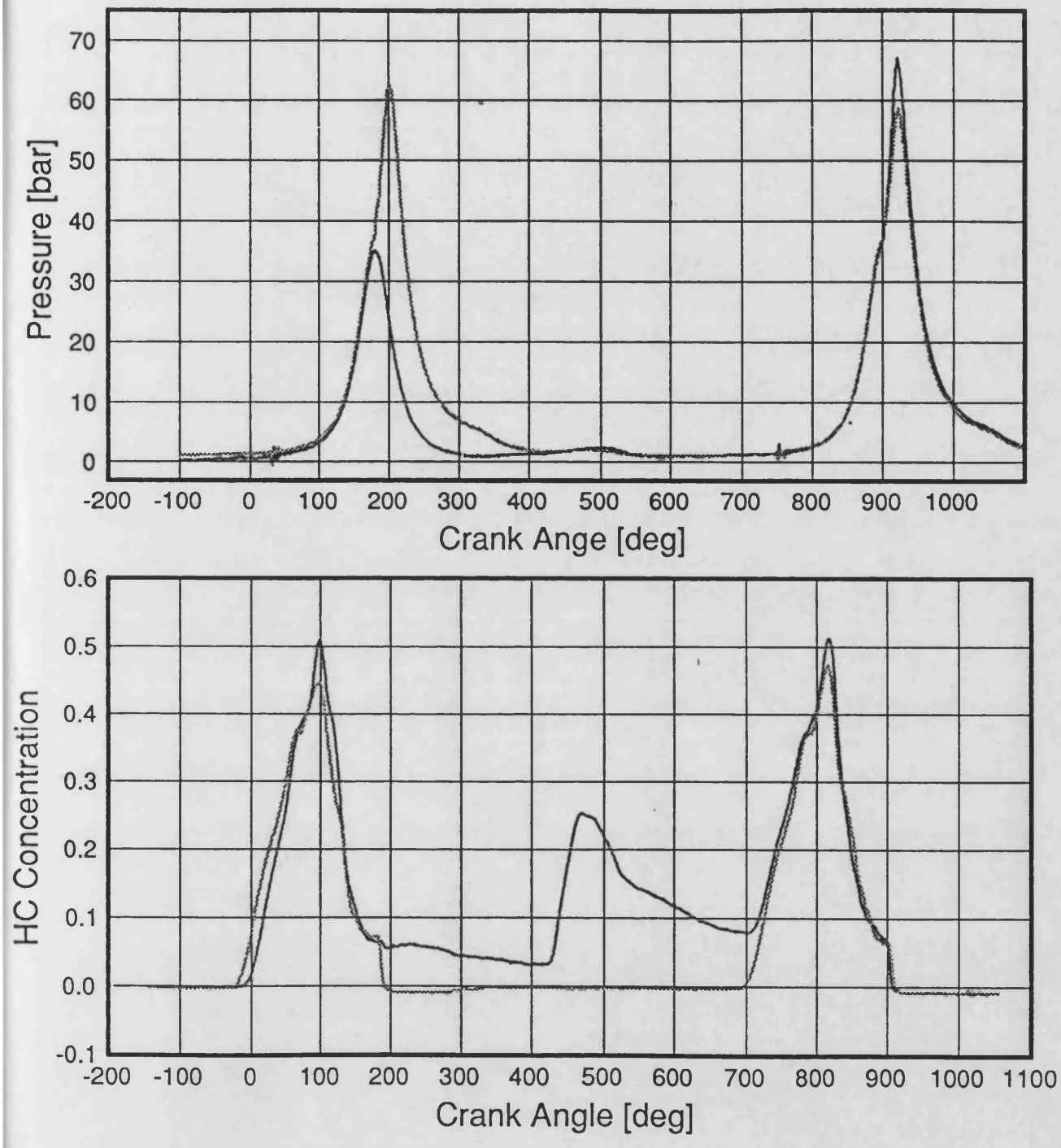

Figure 7.11 FID and Pressure Signals for Consecutive Misfired and Fired Cycles

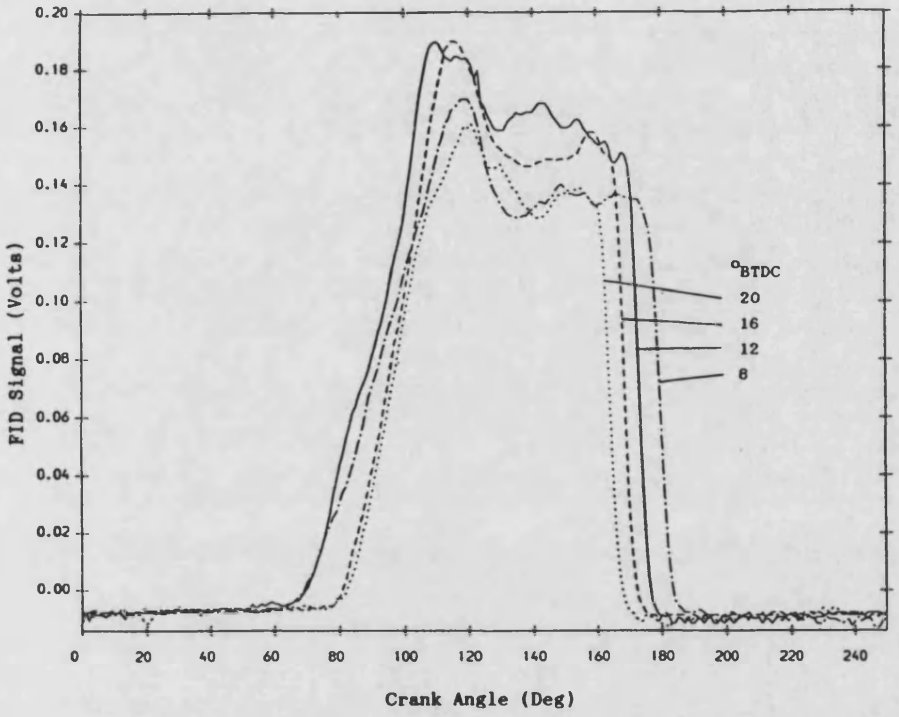

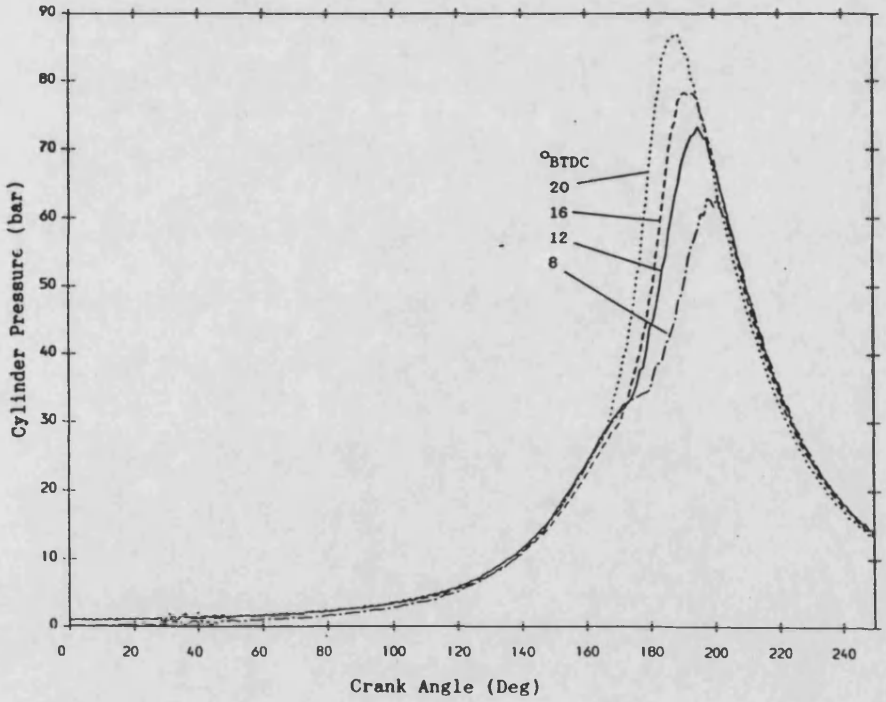

Figure 7.12 Effect of Ignition Timing on Pressure and FID Signals

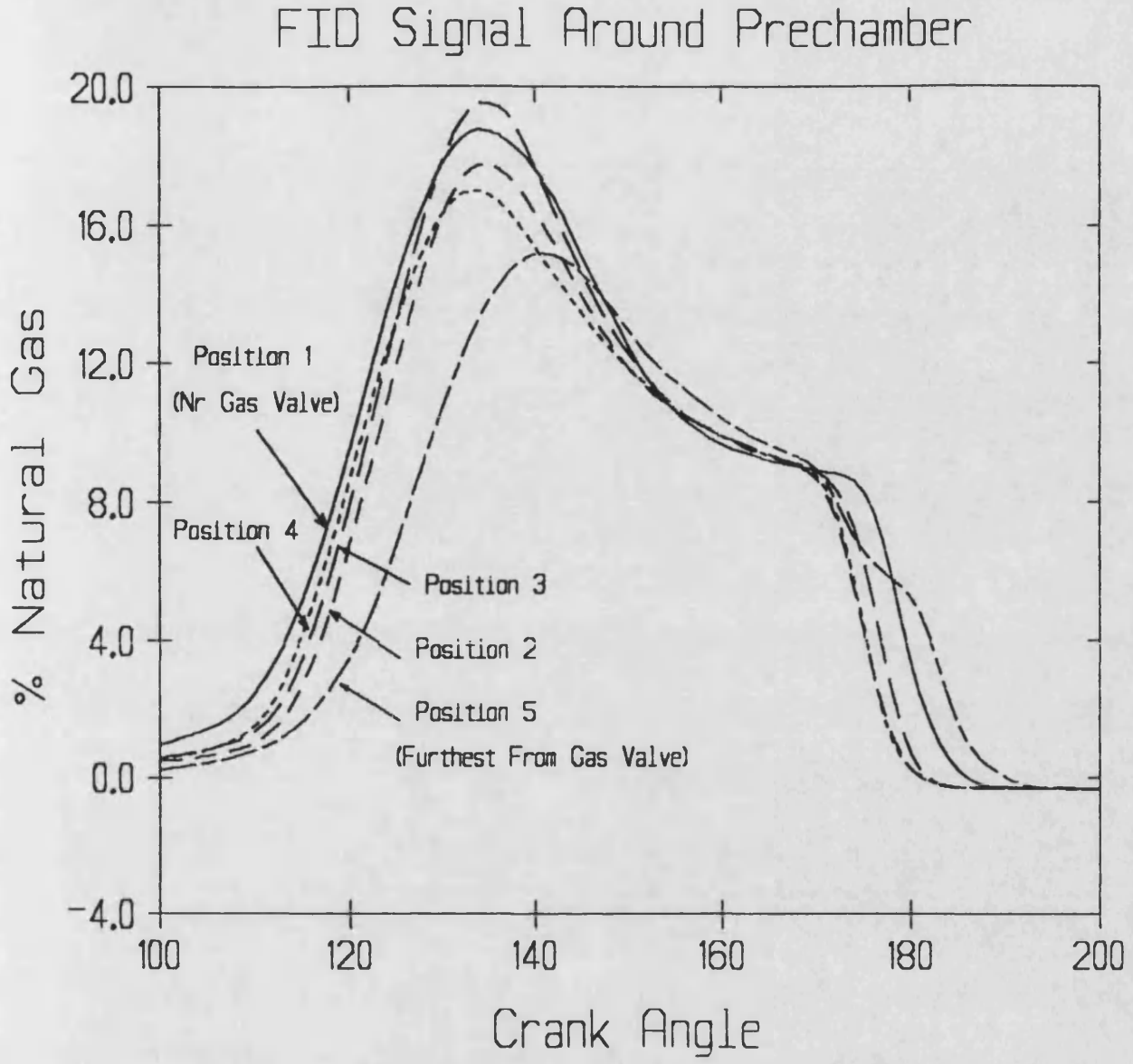

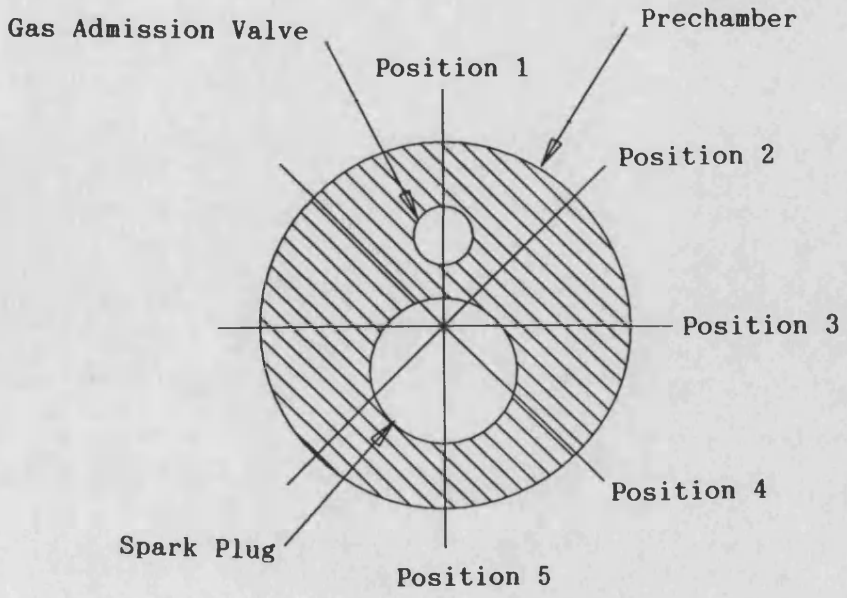

Figure 7.13 Ensemble Averaged FID Signals at the 5 Locations Around Prechamber Perimeter

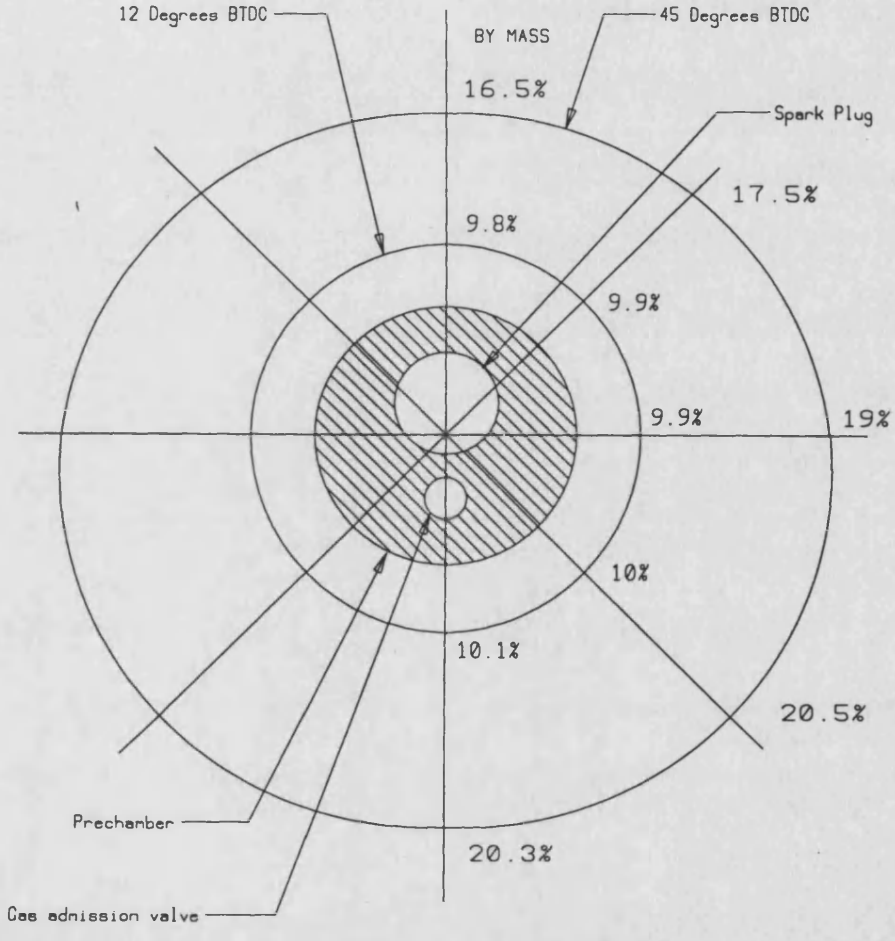

Figure 7.14 Mixture Distribution at Prechamber Perimeter with a Pilot Air-Fuel Ratio of 2.3:1

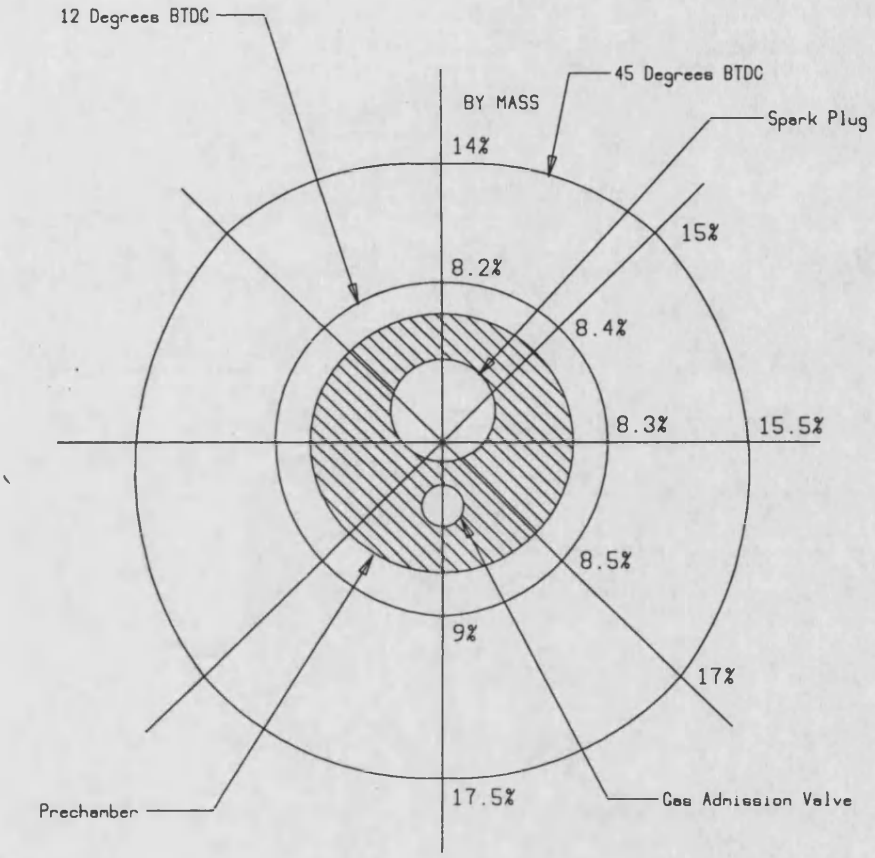

Figure 7.15 Mixture Distribution at Prechamber Perimeter with a Pilot Air-Fuel Ratio of 3:1

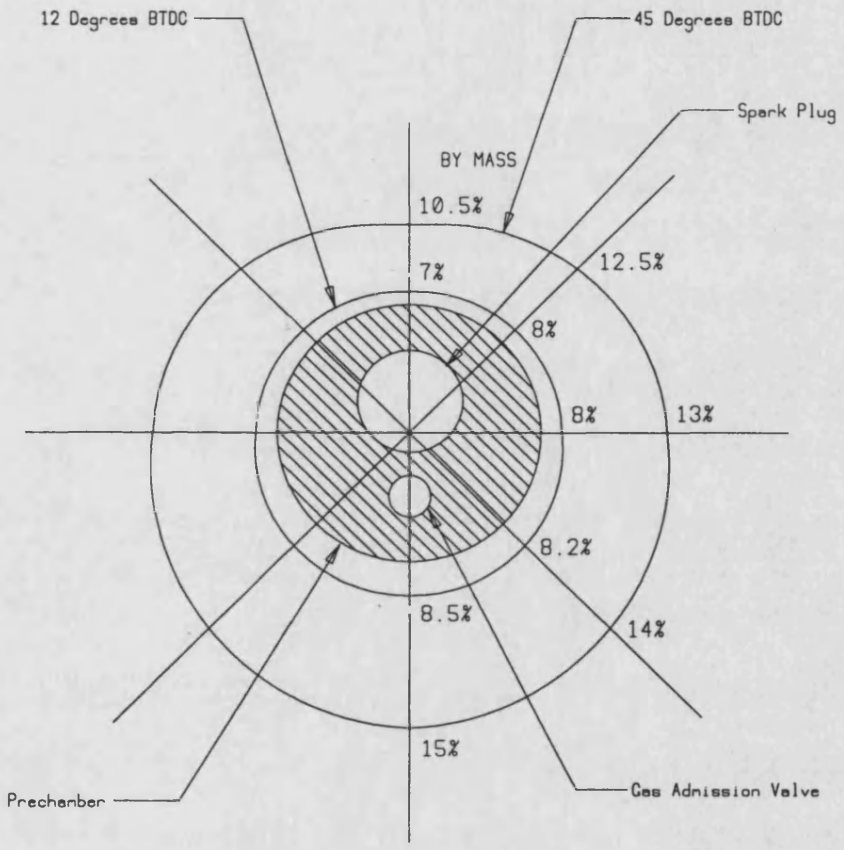

Figure 7.16 Mixture Distribution at Prechamber Perimeter with a Pilot Air-Fuel Ratio of 3.7:1

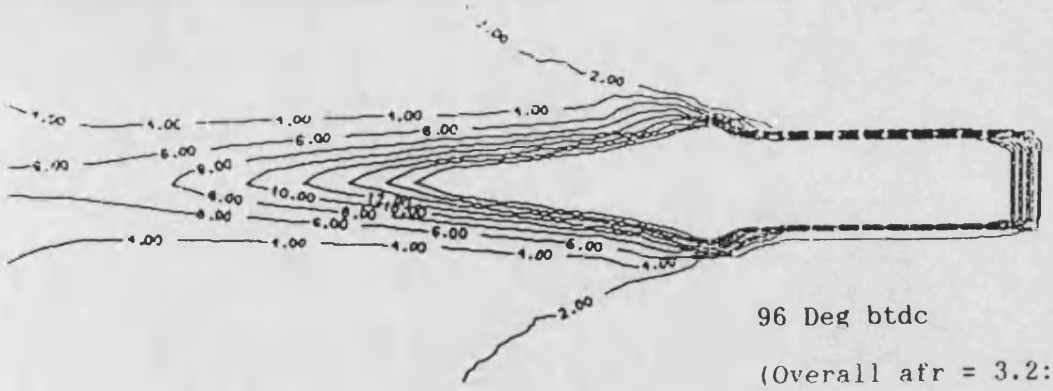

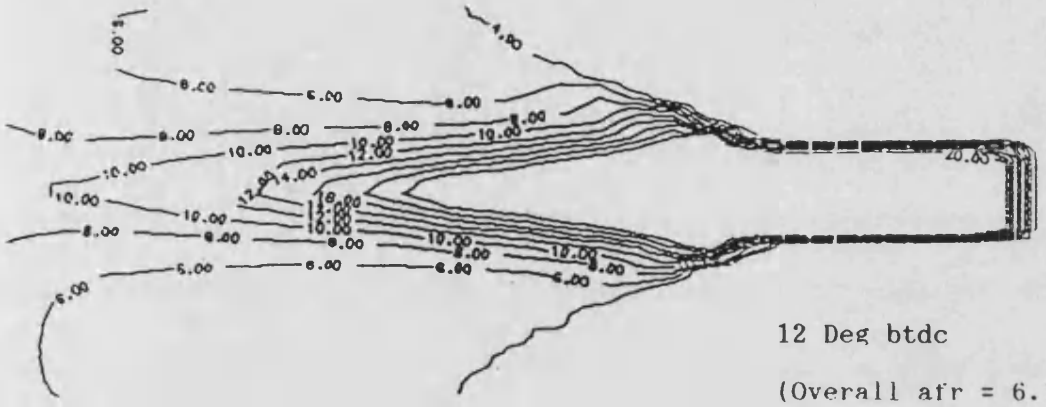

a) Pilot Air-Fuel Ratio = 0.0

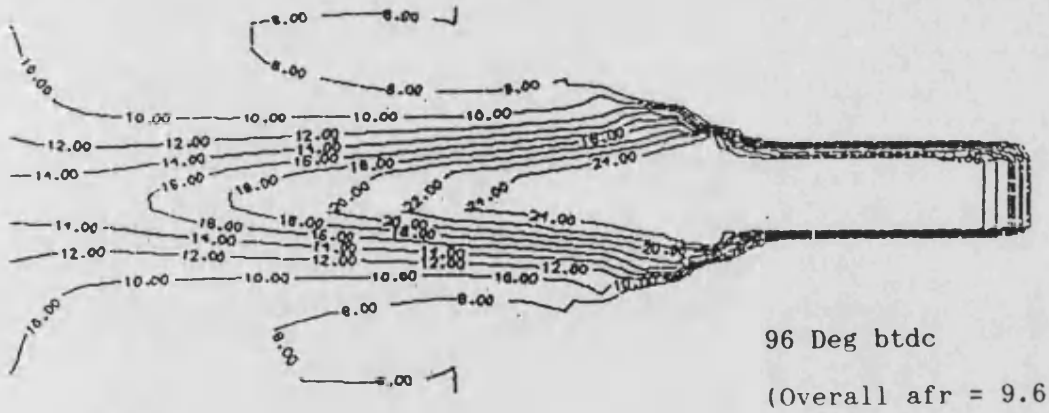

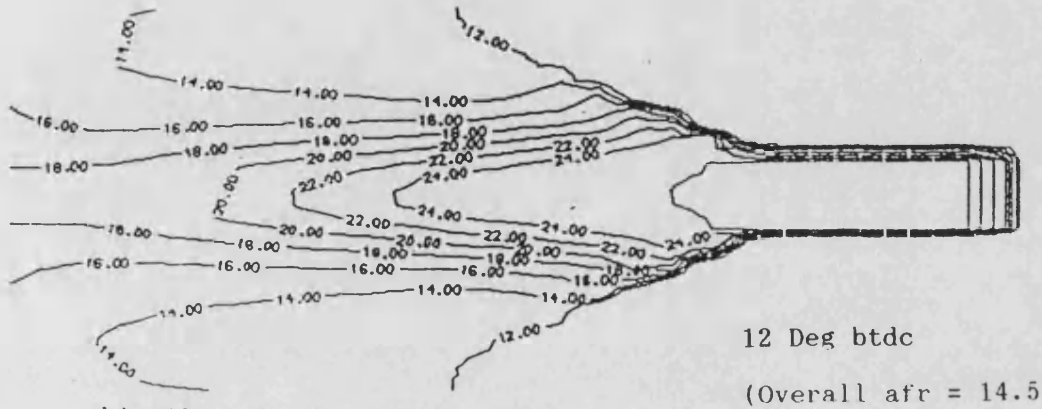

b) Pilot Air-Fuel Ratio = 2.3

Figure 7.17 Contours of Air-Fuel Ratio Obtained using PHOENICS CFD for a Pure Gas Pilot mixture (a) and an Air Fuel Ratio of 2.3:1 (b)

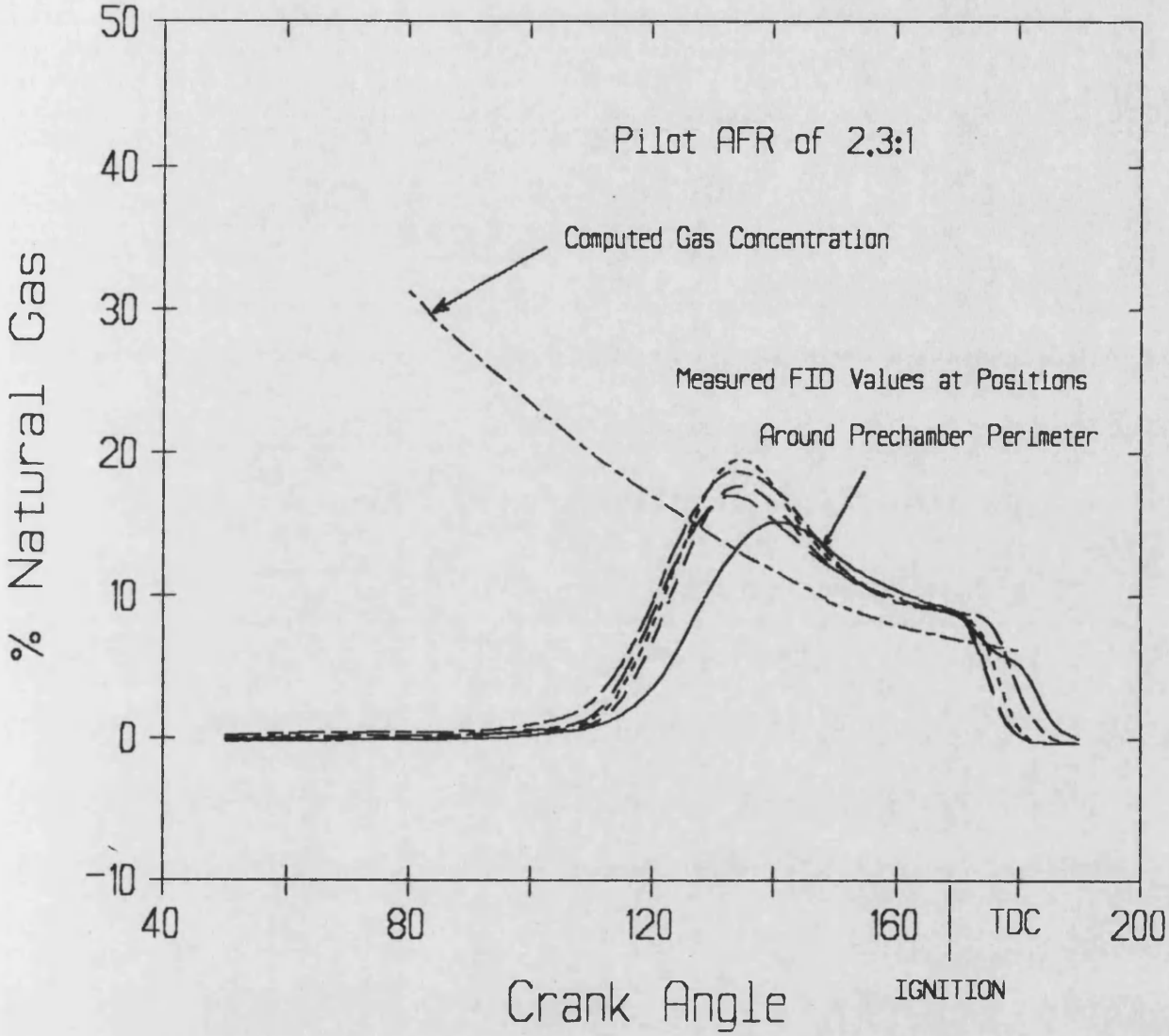

Figure 7.18 Comparison of Overall Prechamber Air-Fuel Ratio Obtained by PHOENICS CFD and Ensemble Averaged FID Signals at Positions around Prechamber Perimeter

Chapter 8

8 Modelling of the Prechamber using CFD

8.1 Introduction

This chapter describes the use of computational fluid dynamics to model the motion and mixing of fuel and air gases within the prechamber of the divided chamber gas engine. The object was to investigate mixture preparation throughout the prechamber volume during the compression stroke, up to the time of ignition. During this period, the fuel rich pilot mixture filling the prechamber is leaned down to an ignitable concentration by a high velocity jet of lean mixture from the main combustion chamber. This process is described in chapter 4 and shown clearly in figure 4.3.

The object of this study was to investigate how the mixture develops throughout the prechamber volume, particularly in the region of the spark plug, under normal operating conditions. The modelling has been done using the computational fluids dynamics program STAR described and validated in chapter 5. Results from this study are compared with earlier experimental measurements of mixture concentration using the fast response FID. The effects of changing the concentration of the mixture supplied to each combustion chamber and increased nozzle size have been investigated.

8.2 The Prechamber Model

The STAR CFD program allows construction of a body fitted mesh so that accurate modelling of the prechamber geometry may be achieved. This is a feature which earlier CFD programs, such as the version of PHOENICS used by Moore (18) did not allow.

Neglecting the gas admission valve and the spark plug electrode, the prechamber geometry is symmetrical about the central axis. As only the compression stroke was modelled, the gas admission valve was not included in this model. This allowed the prechamber geometry to be represented by a 2-dimensional axisymmetric model consisting of a single layer of cells. The advantage of this approach was that the total number of cells required to model the geometry was greatly reduced resulting in a proportionate reduction in computing time.

When constructing the model mesh the total number, shape and distribution of the cells must be carefully considered. The total computing time taken for the model to run will be proportional to the number of cells. The shape of the cells must be constrained to the limits discussed in chapter 5 to avoid convergence and stability problems. The distibution of the cells should be such that cell density is greatest where velocity flux gradients are greatest. Often several trial models must first be tried before an optimum compromise is reached.

Initially an axisymetric model consisting of a 10 degree single layer slice and containing 1504 cells was produced, and this mesh is shown in figure 8.1 (a). With this mesh, however, it was not possible to achieve convergence of the solution throughout the complete period of the compression stroke due to the number and size of the cells, for reasons discussed later in this chapter. A second similar mesh was created containing 400 cells which was able to produce converged solutions for the entire compression stroke. This mesh is shown in figure 8.1 (b). Mesh density is greatest at the prechamber end nearest the location of the spark plug where greatest solution accuracy and resolution was

required.

8.3 Applying Transient Boundary Conditions

Boundary conditions prescribing the incoming flow velocity and temperature at the throat between the prechamber and main chamber were obtained by using the engine simulation program SPICE (4) to model the intake and compression strokes of the engine. Figure 8.2 shows velocity variation during the compression stroke for standard and enlarged size throats with the engine operating at 1500 rpm and a load of 6.89 bar bmep. Turbulence was modelled using the K-ε model. As boundary values of dissipation rate ε were not available, these were calculated from the relationship with mixing length l given in appendix E. Values for turbulence intensity and mixing length were set to recommended levels for pipe flow. Mixture concentration within the main chamber was assumed to be homogeneous throughout the compression stroke.

These boundary conditions were applied to the prechamber throat boundary over the period of the compression stroke using a series of load steps defined by the STAR program. During each of these load steps, a number of time step iterations are performed. The boundary value for velocity and temperature at each of these time steps was determined by linear interpolation between values set at the present and previous load steps.

The size and number of these time steps are important parameters in determining solution accuracy, solution stability or convergence, and computing requirements. Large time step intervals may result in an inaccurate or unstable solution, while too small a time step will require excessive computing time. The

optimum time step size is related to both cell dimensions and the velocity of sound by the Courant Number, C, discussed in chapter 5.

$$C = \frac{V_s \times \delta t}{\delta l}$$

where V_s is the velocity of sound, δt is the time step interval and δl is the cell dimension in the direction of flow.

Ideally the Courant Number should be less than or close to unity for all cells in the mesh. However, this is only a guide and stable converged solutions may still be obtained for Courant Numbers up to 20. The solution for the initial cell mesh containing 1504 cells became unstable and diverged. As a consequence, Courant numbers were calculated for the worst cells and found to have a value of the order of 50 for a time step of 50 μs. As it was impractical to reduce the time step to the required size by limitations of computing time, the second mesh containing 400 cells, previously referred to, was created. This mesh enabled Courant numbers to be reduced to within a more acceptable range without excessive computational times.

8.4 Preliminary Results

Initially, prechamber mixing was modelled for the same 'standard' operating conditions used during the experimental study reported in chapter 7. Main chamber mixture being 4% gas by mass(afr of 25:1) and a pilot mixture of 30% (by mass) gas in air which is assumed to have totally scavenged and filled the prechamber by the start of the compression stroke. The main chamber mixture is assumed to be homogenious.

Figure 8.3 show velocity vectors for the bulk flow within the prechamber at intervals during the compression stroke. At 160 deg btdc a flow of mixture from the main chamber can be seen entering the prechamber through the nozzle. As the compression stroke continues, by 120 deg btdc, a high velocity jet is seen to develop along the prechamber axis and regions of recirculating flow are apparent in the diverging section of the prechamber. By 60 deg btdc, the jet is seen to impinge on the back surface of the prechamber, close to the location of the spark plug. The area of recirculation is shown to have extended to the outer regions of the chamber. At 10 deg btdc the recirculating flow continues, but the core of the jet has begun to weaken.

Contours of mixture concentration within the prechamber are shown in figure 8.4 at the same intervals in the compression stroke. At 120 deg btdc, the mixture concentration is seen to be reducing in a normal direction from core of the lean jet. By 60 degrees btdc the lean jet has reached the back surface of the chamber and leaner mixture has begun to sweep around the wall as a result of the recirculating flow. Near the axis of the chamber, the effect of the high velocity lean jet is shown by almost constant mixture concentrations along the length of the chamber. At 10 deg btdc, the leaner mixture has been swept completely around the prechamber and mixed with the rich pilot mixture. The effects of the lean jet have begun to reduce as the velocities decrease.

The mixing process can be shown more clearly by considering the variation of both overall average mixture concentration, and the variation of mixture at specific locations within the

prechamber during the compression stroke. Figure 8.5 shows, by mass, the overall mixture and the mixture concentration at the spark plug location during this period. The overall mixture varies in a predictable manner. This reduces steadily throughout compression, more rapidly at first as a result of the high velocity jet, then the rate slowing as the jet weakens towards the end of the piston's travel.

The variation of mixture at the spark plug location is perhaps more surprising. The fuel rich mixture is seen to reduce very rapidly at approximately 80 deg btdc. The mixture then remains relatively constant until about 120 deg btdc when it is actually shown to increase slightly up until 150 deg btdc followed by a further smaller reduction before tdc. The initial rapid reduction corresponds to the time when the lean jet reaches the end wall of the chamber where the spark plug is located. Once this has occured, the mixture at this location is within the outer edges of the jet. The observation that the mixture concentration then remains constant followed by a period of slight enrichment may be explained by the effect of the recirculating flow. This will result in rich mixtures being drawn into the edges of the jet from the surrounding volume which mix with the lean mixture within the core of the jet. Eventually the mixture drawn into the jet will become leaner, and this results in the further reduction in concentration seen during the last 30 degrees up to tdc.

8.5 Prechamber Parametric Study

The model was re-run for various main chamber and prechamber fuel mixtures to investigate their effect on mixture preparation within the prechamber, particularly in the region of the spark

plug. Figure 8.6 shows overall prechamber mixture concentrations for main chamber air-fuel ratios of 22.2:1, 25:1 and 28.6:1 for a pilot mixture of 30% gas. These result in overall prechamber mixtures respectively of 11.8:1, 14.2:1 and 15.1:1 at 10 deg btdc, the time of the spark. The effect at the spark plug location is shown in figure 8.7 for the same main chamber air-fuel ratios. For all three conditions there is the same rapid leaning of mixture at between 70 and 80 deg btdc, followed by a period of relatively constant fuel mixture until tdc. The corresponding mixture concentrations at 10 deg btdc are 13:1, 15.6:1 and 16.4:1. These are all well within the flamability limits of natural gas, and close to stoichiometric for the main chamber air-fuel ratios of 25:1 and 28.6:1.

The effect of changing pilot mixture on mixture preparation has also been investigated. Results are shown in figures 8.8 and 8.9 for overall mixture development and mixture variation at the spark plug location for pilot mixtures of 90% gas, 50% gas 30% gas and 20% gas. It is clearly seen that this parameter has a great effect on both overall and localised mixture values. At the time of ignition, the mixture concentration for the richest pilot mixture is approximately 12% gas, too rich for the spark to ignite. For the 50% gas pilot, the mixture is approximately 10% gas, close to the rich limit of flamability. The 30% and 20% cases result in mixtures of 6.4% and 6.3% gas (by mass) respectively, both close to the stoichiometric value of 6.1% gas.

It was believed that the prechamber geometry, particularly the size of the throat, has an important effect on mixture preparation. A brief study was conducted of the effects of changing the size of the prechamber throat. A new prechamber mesh

was created which had a throat area 50% greater than the actual size. Corresponding boundary conditions were calculated using SPICE (4) for the new geometry. Results were computed for the same fuelling conditions. Figures 8.10 and 8.11 compare overall mixture preparation, and mixture variation at the spark plug for the two sizes of nozzle. There is little difference shown in overall mixture preparation during most of the compression stroke, but towards tdc the mixture is shown to lean further with the larger nozzle.

The effect of throat size on mixture variation at the spark plug is more significant. The rapid leaning of mixture at this location is seen to occur much later in the stroke, approximately 100 deg btdc. This would result from the lower velocity jet taking longer to reach the spark plug location. The mixture again remains relatively constant for the remainder of the stroke, but at a greatly reduced value of 4.2%, at the limit of flammability. This lower concentration may be explained by the effect of the wider jet created by the larger nozzle which would have a widened core region of leaner mixture extending further into the spark plug location.

8.6 Comparison of Results with Experimental Measurements and Computational Results by Johns (14)

Comparisons can be made of computed variations in mixture concentration with experimental measurements taken with the HFR FID, reported in chater 7. Figure 8.12 shows measured mixture variation at the position shown in figure 8.1 together with computed values at the same location. The overall computed mixture variation is included for reference. Both computed and

measured values show the mixture to lean rapidly from around 100 deg btdc when the recirculating flow reaches this location at the prechamber wall. The measured value of mixture concentration falls to approximately 6% (by mass) gas, but the computed value is shown to reduce only to about 10% gas concentration. This may be as a result of turbulence levels being too low in the CFD model which would cause an under-estimate of mixing rate.

Results obtained by Johns (14) from a similar computational study have been discussed in chapter 2. These may be compared to results produced by STAR. Figure 8.13 shows mixture variation from both studies at the spark plug location. The prechamber geometries are similar, and in each case the spark plug is located close to the axis of the chamber. Both results show the same effect of placing the spark plug in the path of the lean jet. As the jet reaches the back wall of the chamber, there is shown to be similar rapid leaning of the mixture at this location. The time that this occurs is slightly earlier for Johns (14), this probably resulting from the different combination of throat size and chamber length. Mixture in the case of Johns (14) is seen to lean to a lower value of approximately 4.5% gas (by mass), close to the misfire limit. This may be explained by the fact that the spark plug is located closer to the core of a larger lean jet produced by a greater throat area.

8.7 Summary

A study has been performed of the mixing process occurring within the prechamber during the compression stroke by use of the CFD program STAR. The results show that mixture concentration at the spark plug location drops rapidly early in the stroke and

remains relatively constant for the remaining period. This phenomenon is believed to result from the lean jet reaching the back wall of the chamber and producing recirculating flow.

The effects of changing certain parameters on prechamber mixing has been investigated. Main chamber mixture concentration is shown not to have a great effect on mixture preparation, but it's effects on ultimate overall mixture concentration and mixture at the spark plug are significant.

Pilot mixture concentration is shown to have a more critical effect on mixture variation. It is shown that if the prechamber is filled entirely with a pure gas pilot mixture, the resulting mixture produced at the spark plug location by the time of ignition is too rich to be ignited. Pilot mixtures of between 20% and 30% gas (by mass) result in mixture concentrations close to stoichiometric at the spark plug location at the time of ignition.

The prechamber throat area has been shown to have little effect on overall mixture variation, but an important effect on localised values at the spark plug. This parameter will effect the time at which leaning occurs at this location, as well as ultimate concentration. The larger throat size results in leaning at the spark plug occurring later as a result of reduced jet velocities, and a leaner mixture at the time of ignition.

Comparisons have been made with experimental measurements taken by the HFR FID. Both results show similar rates of leaning occuring at the same point in the compression stroke. A difference in ultimate concentrations may be caused by turbulence levels being set too low in the model.

A comparison has also been made with results taken by Johns (14) for a similar study. Both results show the phenomenon of rapid leaning occurring at the spark plug location followed by a period of relatively constant concentration up to tdc. The leaner mixture experienced by Johns (14) may result from the large throat size and slightly different spark plug location used in that study.

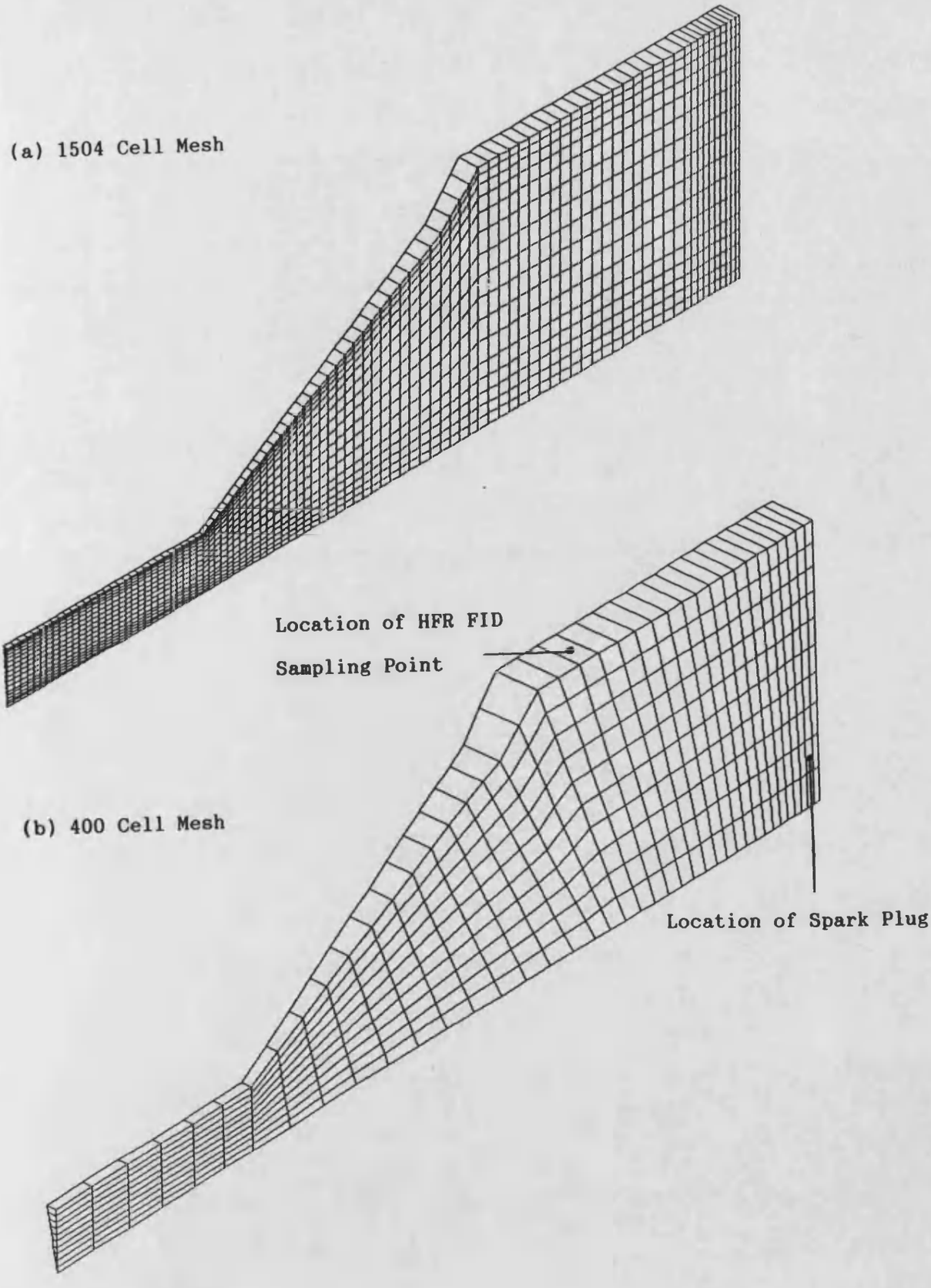

Figure 8.1 STAR Prechamber Models with (a) 1504 cell mesh, (b) 400 cell mesh

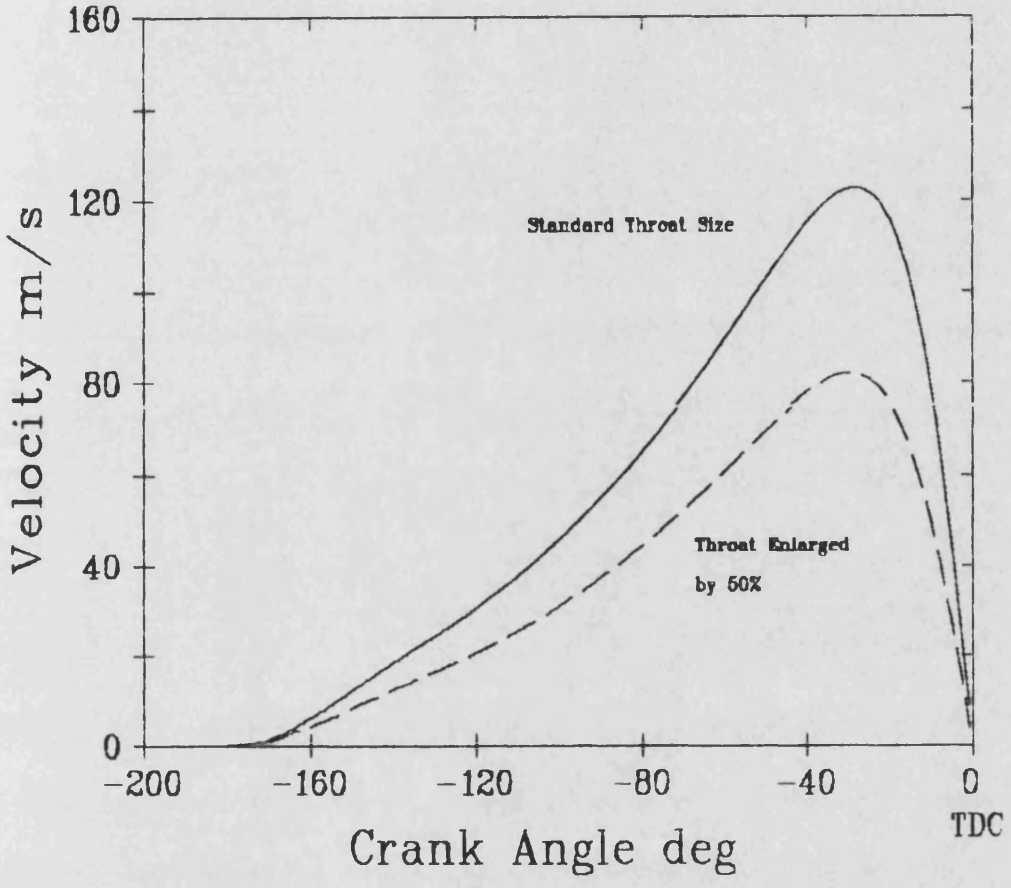

Figure 8.2 Velocity Boundary Conditions at the Prechamber Throat, Calculated using SPICE, for Standard and Enlarged Throat Sizes

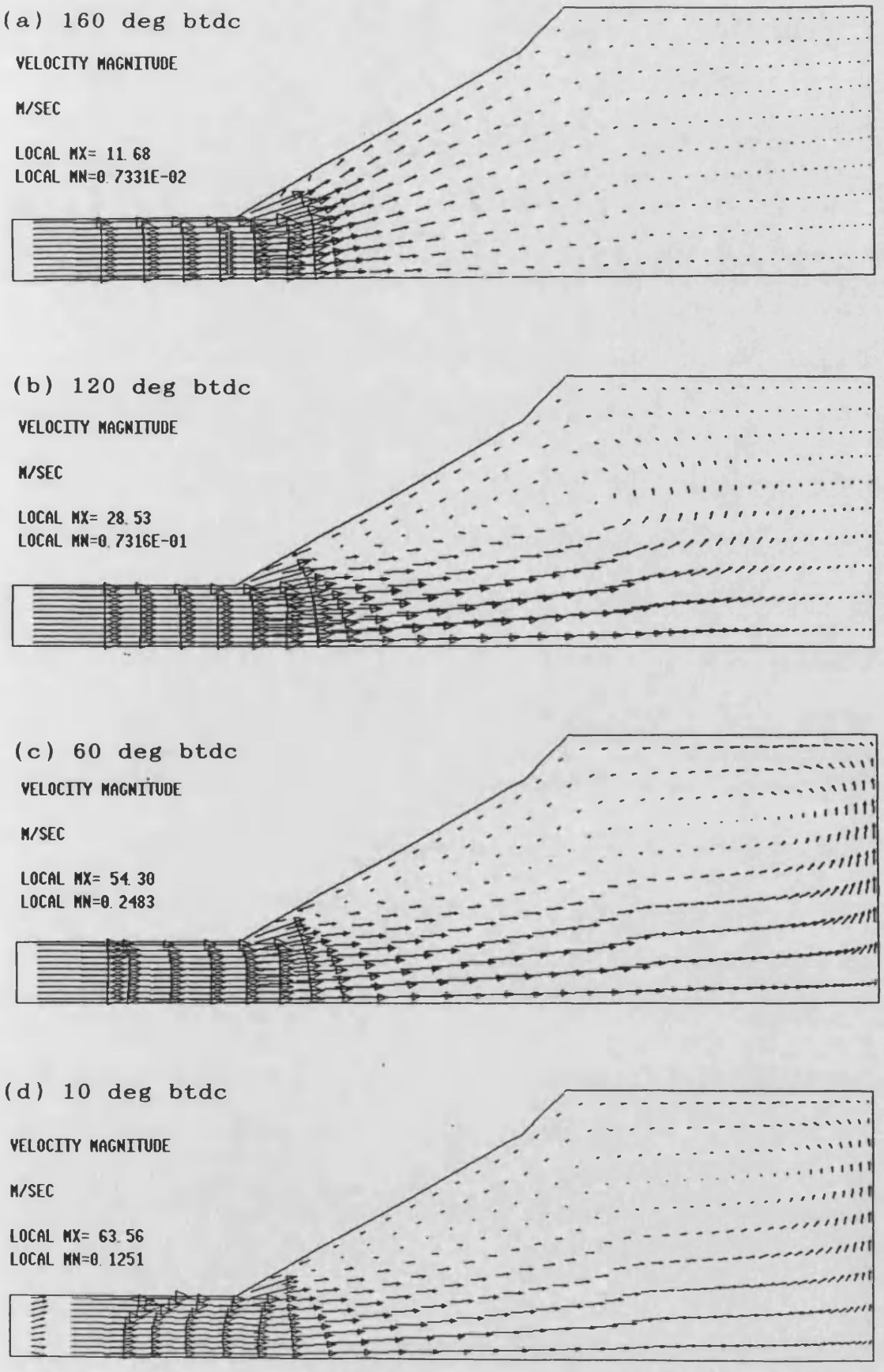

Figure 8.3 Velocity Vector Plots for the Prechamber Operating with a Pilot Mixture of 30 % and a Main Chamber Air-Fuel Ratio of 25:1

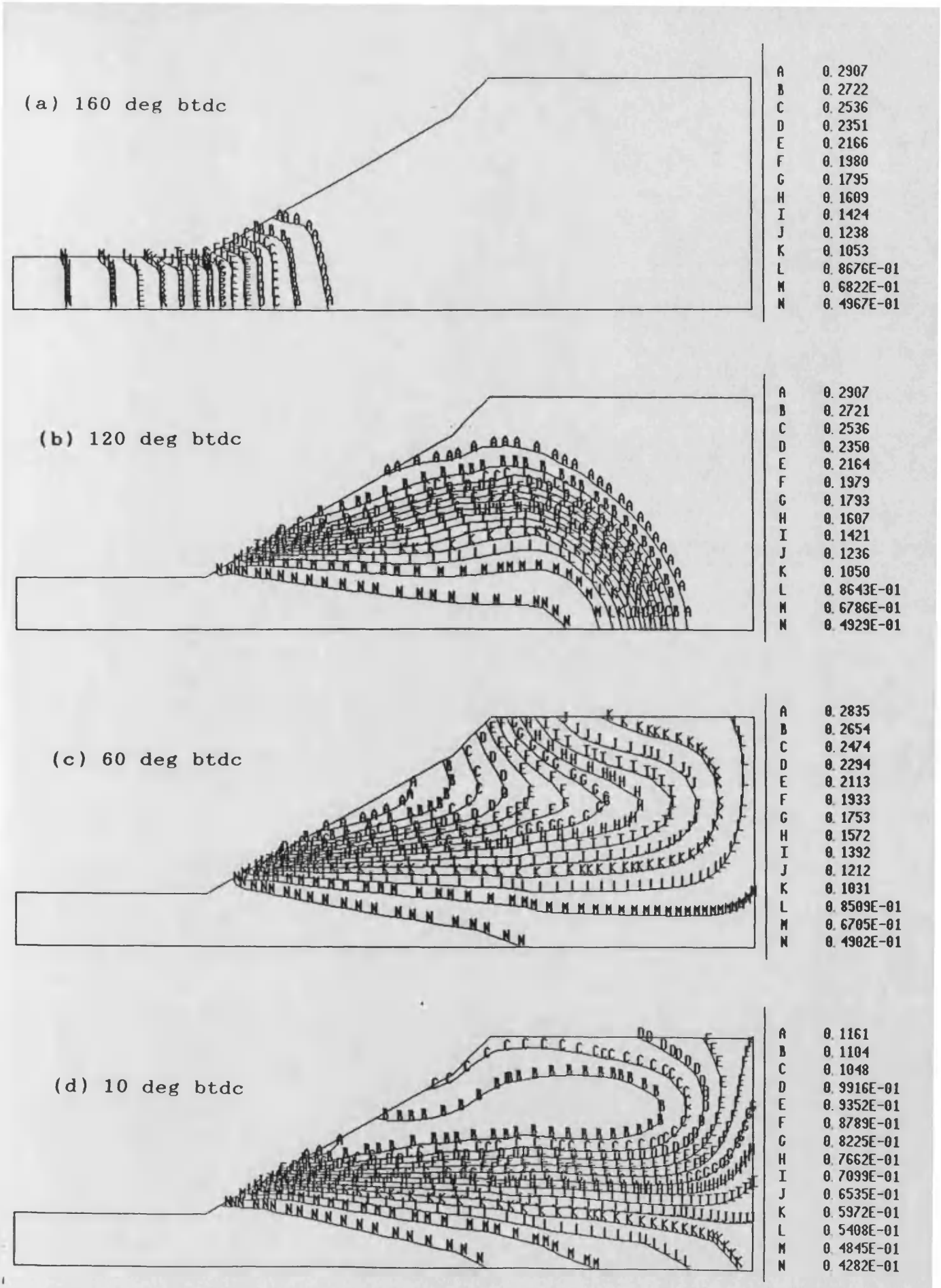

Figure 8.4 Contours of Mixture Concentration for the Prechamber Operating with a Pilot Mixture of 30 % and a Main Chamber Air-Fuel Ratio of 25:1

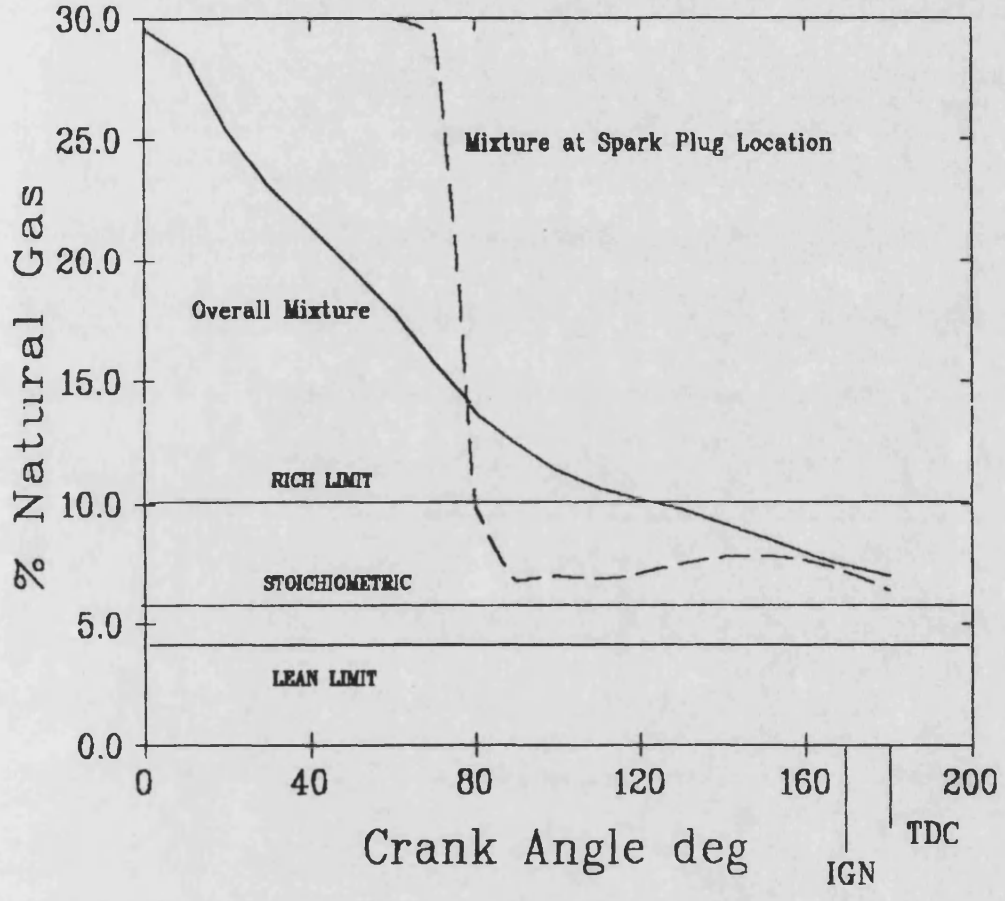

Figure 8.5 Variation of the Overall Mixture and of the Mixture at the Spark Plug Location with a Pilot Mixture of 30 % Natural Gas and a Main Chamber Air-Fuel Ratio of 25:1

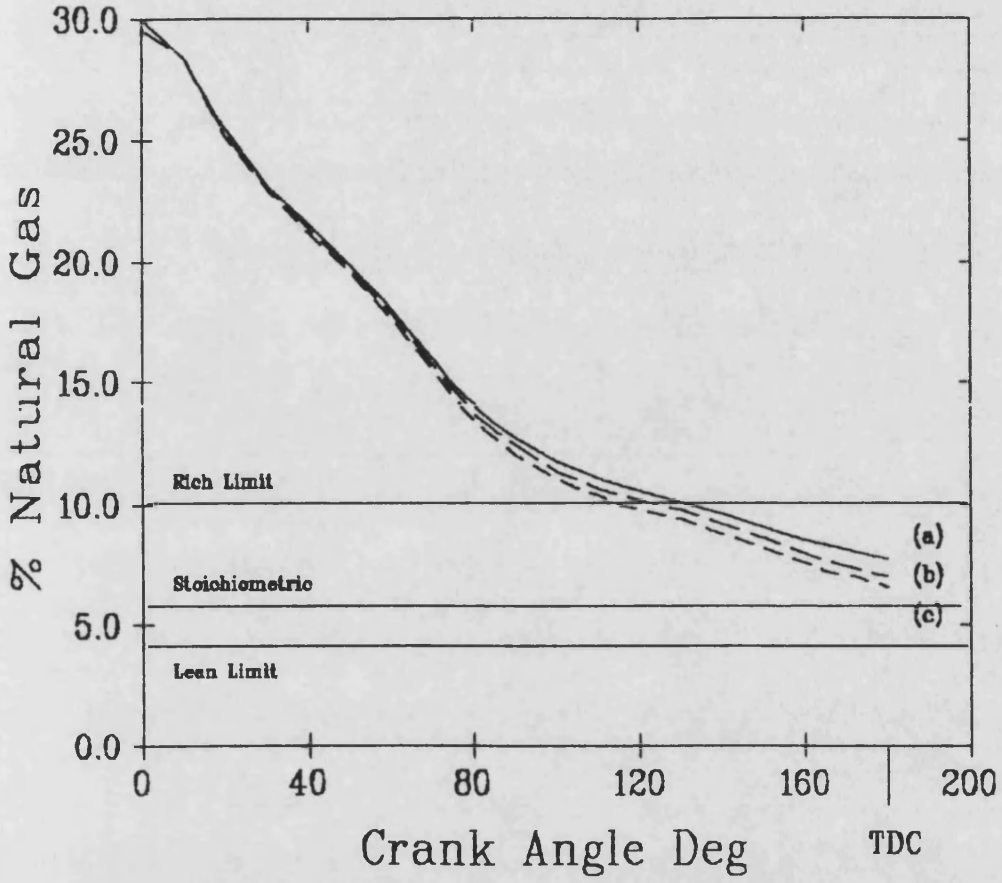

Figure 8.6 Effect of Main Chamber Mixture on Overall Prechamber Mixture Preparation with (a) Main Chamber Mixture of 22.2:1, (b) 25:1 and (c) 28.6:1

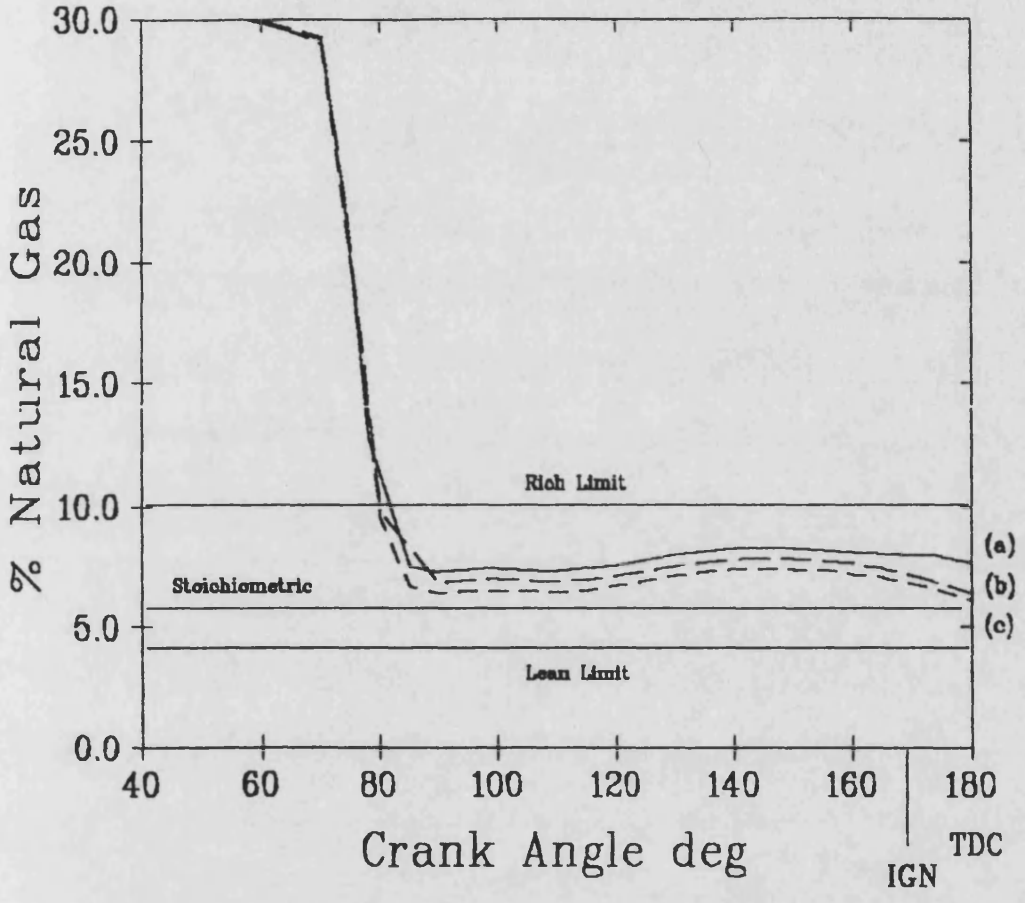

Figure 8.7 Effect of Main Chamber Mixture on Mixture Variation at the Spark Plug Location with (a) Main Chamber Mixture of 22.2:1, (b) 25:1 and (c) 28.6:1

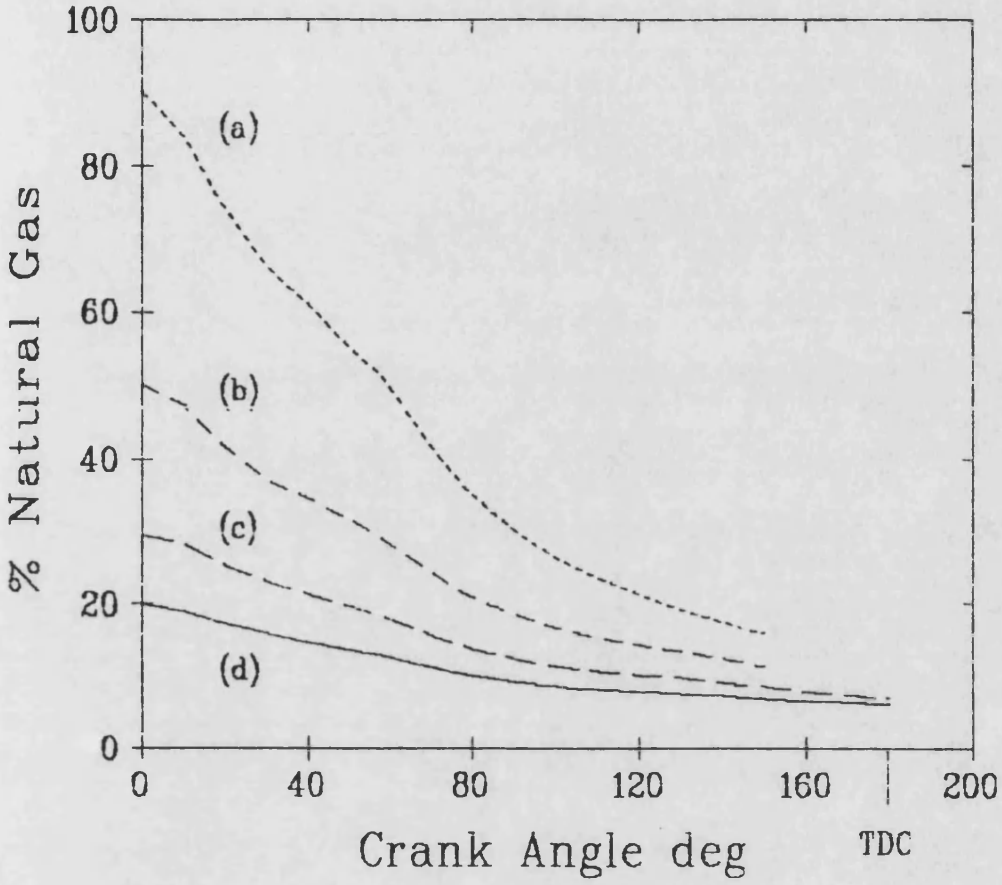

Figure 8.8 Effect of Pilot Mixture on Overall Prechamber Mixture Preparation with (a) Pilot Mixture of 90 % Gas, (b) 50 % Gas, (c) 30 % Gas and (d) 20 % Gas

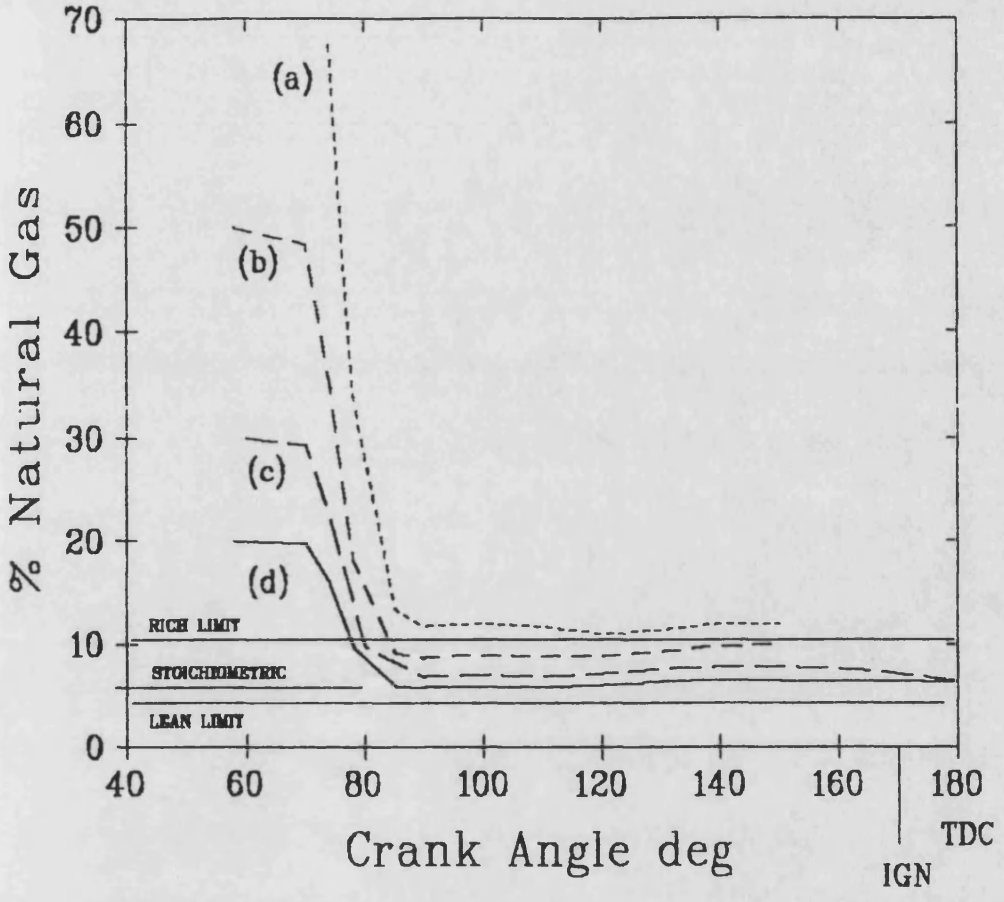

Figure 8.9 Effect of Pilot Mixture on Mixture Variation at the Spark Plug Location for (a) Pilot Mixture of 90 % Gas, (b) 50 % Gas, (c) 30 % Gas and (d) 20 % Gas

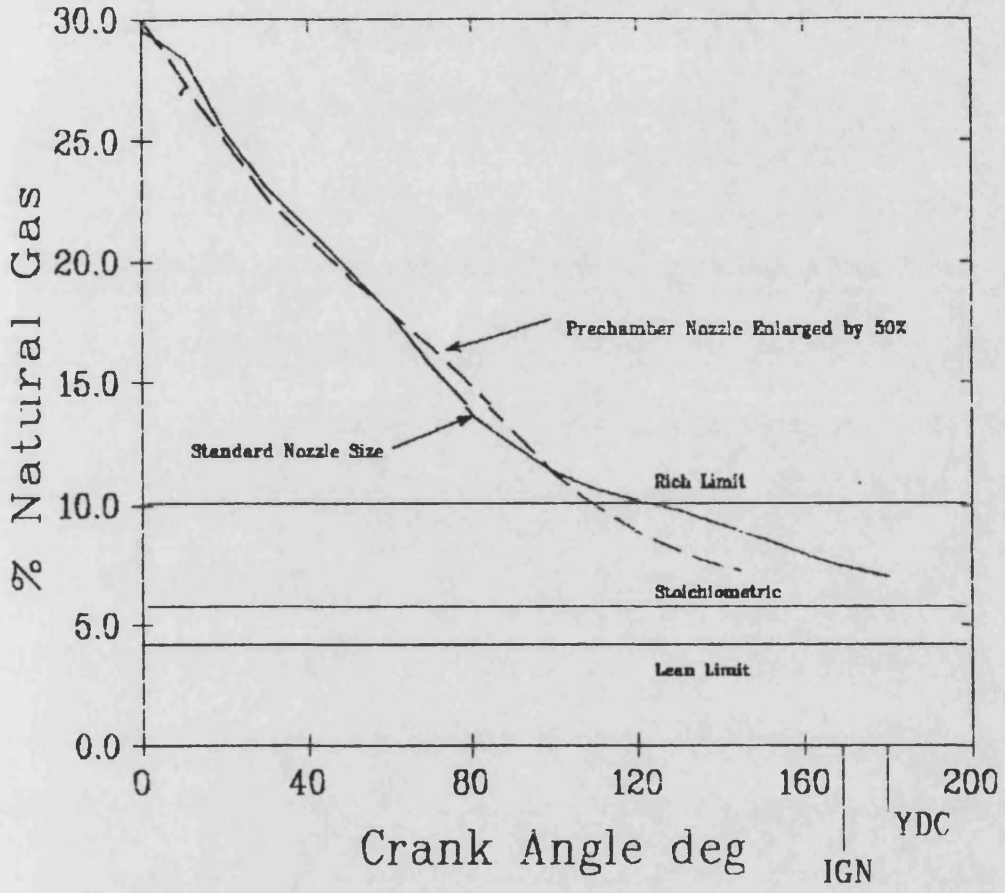

Figure 8.10 Comparison of Overall Prechamber Mixture Preparation for Standard Size Nozzle and Nozzle Area Enlarged by 50 %

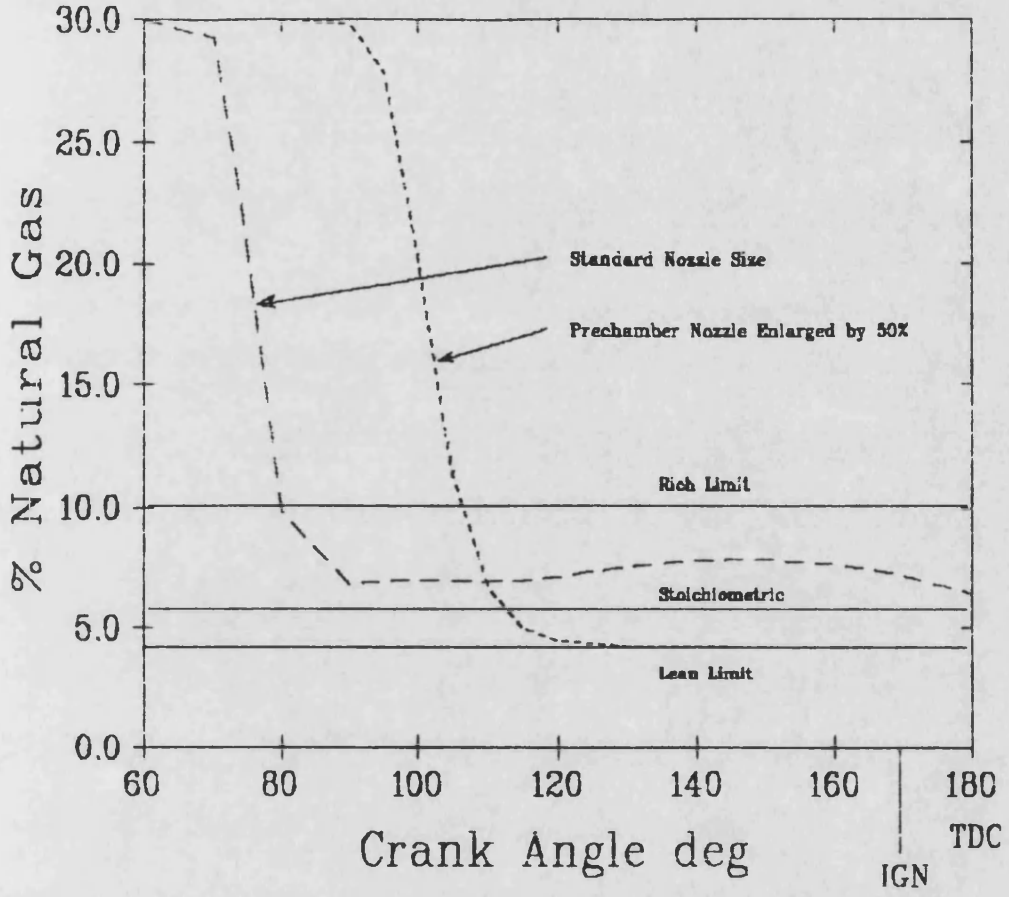

Figure 8.11 Comparison of Mixture Variation at the Spark Plug Location for Standard Size Nozzle and Nozzle Area Enlarged by 50 %

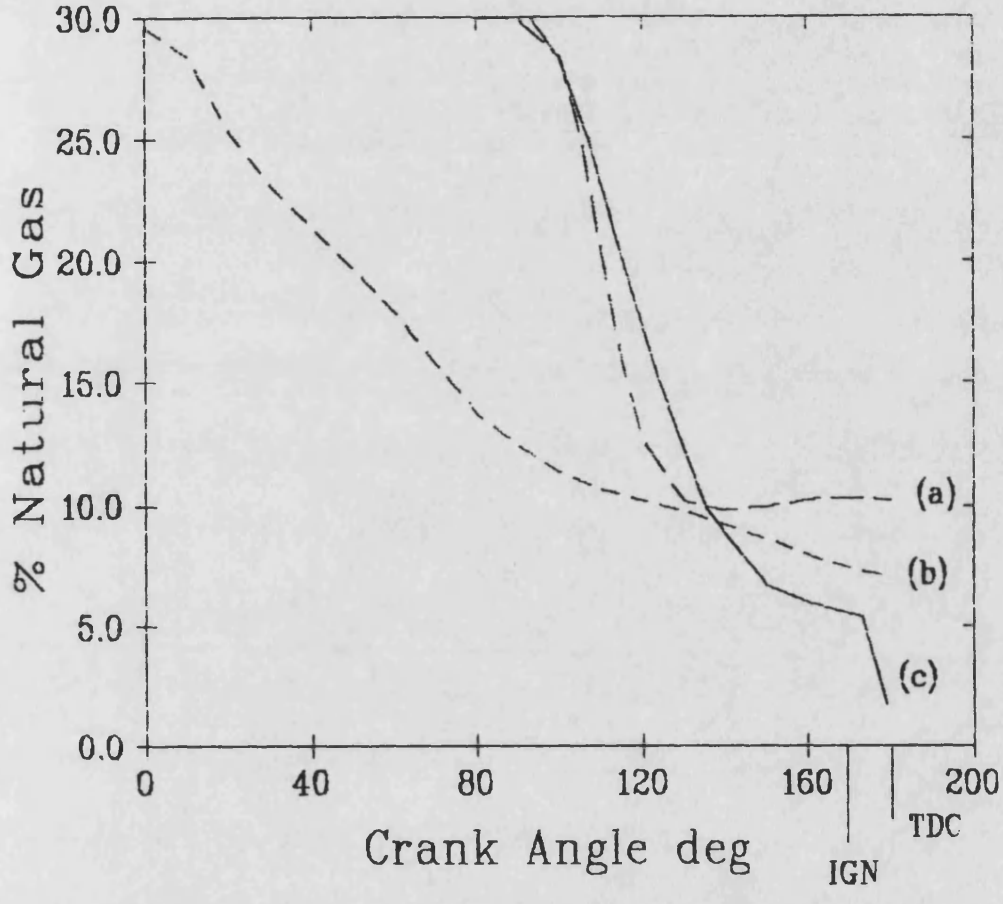

Figure 8.12 Comparison of Computed Mixture Variation with Experimental Measurements taken by the HFR FID. (a) Computed Mixture Variation at the Sampling Point, (b) Computed Overall Mixture Variation and (c) FID Measurements for Similar Conditions

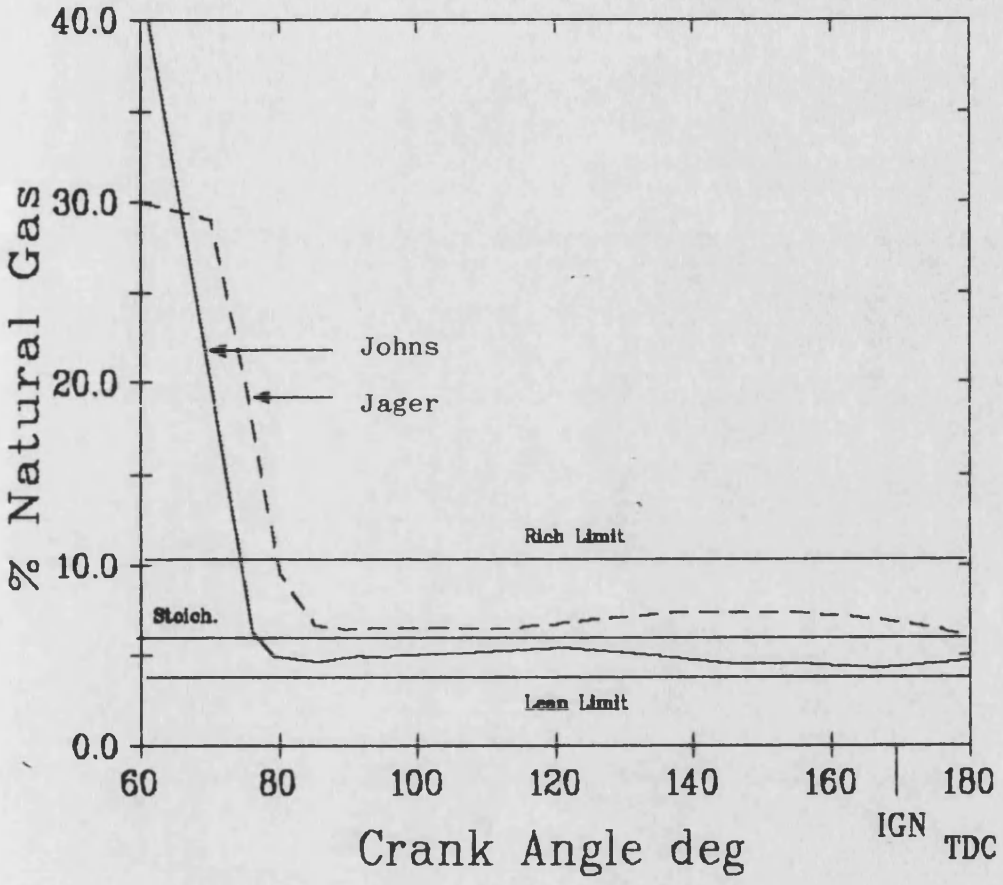

Figure 8.13 Comparison of Mixture Variation at the Spark Plug Location for a Pilot Mixture of 30 % Gas and Main Chamber Air-Fuel Ratio of 28.6:1 with Results from a Similar Computational Study Performed by Johns (14) at the Same Location, but with a Pure Gas Pilot Mixture and a Main Chamber Mixture of 28:1

Chapter 9

9. Discussion and Conclusions

Commissioning of the engine took longer than had originally been thought, but in retrospect this was to be expected when attempting a task of this nature. Apart from the iterative procedures involved in developing the engine and rig, much time was spent in locating and solving faults that frequently developed around the gas supply system, an area where safety must be rigidly maintained. Faults also developed in the instrumentation and analysis equipment and these were often not realised immediately.

The help from Dorman Diesels proved invaluable in both supplying hardware and expertise for the engine's development and maintenance as well as feedback with regard to the realism of assumed engine parameters and the results obtained.

The FID study required much patience and determination in order to obtain meaningful results. The period of validating bench tests took considerably longer than had been anticipated as a result of faults in the sampling system. The results, however, were interesting and could not have been obtained by any other method. Considerable experience has been gained in the application of this technique.

The CFD studies proved time consuming in achieving converged solutions for each of the problems modelled. This was partly as a result of poor documentation, particularly on the later transient version of STAR, and changes in programming format between successive versions. Results to the prechamber study were found to be highly informative, giving an insight into the mixing process.

9.1 Conclusions

Engine Parametric Study

The prechamber ignition system has been proven to be a successful method of reducing NOx emissions for a natural gas engine. Experimental results demonstrate that extremely low (<2g/kWh) emissions of NOx are possible with this system by adopting air-fuel ratios of 27 to 29:1

From the study, it appears that the best control strategy is to operate the prechamber with a pilot supply air-fuel ratio of approximately 3:1 and with a filling ratio just high enough to fill the prechamber with fresh charge. This corresponds well with the results from the CFD study which indicate that a mixture concentration close to stoichiometric will be produced at the spark plug location at the time of ignition.

When the main chamber is optimised for low NOx emission, the prechamber can become an important source of NOx, which may be influenced by the prechamber volume and choice of pilot air-fuel ratio.

The effect of advancing ignition timing is to increase both thermal efficiency and emission of NOx. The effect on NOx is less for leaner mixtures. Prechamber knock is caused by retarding the ignition. This is believed to result from the extremely short duration of burning in the prechamber, completion occurring before peak cylinder pressure has been reached.

Ambient temperature has a significant effect on NOx. When the ambient temperature is artificially varied between 5 degC and 40 degC the level of NOx is increased from 0.6 g/kWh to 2.3 g/kWh.

Closed loop control of the air-fuel ratio is necessary if low NOx emissions are to be maintained under all operating conditions.

HFR FID Study

The Collings FID is not an instrument that can be immediately fitted to an engine with the expectation of obtaining meaningful results. The FID sampling system parameters must be tailored to the application with the supplied computer software and it's performance validated by a series of bench tests.

The HFR FID is an effective instrument for measuring the spatial and temporal development of mixture strength in natural gas engines.

Measurement of mixture concentration within the prechamber has been successively achieved during part of the compression stroke up to the point of ignition. It was not possible to obtain a continuous measurement of mixture concentration throughout the engine cycle because of the inherent inability for the FID to operate over the range of pressures found in engine combustion chambers.

The CFD Study

The STAR CFD program has been shown to accurately model the flow through an orifice plate. Considerable care must be taken in

construction of the model mesh if converged solutions are to be achieved.

CFD has proven a useful method for investigating mixture preparation in the prechamber of the SE1 gas engine. Parametric studies can be easily performed.

Results from CFD modelling have show the mixture in the prechamber to be very inhomogeneous. Mixture variation at the spark plug is very different to that of overall mixture. Leaning of the mixture at this location occurs very rapidly and corresponds to the time when the lean jet reaches this point. This phenomenon is also observed in results by Johns (14) to a similar study.

Pilot mixture concentration has a greater effect on prechamber mixture than the main chamber air-fuel ratio. A pilot mixture of approximately 3:1 air-fuel ratio will produce a mixture at the spark plug location close to stoichiometric at the time of ignition. A pilot mixture of pure gas will produce a mixture too rich to be ignited by a spark, if a filling ratio of 1 (prechamber completely filled with gas at manifold conditions) is adopted.

Changing the throat size of the prechamber has an effect on both the extent to which the prechamber charge is leaned, and the time when this occurs at the spark plug location.

Results from this study agree well with those obtained from the engine parametric study, and from FID sampling in-cylinder sampling.

References

References

1. Brisley R J
"A New Technique to Study the Response of Catalysts to Transient Conditions"
JSAE COMODIA conference, Japan, Sept 1990

2. British Standard 1042, Section 1.1 1981

3. Caton J A, Siebers D L
"Reduction of Nitrogen Oxides in Engine Exhaust Gases by the Addition of Cyanuric Acid"
Journal of Engineering for Gas Turbines and Power
July 1989, Vol. 111/387

4. Charlton S J
"SPICE Users Manual:Simulation Program for Internal Combustion Engines"

5. Charlton S J, Jager D J, Wilson M, & Shooshtarian A
"Computer Modelling and Experimental Investigation of Mixing and Combustion in a Lean-Burn Natural Gas Engine"
Transactions of the SAE, Journal of Engines, 1990.

6. Charlton S J, Jager D J, Wilson M, & Shooshtarian A
"Computer Modelling and Experimental Investigation of Mixing and Combustion in a Lean-Burn Natural Gas Engine"
SAE Paper 900228, International Congress, Detroit, 1990.

7. Charlton S J, Jager D J, Wilson M & Shooshtarian A
"An Investigation of Mixing and Combustion in a Lean-Burn Natural Gas Engine"
ImechE Seminar on Gas Engines and Co-generation
10-11 May 1990

8. Cheng W K, Galliot F, Collings N
"On The Time Delay in Continuous In-Cylinder Sampling From IC Engines"
SAE Paper 1989, 890579

9. Collings N
"A New Technique For Measuring HC Concentration in Real Time in a Running Engine"
SAE Paper 1988, 880517

10. Collings N, Hands T
"A New Technique to Study the Response of Catalysts to Transient Conditions"
JSAE COMODIA Conference, Japan, Sept 1990

11. Eckard D W, Servé J V
"Maintaining Low Exhaust Emissions with9 Turbocharged Gas Engines Using a Feedback Air-Fuel Ratio Control System"
Journal of Engineering for Gas Turbines and Power, October 1987, Vol. 109/487

12. *"Fluid Meters; Their Theory & Application"*
Report by the ASME Research Comittee on Flow Meters
(Sixth Edition)

13. Gosman, Benodekar and Liew
"STAR Users Manual", Versions 1.8 and 2.1

14. Hanu R, Chtsu A and Asanuma T
"Effect of Torch Jet Direction on Combustion and Performance of a Prechamber Spark-Ignition Engine"
Society of Automotive Engineers, 1987, 870167

15. Heywood J B
"Internal Combustion Engine Fundamentals"
McGraw-Hill Books

16. Heywood J B, Galliot F, Cheng W K, Sztenderowics M, Collings N
In-Cylinder Measurements of Residual Gas Concentration in a Spark Ignition Engine"
SAE 1990, 900485

17. Jager D J, Tawfig M E, & Charlton S J
"In-Cylinder Measurement of Mixture Strength in a Divided Chamber Natural Gas Engine"
UnICEG Seminar on the HFR FID, Brunel University, Sept 1990.

18. Jager D J, Charlton S J, Tawfig M E
"In-Cylinder Measurement of Mixture Strength in a Turbocharged Natural Gas Engine"
IMechE Seminar on Experimental Methods in Engine Research and Development 11-12 December 1991.

19. Johns R J R, Jones B M

"Computer Modelling of the Flow in a Lean Burn Natural Gas Engine"

ImechE 1991 C430/058

20. Kingston-Jones M G and Heaton D M

"Nebula Combustion System for Lean Burn Spark Ignited Gas Engines"

SAE 890211

21. Macari N C, Richardson R D

"Operation of a Caterpillar 3516 Spark-Ignited Engine on Low-Btu Fuel"

Journal of Engineering for Gas Turbines and Power, October 1987, Vol. 109/443

22. Mayer C L

"The Waukesha GL Lean Combustion Engine"

Waukesha Engineering, Dresser Industries, USA

23. Moore D S

"Design of a Single Cylinder Research Engine & Development of a Computer Model for Lean Burn Combustion Studies"

Phd thesis, University of Bath 1987

24. Nutton D, Pinnock A

"Closed Loop Ignition and Fuelling Control Using Optical Combustion Sensors"

SAE 1990 900486

25. Pohl J M

"Design and Development of the Waukesha AT25GL Series Gas Engine"

Transactions of the ASME, 1984, 88-ICE-24

26. Ryu H, Chtsu A, Asanuma T

"Effect of Torch Jet Direction on Combustion and Performance of a Prechamber Spark-Ignition Engine"

SAE 870167 1987

27. Snyder W E, Wright M R and Dexter S G

"A Natural Gas Engine Combustion Rig with High-Speed Photography"

Transaction of the ASME, July 1988, Vol. 110/334

28. Servé J V

"NOx Reduction on Large Bore Turbocharged SI Engines"

Transactions of the ASME, 1982, 82-DGP-16

29. Sleightholme, G R

In-Cylinder Measurements of Charge Inhomogeneity in a Spark-Ignition Engine"

SAE 1990, 900484

30. Snyder W E, Wright M R, Dexter S G

"A Natural Gas Engine Combustion Rig With High-Speed Photography"

Transactions of the ASME, July 1988 Vol. 110/334

31. Spalding

"PHOENICS Users Manual"

32. Taylor, G I
"Dispersion of Soluable Matter in Solvent Flowing Slowly Through a Tube"
Proceedings of Roy. Soc. A, 219, 1953, pp. 186-203

33. Taylor, G I
"The Dispersion of Matter in Turbulent Flow Through a Pipe"
Proceedings of Roy. Soc. A, 219, 1954, pp. 446-468

34. Thompson L.D.,Beadle R.H. and Blake B.W.
"A Combustion System for Spark-Fired Gas Engines Using Diesel Compression Ratios"
Transactions of the ASME, Vol 78/743 1956

35. *"United nations Agreement Concerning The Adoption of Uniform Conditions of Approval and Reciprocal Recognition of Approval for Motor Vehicle Equipment and Parts"*
Addendum 48: Regulation No. 49

36. Urban, C.M.
"Emission Control Technology for Stationary Natural Gas Engines"
Journal of Eng. for Gas Turbines and Power, July 1989, Vol. 111 pp 369-374

37. Vinyard S.
"Natural Gas: Old Fuel for New Uses"
Technology Today, June 1988

38. Wadman B.

"Progress with Clean Burn Superior Engines"

Diesel & Gas Turbine Worldwide, May 1987

39. Wilson R.

"Caterpillar Begins Introduction of Broad Gas Engine Line"

Diesel & Gas Turbine Worldwide May 1986

Appendix A

Appendix A

Engine Specification

Model	Dorman SE1 gas engine
Type	Single cylinder divided chamber gas engine
Bore	160 mm
Stroke	190 mm
Capacity	3820 cc (excluding prechamber)
Prechamber capacity	Size 1 - 10 cc; size 2 - 15 cc
Compression ratio	9.77:1 (with 10 cc prechamber)
Valve Type	4 overhead valves; 2 inlet, 2 exhaust, pushrod operated

Fuel system

Fuel	Pipeline natural gas
Carburation	Modified, single Impco 200 series gas mixer

Ignition System

Type	Altronic 3, induction coil with variable timing

Air Compressor Specification

Make:	Bellis/Morcum
Model:	VH150
Type:	2 stage, Reciprocating
Cylinders:	2 Low Pressure, 1 High Pressure
Flow Capacity:	150 cu ft/min

Features: Oil Free Operation by use of Teflon Piston Rings;

Automatic 1/2 load capacity

Appendix B

Appendix B

Fuel Specification

Type: Pipeline natural gas, supplied by British Gas South West Region

Composition

		% Vol	% Mass
N_2	-	1.17	1.81
CO_2	-	0.37	1.37
CH_4	-	94.4	85.64
C_2H_6	-	3.5	7.52
C_3H_8	-	0.4	2.36
C_4H_{10}	-	0.29	0.97
C_5H_{12}	-	0.08	0.33

Octane Rating : 120

Calorific Value : 38.7 MJ/m3

Stoichiometric air-fuel ratio : 16.5 by mass

Appendix C

Appendix C

Nitric Oxide Humidity Correction Factor

To correct for humidity, multiply value by the following correction factor :

$$\frac{1}{1 + A\,(7m - 75) + B * 1.8\,(t - 302)}$$

Where $A = 0.044 \dfrac{Gfuel}{Gair} - 0.0038$

$$B = -0.116 \frac{Gfuel}{Gair} + 0.0053$$

m = humidity of the inlet air in grams of water per kilogram of dry air

T = temperature of the air in K

$\dfrac{Gfuel}{Gair}$ = Fuel air ratio (dry basis)

Appendix D

Appendix D

Stolz Equation (1)

$$Cd = 0.5959 + 0.0312\,\beta^{2.1} - 0.1840\,\beta^{8} + 0.0029\,\beta^{2.5}\,(10^{6}/Re_D)^{0.75} + 0.0900\,L_1\beta^{4}(1-\beta^{4})^{-1} - 0.0337\,L_2\,\beta^{3}$$

where β is the ratio of the orifice and pipe diameters and Re_D is the Reynolds number in the pipe

NOTE - When $L_1 \geq 0.039/0.09$ (=0.4333), use 0.039 for coefficient of $\beta^{4}(1-\beta^{4})^{-1}$

Calculation of Mass Flow Through an Orifice Plate

Equation 2

$$Q = CdA_2\sqrt{(2\Delta P/\rho)/(1 - \beta^{4})^{0.5}}$$

where β is the ratio of the orifice and pipe diameters

ΔP is the pressure drop across the orifice plate

Continuity of Flow

Equation 3

$$w_{in} \times \rho_1 A_{in} = w_{out} \times \rho_2 \times A_{out}$$

Value of Cd for Orifice Plate with Corner Tappings and a Diametric Ratio β of 0.5 Using Stolz Equation:

$$Cd = 0.619$$

Appendix E

Appendix E

Mass and momentum conservation equations solved by STAR for general fluid flows and a moving coordinate frame (the 'Navier Stokes' equations) run in Cartesian tensor notation;

$$\frac{1}{\sqrt{g}}\frac{\partial}{\partial t}(\sqrt{g}\,\rho)+\frac{\partial}{\partial x_j}(\rho\,\tilde{u}_j)=0$$

$$\frac{1}{\sqrt{g}}\frac{\partial}{\partial t}(\sqrt{g}\,\rho\,u_i)+\frac{\partial}{\partial x_j}(\rho\,u_j\,u_i+\tau_{ij})=\frac{\partial p}{\partial x_i}+s_i$$

where

t ≡ time

x_i ≡ cartesian coordinate ($i = 1, 2, 3$)

u_i ≡ absolute fluid velocity component in direction x_i

$\tilde{u}_j$ ≡ $u_j - u_{cj}$, relative velocity between fluid and local (moving) coordinate frame which moves with velocity u_{cj}

p ≡ piezometric pressure = $p_s + \rho_0 g_m x_m$, where p_s is static pressure, ρ_0 is reference density, the g_m are gravitational field components and the x_m are coordinates from a datum

ρ ≡ density

τ_{ij} ≡ stress tensor components

s_i ≡ momentum source components

$\sqrt{g}$ ≡ determinant of metric tensor

and repeated subscripts denote summation*.

The final form of the finite volume, FV, equations is reduced to:

$$\frac{(\rho V)^n - (\rho V)^o}{\delta t} + \sum F_j = 0$$

The result, in its most compact form, is:

$$A_P \phi_P^n = \sum_m A_m \phi_m^n + s_1 + B_P \phi_P^o$$

where Am represents the effects of convection and/or diffusion; the summation is over all neighbouring nodes used in the flux discretisation; $B_P \equiv (\rho V)^o/\delta t$; and

$$A_P = \sum_m A_m + s_2 + B_P$$

The k-e Turbulence Model

Turbulence energy K may be estimated from the relationship;

$$K = \frac{3}{2} \times (U \times I)^2$$

where U is the inlet velocity and I is the turbulence intensity.

The turbulence dissipation rate ε is related to the turbulence length scale l by;

$$\varepsilon = \frac{C_{\mu}^{3/4} k^{3/2}}{l}$$

C_{μ} = 0.09 for pipe flow

the mixing length for pipe flow may be assumed as;

l = 0.1 x Diameter of Pipe

Appendix F

```
   REM ******************************************************
   REM ***                                                ***
   REM *** DORMAN SE1 GAS ENGINE DATA PROCESSING PROGRAM ***
   REM *** ------------------------------------------     ***
   REM ***                By D.J.Jager                    ***
   REM ***       School of Mechanical Engineering         ***
   REM ***                                                ***
   REM ******************************************************
   REM
   REM ********************
   REM * INITIAL SET UP *
   REM ********************
20 CLS
   CR=10:IGN=12:T=25:AP=750:N=1500:ROOTSMETER=18:TE1=25:L=20:MANTEMP=35:ORIFACETEMP=20
   PCGT=25:PCGASPRESS=50:PCET=30:PCAIRPRESS=100:D=6:O=100:B=500:PCEP=100
   I=30:PE1=600:G=30:GB=30:VMC=3:PCA=.5:VPC=.1:P=100
   DATNO=1
40 REM INITIAL PARAMETERS
50 PI=3.1415927£
80 COLOR 3,1,1
90 CLS
    GOSUB 9100
    REM
    REM *************
    REM *** MENU ***
    REM *************
120 CLS
130 PRINT "           DORMAN SE1 GAS ENGINE DATA PROCESSING PROGRAM - DATAPRO"
140 PRINT "           ========================================================"
    REM
    REM
    REM ******************************
    REM ********** MENU ************
    REM ******************************
150 LOCATE 3,30
160 PRINT "*** MENU ***"
    LOCATE 13,15:PRINT "PRESS (L) TO LOAD PREVIOUS DATA"
170 LOCATE 22,13:PRINT "* PRESS SPACE BAR TO DISPLAY & INPUT DATA *"
180 LOCATE 15,15:PRINT "PRESS (E) TO EXIT PROGRAM"
    LOCATE 9 ,15:PRINT "PRESS (M) TO RESET MANOMETER OFFSETS"
    LOCATE 5 ,15:PRINT "PRESS (F) TO CREATE NEW DATA FILE"
    LOCATE 7 ,15:PRINT "PRESS (T) TO SAVE DEFAULT DATA SET"
    LOCATE 17,15:PRINT "PRESS (S) TO SAVE MANOMETER OFFSETS"
    LOCATE 11,15:PRINT "PRESS (R) TO RE-OPEN OLD FILE"
    LOCATE 19,15:PRINT "PRESS (O) TO LOAD DEFAULT FILE
190 I$=INKEY$
210 IF I$="E" THEN CLS:END
220 IF I$=" " THEN GOSUB 250
230 IF I$="M" THEN GOSUB 7000
    IF I$="L" THEN GOSUB 8000
    IF I$="F" THEN GOSUB 4190
    IF I$="S" THEN GOSUB 9000
    IF I$="T" THEN GOSUB 9300
    IF I$="R" THEN GOSUB 9200
    IF I$="O" THEN GOTO 9400
240 GOTO 150
250 CLS
    GOSUB 700
280 X$=INKEY$
290 LOCATE 1,60
300 PRINT" TIME = ";TIME$
310 IF X$="A" THEN GOTO 280
```

```
    IF X$="b" THEN GOSUB 2901
    IF X$="B" THEN GOSUB 3145
320 IF X$="C" THEN GOSUB 2910
330 IF X$="c" THEN GOSUB 2940
340 IF X$="D" THEN GOSUB 3150
350 IF X$="d" THEN GOSUB 3840
360 IF X$="r" THEN GOSUB 3360
370 IF X$="E" THEN GOSUB 3600
380 IF X$="e" THEN GOSUB 2970
390 IF X$="F" THEN GOSUB 3630
400 IF X$="f" THEN GOSUB 3000
410 IF X$="G" THEN GOSUB 3690
420 IF X$="g" THEN GOSUB 3480
430 IF X$="H" THEN GOSUB 3720
440 IF X$="h" THEN GOSUB 3510
450 IF X$="I" THEN GOSUB 3780
460 IF X$="i" THEN GOSUB 3180
470 IF X$="J" THEN GOSUB 3240
480 IF X$="j" THEN GOSUB 3270
490 IF X$="K" THEN GOSUB 3060
500 IF X$="k" THEN GOSUB 3030
510 IF X$="L" THEN GOSUB 3210
520 IF X$="l" THEN GOSUB 3570
530 IF X$="M" THEN GOSUB 3750
540 IF X$="m" THEN GOSUB 3300
550 IF X$="n" THEN GOSUB 3390
560 IF X$="o" THEN GOSUB 3330
580 IF X$="P" THEN GOSUB 3420
590 IF X$="p" THEN GOSUB 3090
600 IF X$="Q" THEN GOSUB 3450
610 IF X$="q" THEN GOSUB 3660
620 IF X$="X" THEN GOTO 120
630 IF X$="a" THEN GOSUB 3540
640 IF X$="R" THEN GOSUB 3880
650 IF X$=" " THEN GOSUB 4240
652 IF X$="S" THEN GOSUB 3870
654 IF X$="T" THEN GOSUB 3872
    IF X$="N" THEN GOSUB 3875
    IF X$="O" THEN GOSUB 3876
    IF X$="U" THEN GOSUB 3877
660 GOTO 280
700 REM
710 REM
711 REM ****************************
712 REM ****** CALCULATIONS ******
713 REM ****************************
    REM
    REM ---------------------------
    REM GAS & AIR FLOW CALCULATIONS
    REM ---------------------------
    REM
714 PI=3.141593
715 TA=T+273
720 GT=ROOTSMETER+273
730 OTEMP=273+ORIFACETEMP
740 BGT=273+L
750 REM
760 REM CAL. POWER
770 REM
780 P=(N*D*.746)/200
782 REM
```

```
783 REM CAL. TORQUE
785 TORQUE=P*1000/(N*2*PI/60)
790 REM
800 REM CAL. DENSITY OF GAS IN MAINS PIPE
810 REM
820 DG=((AP*133.3)+(G*9.8064))/(520*GT)
830 REM
    REM CAL. CALORIFIC VALUE OF FUEL- KJ/KG
835 CV=57000
840 REM CAL. FUEL CON.
850 REM
    IF FTIME=0 THEN GOTO 870
860 REM FTOT IS IN KG/SEC
    F=16967/FTIME
870 FTOT=F*DG/60000!
    REM F=FUEL FLOW IN L/MIN
880 REM
890 REM CAL. DENSITY OF AIR
900 REM
910 DA=((AP+B)*133.3)/(287*OTEMP)
920 REM
930 REM CAL. AIR CON. BY MASS
940 REM
950 AC=6.150001E-04*((2*O*9.8604*DA)^.5)
960 REM
970 REM CAL. OVERALL AIR/FUEL RATIO
980 REM
990 AFR=AC/FTOT
1000 TM=MANTEMP+273
1010 REM
1020 REM CAL. DENSITY OF MIXTURE
1030 REM
1040 DMIX2=(((AP+I)*133.3)*(AFR+1))/(((AFR*287)+520)*TM)
     DMCAIR=(AP+I)*133.3/(287*TM)
     DMCGAS=(AP+I)*133.3/(520*TM)
     DMIX=(DMCAIR*AFR/(AFR+1))+(DMCGAS/(AFR+1))
1050 REM
1060 REM CAL. VOL. EFF.
1070 REM
1090 VEFF=100*(AC+FTOT)/(.0000318*N*DMIX)
1100 REM
1110 REM CAL. THERMAL EFF.
1120 REM
1130 THERMEFF=(P*100)/(FTOT*CV)
1140 REM
1150 REM CAL.SFC
1160 REM
1165 IF D=0 THEN P=.01
1170 SFC=(FTOT*3600)/P
1172 BSFC2=(CV*SFC)/1.055E3
1174 BSFC3=(CV*SFC)/3600
1180 REM
1190 REM CAL. BMEP
1200 REM
1210 SPEED=N/60
1220 WCYCLE=P*1000*2/SPEED
1230 BMEP=WCYCLE*.00001/.0039
1240 REM
1250 REM
1260 REM CAL. GAS AND AIR FLOWS TO PC/MC
```

```
1270 REM
     AMBIENTPRESS=AP*133.3
1280 REM KRMCG=CORRECTION FACTOR FOR MC ROTAMETER
1290 KRMCG=(273/BGT)*(((GB+AP)*133.3/101325)^.5)
     REM DGMC="DENSITY" OF GAS THROUGH MC ROTAMETER AT 1.01325 BAR
     REM DGPC="DENSITY" OF GAS THROUGH PC ROTAMETER AT 1.01325 BAR
     REM DAPC="DENSITY" OF AIR THROUGH PC ROTAMETER AT 1.01308 BAR
     REM BGT = BOOSTED GAS TEMP.
     REM PCGT = PC ROTAMETER GAS TEMP.
     REM PCAT = PC ROTAMETER AIR TEMP.
     PCAPRESS=PCAIRPRESS*6895
     PCGPRESS=PCGASPRESS*6895
     KRPCG=(273/(PCGT+273))*(((AMBIENTPRESS+PCGPRESS)/101325)^.5)
     KRPCA=(288/(PCAT+273))*(((AMBIENTPRESS+PCAPRESS)/101308)^.5)
1300 DGMC=0.71376
     DGPC=0.71376
     DAPC=1.2257
     REM DGBG = ACTUAL PC GAS DENSITY
     DGBG=(AMBIENTPRESS+(GB*133.3))/(520*(PCGT+273))
     REM DABG = ACTUAL PC AIR DENSITY
     DABG=(AMBIENTPRESS+PCAPRESS)/(287*(273+PCAT))
1305 REM BY MASS
1310 PCGAS=(KRPCG*DGPC*VPC*.02832)/60
1320 MCGAS=(KRMCG*DGMC*VMC*.02832)/60
     PCAIR=(KRPCA*DAPC*PCA)/60000
     REM
1325 REM CAL. PC AFR
1327 IF PCGAS=0 THEN GOTO 1340
1328 PCAFR=PCAIR/PCGAS
1330 REM
1331 REM CAL. PC FILLING RATIO BASED ON ACTUAL P.C. ENTRY CONDITIONS
1334 TPCFLOW=N*PCSIZE*1E-6/120
     REM CAL. FILLING RATIO WITH CONDITIONS AT ENTRY TO PC
     PPCMIX=(PCEP*133.3)+AMBIENTPRESS
     DPCAIR=PPCMIX/(287*(PCET+273))
     DPCGAS=PPCMIX/(520*(PCET+273))
     DPCMIX=(DPCAIR*AFR/(AFR+1))+(DPCGAS/(AFR+1))
     MPCMIX=PCGAS+PCAIR
     VPCMIX=MPCMIX/DPCMIX
     PCFILLRAT=VPCMIX/TPCFLOW
     REM CAL. PC FILLING RATIO BASED ON MANIFOLD CONDITIONS
     PPCMIX2=(I*133.3)+AMBIENTPRESS
     DPCAIR2=PPCMIX2/(287*(MANTEMP+273))
     DPCGAS2=PPCMIX2/(520*(MANTEMP+273))
     DPCMIX2=(DPCAIR2*AFR/(AFR+1))+(DPCGAS2/(AFR+1))
     VPCMIX2=MPCMIX/DPCMIX2
     PCFILLRAT2=VPCMIX2/TPCFLOW
     REM P.C. TO MANIFOLD PRESS. RATIO
     PCPR1=((PCEP*133.3)+AMBIENTPRESS)/((I*133.3)+AMBIENTPRESS)
     PCPR2=((PCEP*133.3)+AMBIENTPRESS)/((B*133.3)+AMBIENTPRESS)
1340 REM CAL. AGREEMENT BETWEEN ROOTS METER & ROTAMETER
1350 METERERROR=100*(FTOT-(PCGAS+MCGAS))/FTOT
     REM CAL. M.C. AFR
     MCAFR=AC/(FTOT-PCGAS)
     REM
     REM ----------------------
1360 REM INLET TEMP. SUBROUTINE
     REM ----------------------
1370 REM
1380 TB=TB1+273
```

```
1390 REM TB = BOOST AIR TEMP. AT ENTRY TO INTERCOOLER
1400 PA=AP*133.3:R=AFR:EFFTOT=.55:CPE=1200
1410 TE=TE1+273
1420 GAMMAE=1.33
1430 GAMMAAIR=1.4
1440 PB=PA+(133.3*PB1)
1450 Z1=(GAMMAAIR-1)/GAMMAAIR
1460 Z2=(GAMMAE-1)/GAMMAE
1470 PB=B*133.3+PA
1480 TB=TA+(TA*(((PB/PA)^Z1)-1))
1490 TI=TB-.75*(TB-TA)
1500 TINLET=TI-273
1510 REM
1520 REM ---------------
1530 REM CALC. TURBO EFF.
1540 REM ---------------
1550 REM
1560 CPA=1000
1570 PCOMP=AC*CPA*(TB-TA)
1580 RE=(PA/PE)
1590 PTURB=AC*(1+(1/R))*CPE*TE*(1-((RE)^Z2))
1600 TURBOEFF=PCOMP*100/PTURB
1610 REM
1620 REM ------------------
1630 REM CAL. NOX EMISSIONS
1640 REM ------------------
1650 REM
1660 NOXM=NOX*AC*(1+(1/R))/1000
1670 NOXGKWHR=NOXM*3600/P
1680 REM CAL. NO EMISSIONS
1690 NOM=NO*AC*(1+(1/R))/1000
1700 NOGKWHR=NOM*3600/P
1710 REM
1720 REM ----------------------
1730 REM CAL. ENERGY BALANCE
1740 REM ----------------------
1760 CPW=4190!
1770 CPOIL=1880!
1780 REM OIL FLOW = 0.040611 L/MIN PER RPM
1790 OILFLOW=.089*N*.040611/60
1800 REM Q=(Hp2-Hp0)+dH0+(Hr0-Hr1)
1810 REM P=MECH. WORK-KW
1815 W=P*1000
1820 REM
1830 REM ENERGY FROM FUEL
1850 DH0=CV*FTOT*1000
1860 REM
1870 REM CAL.HEAT TO COOLANT
1880 MW=DMW/60
1890 QCOOLANT=MW*CPW*(WC1-WC2)
1900 REM
1910 REM CAL.HEAT TO OIL
1920 QOIL=OILFLOW*CPOIL*(OC1-OC2)
1930 REM ---------------------------------------------
1940 REM SUBROUTINE TO CAL.ENTHALPY OF AIR/FUEL MIXTURE
     REM ---------------------------------------------
1950 MMIX=AC+FTOT
1960 CPMETHANE=1991
1970 CPAIR=1400
1980 CPMIX=(CPMETHANE+(AFR*CPAIR))/(AFR+1)
```

```
1990 QMIX=MMIX*CPMIX*(T0-T1)
2000 REM
2010 REM CAL.WORK LOST IN EXPANSION THROUGH EXHAUST RESTRICTER
2020 MEX=AC+FTOT
2030 QRESTRICTOR=MEX*CPE*(1-(AP/(PE1+AP))^Z2)
2040 REM
2050 REM CAL. HEAT GAIN TO EXHAUST PRODUCTS
2060 REM CAL. Ho
2070 TM1=273
2090
2095 H0=HEXH
2100 REM
2110 REM CAL.H2
2120 REM
2130 TM1=273+TE1
2140
2150 H2=HEXH
2160 REM
2170 QEXH=CPE*MMIX*(TM1-T0)
2180 REM
2190 Q=QEXH+QMIX
2200 REM BALANCE RATIO
2210 REM EOUT = ENERGY OUT
2220 EOUT=QCOOLANT+QOIL+W+Q+QRESTRICTOR
2230 REM EIN = ENERGY IN
2240 EIN=DH0
2242 REM ERATIO=ENERGY RATIO
     IF EIN=0 THEN GOTO 2375
2244 ERATIO=EOUT/EIN
2246 REM
2247 GOTO 2375
2248 REM
2250 REM SUBROUTINE TO CAL.ENTHALPY OF EX.GAS
2260 REM
2280 CON1=985.03:CON2=993.89:CON3=8.9465E-04:CON4=1.57193:CON5=1.02512E-04
2290 CON6=-5.2384E-04:CON7=-4.552E-08:CON8=1.166083E-07:CON9=6.22E-12
2300 CON10=-1.253348E-11
2310 TM1=TE
2320 TM2=TM1*TM1
2330 TM3=TM2*TM1
2340 TM4=TM3*TM1
2350 TM5=TM4*TM1
2360 HEXH=(CON1*TM1+CON3*TM2+CON5*TM3+CON7*TM4+CON9*TM5+AFR*(CON2*TM1+CON4*TM2+CON6*TM3+CON8*TM4+CON10*TM5))/(1!+AFR)
2370 RETURN
2375 REM CAL. MAX CYLINDER PRESSURE
     PMAX=VPMAX*21.4
2380 REM
     REM **********************************
2390 REM ******** SCREEN DISPLAY ********
2400 REM **********************************
     REM
     REM
2440 LOCATE 1,1
2450 PRINT " DATE = ";DATE$
2460 LOCATE 1,30:PRINT "DATA SET NUMBER ..";DATNO
2470 PRINT" FILE NAME :- ";FILE$;"       TITLE :- ";TITLE$
2480 LOCATE 3,2 :PRINT "KEY     PARAMETER       VALUE"
2490 LOCATE 3,40:PRINT "KEY     PARAMETER       VALUE"
2500 PRINT "--------------------------------------------------------------------------------"
2510 LOCATE 5,2 :PRINT "(A) COMPRESSION RATIO...";CR;":1 "
```

```
2520 LOCATE 6,40:PRINT "(a) IGNITION TIMING.....";IGN;" BTDC "
2530 LOCATE 6,2 :PRINT "(B) PRECHAMBER SIZE.....":PCSIZE:" cc "
2540 LOCATE 5,40:PRINT "(X) FOR MENU
2550 LOCATE 7,2 :PRINT "(C) AMBIENT TEMP........";T
2560 LOCATE 7,40:PRINT "(c) AMBIENT PRESSURE....":AP;" mm Hg "
2570 LOCATE 8,2 :PRINT "(D) ENGINE SPEED........";N;" rpm  "
2580 LOCATE 9,2 :PRINT "(E) HT.EX.IN TEMP..(1/0)";WC1;" C  "
2590 LOCATE 10,2:PRINT "(F) HT.EX.OUT TEMP.(1/1)";WC2;" C  "
2600 LOCATE 11,2:PRINT "(G) OIL COOLER IN..(1/2)";OC1;" C  "
2610 LOCATE 12,2:PRINT "(H) OIL COOLER OUT.(1/4)";OC2;" C  "
2620 LOCATE 13,2:PRINT "(I).ROOTS METER GAS(3/4)";ROOTSMETER:" C  "
2630 LOCATE 14,2:PRINT "(J) EXHAUST TEMP...(3/2)";TE1;" C  "
2640 LOCATE 15,2:PRINT "(K) BOOSTED GAS....(3/5)";L;" C  "
2650 LOCATE 16,2:PRINT "(L) INTAKE MANIFOLD(3/6)";MANTEMP;" C  "
2660 LOCATE 17,2:PRINT "(M).ORIFICE TEMP...(3/7)":ORIFACETEMP;" C  "
2670 LOCATE 18,2 :PRINT "(N) PC GAS ROT.TEMP(3/A)":PCGT;" C  "
2680 LOCATE 19,2 :PRINT "(O) PC GAS PRESSURE.....":USING "££.£ lbs/in2 ";PCGASPRESS
2690 LOCATE 20,2 :PRINT "(P) NOX-";NOX;" ppm (Q) NO-";NO;" ppm "
     LOCATE 21,2 :PRINT "(U) P.C. ENTRY TEMP(3/B)";PCET;" C "
2705 LOCATE 22,2 :PRINT "(S) P.C. AIR TEMP..(3/C)";PCAT;" C "
2707 LOCATE 23,2 :PRINT "(T) P.C. AIR PRESS.....";USING "££.£ lbs/in2";PCAIRPRESS
2710 LOCATE 8,40 :PRINT "(d) DYNANOMETER LOAD....";USING "££.£";D
2720 LOCATE 9,40:PRINT "(e).ORIFICE PRESSURE....";O;" mm H2O  "
2730 LOCATE 10,40:PRINT "(f).AIR BOOST.....";B;" mm Hg  "
2740 LOCATE 11,40:PRINT "(g) M.C. OVERPRESSURE...";MCOP;" mm H2O  "
2750 LOCATE 12,40:PRINT "(h) P.C. ENTRY PRESS....":PCBP;" mm Hg  "
2760 LOCATE 13,40:PRINT "(i) INTAKE PRESSURE.....";I;" mm Hg  "
2770 LOCATE 14,40:PRINT "(j) EXHAUST PRESSURE....":PE1;" mm Hg  "
2780 LOCATE 15,40:PRINT "(k).GAS MAINS PRESSURE..";G;" mm H2O  "
2790 LOCATE 16,40:PRINT "(l) GAS BOOST PRESSURE..";GB;" mm Hg  "
2800 LOCATE 17,40:PRINT "(m) M.C. GAS FLOW ..... ";USING "£.££ CuFt/min ";VMC
2810 LOCATE 18,40:PRINT "(n) P.C. AIR FLOW ......";USING "££.££ l/min ";PCA
2820 LOCATE 19,40:PRINT "(o) P.C. GAS FLOW A/B... ";USING ".£££ CuFt/min ";VPC
2830 LOCATE 20,40:PRINT "(p).TIMED GAS FLOW......";USING "£££.£ sec ";PTIMB
2840 LOCATE 21,40:PRINT "(q) COOLANT FLOW........";DMW;" l/min  "
2850 LOCATE 22,40:PRINT "(r) THROTTLE POSITION...";THROTPOS;" % "
     LOCATE 23,40:PRINT "                                      "
    LOCATE 23,40 :PRINT"(R) SAVE DATA SET TO FILE
2860 X=0
2870 RETURN
     REM
2880 REM ************************************
2890 REM ***** INPUT DATA FROM KEYBOARD *****
2900 REM ************************************
     REM
     REM
2901 LOCATE 23,40
     INPUT "CYLINDER PRESS. (VOLTS) "VPMAX
     GOTO 710
2910 LOCATE 23,40
2920 INPUT "AMBIENT TEMP. (degrees C)";T
2930 GOTO 710
2940 LOCATE 23,40
2950 INPUT "AMBIENT PRESSURE (mm Hg) ";AP
2960 GOTO 710
2970 LOCATE 23,40
2980 INPUT "ORIFACE PRESSURE (mm H2O) ";OTOP
     O=(OTOP-OMO)*2
2990 GOTO 710
3000 LOCATE 23,40
```

```
3010 INPUT "BOOST AIR PRESSURE (mm Hg) ";BTOP
     B=(BTOP-BAMO)*2
3020 GOTO 710
3030 LOCATE 23,40
3040 INPUT "MAINS GAS PRESSURE (mm H2O) ";GTOP
     G=(GTOP-MGMO)*2
3050 GOTO 710
3060 LOCATE 23,40
3070 INPUT "BOOSTED GAS TEMP. (C)   ";L
3080 GOTO 710
3090 LOCATE 23,40
3100 INPUT "GAS FLOW TIME  (sec)    ";FTIME
3110 GOTO 710
3120 LOCATE 23,40
3130 INPUT "DYNANOMETER LOAD        ";D
3140 GOTO 710
3145 LOCATE 23,40
     INPUT"PRECHAMBER SIZE , cc ":PCSIZE
     GOTO 710
3150 LOCATE 23,40
3160 INPUT"ENGINE SPEED (rpm)       ";N
3170 GOTO 710
3180 LOCATE 23,40
3190 INPUT "INTAKE PRESSURE (mm H2O) ";ITOP
     I=(ITOP-IMO)*2
3200 GOTO 710
3210 LOCATE 23,40
3220 INPUT "INTAKE MANIFOLD TEMP. (C) ";MANTEMP
3230 GOTO 710
3240 LOCATE 23,40
3250 INPUT "EXHAUST GAS TEMP.         ";TE1
3260 GOTO 710
3270 LOCATE 23,40
3280 INPUT "EXHAUST PRESSURE          ";PE1TOP
     PE1=(PE1TOP-EMO)*2
3290 GOTO 710
3300 LOCATE 23,40
3310 INPUT "MAIN CHAMBER GAS FLOW (CuFt/min) ";VMC
3320 GOTO 710
3330 LOCATE 23,40
3340 INPUT "PRECHAMBER GAS FLOW (CuFt/min) ";VPC
3350 GOTO 710
3360 LOCATE 23,40
3370 INPUT "THROTTLE POSITION (%)    ";THROTPOS
3380 GOTO 710
3390 LOCATE 23,40
3400 INPUT "P.C. AIR FLOW (l/min)    ";PCA
3410 GOTO 710
3420 LOCATE 23,40
3430 INPUT "NOX READING (ppm)        ";NOX
3440 GOTO 710
3450 LOCATE 23,40
3460 INPUT "NO READING (ppm)         ";NO
3470 GOTO 710
3480 LOCATE 23,40
3490 INPUT "M.C. OVER PRESSURE (mm H2O) ";MCOPTOP
     MCOP=(MCOPTOP-MCMO)*2
3500 GOTO 710
3510 LOCATE 23,40
3520 INPUT "P.C. ENTRY PRESSURE (mm Hg) ";PCEPTOP
```

```
    PCEP=(PCEPTOP-PCMO)*2
3530 GOTO 710
3540 LOCATE 23,40
3550 INPUT "IGNITION TIMING          ";IGN
3560 GOTO 710
3570 LOCATE 23,40
3580 INPUT "GAS BOOST PRESSURE       ";GBTOP
    GB=(GBTOP-BGMO)*2
3590 GOTO 710
3600 LOCATE 23,40
3610 INPUT "HEAT EX. INLET TEMP. (C) ";WC1
3620 GOTO 710
3630 LOCATE 23,40
3640 INPUT "HEAT EX. OUTLET TEMP. (C) ";WC2
3650 GOTO 710
3660 LOCATE 23,40
3670 INPUT "COOLANT FLOW RATE (l/min) ";DMW
3680 GOTO 710
3690 LOCATE 23,40
3700 INPUT "OIL COOLER INLET TEMP. (C)";OC1
3710 GOTO 710
3720 LOCATE 23,40
3730 INPUT "OIL COOLER OUTLET TEMP. (C)";OC2
3740 GOTO 710
3750 LOCATE 23,40
3760 INPUT "AIR ORIFICE TEMP. (C)    ";ORIFACETEMP
3770 GOTO 710
3780 LOCATE 23,40
3790 INPUT "ROOTSMETER GAS TEMP. (C) ";ROOTSMETER
3800 GOTO 710
3810 LOCATE 23,40
3820 INPUT "ACTUAL INLET TEMP. (C)  ";INLETTEMP
3830 GOTO 710
3840 LOCATE 23,40
3850 INPUT "DYNAMOMETER LOAD        ";D
3860 GOTO 710
3870 LOCATE 23,40:INPUT "P.C. AIR TEMP.         ";PCAT
3871 GOTO 710
3872 LOCATE 23,40:INPUT "P.C. AIR PRESS.        ";PCAIRPRESS
3874 GOTO 710
3875 LOCATE 23,40:INPUT "P.C. GAS TEMP.         ";PCGT
    GOTO 710
3876 LOCATE 23,40:INPUT "P.C. GAS PRESS.        ";PCGASPRESS
    GOTO 710
3877 LOCATE 23,40:INPUT "P.C. ENTRY TEMP.       ";PCET
    GOTO 710
3879 REM
3880 REM ******************************
3890 REM **** WRITE DATA TO FILES ****
3900 REM ******************************
    REM
3910 BEEP
    DATNO=DATNO+1
3960 D$=DATE$:T$=TIME$
4030 LOCATE 1,30:PRINT "DATA SET NUMBER ..";DATNO
4040 REM
    OPEN "A",£3,FILE$
4050 REM
4060 REM WRITE RESULTS DATA TO DATA FILE
4070 WRITE£3,D$,T$,DATNO
    REM INPUT DATA
4080 WRITE£3,CR,IGN,PCSIZE,CONENO,T,AP,N,WC1,WC2,OC1,OC2,ROOTSMETER,TE1,L,MANTEMP
    WRITE£3,ORIFACETEMP,PCGT,PCGASPRESS,NOX,NO,PCET,PCAT,PCAIRPRESS,D,O,B,MCOP,PCEP
    WRITE£3,I,PE1,G,GB,VMC,PCA,VPC,F,DMW,THROTPOS,VPMAX
    WRITE£3,FTIME
```

```
     REM PROCESSED DATA
     WRITE£3,AFR,P,VEFF,THERMEFF,TINLET,TURBOEFF,BMEP,SFC,BSFC2,BSFC3,NOXGKWHR
     WRITE£3,NOGKWHR,PCGAS,MCGAS,METERERROR,FTOT,TORQUE,ERATIO,PCAFR,PCFILLRAT
     WRITE£3,PCAIR,PCKN,C$,PMAX
4110 REM
4120 REM
4140 CLOSE £3
4150 RETURN
4160 REM
     REM ************************************
     REM *** SUB. TO CREATE NEW DATA FILE ***
     REM ************************************
     REM
4190 CLS
4200 LOCATE 10,20:INPUT "ENTER NAME OF DATA FILE";FILE$
     CLOSE£3
4210 OPEN "O",£3,FILE$
     LOCATE 14,15:INPUT "ENTER FILE TITLE ";TITLE$
     WRITE£3,TITLE$
     CLOSE£3
     DATNO=1
4220 CLS
4230 RETURN
     REM
     REM ***********************************
     REM ******* PRINT OUT RESULTS ********
     REM ***********************************
     REM
4240 CLS
     LOCATE 2,1:PRINT"-------------------------------------------------------------------------------"
4250 LOCATE 3,1
4260 PRINT "                                RESULTS"
     LOCATE 4,1:PRINT"-------------------------------------------------------------------------------"
4280 LOCATE 6,1
4290 PRINT "AIR TO FUEL RATIO     = ";USING "££.££";AFR
4310 LOCATE 6,40
4320 PRINT "MECHANICAL POWER      = ";USING "££.££ Kw";P
4340 PRINT "VOLUMETRIC  EFF.      = ";USING "££.££ %";VEFF
4350 LOCATE 7,40
4360 PRINT "THERMAL EFFICIENCY    = ";USING "££.££ %";THERMEFF
4380 PRINT "INLET TEMP.           = ";USING "££.££ C";TINLET
4390 LOCATE 8,40
4400 PRINT "TURBO EFFICIENCY      = ";USING "££.££ %";TURBOEFF
4420 PRINT "bmep                  = ";USING "££.££ bar";BMEP
4430 LOCATE 9,40 :PRINT "bsfc                 = ";USING "£.£££ Kg/KwHr";SFC
4432 LOCATE 10,1 :PRINT "bsfc                 = ";USING "££.££ Btu/KwHr";BSFC2
4434 LOCATE 10,40:PRINT "bsfc                 = ";USING "££.££ KJ/Kws";BSFC3
4440 PRINT "NOX EMISSIONS         = ";USING "££.££ g/KwHr";NOXGKWHR
4450 LOCATE 11,40:PRINT "NO EMISSIONS           = ";USING "££.££ g/KwHr";NOGKWHR
4460 PRINT "P.C. GAS FLOW         = ";USING "££.£^^^^ Kg/s";PCGAS
4470 LOCATE 12,40
4480 PRINT "M.C. GAS FLOW         = ";USING "££.£^^^^ Kg/min";MCGAS
     LOCATE 16,40
4490 PRINT "ROOTS METER/ROTAMETER = ";USING "££.££ %";METERERROR
4500 LOCATE 13,40:PRINT "TOTAL GAS FLOW       = ";USING "££.£^^^^ Kg/sec";FTOT
4505 PRINT "ENGINE TORQUE         = ";USING "£££.£ N m";TORQUE
4510 LOCATE 14,40:PRINT "ENERGY BALANCE RATIO  =  ";USING "££.££";ERATIO
4515 LOCATE 16,1 :PRINT "P.C. AFR             = ";USING "££.££";PCAFR
4520 LOCATE 19,1 :PRINT "P.C. FILLING RATIO BASED ON PRECHAMBER ENTRY CONDITIONS      = ";USING "££.££";PCFILLRAT
     LOCATE 13,1 :PRINT "P.C. AIR FLOW         = ";USING "£.£^^^^ Kg/sec";PCAIR
4522 LOCATE 17,1 :PRINT "P.C. KNOCK No. (1-10) =  ";PCKN
     LOCATE 20,1 :PRINT "P.C. FILLING RATIO BASED ON MANIFOLD CONDITIONS (MASS RATIO) =  ";USING "££.££";PCFILLRAT2
     LOCATE 17,40:PRINT "P.C./MAN. PRESS. RATIO= ";USING "£.££";PCPR1
```

```
    LOCATE 15,1 :PRINT "M.C. AFR              = ";USING "££.££";MCAFR
    LOCATE 15,40:PRINT "P.C./BOOST PRESS. RAT.= ";USING "£.££";PCPR2
    LOCATE 18,1 :PRINT "METERED FUEL FLOW (F) = ";USING "£££.£ L/MIN";F
4530 LOCATE 22,1 :PRINT "SPECIAL COMMENTS   :- ";C$
4550 T$=INKEY$
4560 IF T$=" " THEN CLS:GOTO 2400
4565 IF T$="C" THEN GOSUB 6008:GOTO 4240
4566 IF T$="K" THEN GOSUB 6016:GOTO 4240
    IF T$="F" THEN GOSUB 6000:GOTO 710
4570 GOTO 4550
4580 X=0
4590 RETURN
4600 CLS
4610 LOCATE 10,15:INPUT "ENTER FILE TITLE ";TITLE$
    OPEN "A",£3,FILE$
4620 WRITE£3,TITLE$
    CLOSE£3
4630 CLS
4640 RETURN
6000 CLS
6002 LOCATE 10,20:INPUT"METERED GAS FLOW = ";F
    CLS:RETURN
6008 CLS
6010 LOCATE 10,20:INPUT"ENTER COMMENTS :- ";C$
6015 CLS
    RETURN
6016 CLS
6017 LOCATE 10,20:INPUT"ENTER P.C. KNOCK No. : ";PCKN
6018 CLS
6020 RETURN
    REM
    REM ****************************************
7000 REM *** SUB. TO SET MANOMETER OFFSETS ***
    REM ****************************************
    REM
    CLS
    LOCATE 10,10:INPUT"ORIFICE UPPER..... ";OU
    LOCATE 11,10:INPUT"ORIFICE LOWER..... ";OL
    CLS
    LOCATE 10,10:INPUT"BOOST AIR UPPER... ";BU
    LOCATE 11,10:INPUT"BOOST AIR LOWER... ";BL
    CLS
    LOCATE 10,10:INPUT"M.C. UPPER........ ";MCU
    LOCATE 11,10:INPUT"M.C. LOWER........ ";MCL
    CLS
    LOCATE 10,10:INPUT"P.C. UPPER........ ";PCU
    LOCATE 11,10:INPUT"P.C. LOWER........ ";PCL
    CLS
    LOCATE 10,10:INPUT"INTAKE UPPER...... ";IU
    LOCATE 11,10:INPUT"INTAKE LOWER...... ";IL
    CLS
    LOCATE 10,10:INPUT"EXHAUST UPPER..... ";EU
    LOCATE 11,10:INPUT"EXHAUST LOWER..... ";EL
    CLS
    LOCATE 10,10:INPUT"MAINS GAS UPPER... ";MGU
    LOCATE 11,10:INPUT"MAINS GAS LOWER... ";MGL
    CLS
    LOCATE 10,10:INPUT"BOOST GAS UPPER... ";BGU
    LOCATE 11,10:INPUT"BOOST GAS LOWER... ";BGL
    CLS
    OMO=OU-((OU+OL)/2)
    BAMO=BU-((BU+BL)/2)
```

```
     MCMO=MCU-((MCU+MCL)/2)
     PCMO=PCU-((PCU+PCL)/2)
     IMO=IU-((IU+IL)/2)
     EMO=EU-((EU+EL)/2)
     MGMO=MGU-((MGU+MGL)/2)
     BGMO=BGU-((BGU+BGL)/2)
     RETURN
     REM
     REM **********************************
8000 REM ****** SUB. LOAD OLD DATA ******
     REM **********************************
     REM
     CLS
     LOCATE 10,10:INPUT"FILE NAME ...";FILENAME$
     LOCATE 11,10:INPUT"DATA NUMBER ... ";DATANUMBER
8005 DATANUMBER=DATANUMBER+1
     OPEN "I",£4,FILENAME$
     INPUT£4,TITLE$
8010 IF EOF(4) THEN CLOSE£4:RETURN
     INPUT£4,D$,T$,DATNO
     REM INPUT DATA
8020 INPUT£4,CR,IGN,PCSIZE,CONENO,T,AP,N,WC1,WC2,OC1,OC2,ROOTSMETER,TE1,L,MANTEMP
     INPUT£4,ORIFACETEMP,PCGT,PCGASPRESS,NOX,NO,PCET,PCAT,PCAIRPRESS,D,O,B,MCOP,PCEP
     INPUT£4,I,PE1,G,GB,VMC,PCA,VPC,F,DMW,THROTPOS,VPMAX
     INPUT£4,FTIME
     REM PROCESSED DATA
     INPUT£4,AFR,P,VEFF,THERMEFF,TINLET,TURBOEFF,BMEP,SFC,BSFC2,BSFC3,NOXGKWHR
     INPUT£4,NOGKWHR,PCGAS,MCGAS,METERERROR,FTOT,TORQUE,ERATIO,PCAFR,PCFILLRAT
     INPUT£4,PCAIR,PCKN,C$,PMAX
     FILE$=FILENAME$
     IF DATANUMBER=DATNO THEN CLOSE£4:DATNO=DATNO-1:CLS:RETURN
     GOTO 8010
     REM
     REM ********************************
     REM *** SAVE MANOMETER OFFSETS ***
     REM ********************************
     REM
9000 OPEN "O",£5,"MANOFF"
     WRITE£5,OMO,BAMO,MCMO,PCMO,IMO,EMO,MGMO,BGMO
     CLOSE£5
     RETURN
     REM
     REM *** LOAD MANOMETER OFFSETS ***
     REM
9100 OPEN "I",£5,"MANOFF"
     INPUT£5,OMO,BAMO,MCMO,PCMO,IMO,EMO,MGMO,BGMO
     CLOSE£5
     RETURN
     REM
     REM ******************************
9200 REM ***** RE-OPEN FILE SUB *****
     REM ******************************
     REM
     CLS
     LOCATE 15,15:INPUT "ENTER FILE NAME.....";FILE$
     CLOSE£4
     OPEN "I",£4,FILE$
     INPUT£4,TITLE$
9210 IF EOF(4) THEN CLS:FLAG=1:CLOSE£4:RETURN
     INPUT£4,D$,T$,DATNO
     REM INPUT DATA
     INPUT£4,CR,IGN,PCSIZE,CONENO,T,AP,N,WC1,WC2,OC1,OC2,ROOTSMETER,TE1,L,MANTEMP
```

```
     INPUT£4,ORIFACETEMP,PCGT,PCGASPRESS,NOX,NO,PCET,PCAT,PCAIRPRESS,D,O,B,MCOP,PCBP
     INPUT£4,I,PE1,G,GB,VMC,PCA,VPC,F,DMW,THROTPOS,VPMAX
     INPUT£4,FTIME
     REM PROCESSED DATA
     INPUT£4,AFR,P,VEFF,THERMEFF,TINLET,TURBOEFF,BMEP,SFC,BSFC2,BSFC3,NOXGKWHR
     INPUT£4,NOGKWHR,PCGAS,MCGAS,METERERROR,FTOT,TORQUE,ERATIO,PCAFR,PCFILLRAT
     INPUT£4,PCAIR,PCKN,C$,PMAX
     GOTO 9210
     REM
9300 REM ********************************
     REM *** SAVE LAST DATA SET SUB ***
     REM ********************************
     REM
     CLS
     OPEN "O",£6,"DEFAULT"
     WRITE£6,FILE$,TITLE$,D$,T$,DATNO
     REM INPUT DATA
     WRITE£6,CR,IGN,PCSIZE,CONENO,T,AP,N,WC1,WC2,OC1,OC2,ROOTSMETER,TE1,L,MANTEMP
     WRITE£6,ORIFACETEMP,PCGT,PCGASPRESS,NOX,NO,PCET,PCAT,PCAIRPRESS,D,O,B,MCOP,PCBP
     WRITE£6,I,PE1,G,GB,VMC,PCA,VPC,F,DMW,THROTPOS,VPMAX
     WRITE£6,FTIME
     REM PROCESSED DATA
     WRITE£6,AFR,P,VEFF,THERMEFF,TINLET,TURBOEFF,BMEP,SFC,BSFC2,BSFC3,NOXGKWHR
     WRITE£6,NOGKWHR,PCGAS,MCGAS,METERERROR,FTOT,TORQUE,ERATIO,PCAFR,PCFILLRAT
     WRITE£6,PCAIR,PCKN,C$,PMAX
     CLOSE£6
     RETURN
     REM
9400 REM ********************************
     REM * INPUT DEFAULT FILE DATA SUB *
     REM ********************************
     REM
   OPEN "I",£6,"DEFAULT"
   INPUT£6,FILE$,TITLE$,D$,T$,DATNO
   REM INPUT DATA
   INPUT£6,CR,IGN,PCSIZE,CONENO,T,AP,N,WC1,WC2,OC1,OC2,ROOTSMETER,TE1,L,MANTEMP
   INPUT£6,ORIFACETEMP,PCGT,PCGASPRESS,NOX,NO,PCET,PCAT,PCAIRPRESS,D,O,B,MCOP,PCBP
   INPUT£6,I,PE1,G,GB,VMC,PCA,VPC,F,DMW,THROTPOS,VPMAX
   INPUT£6,FTIME
   REM PROCESSED DATA
   INPUT£6,AFR,P,VEFF,THERMEFF,TINLET,TURBOEFF,BMEP,SFC,BSFC2,BSFC3,NOXGKWHR
   INPUT£6,NOGKWHR,PCGAS,MCGAS,METERERROR,FTOT,TORQUE,ERATIO,PCAFR,PCFILLRAT
   INPUT£6,PCAIR,PCKN,C$,PMAX
   CLOSE£6
   GOSUB 250
```

Appendix G

Appendix G

Published Papers by the Author

1. Charlton S J, Jager D J, Wilson M, & Shooshtarian A
"Computer Modelling and Experimental Investigation of Mixing and Combustion in a Lean-Burn Natural Gas Engine"
Transactions of the SAE, Journal of Engines, 1990.

2. Charlton S J, Jager D J, Wilson M, & Shooshtarian A
"Computer Modelling and Experimental Investigation of Mixing and Combustion in a Lean-Burn Natural Gas Engine"
SAE Paper 900228, International Congress, Detroit, 1990.

3. Charlton S J, Jager D J, Wilson M, Shoostharian A
"An Investigation of Mixing and Combustion in a Lean Burn Natural Gas Engine"
ImechE Seminar on Gas Engines and Co-generation
10-11 May 1990

4. Jager D J, Charlton S J, Tawfig M E
"In-Cylinder Measurement of Mixture Strength in a Turbocharged Natural Gas Engine"
IMechE Seminar on Experimental Methods in Engine Research and Development 11-12 December 1991.